January 2015

Understanding The Structure-Function Relationships Between Monoamine Neurotransmitter Transporters And Their Cognate Ions And Ligands

Bruce Felts

Follow this and additional works at: https://commons.und.edu/theses

UNDERSTANDING THE STRUCTURE-FUNCTION RELATIONSHIPS BETWEEN
MONOAMINE NEUROTRANSMITTER TRANSPORTERS AND THEIR COGNATE IONS
AND LIGANDS

by

Bruce F. Felts
Bachelor of Science, University of Minnesota 2009

A dissertation
Submitted to the Graduate Faculty

of the

University of North Dakota
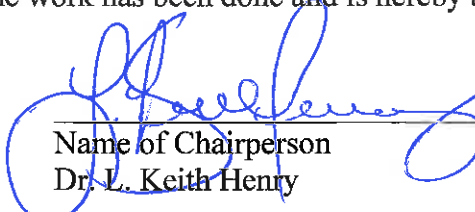
in partial fulfillment of the requirements
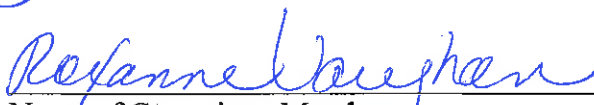

for the degree of

Doctor of Philosophy

Grand Forks, North Dakota
August
2015
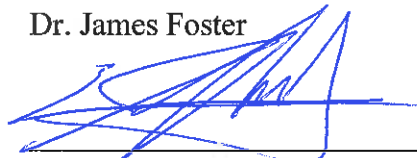
This dissertation, submitted by Bruce F. Felts in partial fulfillment of the requirements for the Degree of Doctor of Philosophy from the University of North Dakota, has been read by the Faculty Advisory Committee under whom the work has been done and is hereby approved.

Name of Chairperson
Dr. L. Keith Henry

Name of Committee Member
Dr. Roxanne Vaughan

Name of Committee Member
Dr. Lucia Carvelli

Name of Committee Member
Dr. James Foster

Name of Committee Member
Dr. Eric Murphy

This dissertation is being submitted by the appointed advisory committee as having met all of the requirements of the School of Graduate Studies at the University of North Dakota and is hereby approved.

Wayne Swisher
Dean of the School of Graduate Studies

July 22, 2015
Date
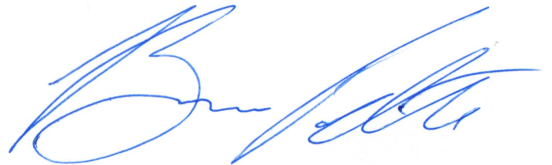
PERMISSION

Title	Understanding the Structure-Function Relationships Between Monoamine Neurotransmitter Transporters and Their Cognate Ions and Ligands
Department	Pharmacology, Physiology and Therapeutics
Degree	Doctor of Philosophy

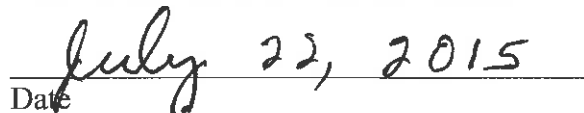In presenting this dissertation in partial fulfillment of the requirements for a graduate degree from the University of North Dakota, I agree that the library of this University shall make it freely available for inspection. I further agree that permission for extensive copying for scholarly purposes may be granted by the professor who supervised my dissertation work or, in his absence, by the Chairperson of the department or the dean of the School of Graduate Studies. It is understood that any copying or publication or other use of this dissertation or part thereof for financial gain shall not be allowed without my written permission. It is also understood that due recognition shall be given to me and to the University of North Dakota in any scholarly use which may be made of any material in my dissertation.

Bruce Felts
June 3, 2015

TABLE OF CONTENTS

CHAPTERS

LIST OF FIGURES

xiii

LIST OF TABLES

ACKNOWLEDGMENTS

First and foremost, I want to thank my mentor, Dr. Keith Henry, for everything he has done for me over the course of our time together. I cannot emphasize enough how grateful I am to have been able to be mentored by such a knowledgeable and understanding person. I owe so much of my professional development to your direction and I am confident that, thanks to you, I now have all the tools I need to succeed at whatever career I decide to pursue.

To each of my committee members, I am so thankful for all of your support and guidance through my tenure at UND. To Dr. Vaughan, Dr. Foster and Dr. Carvelli, thanks especially for sharing all of your monoamine transporter expertise and for lending countless hours of your time to manuscript, poster and presentation editing. To Dr. Murphy, thank you for all the career advice and for the hours of discussion on topics ranging from the profound to the perfunctory.

I'd also like to thank all of the UND faculty and staff members that have, throughout the years, dealt with my consistently late paper work and last minute emails. Jim, Deb, Julie, Laura, John, Victoria, Jennifer and Lisa, thank you for putting up with me. I'd also like to acknowledge all of my fellow graduate students and post-doctoral colleagues who have always supported me through every step along my journey through graduate school. Whether it was celebrating the milestones or commiserating the failures of bench science, I couldn't be more grateful to have been apart of such a good group of people.

I feel it is also important to recognize all of my collaborators from around the world. There are too many of you to name individually, but know that all your hard work and dedication

to your craft has been instrumental to my development as a scientist. Whether we ever met face-to-face or not, I'm am so appreciative of the support network for which each of you are apart of.

Last, but certainly not least, I'd like to recognize my family for all of their continuous support throughout the years. To my parents, Ralph and Doreen, you are both such excellent role models and I owe who I am today to all the counsel, encouragement and love that you have provided me over the years. To my wife, Lily, thank you for being (mostly) understanding of my chronic research-induced tardiness and for always providing the support that I needed to weather the inevitable bumps that occurred along the way. And of course, to Rufus for getting me up early in the morning and reminding me that it's the simple pleasures that truly make us happy.

Dedicated to all the late nights,
The lost hours, the sore backs,
And to those that however so slight,
Helped me to keep on the path.

ABSTRACT

The SLC6 family of secondary active transporters is made up of integral membrane solute carrier proteins characterized by the Na^+-dependent translocation of small amino acid or amino acid-like substrates. SLC6 transporters, particularly the monoamine transporters (MATs) of serotonin, dopamine and norepinephrine, are some of the most heavily studied proteins today due to their association with a number of human diseases and disorders, making MATs a critical target for therapeutic development. In addition, MATs are directly involved in the action of drugs of abuse such as cocaine, amphetamines, and ecstasy.

Following the first cloning of a MAT gene in the early 1990s, much has been uncovered about the structure and function of these proteins. Early studies developed an understanding of the kinetic parameters by which MATs operate and also yielded enough information to model the basic structural characteristics of MATs. This was greatly improved upon within the last decade, as crystallographic and computational advances have provided structural insights that have vastly accelerated our ability to study these proteins and their involvement in complex biological processes. However, despite a wealth of knowledge concerning the structural and kinetic characteristics of MATs, little is understood as to how these features are interrelated and much is still unclear as to the how regulation (and maybe more importantly, dysregulation) of MATs alters the functionality of these proteins at the molecular and synaptic levels.

The overall goal of this dissertation was to comprehensively examine the relationship between MAT structure and the ions and ligands that bind to MATs to promote/prevent

transporter function. This was done using a comprehensive approach that included biological, electrophysiological and computational techniques to target and elucidate the roles of specific amino acid residues in ion/ligand binding and/or mediation of the substrate translocation process. In successfully examining a number of specific MAT residues, this work has lead to the deduction of basic roles for each of the ion binding sites in the translocation mechanism (chapters II and III), as well as detailed the importance of specific structural components of MATs that are vital for functionality (chapters IV and V). Furthermore, this dissertation includes work highlighting the development of several photo-labeled, radio-iodinated antagonist analogues that will be used to further improve the understanding of how inhibitors bind to and block MAT function at the molecular level (chapter VI). In total, the work outlined in this dissertation provides a clearer understanding as to the molecular interactions that are necessary for MAT function and contributes an improved appreciation for the underlying mechanisms of substrate translocation and pharmacological intervention.

CHAPTER I

INTRODUCTION

The Solute Carrier Super-family of Proteins

The solute carrier (SLC) transporter super-family is comprised of approximately 350 transporters organized into 55 families. A majority of SLC members are integral, plasmalemmal proteins that are responsible for the transport of a wide range of impermeant solutes across cell membranes. SLC transporters have an extraordinarily diverse range of substrates that include both charged and uncharged organic molecules along with inorganic ions and the gas ammonia. However, despite such a large array of functions, the overall tertiary structure of SLC transporters has been shown to be remarkably similar, with all the solved SLC structures exhibiting a 5 + 5 arrangement of α-helices that have been termed the "LeuT-fold," after an amino acid transporter from the bacterium *A. aeolicus* that was the first SLC transporter to have a high-resolution crystal structure solved. This 5 + 5 arrangement consists of two bundles of 5 transmembrane helices (TMs) that are bundled together and exhibit inverted symmetry in relation to each other, supporting the idea of a conserved mechanism throughout the SLC family. This similarity in the "super-structure" of SLC proteins is especially surprising, given that very little homology is found in the primary amino acid sequence of SLC transporters from different sub-families.

The SLC6 family is among the largest and most studied of the SLC class, containing 20 genes that encode a group of structurally similar transporter proteins. These proteins transport

amino acids and amino acid derivatives across the plasma membrane against a concentration gradient by coupling substrate movement to the extracellular electrochemical Na^+ gradient. Whereas SLC6 transporters are found from bacteria to man, the vast majority of information concerning the SLC6 family comes from studies of the glycine, γ-amino-butyric acid (GABA), serotonin, norepinephrine and dopamine neurotransmitter transporters, due to their importance in mental health and addiction. In the CNS of higher order species, the cognate substrates for neurotransmitter tranporters are all common neurotransmitters that transmit chemical messages that are critical for a range of essential brain functions. Whereas the neurotransmitters glycine and GABA are considered inhibitory transmitters, as they are associated with the regulation of neuronal excitability throughout the CNS, the monoamine neurotransmitters serotonin (5-HT), dopamine (DA) and norepinephrine exhibit an increased amount of diversity in terms of the roles that each pathway performs. My work will focus primarily on the monoamine neurotransmitter transporters (MATs), with particular emphasis on the serotonin transporter (SERT) and the dopamine transporter (DAT).

The Neurophysiologic Role of MATs

The expression of MATs is primarily associated with their respective monoaminergic neurons, and thus the presence of MATs is typically used as a marker for specific monoaminergic systems (Huang and Lin 2015). MATs are distributed in both the dendrites and along the axons of presynaptic monoaminergic neurons (Figure 1). Here, the MATs mediate the rapid reuptake of neurotransmitter released into the synapse during chemical neurotransmission and also play a role in neurotransmitter recycling, as transport of neurotransmitter back into the

2
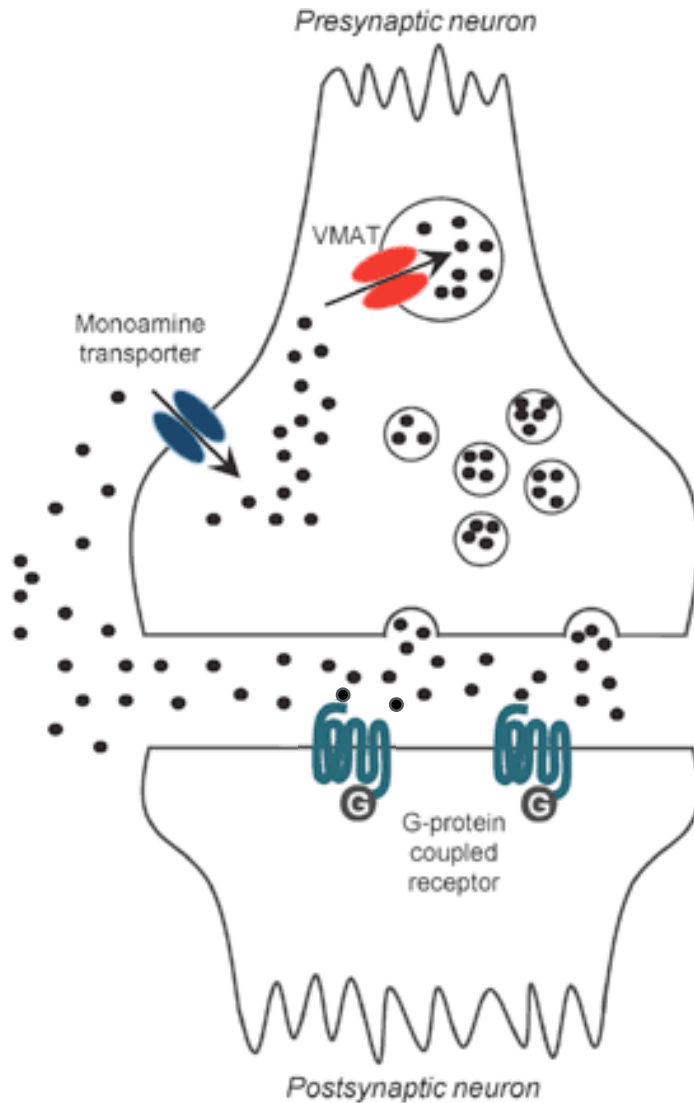
Figure 1. Role of MATs in synaptic transmission. Cartoon depicting a chemical synapse during signal transduction. Neurotransmitter (*black dots*) is cleared from the synapse by MATs. Once transported back into the presynaptic neuron, neurotransmitter can then be repackaged back into vesicles by VMAT.

pre-synaptic neuron thereby allows for the sequestration of neurotransmitter back into synaptic vesicles by vesicular monoamine transporters (VMAT1 and VMAT2) (Iversen 1971; Anne and Gasnier 2014). Thus, MATs have a critical regulatory influence on the process of synaptic transmission by both terminating receptor-mediated signaling events and replenishing vesicular neurotransmitter pools.

Due to their crucial role of keeping basal extracellular concentrations of neurotransmitters low, malfunction or improper regulation of MATs contributes to a number of neurological and neuropsychiatric disorders (Gether et al. 2006; Pramod et al. 2013). MATs alone have been implicated in a variety of mental illnesses including (but not limited to), major depression, anxiety, addiction, autism, attention deficit disorder, schizophrenia and obsessive compulsive disorder (Hahn and Blakely 2002; Sakrikar et al. 2012; Hamilton et al. 2013; Pramod et al. 2013; Hansen et al. 2014). Given their clinical significance, it is unsurprising that MATs are targets for a number of therapeutic and illicit compounds. These include tricyclic antidepressants, selective serotonin reuptake inhibitors and the drugs of abuse cocaine, methamphetamine and methylene-dioxymethamphetamine (MDMA, ecstasy) (Tatsumi et al. 1997; Amara and Sonders 1998; Kristensen et al. 2011). Despite the importance of MATs as drug targets however, surprisingly little is known about their molecular pharmacology, including localization and structure of drug binding sites along with the molecular mechanism of action. Recent progress provided by crystal structures of a single eukaryotic and several prokaryotic SLC6 transporters has provided a new level of insight into the structural biology of the MATs that presents new opportunities to interpret existing knowledge, as well as guide new studies aimed at better understanding how drugs bind, interact with and functionally modulate MATs.

Monoamine Transporter Structure

Following the first cloning of a MAT gene in the early 1990s (Blakely et al. 1991; Hoffman et al. 1991; Pacholczyk et al. 1991), much has been uncovered about the structure and function of MATs. Early studies used extensive biochemical and mutagenesis studies to develop an understanding of the kinetic parameters by which MATs operate and provide indispensable insight into transporter topology and secondary structure. However, this work was limited as it was not able to successfully produce much information on the tertiary structure of MATs. This was greatly improved upon within the last decade, as a number of prokaryotic as well as a single eukaryotic SLC family member have been crystallized.

The first crystal structure of an SLC6 family member was reported by Yamashita et al. in 2005, whereby a high-resolution X-ray crystallographic structure of a prokaryotic homolog to the SLC6 transporters, dubbed the leucine transporter (LeuT), was obtained from the thermophile bacterium *A. aeolicus*. This first crystal structure provided unambiguous insight into central aspects of the structural biology of SLC6 transporters, including long-sought details for how SLC6 transporters accommodate substrate and ions. Importantly, this crystal structure displayed features that closely matched what the previous biochemical analysis had predicted, suggesting that LeuT was a useful structural and functional template for understanding MATs (Singh et al. 2008). This has since been confirmed with the successful crystallization of the first eukaryotic SLC6 protein, a dopamine transporter from *Drosophila melanogaster* (dDAT) (Penmatsa and Gouaux 2013). In addition, the discovery of a remarkable structural conservation between LeuT and secondary active transporters from other transporter families, not originally thought to be structurally or mechanistically related to SLC6 transporters (Abramson and Wright 2009), have

further strengthened the validity of using LeuT as a structural template for understanding fundamental aspects of MAT function.

In general, SLC6 proteins have twelve defined TMs with intracellularly-facing N- and C-termini (Figure 2). Unlike the prokaryotic SLC6 family members, MATs feature N- and C-termini that are significantly longer and have been shown to mediate complex regulatory processes, such as transporter trafficking, ion stoichiometry and protein function (Kristensen et al. 2011; Pramod et al. 2013; Vaughan and Foster 2013). Moreover, MATs also feature a number of intracellular sites for post-translational modifications such as phosphorylation and palmitoylation and an extended extracellular loop 2 domain (EL2) between TMs 3 and 4 which contains a several glycosylation sites as well as a critical disulfide bond (discussed further in chapter V) (Vaughan and Foster 2013) (Figure 2). Nevertheless, MATs and LeuT share only a modest 20-25% overall sequence identity that increases to greater than 50% identity when focusing on the core binding region where the bound substrate is located in the LeuT crystal (Yamashita et al. 2005). The LeuT and dDAT crystal structures have revealed that SLC6 transporters are based on a 5 + 5 helical architecture where TMs 1–5 and TMs 6–10 form two pentihelical bundles aligned antiparallel to one another yielding a pseudo-twofold axis of symmetry (Figure 3A). TMs 11 and 12 in LeuT lie peripheral to the 5 + 5 core and may play a less critical role in transport but important functions in other aspects of structure or regulation.

The substrate permeation pathway is formed almost exclusively by TM1, TM3, TM6, and TM8 and holds a central substrate-binding site (S1) in which the substrate and two Na^+ ions are accommodated (Figure 3, A and B) (Yamashita et al. 2005). Directly above the binding site is an external "lid" formed by the aromatic side chains of Y108 on TM3 and F253 on TM6. This
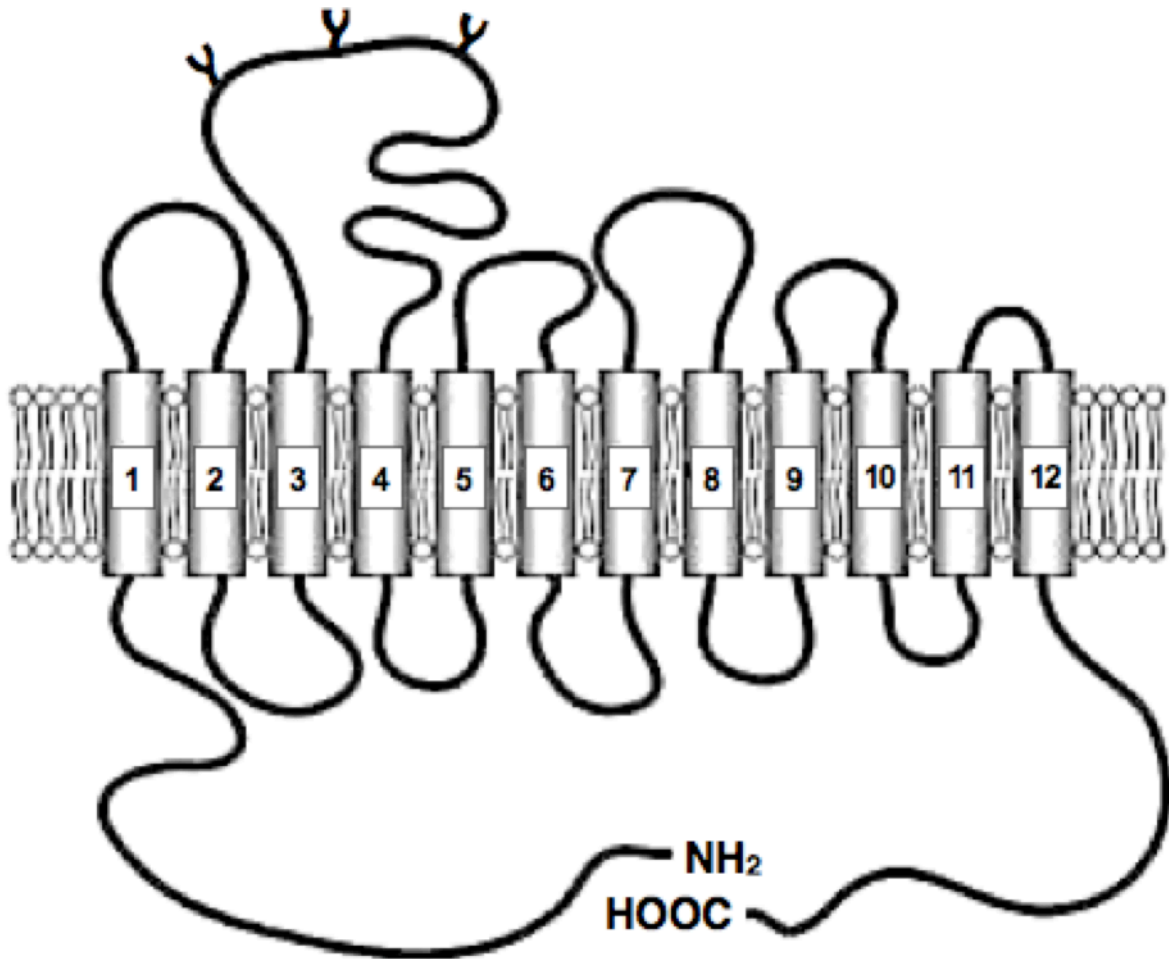
Figure 2. Basic structure of a MAT. Cartoon representing a simplified layout of a MAT's structure. There are 12 transmembrane-spanning helical domains, as well as intra- and extracellular loop regions (glycosolation sites in extracellular loop 2 are represented as Ys) including both N- and C-termini that face intracellularly.
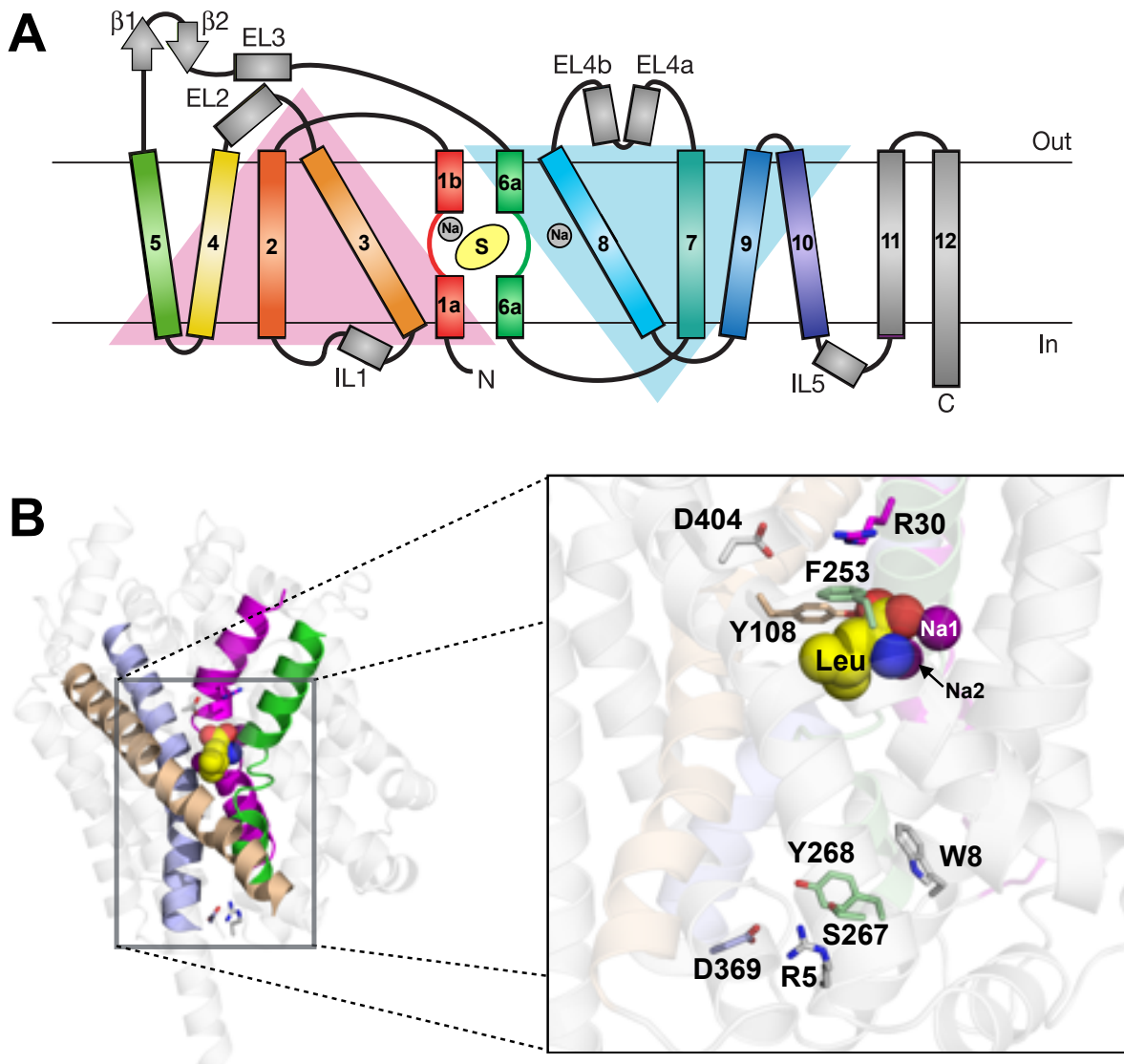
Figure 3. X-ray crystal structure and topology of the SLC6 bacterial homologue, LeuT. (*A*) A two-dimensional representation of the topology of LeuT. The positions of the substrate and the two sodium ions are depicted as a yellow oval and gray circles, respectively. The 5 + 5 inverted symmetry of TMs 1-5 and 6-10 is highlighted by the large pink and blue triangles. Figure adapted from Yamashita *et al*, 2005. (*B, left*) A three-dimensional representation of the occluded LeuT crystal structure with leucine (*yellow space-filling molecule*) and two sodiums (*purple spheres*) bound. TMs 1 (*purple*), 3 (*pale brown*), 6 (*green*) and 8 (*lavender*) are colored to outline the general substrate permeation pathway. (*B, right*) A closeup view of the central core of LeuT. Amino acid side chains associated with the external and internal gates are depicted as sticks.

hydrophobic lid is supported by the presence of a water-mediated ionic interaction between R30 on TM1 and D404 on TM10 (Figure 3B). In a LeuT crystal structure with the noncompetitive inhibitor tryptophan complexed, a direct interaction between the inhibitor and the side chains of R30 and D404 is observed, suggesting that this ionic interaction may be important for proper function of the translocation mechanism (Singh et al. 2007; Zhou et al. 2007; 2009). Importantly, this ionic interaction at the outer gate is conserved in MATs (although the Asp is replaced by a Glu in SERT). The importance of the formation of this putative salt bridge in AMPH recognition and translocation by SERT is the topic of chapter V.

The intracellular gate found just below the binding site is much thicker than its extracellular counterpart. This structure is stabilized mainly by an interaction network formed between the ionic pairing of R5 and D369, as well as by S267 and Y268 (Figure 3B). Adjacent to these residues is a bulky side chain of a tryptophan (W8), which has also been suggested to provide strength to the substructure (Yamashita et al. 2005; Singh et al. 2007; Zhou et al. 2007; Singh et al. 2008; Zhou et al. 2009).

The extracellular and intracellular gating regions prevent access to the binding region when in an occluded or closed conformation, eliminating the non-specific movement of substrate or ions in either direction and forcing the substrate to move into the cell following translocation (Yamashita et al. 2005; Kanner 2008; Singh et al. 2008). This crucial role is supported by the observation that all residues participating in the two networks are strictly conserved across the MATs except for D404, which is conservatively substituted by a Glu in SERT (Beuming et al. 2006).

The Substrate Binding Pocket

LeuT and the MATs share a remarkably high sequence similarity (upwards of 65%) in the regions that contain core transport machinery, especially within TMs 1, 3, 6 and 8, which makeup the substrate permeation pathway and house the substrate binding site (S1) along with the Na^+ binding sites (Yamashita et al. 2005; Beuming et al. 2006)(Figure 3B). Consequently, the LeuT crystal structures provide sound templates for which homology models of MATs can be constructed (Yamashita et al. 2005; Beuming et al. 2006; Rudnick 2006; Henry et al. 2006a). In general, the high degree of sequence similarity observed between the core region of LeuT and the MATs produce models with very similar overall structure. By contrast, some of the more variable loop regions have little to no homology and are therefore more difficult to align with the LeuT template (Beuming et al. 2006). Similarly, LeuT has considerably shorter N- and C-termini and thus these regions have also been very difficult to recreate computationally. However, the recent solving of the dDAT crystal structure does provide a more detailed look into some of the regions that previously were unsolved, with the caveat that several point mutations, a large deletion in EL2 and use of a Fab fragment were needed in order to thermo-stabilize dDAT for crystallography (Penmatsa et al. 2013).

Due to the large number and variety of crystal structure conformations available for LeuT, much of this introduction will focus on the particular structural features that are important for substrate/ion binding and the translocation machinery of LeuT. Importantly, many of the amino acids that are functionally important for LeuT are conserved in MATs. Likewise, important functional residues that are not highly conserved between LeuT and the MATs generally suggest an evolutionary reason for this discrepancy. Throughout this introduction I will highlight these

divergent residues in order to emphasize the structural nuances between LeuT and the MATs that are vital for their contrasting cellular responsibilities.

The S1 binding site of LeuT. In all substrate-bound LeuT structures reported, a single substrate molecule is accommodated in a common binding site, designated S1, which is located centrally within the permeation pathway (Figure 4A) (Yamashita et al. 2005; Singh et al. 2008; Krishnamurthy and Gouaux 2012; Piscitelli and Gouaux 2012). The S1 pocket is composed almost entirely of TMs 1, 3, 6 and 8, whereby residues from these TMs that face the permeation pathway create a lining of aromatic, aliphatic and polar amino acid side chains. In addition, the backbone amide groups from the unwound regions of TMs 1 and 6 also contribute to the S1 binding site (Yamashita et al. 2005; Singh et al. 2008)(Figure 4A).

The S1 pocket of LeuT can be divided into two regions: a polar region formed exclusively by the unwound regions of TM1 and TM6 that accommodates the α-amino and α-carboxylate groups of the amino acid substrates, and a hydrophobic pocket formed by aliphatic side chains from TM1, TM3, and TM6 accommodating the hydrophobic side chain of the substrate (Yamashita et al. 2005; Singh et al. 2008) (Figure 4A) Within the polar region, the hydrophilic components of the substrate form hydrogen bonds with backbone amide groups of TM1 and TM6. The α-amino group of the substrate interacts with backbone carbonyls from A22 in TM1, along with F253 and T254 in TM6, and with a side-chain hydroxyl from S256 in TM6. The α-carboxyl group of the substrate interacts with a backbone amide nitrogen from L25 and G26 in TM1, a phenolic hydroxyl moiety from Y108 in TM3 and with one of the bound Na^+ ions (Na1) (Yamashita et al. 2005). The hydrophobic region accommodating the aliphatic portion of the substrate is formed by the side chains of residues from TM3 (V104 and Y108), TM6 (F253,

11
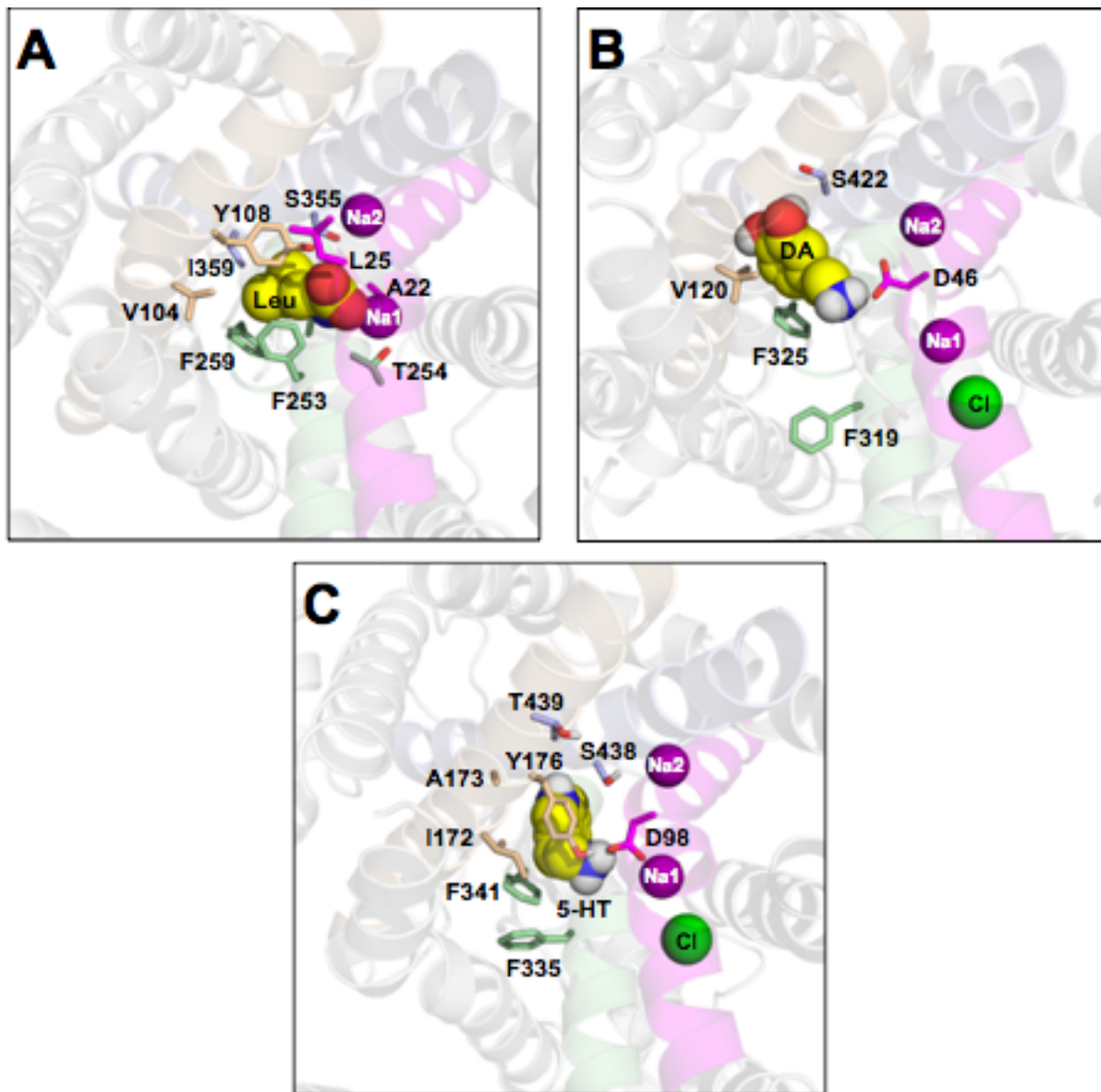
Figure 4. The S1 binding site of LeuT, dDAT and hSERT. Pictured are three-dimesional representations of the S1 binding sites of (*A*) LeuT, (*B*) dDAT and (*C*) hSERT with their respective substrates bound. Panels (*A*) and (*B*) are taken from occluded or semi-occluded crystal structures, respectively, whereas panel (*C*) is a computational homology model of hSERT based off of the structure of LeuT. Each substrate is depicted as a yellow space-filling molecule (with hydrogens capable of hydrogen bonding included) and the bound Na^+ and Cl^- ions are represented as purple and green spheres, respectively. Amino acid side chains that makeup the substrate binding site are shown as colored sticks, with their respective colors illustrating whether they are in TMs 1(*purple*), 3 (*pale brown*), 6 (*green*), or 8 (*lavender*).

S256 and F259) and TM8 (S355 and I359). This region is a major determinant for substrate specificity of the MAT binding pocket (Gouaux 2009). Lastly, the position of the side chains from residues Y108 and F253 are oriented above the bound substrate and thus these side chains form a pseudo-barrier between the binding site and the extracellular vestibule. It is important to note that these two aromatic side chains are part of the predicted extracellular gate that separates the substrate from the extracellular vestibule (Figure 4B) (Singh et al. 2008).

The sharing of upwards of 65% sequence identity between the core binding regions of LeuT and the MATs, along with the high degree of conservation between substrate coordinating residues, strongly suggests that the S1 site is structurally conserved between LeuT and MATs. This is consistent with a large amount of biochemical evidence that has identified S1 residues that alter substrate affinity in MATs (Beuming et al. 2006; Rudnick 2006; Henry et al. 2007) and has since been confirmed by the dDAT crystal structure (Wang et al. 2015).

The S1 binding site in MATs. For the MATs, docking 5-HT and DA into homology models of the S1 site in SERT and DAT, respectively, have obtained strikingly similar poses of the substrates (Huang and Zhan 2007; Beuming et al. 2008; Celik et al. 2008; Field et al. 2010). Importantly, these homology models not only look highly similar to the LeuT crystal structure, but they have also been corroborated by the recent crystal structure obtained for dDAT (Penmatsa et al. 2013; Wang et al. 2015) (Figure 4B). The aromatic moieties of the substrates are accommodated in a hydrophobic region of the pocket, formed by hydrophobic and aliphatic residues in TM1, TM3, and TM6 (Figure 4, B and C), whereas the alkylamine side chains of dopamine both occupy a region equivalent to the polar region in LeuT that accommodates the α-carboxyl group on its amino acid substrates. An important feature in this region of SERT, DAT,

and NET is the presence of an Asp residue close to the TM1 helical break (D46 in dDAT, D98 in hSERT) at a position where LeuT contains a Gly (G24). The acidic side chain in this position is strictly required for the function of the MATs (Kitayama et al. 1992; Barker et al. 1999; Henry 2003; Celik et al. 2008; Andersen et al. 2010), leading to the early suggestion that this residue is involved in a critical interaction with the monoamine substrate, possibly by a direct interaction with the amino group of the substrate (Kitayama et al. 1992; Barker et al. 1999). This has since been validated in the crystal structure of dDAT (Penmatsa et al. 2013; Wang et al. 2015), as well as mutational studies of SERT showing that the loss of affinity observed when shortening the alkyl-amine side chain of 5-HT derivatives by one methyl can be compensated for by extending the amino acid side chain by one methyl via substitution of Asp with Glu at this position (Barker et al. 1999; Celik et al. 2008). Thus, as the monoamine substrates lack a negatively charged carboxylate group, the unique presence of an Asp residue in this position in the MATs is present to compensate for the inability of the monoamine substrates to coordinate with one of the Na^+ ions.

The S2 binding site in the extracellular vestibule. Several reports have suggested that the extracellular portion of the substrate permeation pathway (often referred to as the extracellular vestibule) contains a second substrate binding site in LeuT, designated the S2 site (Shi et al. 2008). The S2 site is located just above the extracellular gate, in an amorphous region housed near the bottom of the extracellular vestibule (Figure 5). Substrate binding to the S2 site was first suggested by Shi et al. (2008), who used molecular dynamics (MD) simulations in combination with biochemical experiments on reconstituted LeuT to propose that occupation of the S2 site is required to trigger conformational changes that releases substrate from the S1 to
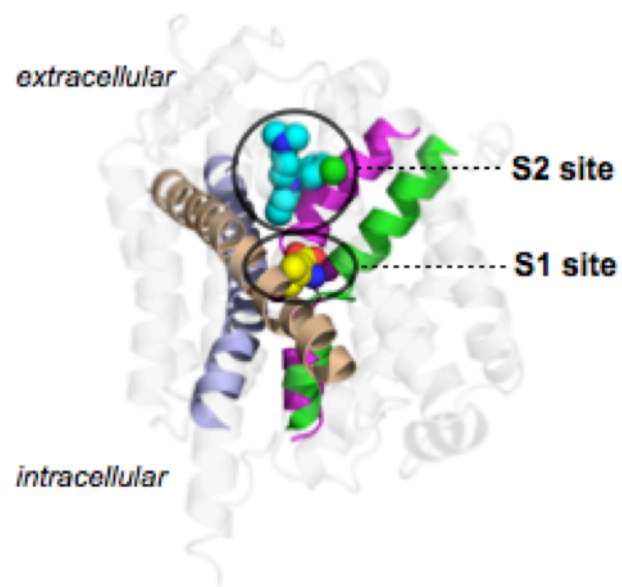
Figure 5. The location of the S1 and S2 binding sites in LeuT. A crystal structure of LeuT with the inhibitor clomipramine bound to the S2 binding site in the extracellular vestibule. The substrate, leucine is bound at the S1 binding site in the central binding region, while both sodium sites are occupied by Na$^+$ (*purple spheres*). TMs 1 (*purple*), 3 (*pale brown*), 6 (*green*) and 8 (*lavender*) are colored to outline the general substrate permeation pathway.

intracellular side (Quick et al. 2012). These results remain controversial, as other reports refute the existence of the S2 site in LeuT (Piscitelli et al. 2010).

Although the S2 site has not been found to occupy substrates in any structure of LeuT crystallized in presence of substrates, other structures of LeuT crystallized in presence of certain LeuT inhibitors or detergents have found that these molecules bind within the S2 site (Figure 5) (Zhou et al. 2007; Singh et al. 2008; Quick et al. 2009; Zhou et al. 2009), hereby preventing conformational changes necessary for substrate translocation (Singh et al. 2007; Quick et al. 2009; Zhou et al. 2009), a mechanism that might be relevant for the mechanism of action of MAT inhibitors (Zhou et al. 2007; 2009). This model has been supported by a wealth of biochemical evidence from SERT, whereby site-directed mutagenesis was used to identify a low-affinity S2 binding site whereby both TCAs (Sarker et al. 2010) and SSRIs (Chen et al. 2005b; Plenge et al. 2007) can occupy. Binding of an antagonist in the S2 site is thought to produce an allosteric effect on the S1 binding site, whereby the S1 site exhibits an increased affinity for a bound antagonist while the S2 site also acts as a functional lid that further decreases the likelihood that the antagonist bound to S1 will dissociate (Chen et al. 2005b; Neubauer 2006; Plenge et al. 2012). Recently, the synthesis of several novel citalopram analogues that favor the S2 site over the S1 site has been reported (Banala et al. 2013). Similarly, the lab of Amy Newman has recently developed three photo-tagged, radiolabeled citalopram analogues that are capable of creating a covalent attachment to within its SERT binding site when flashed with UV light (chapter VI). Both these sets of citalopram analogues could be used as tools to elucidate the residues that are critical for binding of an antagonist at the S2 site.

Ion Binding Sites in MATs

The cotransport of Na^+ ions with the substrate molecule is a principal characteristic of the SLC6 subfamily. It is the utilization of the chemiosmotic Na^+ gradient that contributes the energy needed to complete the thermodynamically-unfavorable movement of substrate across the plasma membrane. Furthermore, binding and, in some cases, cotransport of additional Na^+, Cl^-, K^+ and/or H^+ ions is necessary for the function of most SLC6 transporters (Kristensen et al. 2011). For instance, SERT contains two putative Na^+ binding sites and one Cl^- binding site within close proximity to the substrate-binding site. Interestingly, the SERT translocation shoichiometry requires the symport of one Cl^- and only one Na^+ (despite the purported presence of two bound Na^+) with one 5-HT molecule, while the antiport of one K^+ ion is also required to complete one transport cycle. By contrast, DAT transport stoichiometry consists of the symport of two Na^+ and one Cl^- per molecule of DA and does not require intracellular K^+ antiport. Since the first crystal structures of LeuT were solved (and especially with the recent crystallization of dDAT), a considerable amount of structural knowledge has been gained concerning the overall structural components of the ion binding sites in MATs. This has ushered in a new understanding of how ions interact with MATs and thus has allowed for considerable investigation into the mechanism by which ions couple to and drive substrate transport by MATs, a feature of much of my work discussed in this dissertation (chapters II and III).

The Na^+ binding sites. One of the primary features of all of the outward-facing and occluded LeuT structures is the presence of two distinct ion-binding sites in the S1 pocket that are occupied by Na^+ ions, designated Na1 and Na2 (Yamashita et al. 2005; Zhou et al. 2007; Singh et al. 2008; Zhou et al. 2009). Both Na^+ binding sites are believed to be important in the

stabilization of the unwound regions of TMs 1 and 6, which contain several residues purported to coordinate the binding of substrate (Figure 6A). In addition, the Na^+ ion located in Na1 interacts directly with substrate bound to LeuT, further corroborating the importance of the Na^+ ions in the proper organization of the binding region and explaining the strict selectivity of Na^+ over similarly charged but different sized cations by SLC6 transporters.

In the Na1 and Na2 sites, six and five backbone carbonyls or side-chain oxygens coordinate Na^+, respectively (Figure 6A). The residues forming the Na1 site are highly conserved across the SLC6 family, strongly indicating that an equivalent site is present in MATs (Rudnick 2006; Singh et al. 2008; Gouaux 2009). The only major difference among these residues when comparing LeuT and MATs is the substitution of an Asp (D98 in SERT) at the position equivalent to G24 in LeuT (Figure 6, B and C). As mentioned previously, it has been shown that this variation in MATs is important in order to compensate for the lack of a carboxyl group in the structure of monoamine neurotransmitters.

Of the five residues that coordinate Na2 in LeuT, one is identical and three are highly similar to the equivalent residues in MATs. The single nonconserved residue is T354 in LeuT, which has an Asp (D437) at the homologous position in the MATs. Despite this variation between LeuT and MATs in the constituents that form the putative Na2 site, a number of studies supplied evidence supporting the presence of two Na^+ binding sites, even in those MATs that only cotransport a single Na^+ (Rudnick 2006; Singh et al. 2008).

Although Na^+ binding sites similar to Na1 and Na2 exist in the mammalian MATs, as demonstrated in the dDAT crystal structure, the exact role of Na^+ at each of these sites is largely uncertain. For example, it has been suggested that MATs translocating one Na^+ (SERT and NET)
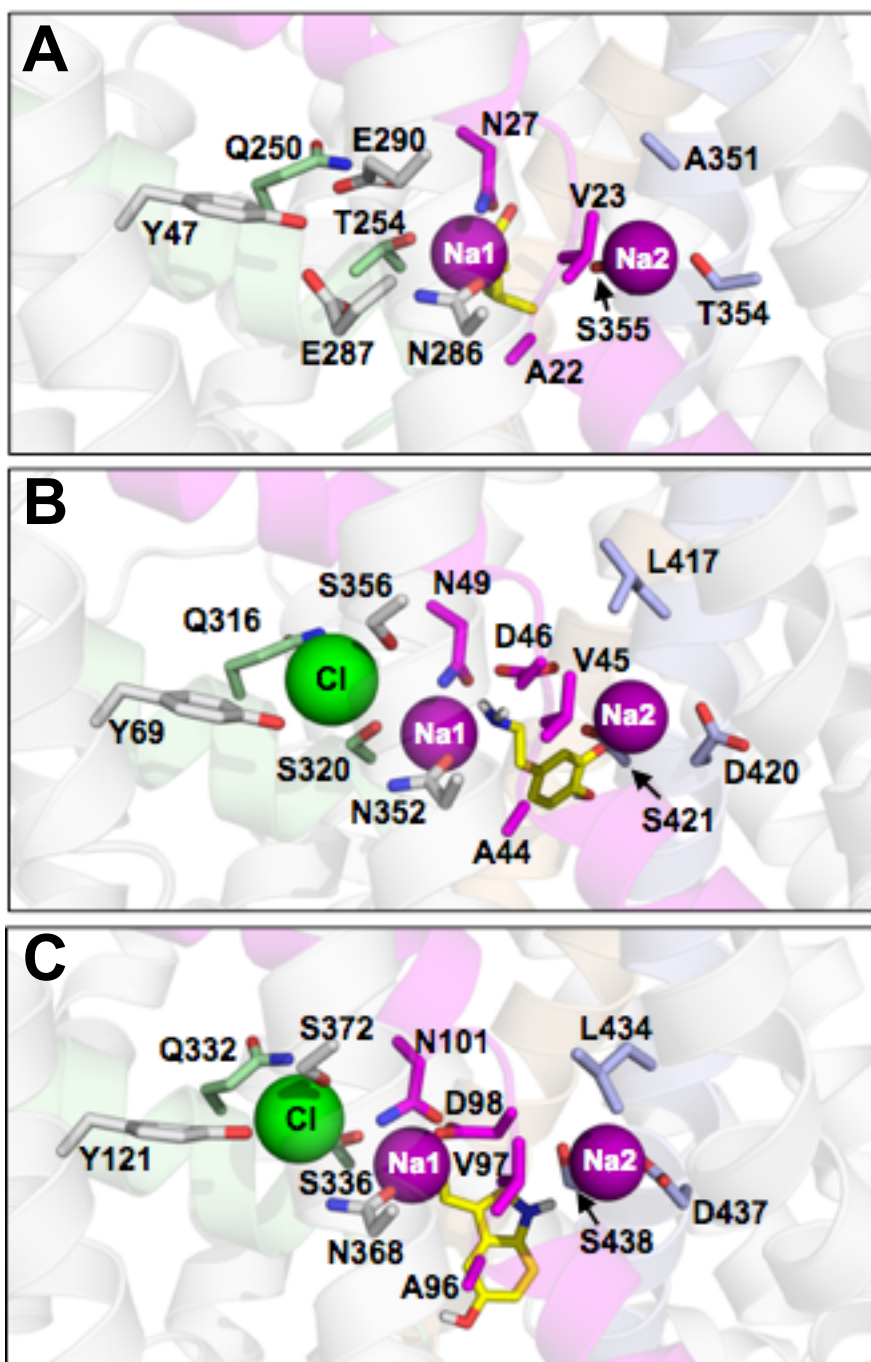
Figure 6. The ion binding sites in LeuT, dDAT and hSERT. Ions and their respective coordination sites are represented for (*A*) LeuT, (*B*) dDAT and (*C*) hSERT. Sodium and chloride ions are depicted as purple and green spheres, respectively. Bound substrate in each model is represented as a yellow sticks with those hydrogens capable of hydrogen bonding included. Side chains from amino acids that makeup part of an ion coordination network are depicted as sticks (note that some interactions are from the amino acid backbone of labeled residues, however for clarity these were not included).

use only the Na1 site, whereas the transporters that translocate two Na$^+$ per substrate also use the Na2 site (Rudnick 2006; Singh et al. 2008). However, in direct opposition to this hypothesis, a crystal structure has been characterized for a bacterial galactose transporter (vSGLT) that is very similar structurally to LeuT but only has a single Na$^+$ binding site, of which is found in a homologous position to the Na2 site in LeuT (Faham et al. 2008). This would suggest that only the Na2 site is conserved throughout the LeuT super-family, and given the fact that the Na1 site is not present in vSGLT, this would suggest that Na2, and not Na1, may be the Na$^+$ of action in MATs that only cotransport a single Na$^+$ (Watanabe et al. 2010).

In chapter III, I will present work that utilizes a mutation at one of the Na1 coordinating residues (N101) in the human (h)SERT which changes the selectivity of this site and thereby allows for the parsing of roles between the Na1 and Na2 sites. There I will also present a mechanism by which the Na$^+$ at Na2 is cotransported with 5-HT and the Na$^+$ at the Na1 site plays more of a regulatory role, thereby mediating the cascade of conformational changes that triggers the translocation mechanism (Felts et al. 2014).

The Cl$^-$ binding site. The majority of mammalian SLC6 transporters, including the three MATs, are dependent on the symport of one Cl$^-$. This is not the case for the prokaryotic SLC6 homolouges, including LeuT, which are characterized by a Cl$^-$-independent mechanism (Zomot et al. 2007; Kanner 2008; Zhao et al. 2010). Given the lack of a Cl$^-$-binding site in LeuT, the characterization of the Cl binding site in mammalian SLC6 transporters was instead successfully mapped via two independent biochemical studies using site-directed mutagenesis and computational modeling (Forrest et al. 2007; Zomot et al. 2007). Comparative sequence analysis of mammalian SLC6 transporters and LeuT provided hints that eventually lead to identification

of Glu290 in TM7 of LeuT as a candidate position for the Cl⁻-binding site in mammalian transporters. Importantly, this negatively charged residue is conserved in Cl⁻-independent prokaryotic SLC6 transporters but not in the Cl⁻-dependent mammalian SLC6 transporters (Forrest et al. 2007; Zomot et al. 2007).

Computational homology models of SERT and the GABA transporter revealed that with Cl⁻ docked into the equivalent position of Glu290 in LeuT, that this positioning could accommodate the Cl⁻ ion via coordination by Y121, S336, N368, S372, along with possible additional coordination by Q332 and C369 (hSERT numbering; Figure 6C). The essential role of Cl⁻ at this site was further supported by site-directed mutagenesis targeting Cl⁻ coordinating residues, where mutation of these residues resulted in considerable alteration of transport activity and a subsequent elimination of Cl⁻ dependence (Forrest et al. 2007; Zomot et al. 2007).

Recently, several groups have shown that mutation of the negatively-charged residue demonstrated to take the place of Cl⁻ in prokaryotic SLC6 transporters results in a Cl⁻ dependent transporter with a Cl binding site coordinated by many of the residues associated with Cl⁻ coordination in MATs (Kantcheva et al. 2013). Moreover, the acquisition of the dDAT crystal structure has similarly confirmed the residues originally forwarded as Cl⁻ coordinating residues in MATs (Figure 6B) (Penmatsa et al. 2013). However, despite the wealth of both biological and structural data that outlines the positioning of the Cl binding site, little remains know as to the actual function of this Cl site during the translocation mechanism (Erreger et al. 2008). This gap in knowledge is the basis for the project outlined in chapter II, where use of a mutant associated with the Na1 site (N101) alters the dependence of the transporter for extracellular Cl⁻, without a relative diminishment in transport activity. This work better describes the selectivity of the Cl

site and speculates on a functional role of Cl⁻ binding (Henry et al. 2011).

Chemiosmotic Coupling and the Translocation Mechanism

The Alternating Access Mechanism of Substrate Transport

The main mechanistic theory for how secondary-active transport selectively moves substrate across the membrane is known as the alternating access mechanism (Jardetzky 1966). The basic concept of this model is that transporters function by having a central core region where substrate binds that can be sealed off from both the extracellular and intracellular faces of the membrane (Figure 7). This is managed by the existence of substructures of the protein that can be sequentially rearranged in order to allow or prevent access to the protein's core, thereby acting as functional gates. The gates can both be closed to form an occluded binding pocket, however the sequential closing off of one gate generally results in the rearrangement and opening of its counterpart, thereby alternatively granting access of the binding region to the opposing faces of the membrane. In the case of ion-coupled transporters, such as MATs, the toggle between extracellular and intracellular facing conformations is determined by the binding of substrate and ions.

Prior to the availability of crystal structures, numerous biochemical studies identified that there is a considerable amount of structural rearrangement of many of the TMs and extracellular loops during transport (Loland et al. 1999; Androutsellis-Theotokis et al. 2001; Ni 2001; Androutsellis-Theotokis and Rudnick 2002; Zomot 2003; Loland et al. 2004). However, despite this wealth of information a mechanistic model remained impossible to generate without a structural template by which to base it on.
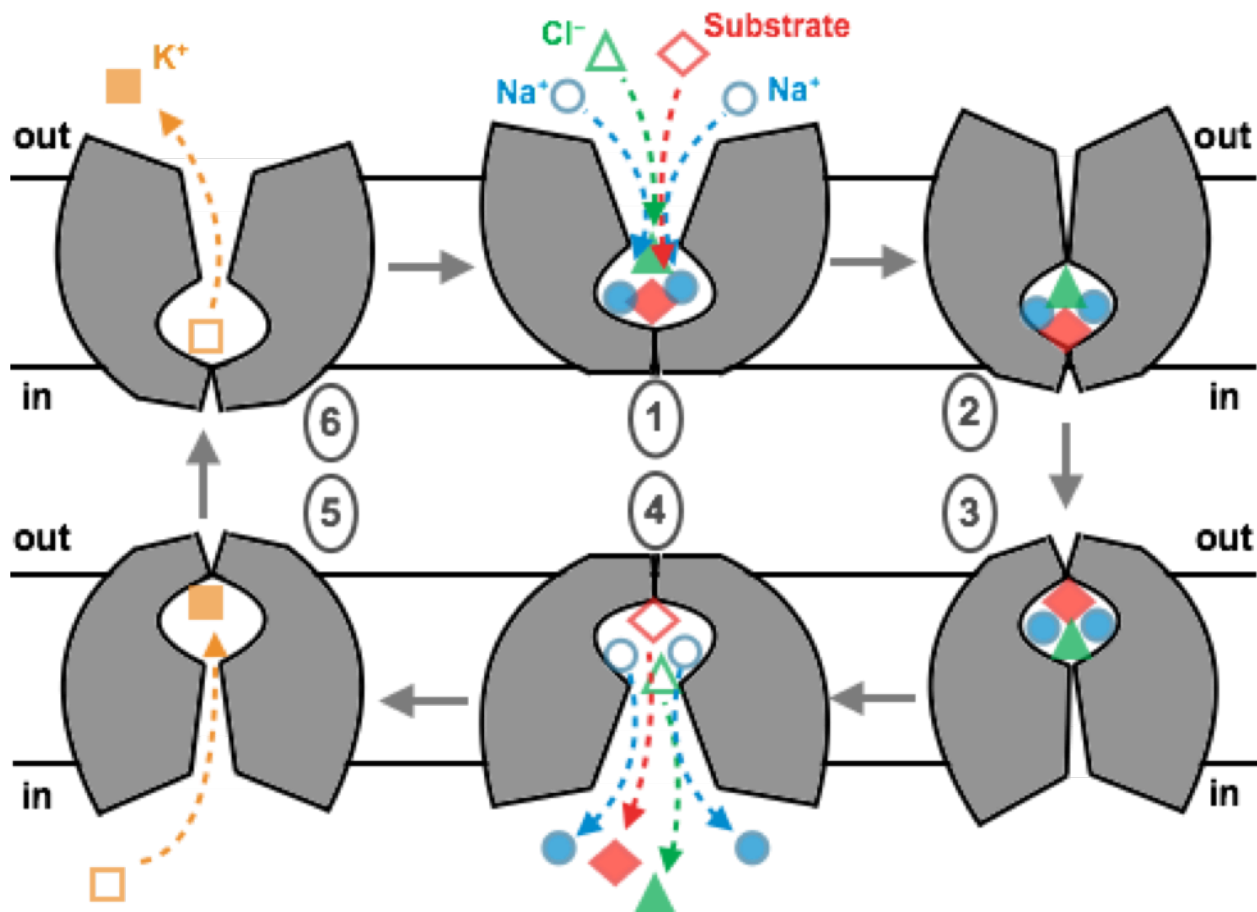
Figure 7. The alternating access model of transport. Cartoon depicting the basic stages of the alternating access model of transport. Substrate (*red diamond*), two sodium ions (*blue circles*) and a chloride ion (*green triangle*) bind to the outward facing structure (*1*). This causes a cascade of confomational changes that closes the extracellular gate (*2*), placing the transporter in the occluded state, and then continues in opening the intracellular gate (*3*). Substrate and ions are then released into the cell (*4*; note that only one sodium is cotransported with the substrate by SERT and NET, while two are cotransported by DAT). For SERT, a potassium ion (*orange square*) binds to the intracellular facing conformation (*5*), causing the rectification of the transporter to the outward facing conformation (note that no ion antiport is needed for rectification of DAT or NET to the outward facing conformation). In returning to the outward facing conformation, the potassium ion is released (*6*) and a new cycle can begin.

The emerging crystal structures of the LeuT-fold family of proteins have since provided snapshots of the transporter in various stages of substrate translocation, such as the outward-facing, occluded and inward-facing conformations (Figure 8, A–C) (Yamashita et al. 2005; Singh et al. 2008; Krishnamurthy and Gouaux 2012). By assuming that the conformational changes necessary to move substrate will be conserved among the LeuT-like transporters, several groups have put the snapshots together to describe the alternating access system in these proteins. Two prevalent models are the "rocking bundle" (Forrest and Rudnick 2009), where a bundle (TMs 1, 2, 6 and 7) and scaffold (TMs 3, 4, 5, 8, 9 and 10) rock in relation to one another resulting in transition from outward to inward facing conformations, and the "hinge" model (Krishnamurthy et al. 2009), where flexing movements in TMs 1 and 6 followed by side chain rearrangement is sufficient to open and close the outer and inner gating densities and allow the subsequent passage of substrate. A relatively complete set of crystal structures for the transporter Mhp1, representing the outward-facing, occluded and inward-facing conformations, have demonstrated that the transporter undergoes rigid body movements similar to those proposed in the rocking bundle model (Shimamura et al. 2010; Weyand et al. 2010). Recently, using antibody stabilization and mutagenesis primarily at the Na2 binding site, a set of LeuT crystals were generated that captured a substrate-free outwards-facing and apo-inward facing set of conformations (Krishnamurthy and Gouaux 2012) (Figure 8, A and C). In this report, the authors propose these new structures reveal a hybrid mechanism of transport for LeuT that involves a combination of both hinge and rigid-body movements to permit substrate and ion passages across the membrane. Indeed, as more LeuT-fold crystal structures are resolved, inevitably a clearer picture of the transport mechanism by this family will emerge. However, even with an
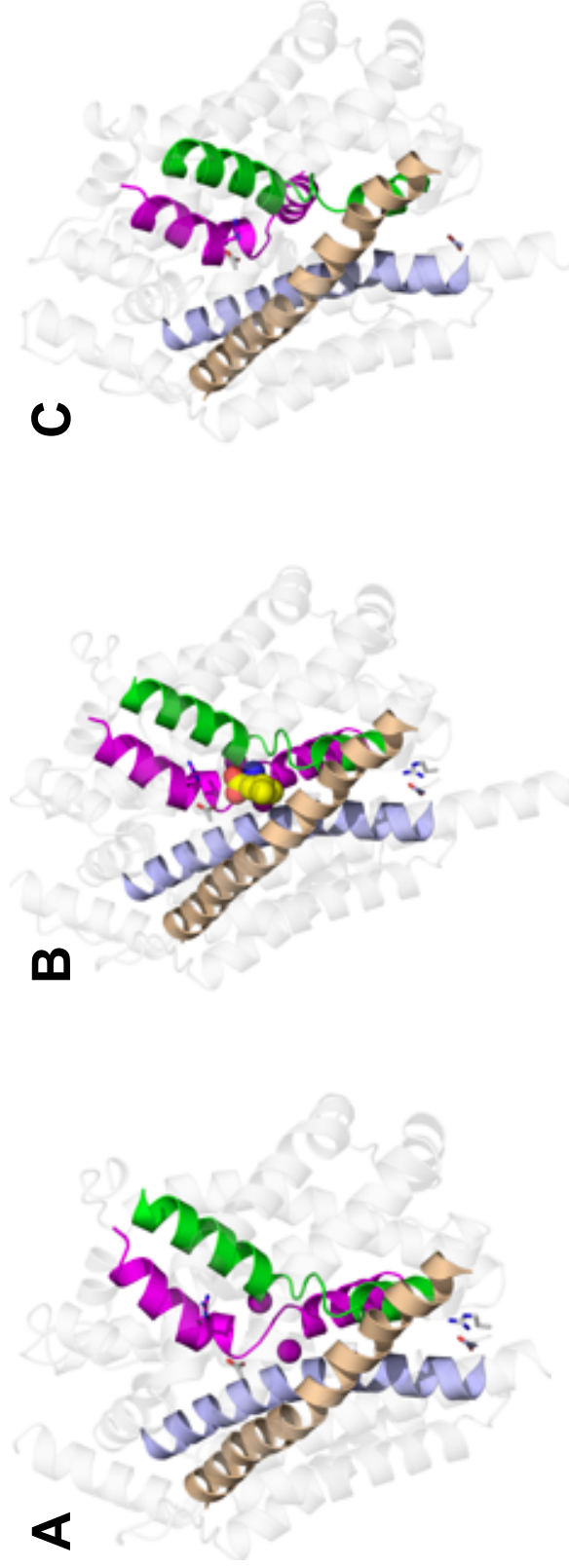
Figure 8. Three distinct structural conformations of LeuT provide a general outline of the alternating access mechanism of transport. Shown are three models representing solved crystal structures of LeuT in the (*A*) substrate-free, open to out conformation, the (*B*) leucing-bound occluded conformation and the (*C*) ion and substrate-free inward open conformation. TMs 1(*purple*), 3 (*pale brown*), 6 (*green*) and 8 (*lavender*) are colored to outline the general substrate permeation pathway. Substrate is depicted as a yellow, space-filling molecule and sodium ions are shown as purple sheres. The outer ionic gating residues (*R30 & D404*) and the inner ionic gating residues (*R5 & D369*) are included in each model as a reference point to highlight the opening of the permeation pathway when outward- or inward-facing.

increasing number of crystal structures captured in various states of mechanistic movement, it is important to remember that each structure represents a simple snapshot of an incredibly dynamic process. As such, much of our understanding of the mechanistic interworkings of MAT machinery remains elusive.

Kinetic and Electrogenic Properties of MATs

The primary role of the MATs is to mediate the rapid removal of neurotransmitter from the synapse, a process that requires transport against very large concentration gradients. Studies using radiolabeled substrates have been the gold standard for the study of the kinetic properties of MATs. These studies have shown that the relationship between concentrations of substrate, along with Na^+ and Cl^-, and transport activity follows Michaelis-Menten kinetics with K_m values in the lower micromolar range for the substrate (Sneddon 1973; Humphreys et al. 1994) and millimolar range for the two ions (Sneddon 1969; Nelson and Rudnick 1979; 1982). However, despite a wealth of knowledge concerning the structural and kinetic characteristics of MATs, little is understood as to how these features are interrelated and much is still unclear as to the how regulation (and maybe more importantly, dysregulation) of MATs alters the functionality of these proteins at the molecular and synaptic levels. My work on the characterization of the role that the ion binding sites play in the SERT transport mechanism can be found in chapters II and III.

Along with defining the kinetic properties of the MAT transport process, flux experiments have also determined that the process of stoichiometric substrate translocation is electrogenic for some MATs (DAT and NET) and electroneutral for others (SERT) (Rudnick and Nelson 1978; Mager et al. 1994; Sonders and Amara 1996). As MAT transport can produce

membrane potential-dependent currents, transporters operating via an electrogenic mechanism therefore also add conductance to the membrane. However, several studies have shown the conducting properties of MATs can be considerably larger than the electrogenic values predicted by the stoichiometric transport mechanism (Sonders et al. 1997; Carvelli et al. 2004). Moreover, in addition to this substrate-dependent ion flux there also exists an uncoupled, substrate independent ion flux. In fact, MATs are thought to exhibit at least four distinct conducting states (Mager et al. 1994).

The mechanism by which these distinctive conducting states operate is yet to be elucidated, however several studies have demonstrated that interacting proteins, such as the SNARE protein syntaxin1A, can bind to and regulate MAT activity and conducting states (Quick 2003; Carvelli et al. 2008). These studies have demonstrated that the interaction between MATs and their binding partners can result in the toggling between the uncoupled and coupled ion conducting states of MATs, and thus that both cell excitability and ligand-mediated effects may be dependent on the association of MATs and their respective interacting proteins (Quick 2003). Moreover, electrogenic substrate transport and inward currents have also been described for other SLC6 members who do not necessarily translocate neurotransmitters (i.e. amino acid, creatine and taurine transporters), thus it is conceivable that in addition to moving substrates across membranes this protein family also controls ion concentrations within cellular microdomains. For example, data from native neurons suggest that DAT-mediated conductances generated by DA or AMPH increase excitability of midbrain dopaminergic neurons (Ingram et al. 2002; Carvelli et al. 2004).

These transport-associated currents provide useful tools for quantitative functional

characterization, as well as for qualitative distinctions between substrates and blockers. For example, amphetamine-like dopamine-releasing drugs produce transport-associated currents at dopamine transporters, but cocaine-like drugs block such currents (Galli et al. 1995; Sonders and Amara 1996). Furthermore, it has been postulated that dysregulation of these MAT conducting states may result in alteration of the firing rates of MAT-associated neurons, possibly explaining disease states such as depression and anxiety (Ingram et al. 2002; Carvelli et al. 2004).

Pharmacological Intervention and MATs

Given the critical role that MATs play in the regulation of neurotransmission, it is unsurprising that these proteins are attractive pharmacologic targets for both therapeutic and illicit substances. Decades ago, MATs were found to be important for the mechanism by which classic mood stabilizers produce their effects (Brill and Patton 1957; Iversen 2000). Since this discovery, the pharmaceutical industry has initiated an extensive drug discovery campaign in order to develop and synthesize compounds that selectively target DAT, NET and SERT. This has led to the successful development of an abundance of ligands for MATs, including compounds that exhibit both high affinity and selectivity for each of the three transporters (Figure 9).

The first class of ligand developed for use as MAT antagonists was the tricyclic antidepressants (TCA)(Marshall et al. 1960), including imipramine (Trofanil) and desipramine (Norpramin), however TCAs demonstrate activity across a variety of different receptors along with MATs (Gillman 2007). A further, more specific set of antagonists have since been developed that exhibit far more selectivity for target protein(s) (Tatsumi et al. 1997). These new
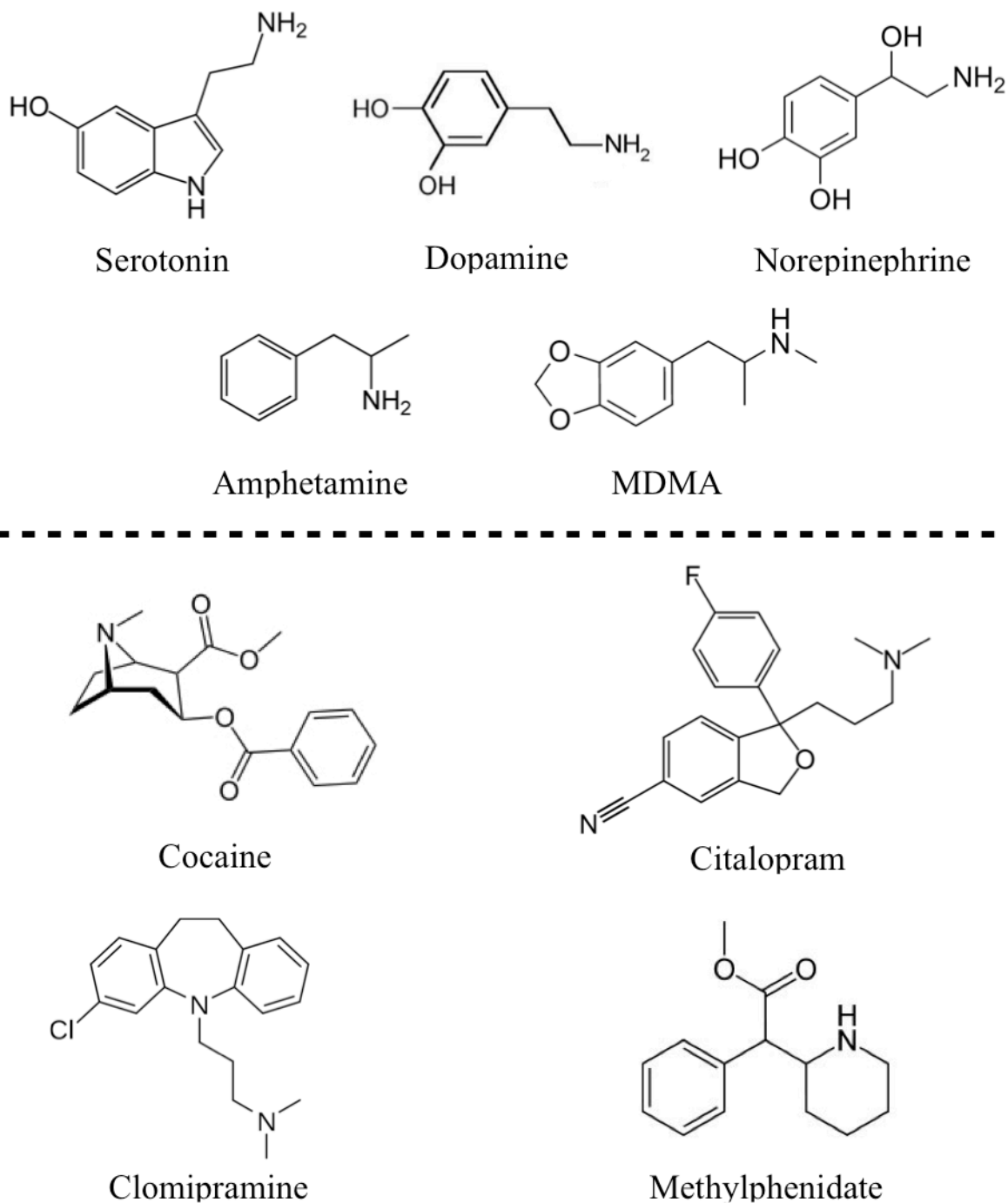
Figure 9. - Chemical structures of classic MAT substrates and inhibitors. Depicted are the chemical structures and names of classic MAT agonists (*top*) and antagonists (*bottom*).

classes are termed selective serotonin reuptake inhibitors (SSRIs), such as fluoxetine (Prozac), citalopram (Celexa) and paroxetine (paxil), norepinephrine reuptake inhibitors, such as reboxetine (Vestra), and selective dopamine reuptake inhibitors, such as bupropion (Wellbutrin). Two classes of dual-acting antagonists with affinity for two of the three MATs have also been developed, including serotonin-norepinephrine reuptake inhibitors, such as duloxetine (Cymbalta), and norepinepherine-dopamine reuptake inhibitors, such as nomifensine (Merital). Many of these drugs have various authorized clinical usages, however knowledge of the structural features of the binding sites for many of these ligands or overall mechanism by which these drugs modulate neurotransmission remains undetermined. Research into defining the binding site(s) of the SSRI citalopram is discussed in chapter VI.

Along with therapeutic compounds, there are also a host of illicit substances, both natural and synthetic, that target MATs (Figure 9) (Rothman and Baumann 2003; Baumann et al. 2014). For instance, cocaine, one of the most abused drugs of addiction, is a potent inhibitor of DAT, NET and SERT. As DAT has been suggested to be the source of the rewarding properties of cocaine (Giros et al. 1996; Chen et al. 2006), the DAT-cocaine interaction has been of particular interest for researchers. Recently, a photo-tagged, radiolabeled cocaine analogue called RTI-82 was used to biochemically determine a specific ligand attachment point when binding to DAT. This allowed for an increase in the constraints used for the development of computational docking studies and resulted in an eloquent prediction of the relative positioning of cocaine bound to DAT (Dahal et al. 2014). Furthermore, a recent crystal structure of a cocaine-bound dDAT revealed a highly similar molecular arrangement (Wang et al. 2015) to that predicted by the work of Dahal *et al*. This exemplifies the power of the combination of biochemical and

computational approaches to determining structural features of the interactions between MATs and their respective ligands. This is critical, as much of my work utilizes this comprehensive approach to obtain structural insights as to the importance of specific binding domains or critical coordinating residues.

Despite cocaine being the most studied MAT ligand and many of the therapeutic compounds having a similar antagonistic effect of MATs, not all drugs act as functional antagonists of MAT transport. In fact, multiple synthetic substrates are available for all three of the MATs (Rothman and Baumann 2003; Baumann et al. 2014). The best examples of these synthetic substrates are amphetamine and a number of amphetamine-like derivatives. This includes one of the most problematic drugs of abuse in today's society, methamphetamine, as well as methylphenidate, which is used to treat attention deficit hyperactivity disorder, and 3,4-methylenedioxymethamphetamine (MDMA or ecstasy), which is an increasingly popular club drug. Moreover, a new class of banned substances known as bath salts target MATs, with some acting as antagonists and other being functional substrates to MATs (Baumann et al. 2014). Critically, each of these synthetic substrates are thought to not only compete with primary neurotransmitters for reuptake by MATs, but they are also thought to induce reverse transport, or efflux, of neurotransmitter back into the synapse, thereby causing an even more pronounced increase in synaptic neurotransmitter levels. How ligands are recognized as substrates and the mechanism by which substrate-induced efflux occurs both remain poorly understood. Research into the importance of an acidic amino acid at the external gate of SERT and the role it plays in substrate recognition and the transport/efflux mechanisms of MDMA is the topic of chapter V.

CHAPTER II

A CONSERVED ASPARAGINE RESIDUE IN TRANSMEMBRANE SEGMENT ONE OF THE SEROTONIN TRANSPORTER DICTATES CHLORIDE-COUPLED NEUROTRANSMITTER TRANSPORT

Introduction

The human (h)SERT, like other neurotransmitter transporters of the SLC1 and SLC6 families, displays secondary-active substrate transport (Mitchell 1961), coupling the concentrative movement of neurotransmitter to the transmembrane gradients of Na^+ and other ions (Humphreys et al. 1994; Rudnick 2002). A distinguishing feature of neurotransmitter transport by the SLC6 family relative to the SLC1 family is a strong dependence on extracellular Cl^- for transport (Lingjærde 1971; Nelson and Blaustein 1982). During a single cycle of substrate transport in hSERT, a stoichiometry of $1\text{-}5\text{-}HT^+in\text{:}1\text{-}Na^+in\text{:}1\text{-}Cl^-in\text{:}1\text{-}K^+out$ has been advanced on the basis of ion dependence studies in cells and resealed membrane vesicles that predicts an overall electroneutral coupling mechanism. Such studies have led to the belief that the energy stored in the Cl^- concentration gradient contributes directly to transmembrane 5-HT flux (Rudnick 2002; Quick 2003). However, electrophysiological experiments reveal that SERT can exhibit nonstoichiometric flux states where additional 5-HT-induced charge movements occur (Lin et al. 1996; Adams and DeFelice 2002; Ramsey 2002; Quick 2003). For the dopamine transporter, a homologue of hSERT, Cl^- has been implicated as a charge carrier in nonstoichiometric flux states (Ingram et al. 2002; Carvelli et al. 2004), suggesting that the role of Cl^- in neurotransmitter transport is more complex than originally suspected. Interacting proteins,

including syntaxin 1A, can modulate the stoichiometry of charge movements across hSERT and other monoamine transporters (Ingram et al. 2002; Quick 2003; Binda et al. 2008; Carvelli et al. 2008), changes that can alter neuronal firing rates (Ingram et al. 2002; Carvelli et al. 2008). In addition, SERTs are expressed early in the embryo (Hoffman and Mezey 1989; Schroeter and Blakely 1996), and in many distinct membrane environments (*e.g.* neurons, placenta, lymphoblasts, platelets, and epithelial cells), where Cl^- gradients can change over time (Jang et al. 2001; Adragna et al. 2004). Together these findings indicate that the contribution of Cl^- to neurotransmitter transport deserves further investigation.

High-resolution structures of a Cl^--independent SLC6 family member, the leucine transporter from *Aquifex aeolicus* (LeuT) (Yamashita et al. 2005), have afforded opportunities to elucidate details of neurotransmitter transporter ionic coupling. Although overall sequence identity between LeuT and neurotransmitter transporters is low, amino acid identity approaches 50% for residues surrounding the binding sites for leucine and Na^+, propelling homology-guided structural studies. In addition, crystal structures of the transporters ApcT (Shaffer et al. 2009), BetP (Ressl et al. 2009), vSGLT (Faham et al. 2008), and Mhp1 (Weyand et al. 2008) that have no significant sequence homology to SLC6 family members exhibit the same helical packing pattern as LeuT (Abramson and Wright 2009). Therefore, a model-guided study of SLC6 family members may identify important mechanisms that are likely difficult to derive from patterns of sequence conservation.

In a prior study (Henry 2003), we demonstrated that an asparagine (N101) in hSERT transmembrane segment (TM) 1 tolerates substitution by cysteine and that cells transfected with N101C are sensitive to transport inactivation by positively charged cysteine-directed MTS

reagents. Because this inactivation was largely eliminated by the presence of 5-HT, we proposed that N101 might lie at or near the substrate-binding site.

The following work demonstrates that the N101 residue, homologous to the sodium-coordinating residue N27 in LeuT, contributes an important role in facilitating the coupling of Cl^- to 5-HT transport. Rather than directly coordinating Cl^- binding, our evidence indicates that N101 translates Cl^- binding to the stabilization of a TM1–TM6 interhelical network, with the participation of TM6 residue S336, to promote efficient coupling between 5-HT and Na^+.

Methodology

Site-directed Mutagenesis and Construction of Mutant Plasmids

Mutation of hSERT cDNA in pcDNA3.1 or pOTV to generate N101A, N101C, and S336C constructs in hSERT and hSERT C109A backgrounds was performed using the Stratagene QuikChange kit, as described previously (Henry 2003), with confirmation of all mutants by DNA sequencing (Center for Molecular Neuroscience Neurogenomics, Vanderbilt DNA Sequencing Core Facility or Northwoods DNA, Inc., Bemidji, MN). For cysteine modification studies to probe for N101-sensitive conformational movements, rSERT N101 mutants were generated in the background of Cys substitutions S277C and S404C using a Cys reduced transporter (X5C; C15A/C21A/C109A/C357I/C622A).

5-HT and NE Transport Measurements

HeLa and HEK-293 cells, maintained at 37 °C in a 5% CO_2-humidified incubator, were grown in complete medium (DMEM, 10% FBS, 2 mM L-glutamine, 100 units/ml penicillin, and 100 µg/ml streptomycin). For initial evaluation of mutant transporter activity, cells were plated at

a density of 50,000 cells/cm^2 in 96- or 24-well culture plates. Cells were transfected with hSERT, rSERT, or hNE transporter constructs with TransIT transfection reagent (Mirus Inc., 6μl/μg of DNA), also in OptiMEM medium as described previously (Henry 2003), or with Lipofectin followed by infection with vTF7-3 vaccinia virus as described (Blakely et al. 1991). Following transfection (20–48 hours), cells were washed with one of the following buffers: MKRHG assay buffer (120mM NaCl, 4.7mM KCl, 2.2mM CaCl$_2$, 1.2mM MgSO$_4$, 1.2mM KH$_2$PO$_4$, 10mM glucose, 10mM HEPES, pH 7.4); chloride-containing assay buffer (5.4mM potassium gluconate, 1.2mM calcium gluconate, 7.5mM HEPES, and either NaCl or NMDG-Cl at 120mM) chloride-free assay buffer (same as chloride-containing buffer except 120mM NaCl is replaced with 120mM NaX (X= Br, I, NO$_2$, NO$_3$, thiocyanate, acetate, methanesulfonate, or gluconate) and assayed for [^{3}H]5-HT (5-hydroxy[^{3}H]tryptamine-trifluoroacetate, (121 Ci/mmol) Amersham Biosciences) transport as described previously (Henry 2003). For Na$^+$ replacements assays, NMDG-Cl was used in place of NaCl. Transport was linear with time under these conditions for up to 15 minutes. Saturation kinetic profiles for derivation of 5-HT K_m and V_{max} values were established in 24-well plates as described above except 2-fold serial dilutions were used maintaining 5-HT-specific activity, starting at 5μM of a mixture of labeled and unlabeled 5-HT. Transport assays were terminated by washes with ice-cold assay buffer, and cells were then dissolved in MicroScint 20 (Packard) scintillant. Uptake from parental cells was subtracted from transporter-transfected cells to determine specific uptake. Nontransfected cells exhibited comparable uptake to assays performed in the presence of 1μM paroxetine, 1μM RTI-55, or 100nM cocaine. K_m and V_{max} values were derived using a nonlinear curve fit as a function of 5-HT or NE concentration (40nM to 5μM) (Prism 4,

Graphpad). All experiments were performed in triplicate and repeated in three or more separate assays.

Spontaneous 5-HT Efflux

Cells were loaded as described above for transport studies with 40nM [^{3}H]5-HT. Loading was allowed to proceed for 30 or 90 minutes at 37 °C and was terminated by aspiration of assay buffer and a single wash with 0.5ml of ice-cold MKRHG buffer. MKRHG buffer (0.5ml) was added to one-half of the wells and returned to 37 °C for 30 minutes. The wells that did not receive buffer represent the total 5-HT taken up at $T = 0$. Buffer from the efflux wells (representing 5-HT efflux) was collected, transferred to scintillation vials with 5ml of EcoScint H, and counted. 5-HT remaining in the cells at $T = 30$ or 90 minutes was assessed by scintillation photometry. Percent efflux was calculated as the ratio ($\times 100$) of 5-HT efflux divided by 5-HT accumulated in parallel plates, not subjected to efflux, at $T = 0$. No difference was observed in % efflux for plates pre-loaded for 30 or 90 minutes (data not shown).

Total and Cell Surface Expression Protein Analysis

To determine total and surface expression of hSERT with wild type and/or mutant constructs, HeLa cells were plated in 24 or 12 well dishes at 100,000 or 500,000 cells per well, respectively, and transfected 18–24 hours later as detailed above. Seventy two hours after transfection, cell surface proteins were biotinylated and analyzed via Western blotting as described previously (Henry 2003). Oocyte biotinylation experiments to quantitate surface expression of hSERT and hSERT mutants were performed as described previously (Ramsey 2002) using 1.5 ng of cRNA and substituting EZ-Link Sulfo-NHS-biotin (Pierce) with EZ-Link Sulfo-NHS-SS-Biotin. Blots of total and surface protein were probed with ST-01 from Mab

Technologies., Inc. (Stone Mountain, GA), and developed using Western Lightening Chemiluminescent Plus reagent (PerkinElmer Life Sciences).

Evaluation of Cysteine Accessibility

To probe for ion-dependent hSERT conformational movements, HeLa cells were plated on poly-D-lysine-coated 24-well TopCount plates at a density of 50,000 cells/well and transfected as described above. Twenty four hours post-transfection, cells were washed one time with 2 ml, one time with 1 ml, and one time with 500μl of MKRH (MKRHG without glucose) ± 120mM Cl^- and ± 50μM 5-HT. Following a 5-minute incubation, solutions were aspirated and replaced with 500μl of 2mM MTSET in MKRH. MKRH alone was added to one set of wells as a control. MTSET-treated wells were washed twice with 750μl of MKRH followed by aspiration and addition of 225μl of MKRHG. Cells were allowed to equilibrate to 37°C for 10 minutes followed by addition of $[^3H]$5-HT containing ascorbic acid and iproniazid phosphate. After 10 minutes at 37°C, wells were washed three times with 500μl of ice-cold MKRH. MicroScint 20 (0.5ml) was added to each well, and the accumulated 5-HT was quantified.

rSERT N101A/S404C accessibility was examined using MTSEA. HeLa cells were plated in 96-well plates at a density of 50,000 cells/well transfected and infected with vTF7-3 as described above. Twenty hours post-transfection, cells were washed three times with phosphate-buffered saline with magnesium and calcium (PBS: 137mM NaCl or equimolar concentration of NMDG-Cl or sodium isethionate, 2.7mM KCl, 4.3mM Na_2HPO_4, and 1.4mM KH_2PO_4, pH 7.3) containing 0.1mM $CaCl_2$ and 1mM $MgCl_2$ (PBSCM). Following a 5-minute incubation, solutions were aspirated and replaced with 50μl of MTSEA in the indicated concentrations in 50μl of PBSCM. After 10 minutes, the cells were washed five times with 100μl of PBSCM

followed by incubation with 20nM [^{3}H]5-HT for 10 minutes in 50μl of PBSCM. After 10 minutes, wells were washed three times with 100μl of PBSCM. Optifluor (PerkinElmer Life Sciences) (150μl) was added to each well, and accumulated 5-HT was measured in a Wallac MicroBeta plate counter. Cells transfected with S404C was used as the control.

hSERT Expression in *Xenopus laevis* Oocytes

Oocytes were isolated, and cRNA was prepared as described previously (Ramsey 2002; Adams and DeFelice 2003). cRNA was injected on the day of oocyte harvest. hSERT, N101A, N101C, S336C, N101A/S336C, and N101C/S336C cRNA were transcribed from NotI-linearized constructs in pOTV vector (a gift of Dr. Mark Sonders, Columbia University) using Ambion mMessage Machine T7 kit (Ambion, Austin, TX). Each oocyte was injected with 1.5ng of cRNA and incubated at 18°C for 4–6 days in Ringer's buffer (100mM NaCl, 2mM KCl, 5mM MgCl$_2$, 5mM HEPES, pH 7.4) supplemented with 550μM/ml sodium pyruvate, 100μg/ml streptomycin, 50μg/ml tetracycline, and 5% dialyzed horse serum. Whole-cell currents were measured by two-electrode voltage clamp techniques using a GeneClamp 500 (Molecular Devices, Palo Alto, CA). Microelectrodes were pulled using a programmable puller (Model P-87, Sutter Instrument, Novato, CA) and filled with 3M KCl (0.5–3-megohm resistance). A 16-bit A/D converter (Digidata 1322A, Molecular Devices) interfaced to a PC computer running Clampex 9 software (Molecular Devices) was used to control membrane voltage and to acquire data. To induce hSERT-associated current, oocytes were perfused with 5-HT (typically 5μM) in buffer (120mM NaCl, 5.4mM potassium-gluconate, 1.2mM calcium-gluconate, 7.2mM HEPES, 0.1mM iproniazid, pH 7.4) using a gravity flow system (4–5ml/minute). Buffer pH was adjusted with KOH or KHPO$_4$. The 5-HT-induced current was defined as current in the presence of 5-HT

minus current in the absence of 5-HT. Substitution of Cl⁻ was performed as with the tissue culture studies above and is indicated in the text and figures. To minimize liquid junction potentials, Cl⁻ substitution experiments were performed using a 1M KCl, 2% agar salt bridge to isolate the Ag-AgCl electrode from the bath. For constant voltage recordings, data were low pass filtered at 10Hz and digitized at 20Hz. For current-voltage (*I-V*) recordings, the voltage was changed stepwise every 500ms. Currents were low pass filtered at 100Hz and digitized at 200Hz. All analyses were performed using Origin 7 (OriginLab, Northampton, MA) and GraphPad Prism (GraphPad software, San Diego).

Simultaneous Measurement of 5-HT Uptake and 5-HT-induced Currents

Simultaneous measurement of 5-HT uptake and 5-HT-induced current was performed under voltage clamp conditions, using techniques described previously (Petersen and DeFelice 1999). Oocytes were perfused for 150s under voltage clamp with 1μM [³H]5-HT (specific activity = 3.12Ci/mmol). To minimize loss of 5-HT, oocytes were perfused with ice-cold buffer for 250s prior to removal from the chamber. The total charge movement was calculated by time integration of 5-HT-induced inward currents and related to the amount of 5-HT taken up in the same oocyte. Nonspecific 5-HT uptake was determined using water-injected control oocytes analyzed under the same conditions. Oocytes were solubilized with 200μl of 0.1% SDS and 10ml of EcoScint H (National Diagnostics, Atlanta, GA), and 5-HT accumulation was quantified by liquid scintillation photometry (Packard Instrument Co.).

hSERT Molecular Modeling

Molecular models for hSERT were generated using the template structure of LeuT (PDB_ID 2A65) as detailed elsewhere (Kaufmann et al. 2009). The binding mode for 5-HT

identified as the one most consistent with available experimental data by Kaufmann *et al.* (Kaufmann et al. 2009) was taken as the starting point for model refinement using the AMBER forcefield. Briefly, ions were added to the energy-minimized model of 5-HT in complex with hSERT to generate refined models that either contained NaCl or omitted Cl^- (Na^+ only). Two Na^+ ions were added to both the Na^+ (without Cl^-) and NaCl models by superimposing the hSERT model reported by Kaufmann *et al.* (Kaufmann et al. 2009) with the x-ray structure of LeuT and utilizing the coordinates of atom NA 752 (Na1-binding site) and NA 751 (Na2-binding site). For the NaCl model, a single Cl^- ion was centered on the region of the hSERT model occupied by the side-chain carboxyl group of residue E290 in LeuT, as recently validated in studies of SERT and GAT (Forrest et al. 2007; Zomot et al. 2007). Models of the hSERT ion-binding sites were then refined with 50 steps of "steepest descents" and 450 steps of gradient-based minimization in AMBER9 (Kaufmann et al. 2009) followed by brief (1ns) low temperature (50K) molecular dynamics simulations *in vacuo*, using a distance-dependent dielectric constant and 12Å cutoff for non-bonded interactions to energetically relax the system. The resulting structures were then subjected to an additional round of energy minimization as described above to generate the reported models. Partial charges for 5-HT were ascribed using the atom-centered point charge method of Bayly and Kollman (Bayly and Kollman 1994). All other molecular mechanics parameters for 5-HT and ions were taken from the standard AMBER force field with the exception of acetate. Acetate parameters were derived by analogy to the ionized form of the carboxylic acid side chain of aspartate from the standard AMBER9 database truncated at the CB atom with total partial charge equal to −1.0). Two-dimensional schematics of

the refined hSERT ion-binding sites were generated with ChemDraw 10.0 (Cambridge Soft), and three-dimensional representations were rendered with PyMol (Schrödinger, LLC).

Molecular Dynamics and Free Energy Perturbation (FEP) Simulations

Molecular models of a protonated 5-HT were developed where the geometry parameters (bond lengths and angles) were obtained by quantum mechanics minimization at the B3LYP/6–31G* level of theory using the restrained electrostatic potential fitting approach described by Anisimov *et al.* (Anisimov et al. 2005). The net charge of 5-HT molecule was set to +1 with the side-chain nitrogen protonated based on the reported pK_a values. Parameters for deprotonated cysteine (thiolate ion) for pK_a computations have been validated and published before by Foloppe and Nillson (Foloppe and Nilsson 2007). For equilibrium MD simulations, the starting configuration for SERT complexed with the 5-HT, two sodiums, and one chloride ion was taken from the minimized molecular model described above. The S352C, S336C, and N101A mutants were obtained with a side-chain rotamer library search using SCWRL3.0 software (Canutescu et al. 2003). The complexes were next embedded into a lipid membrane using a multiple step membrane building procedure used in previous studies (Jo et al. 2009). The simulation box contains the 5-HT transporter, bound sodium ions with (or without) chloride/acetate ions, one serotonin substrate, and 204 1-palmitoyl-2-oleoylphosphatidylcholine lipid molecules solvated in an explicit 150mM NaCl aqueous solution. All computations were carried out by NAMD version 2.7b1 (Phillips et al. 2005), and analysis was done with CHARMM version c36b2 with the CHARMM27 force fields for proteins and lipids (Brooks et al. 2009). MD simulation methods used here are similar to those used in previous studies of membrane systems (Caplan et al. 2008; Noskov 2008). Briefly, constant temperature/constant pressure algorithms were applied (with

41

pressure at 1 atm and temperature at 315K). Electrostatic interactions were treated with the Particle Mesh Ewald algorithm with a 104/104/96-Å grid for fast Fourier transform, $\kappa = 0.34\text{Å}^{-1}$, and a 6th order spline interpolation. The nonbonded interactions were smoothly switched off at 12–14Å. All simulation systems were equilibrated for 5 ns each without any constraints, and the production was run for another 15 ns.

Results

hSERT N101 Mutation Eliminates Cl⁻ Dependence of 5-HT Uptake

To examine a role of hSERT N101 in the Cl⁻ dependence of 5-HT transport, we transfected HeLa cells with hSERT or hSERT N101A and N101C mutants and measured the effect of extracellular Cl⁻ on 5-HT transport saturation kinetics (Figure 10). As described previously (Chang and Lam 1998), removal of external Cl⁻ from the medium of hSERT-transfected cells resulted in a significant (5-fold) decrease in 5-HT transport V_{max} (NaCl, 0.068 ± 0.006 fmol/cell/minute; sodium gluconate, 0.014 ± 0.002) and a significant (3.6-fold) increase in 5-HT K_m (NaCl, $0.9 \pm 0.2\mu$M; sodium gluconate, $3.2 \pm 0.36\mu$M, one-way ANOVA, Dunnett's post hoc, $p < 0.002$). Remarkably, the hSERT N101A and N101C mutants were largely insensitive to Cl⁻ substitution with gluconate (Figure 10, B and C). Moreover, the 5-HT K_m values of N101A and N101C were not influenced by the presence of Cl⁻, unlike hSERT, and were comparable with the 5-HT K_m values obtained for hSERT in the presence of Cl⁻ (N101A$_{+Cl}$ $1.45 \pm 0.4\mu$M, N101A$_{-Cl}$ $1.66 \pm 0.2\mu$M; N101C$_{+Cl}$ $1.20 \pm 0.3\mu$M, N101C$_{-Cl}$ $1.4 \pm 0.2\mu$M; hSERT$_{+Cl}$ $0.87 \pm 0.2\mu$M, hSERT$_{-Cl}$ $3.2 \pm 0.4\mu$M). The rate of 5-HT transport by hSERT was a monotonic function of extracellular Cl⁻ concentration (Hill = 0.8 ± 0.1) with an EC$_{50}$ of

42
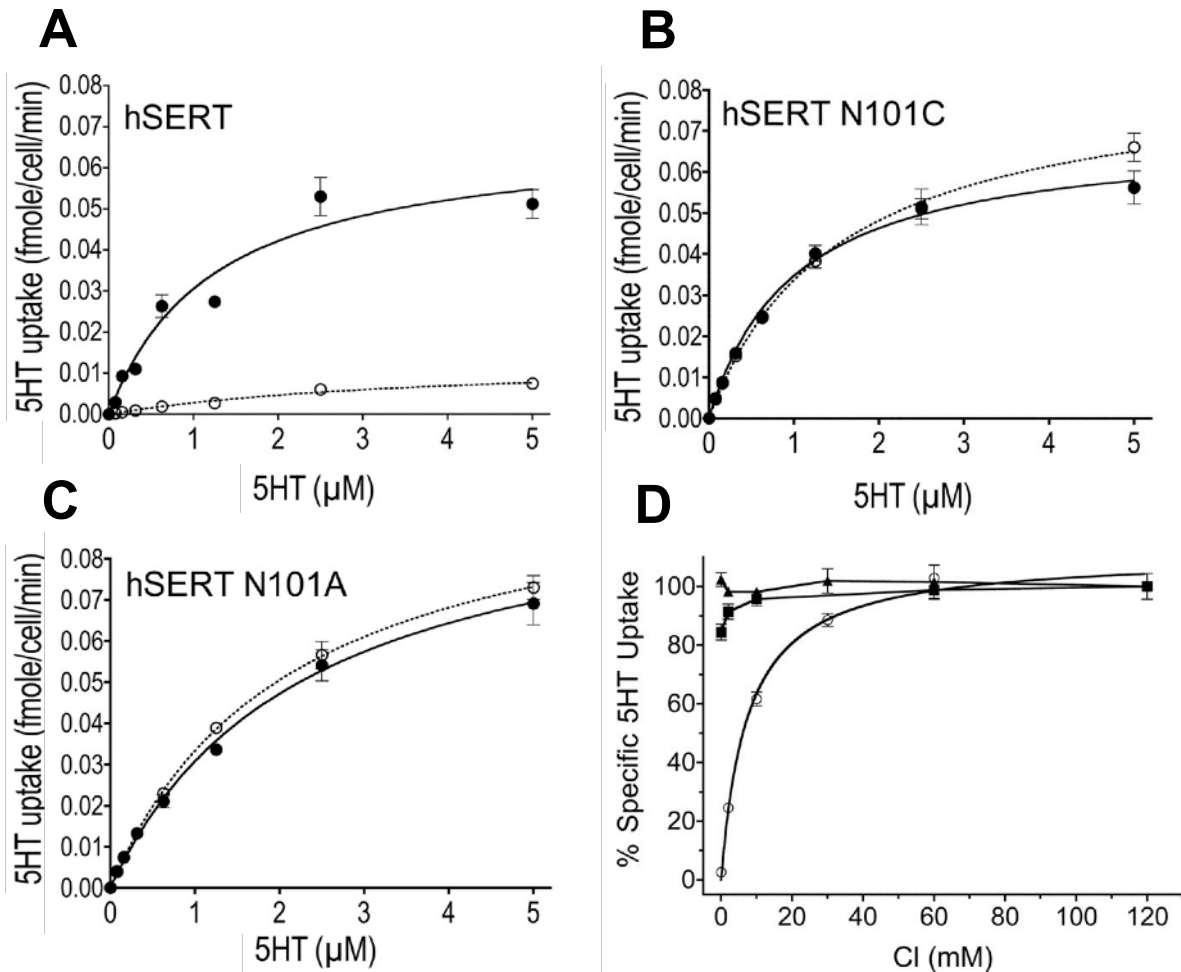
Figure 10. Kinetic analysis and Cl⁻ dependence of 5-HT uptake in hSERT N101 mutants. HeLa cells transiently expressing the hSERT (*A*), hSERT N101A (*B*), or hSERT N101C (*C*) were evaluated for dose-dependent 5-HT uptake after 10 min in the presence (*solid line/filled circles*) or absence (*dashed line/open circles*) of Cl⁻. Dependence of 5-HT uptake on Cl⁻ concentration is lost in N101 mutants (*D*). HeLa cells transiently expressing hSERT (*open circles*), hSERT N101A (*filled boxes*), or hSERT N101C (*filled triangle*) were incubated with increasing concentrations of Cl⁻ and assayed for uptake of [³H]5-HT for 10 min. Remaining anion concentration was accounted for by addition of methanesulfonate. Different amounts of plasmid DNA were used to transfect hSERT, N101A and N101C to account for differences in surface expression.

43

7.5mM (Figure 10D), in line with previous studies of rSERT (Barker et al. 1999). Across the same Cl$^-$ concentration range, the N101C and N101A mutants exhibited virtually no further stimulation of 5-HT transport.

N101 Dictates Cl$^-$-dependent Conformational Changes in TM1 and EL4

N101 could dictate the Cl$^-$ sensitivity of hSERT simply by stabilizing binding of the anion. Alternatively, N101 may be required to translate anion binding into critical conformational changes linked to the Na$^+$-coupled, 5-HT transport process. To examine these issues, we first examined the ability of Cl$^-$ to alter aqueous exposure of three residues proposed to report steps in the transport cycle, C109, S404, and S277 (Figure 11). Each of these positions is distant from the 5-HT- and Cl$^-$-binding sites, so changes in their accessibility are likely to reflect conformational changes because of ligand binding rather than direct binding itself. C109 lies at the extracellular end of TM1 and is the major determinant of wild type SERT sensitivity to MTS reagents (Figure 11) (Chen 1997; Chen et al. 1997). MTS-mediated inactivation of C109 is sensitive to Na$^+$ replacement with Li$^+$ and is also modulated by 5-HT (Chen et al. 1997; Ni 2001), possibly a sign that this residue sits within a conformationally-active domain that is mobilized by ion and neurotransmitter binding. We found that the presence of Cl$^-$ significantly protected C109 against inactivation by the positively charged MTSET (Figure 12A), independent of the presence of 5-HT. In contrast, hSERT N101A was not protected against MTSET inactivation by Cl$^-$, consistent with the lack of Cl$^-$ dependence measured for N101A in 5-HT transport assays (Figure 10). As C109 was the target for inactivation by MTSET in hSERT N101A, as opposed to another endogenous cysteine, we found that the C109A/N101A double mutant was insensitive to MTSET (data not shown). Strikingly, whereas 5-HT had little or no
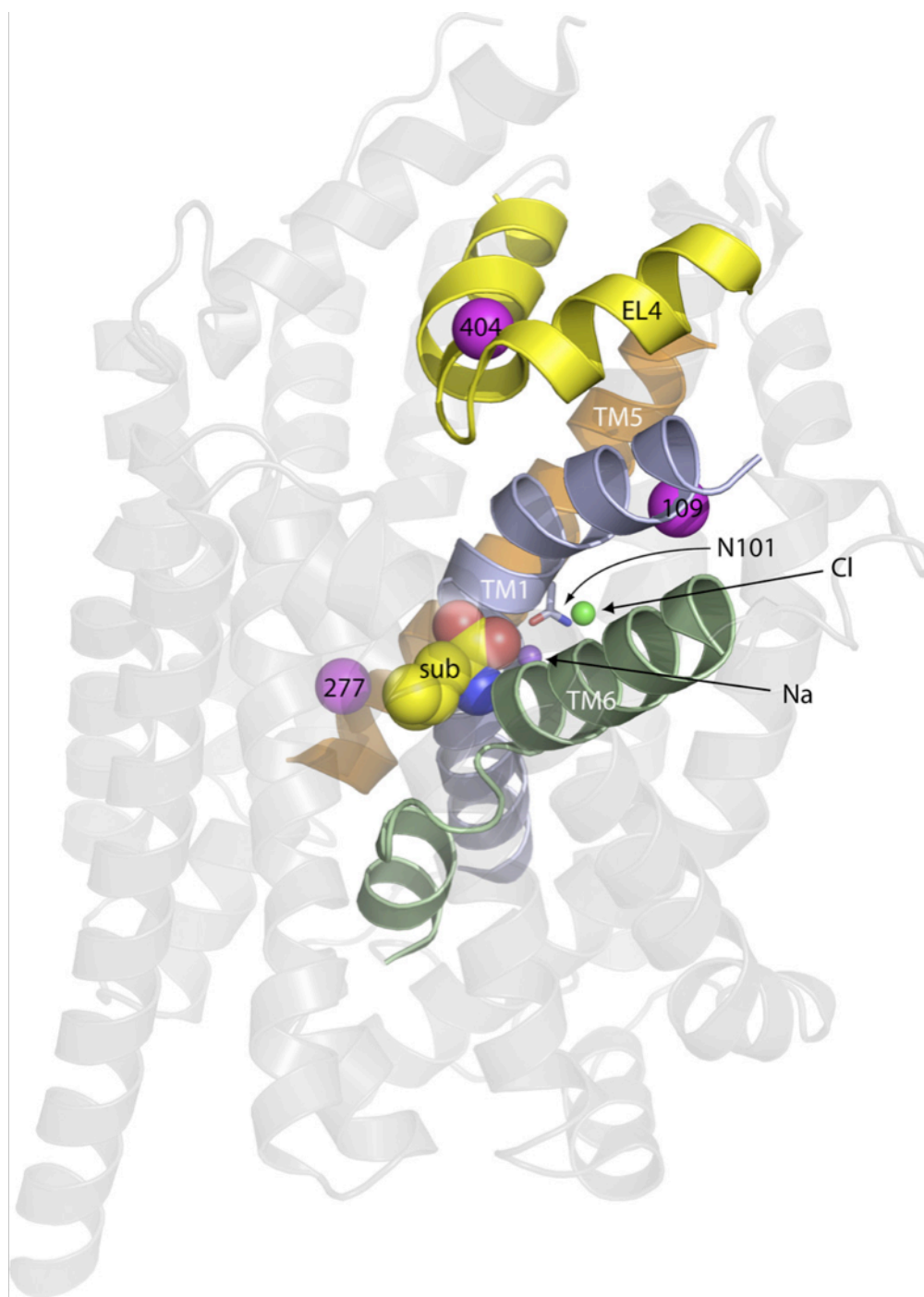
Figure 11. Mapping of MTSET probes and Cl⁻-binding site from hSERT onto the LeuT crystal structure. Illustration shows hSERT features discussed in this study as follows: 1) MTSET targeted cysteine mutants (*magenta spheres* numbered with the corresponding hSERT residue and their respective domains (TM1, *blue*; TM5, *orange*; EL4, *yellow,* and TM6, *green*); 2) space filling model of substrate in the binding site (sub); 3) ions Na⁺ and Cl⁻ (*purple* and *green spheres*, respectively); and 4) *stick* representation of the N101 side chain.
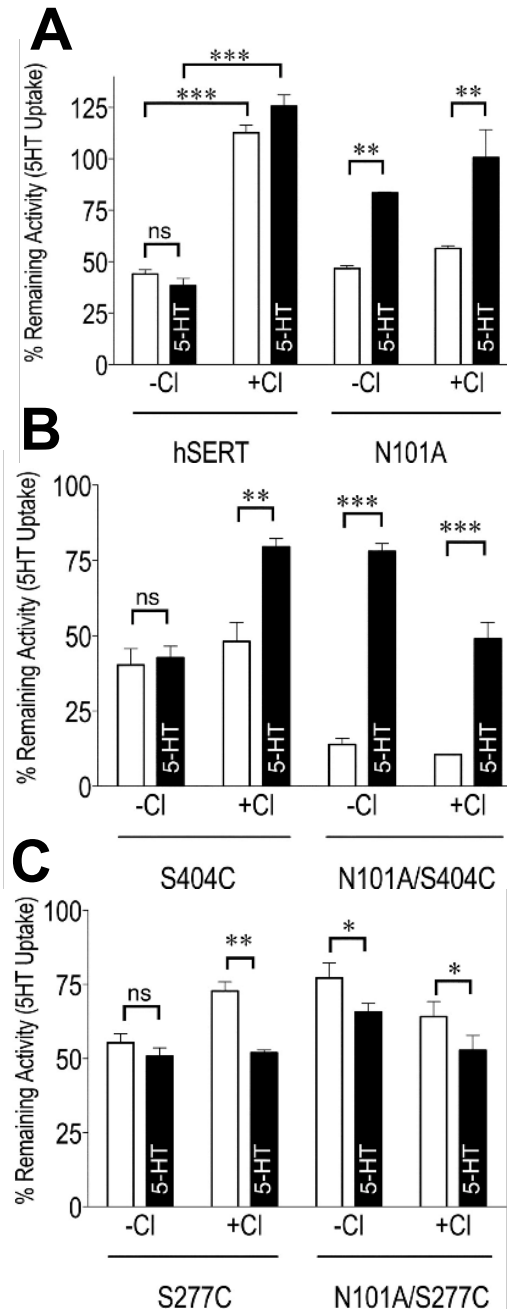
Figure 12. Assessment of MTSET accessibility of targeted cysteines as a prediction of conformation change. Tissue culture cells expressing hSERT or hSERT N101A (*A*), rSERT S404C or rSERT N101A/S404C (*B*), and rSERT S277C or rSERT N101A/S277C (*C*) were pretreated with MTSET in the absence (*open bars*) or presence (*black bars*) of 5-HT (50μM) and in the absence or presence of Cl⁻ as indicated. Following treatment, 5-HT uptake assays were performed in normal uptake buffer to quantitate activity. Percent remaining activity is plotted and is defined as the amount of 5-HT uptake of MTSET- (*A*) or MTSEA- *(B & C)* treated cells as a percent of untreated cells. A two-tailed *t* test was performed on sample sets as indicated with brackets; * = $p \leq 0.05$; ** = $p \leq 0.01$; *** = $p \leq 0.001$. *n.s.,* not significant.

ability to protect wild type hSERT against MTSET inactivation in Cl$^-$-free conditions, 5-HT

provided significant protection to hSERT N101A (Figure 12A) in the absence or presence of the

anion. These data suggest that N101 is required to transduce Cl$^-$ binding to allow 5-HT-

dependent conformational changes that involve TM1 and associated elements, as reported by

C109 modification. In the N101 mutants, 5-HT induced a similar conformational change, but this

effect did not require the presence of Cl$^-$. S404, located in the middle of EL4 (Figure 11), has

been proposed to report reorientation of another external component of the 5-HT permeation

pathway (Mitchell et al. 2004). Unlike C109 in hSERT, however, Cl$^-$ substitution in the absence

of 5-HT does not afford protection of S404C (in a C109A background) to the membrane-

permeant MTSEA (Figure 12B), although Cl$^-$ and 5-HT together do induce protection. We found

that, just as with C109, the aqueous accessibility of S404C in an N101A background is sensitive

to 5-HT in either Cl$^-$-containing or Cl$^-$-free medium. These studies confirm previous data

(Mitchell et al. 2004) that transport-linked conformational changes in EL4 are associated with

the loading of all three substrates and demonstrate that mutation of N101 allows just 5-HT and

Na$^+$ to trigger conformational changes in EL4. C109 and S404 are external reporters of

conformational changes arising with substrate binding. In contrast, S277 in TM5 (Figure 11) is

positioned to contribute to the cytoplasmic permeation pathway for 5-HT. Indeed, increased

S277 accessibility is believed to report an "open-to-in" conformation of the transporter (Zhang

and Rudnick 2006; Forrest et al. 2008). Na$^+$ and Cl$^-$ are required for the 5-HT-dependent

exposure of residues in the cytoplasmic permeation pathway of SERT (Zhang and Rudnick 2006;

Forrest et al. 2008). Figure 12C demonstrates that 5-HT increases the extent of MTSEA

inactivation in rSERT S277C only when Cl$^-$ is present. In the N101A/S277C double mutant,

however, 5-HT alone increased the extent of MTSEA inactivation demonstrating Cl$^-$ independence. As the sensitization of S277C afforded by 5-HT in the N101A background still required the presence of Na$^+$ (data not shown), the cytoplasmic pathway appears to still be coupled to Na$^+$ with N101 substitution, reinforcing a specificity for disruption of Cl$^-$ coupling in N101 mutants.

hSERT N101 Dictates Ion Selectivity of 5-HT-independent Charge Flux

hSERT expressed in *X. laevis* oocytes (Cao et al. 1998) and mammalian cells (Hilber et al. 2005) conducts both 5-HT-independent and -dependent currents, in addition to transporting 5-HT. Both 5-HT-independent ("leak current") and -dependent currents require extracellular Na$^+$ and Cl$^-$ (Corey et al. 1994; 1998), although it is unknown whether the 5-HT-dependent and -independent currents share a common pathway and/or molecular contacts as they permeate SERT. To assess whether mutation of N101 removes the Cl$^-$ dependence of SERT currents or affects stoichiometric charge movements, or both, we monitored hSERT-mediated currents in oocytes recorded under two-electrode voltage clamp. Prior to measuring currents, we determined the abundance of wild type and N101 mutant hSERT expressed on the oocyte surface by biotinylation. Consistent with prior measurements of hSERT N101C surface expression in HeLa cells (Henry 2003), whole-oocyte biotinylation studies revealed reduced cell surface expression of N101 mutants (N101A and N101C, 61 ± 5.7 and 32 ± 8.7% of hSERT, respectively; Figure 13D), although SERT-dependent transport and currents were readily detectable. In the oocyte biotinylation studies, a band was observed in the total (uninjected) control lane similar in size to mature hSERT. However, the band appears to be nonspecific as the same control lane lacks the immature and oligomeric hSERT bands observed in the hSERT-expressing oocytes, and this

band is not observed in the surface control lane. As shown in Figure 13A, 5-HT induced larger currents in N101 mutants compared with wild type hSERT despite reduced surface expression. These currents were absent from mock-injected oocytes and were blocked by co-application of SERT antagonists (data not shown). Additionally, as first described by Mager *et al.* (Mager et al. 1994), antagonist (RTI-55) treatment of hSERT-expressing oocytes revealed a 5-HT-independent current that appears as an outward current at −60mV (Figure 13A) and that reverses at approximately +30mV (Figure 13B). The apparent outward current is interpreted as RTI-55 block of inward leak current. In contrast to 5-HT transport (Mager et al. 1994), the hSERT leak current was insensitive to extracellular Cl^-, except at high positive potentials where a slight reduction in maximal outward current was evident (Figure 13B). These data indicate that Cl^- flux does not constitute a significant fraction of the 5-HT-independent current, consistent with the reversal potential of +30mV. Like hSERT, the N101A mutant was insensitive to external Cl^-. However, in this mutant, the reversal potential for these currents (using RTI-55 to define the leak) shifted from approximately +30 to approximately +70mV (Figure 13C). The movement of ions during these experiments is insufficient to alter the internal ionic concentration of the oocyte, even less so in the presence of endogenous ion pumps. Thus, the shift in reversal potential we observe toward E_{Na} is most likely an inherent effect of the mutant on the ion selectivity of 5-HT independent currents. In support of this hypothesis, replacing all Na^+ with NMDG in normal Cl^- buffer shifts the hSERT reversal negative by 40.1 ± 3.8mV, $p < 0.05$, $n = 7$, whereas N101A shifts by 52.6 ± 3.3mV ($p < 0.05$, $n = 6$). These changes are consistent with a shift toward a greater contribution of Na^+ to 5-HT independent currents in the N101A mutant than in hSERT.
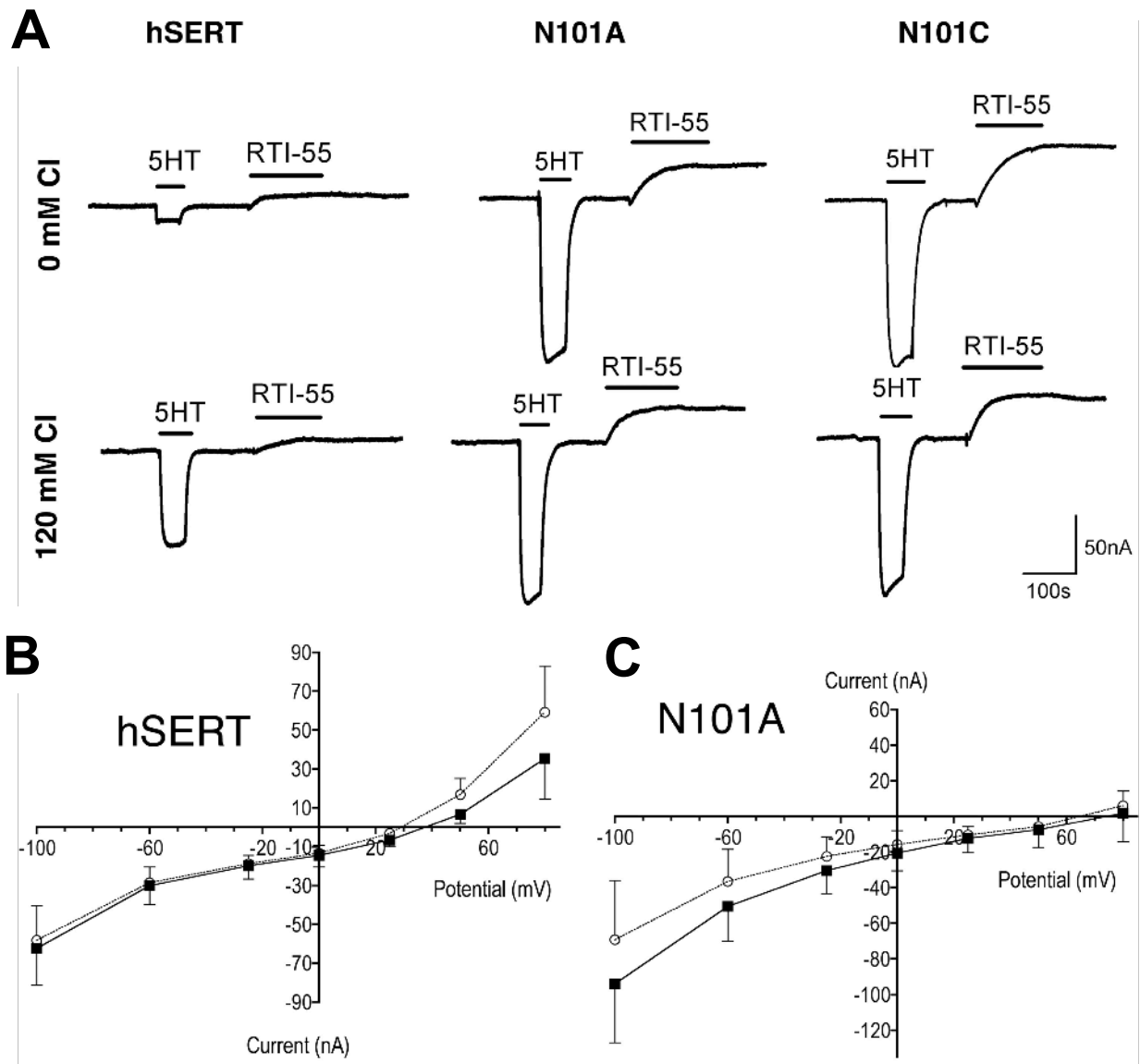
Figure 13. Current-voltage relationship analysis of the hSERT leak conductance of N101A mutant. (*A*) Current traces of 5 HT-induced (5µM 5-HT) and leak current (revealed by application of the SERT antagonist RTI-55 (5 µM)) from oocytes expressing hSERT mutants. Oocytes were injected with equimolar amounts of cRNA. Steady-state *I/V* analyses of leak currents for hSERT (*B*) and N101A (*C*) recorded in Ringer's buffer containing either 120mM NaCl (*open circles*) or 120mM sodium methanesulfonate (*filled boxes*). Values plotted represent the difference between conductances in buffer alone *versus* addition of 5µM RTI-55. Because of the low levels of leak current observed in the hSERT-expressing oocytes compared with the N101 mutants, only hSERT-expressing oocytes showing relatively higher leak currents were used to have sufficient signal for the *I/V* analysis.

50
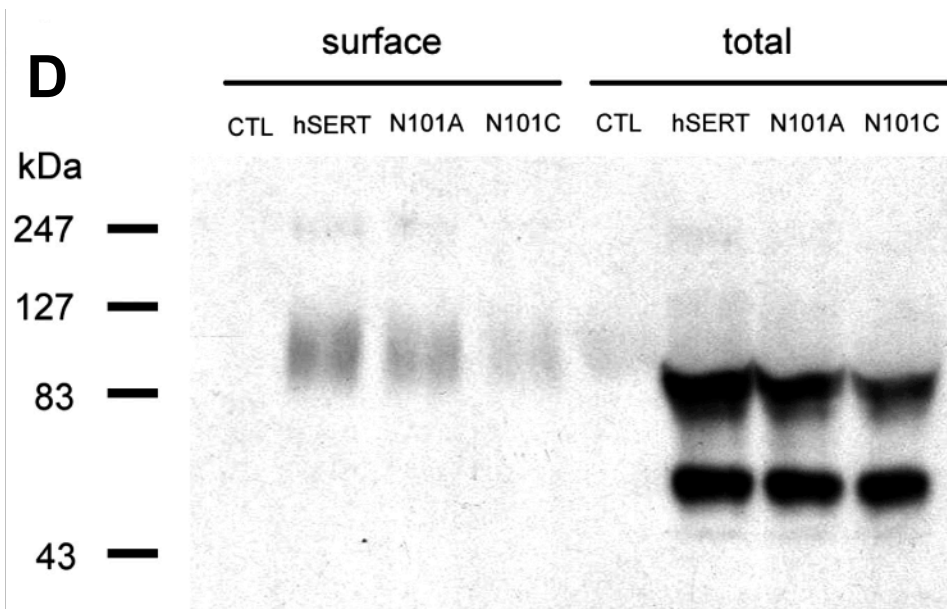
Figure 13 (continued). Current-voltage relationship analysis of the hSERT leak conductance of N101A mutant. (*D*) Western blot analysis of total and surface expression of hSERT detected with hSERT-specific monoclonal antibody ST-51. Equal amounts of protein were loaded in each lane. A band of similar size to mature hSERT was noted in the total (uninjected) control lane. However, the band is nonspecific as the total control lane lacks the immature and oligomeric hSERT bands observed in the hSERT-expressing oocytes, and no bands are observed in the surface control (*CTL*) lane.

N101 Dictates Cl⁻ Dependence of 5-HT-induced Currents

Similar to leak currents, currents elicited by 5-HT were significantly larger in the N101 mutants than in wild type hSERT when normalized for surface expression (Figure 14A). Even more striking was the loss of Cl⁻ dependence for these currents in N101 mutants (Figure 14, A–D). In the hSERT N101C mutant, 5-HT actually induced slightly larger current (I_{max}) at negative potentials in the absence of Cl⁻ and current decreased in response to increasing Cl⁻ concentrations (Figure 14D). These data can be explained if Cl⁻ is still transported through the N101C mutant, offsetting the Na⁺ current. As described previously, 5-HT-induced currents in hSERT and rSERT did not reverse at positive potentials (Cao et al. 1998) because of outward leak currents that begin to dominate at positive potentials (Figure 14B) (Sonders et al. 1997). In contrast, a reversal of 5-HT-induced currents is evident at approximately +75mV for both hSERT N101A and N101C. This finding is consistent with the loss of outward leak currents in the N101 mutants at positive potentials (Figure 14, C and D). Analysis of the Cl⁻ concentration dependence of 5-HT-induced currents (−60mV, 5µM 5-HT) confirms that although 5-HT-activated current in hSERT required Cl⁻ (EC_{50} = 0.5mM), N101 mutants did not require Cl⁻ over the same concentration range (Figure 14E). Unlike the shifted K_m value for 5-HT transport in the absence of Cl⁻ (Figure 10A), the EC_{50} values for 5-HT-elicited currents in hSERT were unaffected by external Cl⁻ (1.6 *versus* 1.8µM, respectively) (Figure 14F). The 5-HT EC_{50} values for N101A and N101C were also Cl⁻-insensitive but were significantly decreased relative to hSERT values (N101A$_{-Cl}$ 0.78 ± 0.14µM, N101A$_{+Cl}$ 0.64 ± 0.11µM; N101C$_{-Cl}$ 0.72 ± 0.13µM, N101C$_{+Cl}$ 0.39 ± 0.05µM, p < 0.05 one-way ANOVA, Dunnett's post hoc test) consistent with the lower K_m value for 5-HT measured in the mutants (Figure 10).
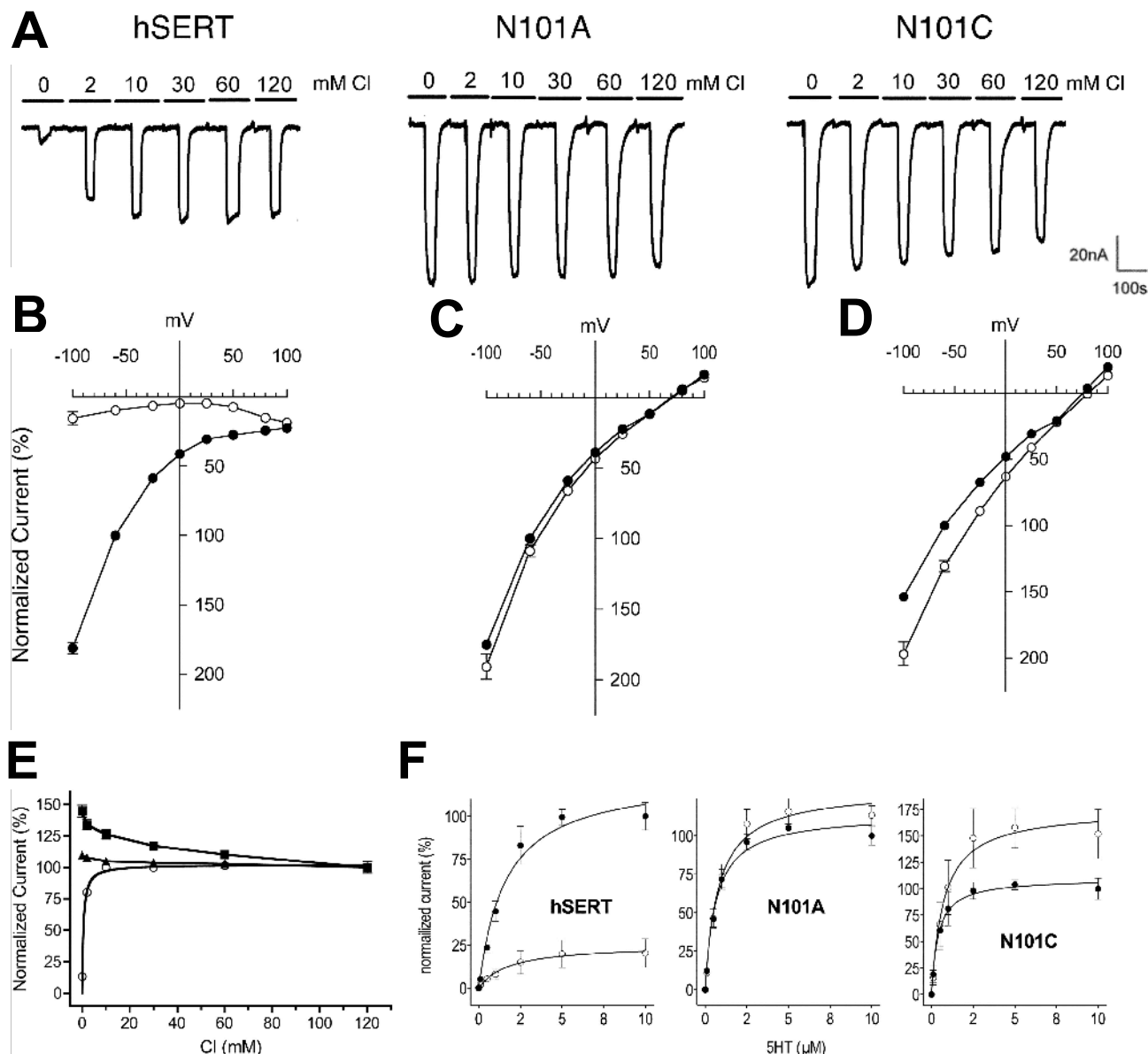
Figure 14. TEVC analysis of N101 mutants. (*A*) Raw traces of Cl⁻ dose-dependent 5-HT-induced currents (5-HT, 5μM). Cl⁻ addition is designated by bars along with concentration used. Anion concentration was adjusted with 120mM with methanesulfonate. Current-voltage relationship for the 5-HT-induced current reveals a reversal equilibrium for N101 mutants. Steady-state currents evoked upon application of 5μM 5-HT in the presence (*filled circles*) or absence (*empty circles*) of Cl⁻ and normalized to % current obtained with 120mM Cl⁻ at –60mV are plotted in relation to membrane potential for hSERT (*B*), N101A (*C*), and N101C (*D*). (*E*) Plot of induced current amplitudes from hSERT (*open circles*), N101A (*filled boxes*), and N101C (*filled triangles*) from (*A*). Currents were normalized to current obtained at 120 mM Cl⁻. Cl⁻ was replaced with 120mM MS. (*F*), plot of induced current as a function of 5-HT concentration in the presence (*filled circles*) or absence (*empty circles*) of Cl⁻ and normalized to percent current at saturation conditions in the presence of Cl⁻.

53

N101 Dictates hSERT Coupling and Stoichiometry

To investigate the larger 5-HT-induced currents exhibited by the N101 mutants, we determined 5-HT flux and total charge movements in hSERT and hSERT N101 mutants in single voltage-clamped (−600mV) oocytes (Ramsey 2002). As shown in Figure 15A, in normal extracellular Cl^- hSERT supported the net inward movement of ~7 positive charges per 5-HT molecule, consistent with previous studies (Mager et al. 1994; Quick 2003). Removal of Cl^- caused a modest but significant increase in the flux ratio (~10 charges/5-HT), arising from a relative retention of 5-HT-gated currents despite a reduction in 5-HT transport. Charge/5-HT flux ratios in the N101 mutants were significantly greater than for hSERT, in the presence or absence of Cl^-, with ~40 charges moved per 5-HT. When normalized for transporter surface expression, this dramatic increase in the charge/5-HT flux ratio resulted from increased charge movement (rather than a reduction in 5-HT transport; data not shown), suggesting a disruption of coupling between transmembrane flux of Na^+ (or other ions) and 5-HT. To test this idea, we returned to mammalian cells where the smaller internal volume facilitates an assessment of equilibrium accumulation of 5-HT. After 2 hours of incubation in 50nM 5-HT, hSERT-transfected HeLa cells established a 281-fold (±14) gradient of 5-HT$_{in}$/5-HT$_{out}$ (Figure 15B). In contrast, the N101 mutants concentrated 5-HT to a significantly lesser extent (N101A, 18-fold (±1); N101C, 31-fold (±1); $p < 0.01$, one-way ANOVA and Dunnett's post hoc analysis). Removal of the Cl^- gradient as a driving force in platelet plasma membrane vesicles led to a much smaller (~50%) decrease in 5-HT accumulation (Nelson and Blaustein 1982), consistent with an important role for N101 in optimal coupling of 5-HT transport to the Na^+ gradient. Moreover, when transfected cells with accumulated 5-HT were washed and then incubated in 5-
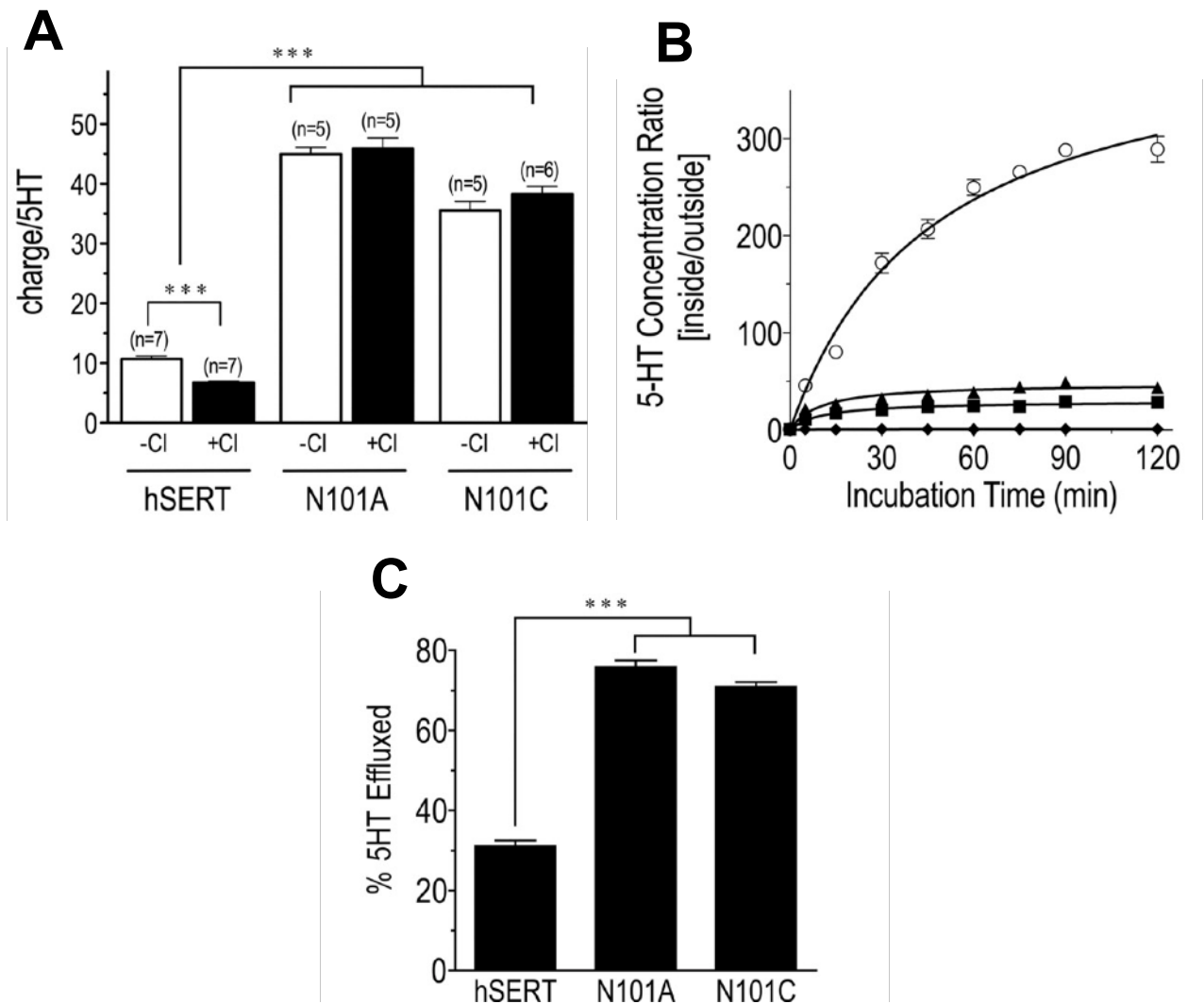
Figure 15. Ion-substrate coupling analysis of hSERT N101 mutants. (*A*) TEVC analysis of charge-to-substrate flux ratio: TEVC oocytes expressing hSERT or the N101 mutants were exposed to [^{3}H]5-HT in the presence or absence of Cl$^-$. Induced current was monitored during the incubation period followed by quantization of total 5-HT incorporated. Total current was converted to charge. The net charge movement per 5-HT molecule translocated was plotted for both presence (*filled bars*) and absence (*open bars*) of Cl$^-$. (***=$p \leq 0.001$). (*B*) Steady-state uptake kinetics: [^{3}H]5-HT (20 nM) uptake in NaCl-containing assay buffer by HeLa cells transiently transfected with hSERT (*open circles*), N101A (*filled boxes*), N101C (*filled triangles*) or nontransfected (*filled diamonds*) is monitored over 120 min. Data are normalized by calculating the concentration ratio of [^{3}H]5-HT inside the cell over the concentration in the buffer. The data were fit to a Michaelis-Menten nonlinear regression equation. (*C*) Substrate efflux from cells preloaded with [^{3}H]5-HT: HeLa cells transiently transfected with hSERT, N101A, or N101C are incubated with 20 nM [^{3}H]5-HT for 30 min washed and allowed to efflux for 30 min in MKRH buffer. % [^{3}H]5-HT efflux is plotted and determined by comparing [^{3}H]5-HT remaining in the cells from efflux assay to duplicate samples halted prior to the efflux step. (***=$p \leq 0.001$).

HT-free medium, hSERT N101 mutant cells exhibited significantly more efflux of 5-HT (hSERT $31 \pm 1.3\%$ in 30 minutes; N101A $76 \pm 1.7\%$ ($p < 0.001$); N101C $71 \pm 1.1\%$ ($p < 0.001$, one-way ANOVA and Dunnett's post hoc analysis) (Figure 15C). Together, these data reveal that mutation of N101 disrupts the ability of hSERT to utilize energy stored in transmembrane ion gradients to support the intracellular accumulation of 5-HT.

Molecular Modeling Suggests a Mechanism for N101 Participation in Ion-coupled 5-HT Transport

The lack of evidence for direct interaction between N101 and Cl^- (Forrest et al. 2007; Zomot et al. 2007; Ben-Yona et al. 2011; Tavoulari et al. 2011) suggests that N101 effects derive not from Cl^- binding. We investigated the possibility that N101 served an essential role in propagating Cl^- binding at nearby sites to other critical determinants of 5-HT transport using RosettaLigand (Meiler and Baker 2006) to dock 5-HT into an hSERT homology model and performed relaxation and energy minimization *in vacuo* with AMBER (Kaufmann et al. 2009). Subsequently, models of wild type hSERT and the N101A mutant were evaluated both in the absence and in the presence of the Cl^- and acetate ions using the same protocol. The placement of 5-HT in our model is consistent with biochemical data that indicate coordination of the 5-HT amine by D98 as well as sensitivity of 5-HT to substitution at various positions around the indole ring (Barker et al. 1998; Adkins et al. 2001). In hSERT, with Na^+, Cl^-, and 5-HT bound, our depiction illustrates these three substrates co-localized around the Na1 binding pocket through their coordination by residues of TM1, -2, -6, and -7 (Table 1). These four helices have been proposed to form a bundle whose movement within the protein closes the extracellular permeation pathway and opens a pathway to the cytoplasm (Forrest et al. 2008). Our minimized structures also predict that Cl^- and Na^+ coordination is linked via dual interacting residues S336

hSERT WT:

> *Na1:* A96 O, D98 Oδ-, N101 Oδ, S336 O, S336 Oγ; n=6
>
> *Na2:* G94 O, V77 O, L434 O, D437Oδ-, S438 Oγ, n=5
>
> *Cl:* Y121 HH, Q332 Hε, S336 Hγ1, N368 Hδ, S372 Hγ; n=5

hSERT WT: No Cl⁻

> *Na1:* A96 O (0.3), D98 Oδ1 Oδ2, N101 Oδ, F335 O, S336 O, n=5.1
>
> *Na2:* G94 O, V77 O, L434 O, D437 Oδ1 Oδ2; n=5

N101A: Cl⁻

> *Na1:* A96 O, D98 Oδ1 Oδ2, S336 O, Oγ, N368 Oδ n=5.8
>
> *Cl:* Y121 HH, Q332 Hε, S336 Hγ1, N368 Hδ, S372 Hγ; n=5

N101A: No Cl⁻

> *Na1:* A96 O, D98 Oδ1 Oδ2, S336 O, Oγ, N368 Oδ n=6
>
> *Na2:* G94 O, V97 O, L434 O, D437 Oδ1 Oδ2; n=5

Table 1. Ion coordination in the presence or absence of Cl⁻ for hSERT and N101. The table presents data from computation models of hSERT WT and N101A with and without Cl⁻ included in the system. Listed are the residues within range of forming a hydrogen bond to each respective bound ion. For each ion-binding site, coordinating residues are listed along with the respective chemical component of the residue that forms a hydrogen bond with the ion. The total number of coordinating interactions is listed at the end of each row. Those residues with low occupancy have their occupancy values included in parentheses.
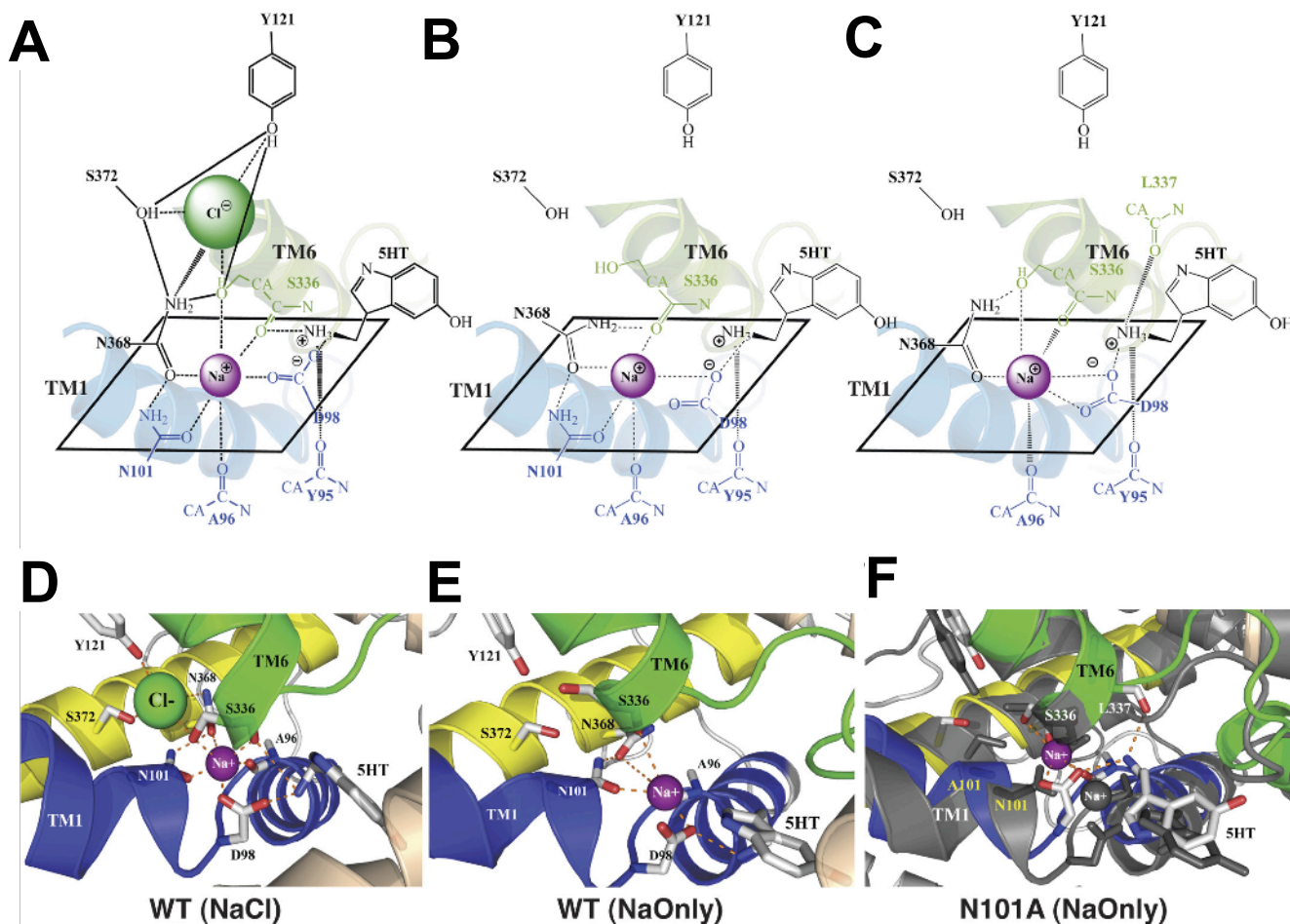
Figure 16. Molecular models of putative hSERT ion-binding sites. The top panels (*A-C*) are 2.5-dimensional representations emphasizing differences in ion coordination geometry observed after a 20-ns MD simulation of computational models of hSERT and hSERT N101A in the presence and absence of Na$^+$. Residues participating in the ion-binding site of each model are color coded *blue* (TM1), *green* (TM6), and *yellow* (TM7). Note the apparent importance of residue Ser-336 in stabilization of favorable ion-coordination geometry in both the models for hSERT with NaCl (*A*) and the N101A mutant without Cl$^-$ (*C*). This positioning of S336 is not found in the model of hSERT without Cl$^-$ (*B*). (*D-F*) A three-dimensional rendering of (*D*) hSERT with NaCl, (*E*) hSERT without Cl$^-$, and (*F*) hSERT N101A without Cl$^-$ superimposed on top of hSERT WT without Cl$^-$ (*black*). All *dashed lines* represent stable hydrogen bonds observed after 20 ns of MD simulation in lipid membrane and aqueous solution.

(TM6) and N368 (TM7). 5-HT engages both the Na^+ and Cl^- coordination networks via a salt bridge provided by its ethylamine nitrogen. N101 participates in Cl^- interactions in these models through stabilization of N368 in TM7 and Na1. To test predictions from the gas-phase computations, we constructed a solvated lipid membrane system with our SERT models and performed all-atom MD simulations with the CHARMM-27 force field (data not shown; see (Henry et al. 2011)).

Using different methods (comparative modeling, docking, minimization, and then all-atom MD simulations), we consistently observed distinct backbone conformational shifts at residue S336 in response to Cl^- removal (Figure 16, A, B, D and E) that result in a shift of hydrogen-bonding interactions of the S336 side-chain OH away from interaction with the N368 side-chain amide (Figure 16, A and D), where many residue contacts in TM1, -2, -6, and -7 are affected, including Y121 and S372. The multiple interactions of N101 observed in hSERT are likely critical to coupling as they lead to an extensive hydrogen bond and coordination network around the bound ion substrates. Conversely, Cl^- coordination by N368 permits an interaction of the S336 side-chain OH with N368 via an improved geometry for coordination of the Na1 site Na^+ ion. In turn, these interactions link TM2 and TM7 to TM1, where critical aspects of 5-HT coordination are located (residue D98 and the backbone carbonyl of Y95) (Figure 16, A and D). Notably, our recent substituted cysteine accessibility method analysis of TM6 (Field et al. 2010) revealed S336C exhibits the same phenotype as the N101C mutant in that it is sensitive to (+)-charged MTS reagents and insensitive to (−)-charged MTS reagents.

Importantly, analyses of MD trajectories allow us to predict the residue interaction changes likely to arise in N101 mutants that allow for Cl^--independent 5-HT transport. Analysis

59

of the inter-residue contacts from MD simulations predicted that the N101A mutation could considerably disrupt the H-bond interaction network found in the hSERT substrate-Na1 ion-binding pocket (Table 1). Coordination of Na^+ by the N101 side-chain amide oxygen is predicted to be lost as is the H-bond between 5-HT and S336. A number of long lived (stable) bonds connecting TM2 and -7 are also lost in the hSERT WT models absent of Cl^- (Figure 16, B and E). However, the A101 side chain, being considerably smaller than N101, permits a local repacking of the residues forming the Na1-binding site and displacement of the Na^+ ion by ~2.0Å (Figure 16F, gray and magenta spheres). This change allows formation of a novel Na^+ coordination site in which the backbone carbonyl of S336 supplements the S336 side chain, restoring WT-like ion coordination number ($n = 6$) with the backbone carbonyl of L337 (TM6) forming an H-bond with the 5-HT ethylamine moiety. Interestingly, a conservative but bulkier N101Q mutation results in almost complete loss of function (data not shown), suggesting side chains larger than Asn may significantly impact interactions in the binding site. The Na1 site is further stabilized by S336 forming an H-bond to the side chain of the N368 amide. There is also a long living hydrogen bond (>80% of all analyzed MD frames) between Y121 and S372 (TM6). These interactions effectively mimic the relative positioning of the same residues from TM1, -2, -6, -7 found in the WT hSERT Cl^- ion coordination models (Figure 16, A, D, E and F)).

Effect of Cl^- and Different Mutations on Ion and Solute Binding to the Transporter

To better understand the role of Cl^- in binding of Na^+ and 5-HT, we computed binding enthalpies using MM/PBSA approximation (Swanson et al. 2004). The evaluation of binding enthalpies for mutants (101A and 336C) may help highlight the role of the anion in the transport cycle and its modulation by N101 and S336. The $\Delta\Delta H$ for the Cl^--free WT protein shows

significant inhibition of both Na^+ and 5-HT binding to the transporter indicating an important role of Cl^- in the stabilization of the entire binding pocket. The analysis of the ion coordination within the Na1 site shows that the anion-depleted transporter displays different ion coordination for Na1 than the anion-bound complex. In particular, the hydroxyl oxygen from the side chain of S336 no longer coordinates the Na^+ ion, and the Na1 coordination number is reduced from ~6 to ~5 ligands producing an immediate effect on ion binding affinity to Na1. In contrast, removal of Cl^- from the N101A mutant led to relatively modest changes in the binding enthalpies for solute and ions to the Na1/Na2 sites as compared with WT. In the N101A system, both side-chain carboxylate oxygens of D98 and the side-chain OH and backbone carbonyl oxygen of S336 are now participating in the coordination shell for the Na^+ ion bound to the Na1 site thereby compensating for the substitution at N101 (Figure 16F). S336 contributes both main chain and side-chain oxygens to ion coordination in the N101A mutant (with and without Cl^- bound). However, binding of Cl^- to the N101A mutant destabilizes ion coordination at the Na2 site such that the affinity of Cl^- for the transporter is reduced relative to that of a wild type transporter. Thermodynamic analysis of binding enthalpies suggest that N101 plays an important role in modulation of binding affinity at the Na1 and Na2 sites as well as a contribution to the modulation of Cl^- binding.

Validation of the Partnership Between N101 and S336 in Cl^--dependent 5-HT Transport

As noted above, our models suggest a critical relationship between N101 in TM1 and S336 in TM6 on the coupling of Na^+ and Cl^- binding to 5-HT transport. To test this hypothesis, we generated the Cys substitution S336C, reducing the length of the side-chain hydrogen bond donor because our model proposes that this side chain directly coordinates Cl^- as well as N368

(Figure 16A) (Yamashita et al. 2005; Forrest et al. 2007). Indeed, although surface expression of hSERT S336C was 70% of hSERT (Figure 17D), transport activity was only $11 \pm 2.7\%$ ($n = 3$) that of wild type. Importantly, the residual 5-HT transport activity observed with S336C was largely Cl$^-$-independent and was actually enhanced by full anion replacement with acetate (Figure 17, A–C).

The findings with S336C are similar to results obtained by Forrest *et al.* (Forrest et al. 2007), who proposed S372 was a Cl$^-$-coordinating residue in SERT and found that mutation of S372 to the negatively charged Asp or Glu yielded Cl$^-$ independence. However, unlike N101C, S372C did not result in Cl$^-$-independent uptake but rather yielded an increase in the apparent K_m value for Cl$^-$. This difference in Cys substitution at these two sites in terms of Cl$^-$ independence could be explained by the pK_a at S336 and S372 in the absence of Cl$^-$. C372 is proposed to be in the noncharged SH form (Forrest et al. 2007). We constructed equilibrated anminimized hSERT models in a solvated membrane system and used free energy perturbation FEP analysis using dual topology methods (Simonson et al. 2004) to evaluate pK_a shift upon deprotonation for cysteines at the positions 336 and 372 relative to model solution (150mM aqueous solution of NaCl). FEP simulations of the pK_a shift for buried cysteines. These analyses reveal that in the presence of Na$^+$ in the Na1 site, C336 can be deprotonated at pH 7 with a large ΔpK_a shift of approximately -5.0. The experimental pK_a for the Cys side chain is ~8.0, and therefore the pK_a for C336 is ~3.0, suggesting that there is a high probability that the side chain of C336 is deprotonated with Na$^+$ present at the Na1 site. However, analysis of C372 shows the resulting ΔpK_a shift is approximately -0.9 and the net pK_a for C372 is ~7.1. The reason for the apparent difference in protonation state at these two positions lies in the proximity
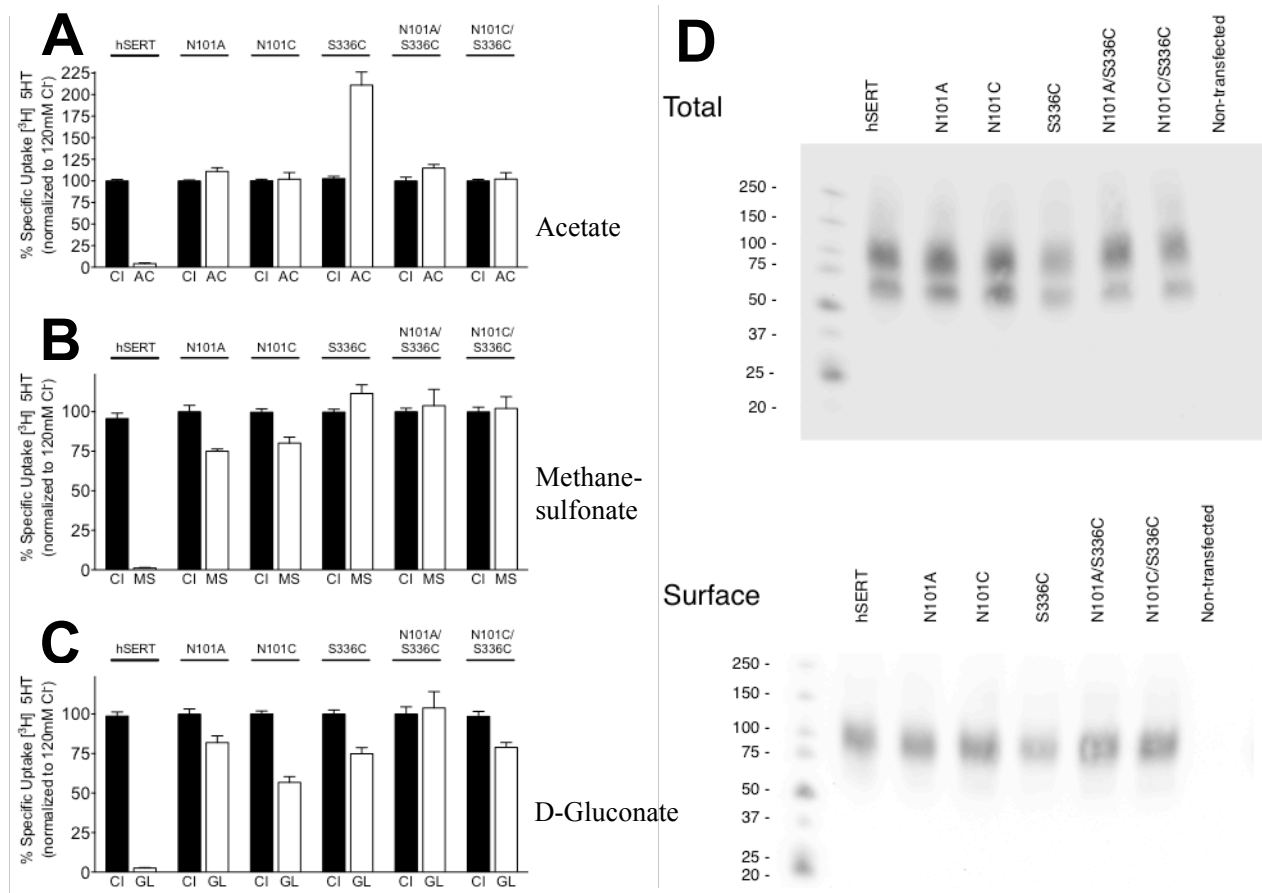
Figure 17. Anion replacement impact on 5-HT transport and substrate induced current in N101 and S336 mutants. [³H]5-HT (30 nM) uptake in HeLa cells was determined under Cl⁻-replacement with the anions (*A*) acetate, (*B*) methanesulfonate and (*C*) D-gluconate in hSERT and mutants as marked. Data were normalized to uptake of Cl⁻-containing buffer for each mutant. (*D*) Western blot analysis was conducted to determine the surface expression of each hSERT mutant. Surface proteins were labeled with a biotin tag, purified using neutravidin beads. hSERT was detected using the monoclonal antibody ST51-1. Parental cells are included as a control.
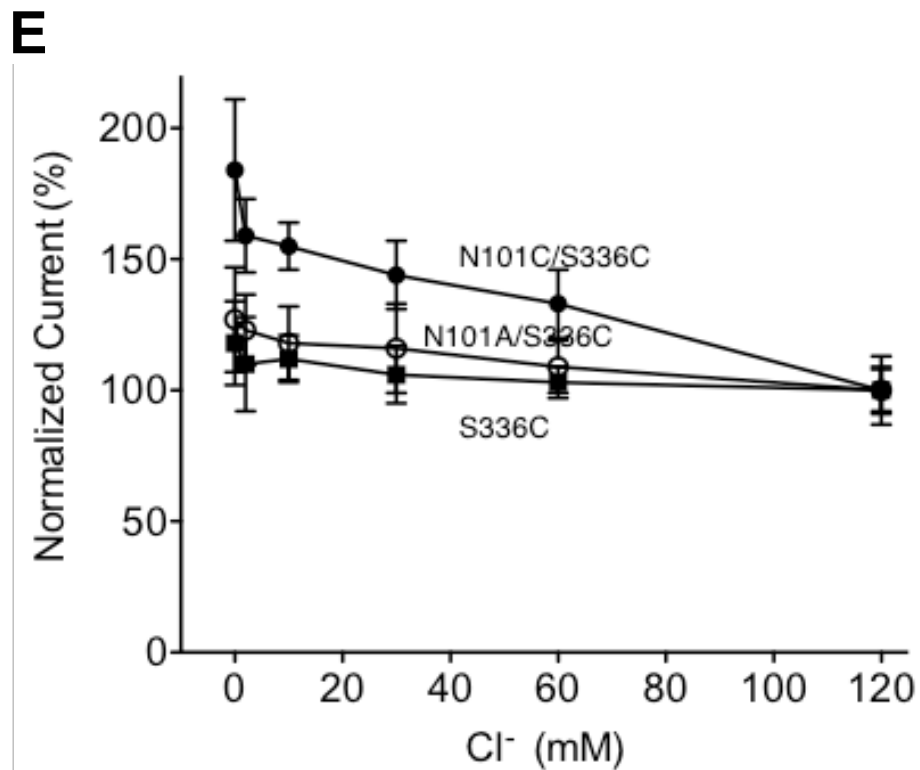
Figure 17 (continued). Anion replacement impact on 5-HT transport and substrate induced current in N101 and S336 mutants. (*E*) TEVC analysis in oocytes of S336C (*filled boxes*), N101A/S336C (*open circles*) and N101C/S336C (*filled circles*) double mutants plotting steady-state currents evoked upon application of 5 μM 5HT in response to Cl⁻ concentration. Currents were normalized to % current obtained with 120 mM Cl⁻ at −60 mV.

to bound Na^+. MD simulations with $C336^-$ show that the negatively charged side chain partially occupies the site for Cl^- and could coordinate Na^+ (with occupancy of ~40%). C372 cannot coordinate to the positive ion, and therefore its deprotonation in the low dielectric environment is energetically unfavorable. These findings are consistent with the proposition that C336 acts similar to charge-changing (Asp or Glu) mutations at the position 372 in providing a localized negative charge and thereby results in Cl^- independence. Whereas the convergence of free energy simulations is known to be a bottleneck of the method, large shifts in pK_a values are suggestive of different propensities in the protonation states of these two cysteines (Li et al. 2008).

Interestingly, whereas in tissue culture studies S336C transported 5-HT at only ~11% the rate of wild type hSERT, introduction of N101A into the S336C background transport rate was three times faster, similar to that of the N101A single mutant alone (Figure 18) (Henry 2003). Like the N101 and S336 single mutants, 5-HT transport by the N101A/S336C and N101C/S336C double mutants is Cl^--independent (Figure 18). Side-chain rotamer modeling of S336C in both wild type and N101A mutant backgrounds suggest steric packing effects in the Na1 ion-binding site were significant structural factors contributing to this phenotype (data not shown; see (Henry et al. 2011)). Consistent with [³H]5-HT transport assays, TEVC analysis of S336C single and N101A/S336C and N101C/S336C double mutants yields results similar to N101A and N101C mutants, where 5-HT-induced currents are Cl^--independent (Figure 17E). As with the N101C single mutant (Figure 14E), the N101C/S336C mutant shows a dose-dependent reduction in observed current in response to increasing Cl^- concentration suggesting the
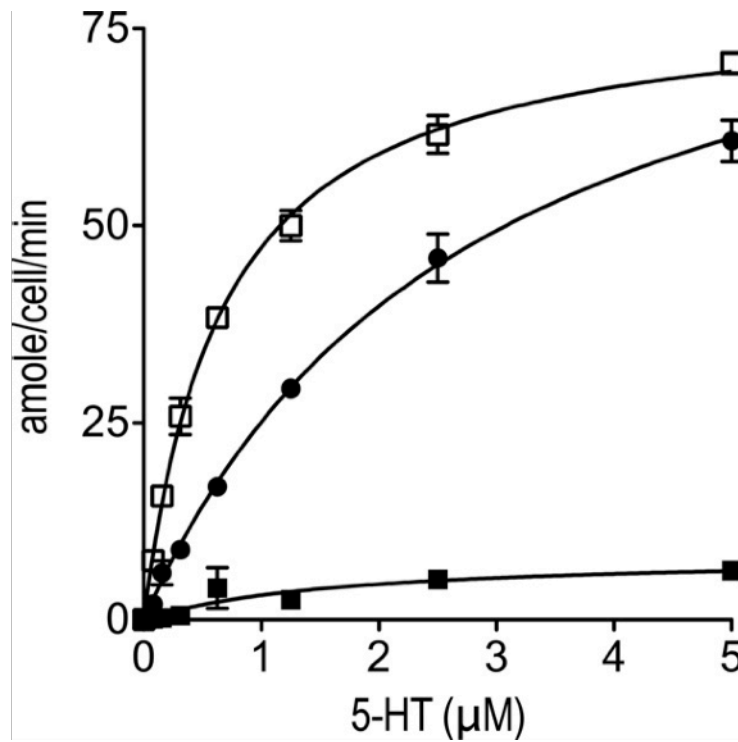
Figure 18. Kinetic analysis of 5-HT transport in hSERT S336C and N101A/ S336C mutants. HeLa cells transiently expressing the hSERT N101A (*open squares*), hSERT S336C (*filled squares*), or hSERT N101A/S336C (*filled circles*) mutants were evaluated for dose-dependent 5-HT uptake after 10 min in NaCl containing buffer (*n=3*).

possibility of Cl⁻ co-transport in the N101C-containing mutant that could offset the movement of positive (Na⁺) ions, appearing as a reduction in current.

Discussion

In previous biochemical analysis of hSERT TM1, it was suggested that the conserved residue N101 was proximal to the substrate- and cocaine-binding sites (Henry 2003). A position proximal to the substrate-binding site was later substantiated by the LeuT crystal structure (Yamashita et al. 2005) and in relation to the competitive antagonist cocaine by subsequent LeuT model-guided studies of dopamine transporter (Beuming et al. 2008). Interestingly, during the substituted cysteine accessibility method analysis, we found N101C could be modified by the positively charged reagent MTSET but not by the negatively charged MTSES (Henry 2003). This distinction does not reflect a direct antagonism of MTSES by Cl⁻ as N101 is not likely to be directly involved in Cl⁻ binding (Forrest et al. 2007; Ben-Yona et al. 2011; Tavoulari et al. 2011). In fact, Cl⁻-free conditions fail to promote MTSES inactivation of the N101C transporter (Rudnick 2002). The inability of MTSES to inactivate the N101C mutant may arise from repulsion by the transmembrane dipoles that are predicted to exist at the central unwound regions in TM1 and -6 (Screpanti and Hunte 2007). Moreover, four recent reports that identify Cl⁻-binding sites and the coordinating residues in SERT and GAT1 do not implicate N101 in this role (Forrest et al. 2007; Zomot et al. 2007; Ben-Yona et al. 2011; Tavoulari et al. 2011).

In this study, we provide several lines of evidence regarding a critical role that N101 plays in coupling Cl⁻ binding to the conformational changes that are essential for Na⁺-coupled 5-HT transport. In particular, our substituted cysteine accessibility method analysis reveals that the

N101 mutants no longer require Cl$^-$ for 5-HT-induced conformational changes, providing more specific evidence for the involvement of N101 in Cl$^-$ dependence. The N101 mutations increase nonstoichiometric charge movements carried by hSERT, both in the presence and the absence of 5-HT, indicating uncoupled ion movements. Conversely, although N101 mutants transported 5-HT at initial rates comparable with that of hSERT, steady-state 5-HT accumulation was reduced ~90%, further indicating a loss of thermodynamic coupling between transmembrane gradients of ions and 5-HT. This loss of coupling was even more severe than would be expected simply from the contribution of a transmembrane Cl$^-$ gradient to 5-HT accumulation, which was less than 2-fold in measurements with resealed vesicles expressing native SERT (Nelson and Blaustein 1982), suggesting a more profound defect in ion coupling in the N101 mutants.

Slight differences in the extent of Cl$^-$ substitution by the anions acetate (105%), methanesulfonate (78%), and gluconate (70%) correlate with their Stokes diameters of 4.5, 5, and 6.2Å, respectively, and suggest that N101 substitution may impart changes in anion selectivity at the Cl$^-$-binding site in SERT. These results indicate that anions may still interact with hSERT in the N101 mutants and are consistent with the presence of all previously proposed Cl$^-$-binding site residues (Forrest et al. 2007; Zomot et al. 2007) in these mutants. Further evidence comes from Cl$^-$ substitution with multivalent anions such as phosphate, resulting in poor functional replacement compared with monovalent species ($\leq$40% compared with Cl$^-$-containing conditions, data not shown). These data also suggest that the anion-binding site is still available, and its functional role can be inhibited by multiple charged species. The N101/S336 double mutants appear less sensitive to the anion size in replacement of Cl$^-$ (Figure 17, B and C) and Cl$^-$ substitution.

Further insight into the role of N101 and the impact of N101 substitutions derives from our MD simulations. We utilized homology-based molecular modeling of hSERT using the LeuT coordinates as well as small molecule docking of 5-HT with RosettaLigand. The results predict that N101 extends into the substrate binding pocket where the side-chain carbonyl oxygen, homologous to LeuT N27 (Yamashita et al. 2005; Kaufmann et al. 2009), as proposed previously (Barker et al. 1999; Yamashita et al. 2005), places N101 in a critical position to contribute to the stabilization of both Na^+- and 5-HT-binding sites. Consistent with these findings, a docking study by Celik *et al.* (Celik et al. 2008) identified a similar pose for 5-HT in SERT as one of the three top-scoring clusters.

Ion and substrate dynamics are controlled by occupancy of Na1 and Cl^- sites. The mutations that affect ion binding to either site (S336 or N101) have a global impact on the entire transport mechanism. For example, our MD analysis implicated S336 as an important residue in the Cl^- dependence of transport coupling. This residue was previously proposed to coordinate Cl^- in SERT (Forrest et al. 2007; Tavoulari et al. 2011) and GAT-1 (Zomot et al. 2007; Ben-Yona et al. 2011), and we found that S336C exhibits the same insensitivity to MTSES as N101C (Field et al. 2010). Experimental analysis of the hSERT S336C mutant subsequently revealed that like in N101C, 5-HT transport by S336C was not dramatically stimulated by Cl^-. However, our MD pK_a analysis suggests that this effect may also be due to replacement of Cl^- by the Cys thiolate anion, similar to replacement of other Cl^--coordinating residues with carboxylic amino acids in SERT and GAT-1 (Forrest et al. 2007; Zomot et al. 2007). Finally, analysis of docking conformations indicates that the coordination geometry of acetate in the wild type is less favorable than in N101A and can explain why acetate can fully replace Cl^- in an N101 mutant

background but not in hSERT. In hSERT, acetate forms an H-bond with the C=O backbone of S336 that would limit adoption of a Cl^--like geometry (data not included; see (Henry et al. 2011)). In N101A, the N368 amide side chain is no longer constrained by the H-bond network imposed by N101 and is thus free to interact with acetate in a manner that reproduces the ion coordination geometry of the WT NaCl model (data not included; see (Henry et al. 2011)).

More generally, our findings illustrate that both the direct interaction of N101 with N368 and the more indirect interaction with S336 via coordination of the NA1 sodium ion suggest that establishment of physical interactions between TM1 and -6 is a critical facet of ion-coupled substrate movement. This idea is further supported and expanded by our inter-helical interaction energy analysis conducted on MD trajectories for WT and mutants (data not shown), which suggests that Cl^- removal has an adverse impact on transport by disruption of interactions between TM1 and -3, TM1 and -6, and TM5 and -8. In contrast, the removal of Cl^- is energetically much less disruptive to inter-helical interactions in the N101 mutants. Recent crystal structure and MD studies suggest that the primary transport mechanism for the LeuT structural superfamily involves helical bundles that move relative to one another to allow entry to and exit from the substrate- and ion-binding sites (Forrest et al. 2008; Ressl et al. 2009; Shimamura et al. 2010; Watanabe et al. 2010) via gating residues originally described by Yamashita *et al.* (Yamashita et al. 2005). However, disagreements do exist between the models, and these differences may reflect mechanistic subtleties between transporters influenced by the substrates and ions involved.

Within the SLC6 family, some bacterial, insect, and mammalian family members differ in the identity of the residue homologous to hSERT N101 and contain instead a His, Ala, Cys,

Gly, Thr, Ser, or Asp (Beuming et al. 2006), whereas all known Cl$^-$-dependent SLC6 neurotransmitter transporters contain Asn at this site. This observation suggests that this residue plays a critical role in promoting optimal coordination of sodium, Cl$^-$, and substrate while limiting movement of additional charges, a role that appears relaxed in the N101 mutants. As we and others (Ingram et al. 2002; Quick 2003; Carvelli et al. 2004; 2008) have published that serotonin and dopamine transporter charge flux is an important contributor to neuronal excitability, we believe that the charge flux-limiting property of this residue is particularly important at synapses.

Neurotransmitter transporters are now known to exist in regulated protein complexes that can modulate multiple aspects of transport, including substrate affinity, membrane trafficking, and ion conductance states. Our observation of a >7-fold increase in Na$^+$ flux in the N101 mutants and the finding that syntaxin1A interaction with the N terminus of SERT can modulate Na$^+$ stoichiometry during the transport cycle (Quick 2003) raise the possibility that syntaxin1A binding may modulate transporter conductance states by orienting residues in TM1, likely including N101, to restrict nonstoichiometric ion flow during the transport cycle. Although Ala (or Cys) can functionally replace N101, the loss of optimal coupling is accompanied by dramatic increases in both leak and 5-HT-gated currents, properties that may be captured by syntaxin1A-linked regulatory mechanisms. The remarkable >2-fold increase in 5-HT efflux from cells expressing the N101 mutants also supports the idea that precise orientation of the amide side chain of this residue can control coupling between ion gradients and efflux of intracellular 5-HT. In fact, initial cation replacement studies using NMDG-Cl suggests that Na$^+$ dependence may be altered in the N101 mutants (Figure 19). In addition, it has been shown that amphetamine-
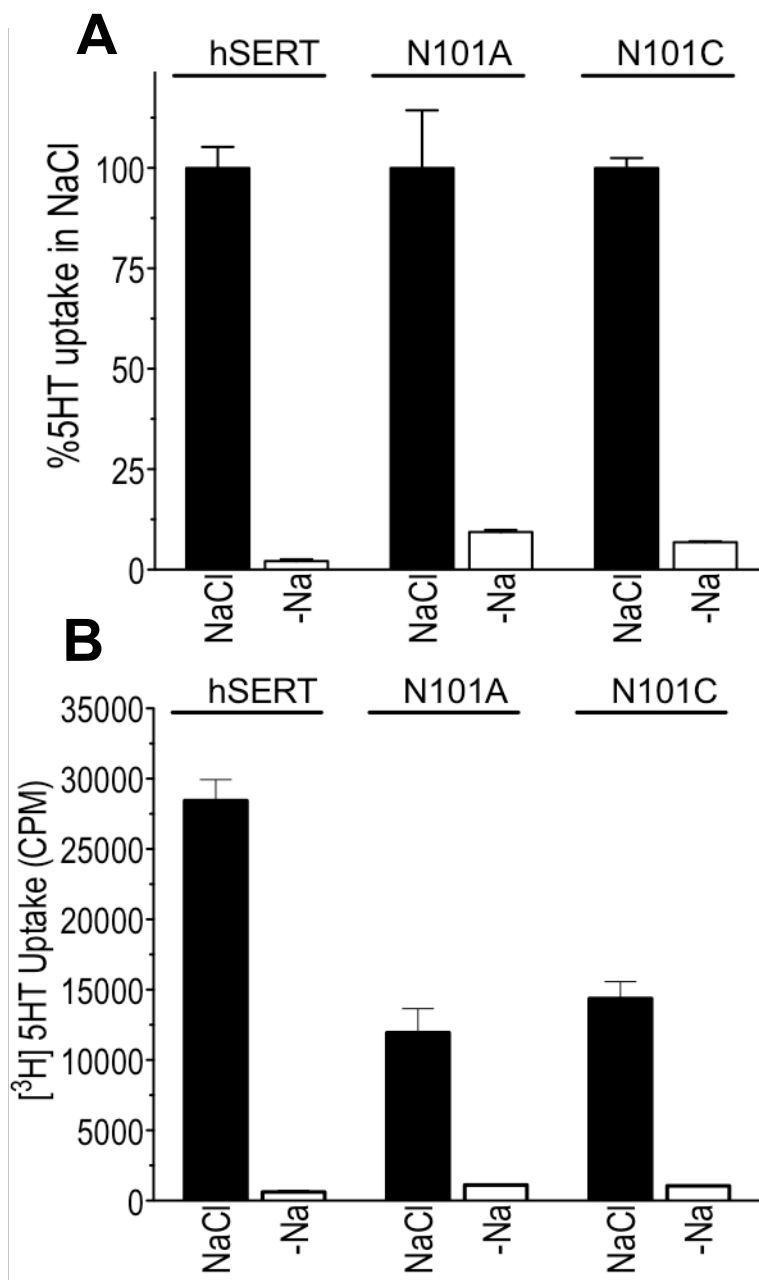
Figure 19. Na$^+$ dependence of hSERT N101A and N101C mutants. Uptake of [^{3}H]5-HT (20 nM) after incubation for 15 minutes in medium with and without Na$^+$ (replaced with NMDG-Cl) is plotted as (*A*) percent uptake of Na$^+$ containing buffer and (*B*) raw [^{3}H] counts per minute (CPM). CPMs for N101A and N101C in panel B are ~30% those of the hSERT WT and are expected based upon the mutants surface expression relative to hSERT WT.

induced efflux through dopamine transporter requires phosphorylation of its cytosolic N-terminus (Fog et al. 2006) as a result of CaMKII activation by amphetamine. Phosphorylation of the N-terminus may propagate changes in structure upward to TM1, recapitulating the impact of N101 mutants. Finally, high NE flux rates mediated by channel-like states have been identified in the norepinephrine transporter (Galli et al. 1998). As these conductance states can be inhibited by syntaxin1A (Sung and Blakely 2007), we speculate that the presence of the Asn in TM1 may provide Cl^--coupled SLC6 transporters not only with the opportunity to more efficiently tap the Na^+ gradient for uphill transport but also allows transporters to move between coupled transporter modes of substrate conduction and channel-like modes of neurotransmitter transport.

CHAPTER III

THE TWO SODIUM SITES IN THE HUMAN SEROTONIN TRANSPORTER PLAY DISTINCT ROLES IN THE ION COUPLING AND ELECTROGENICITY OF TRANSPORT

Introduction

Secondary active solute transporters are a critical feature of biological systems that utilize chemiosmotic gradients to support energetically unfavorable concentrative movement of substrates across the plasma membrane. Evidence suggests that substrate translocation occurs via an alternating access mechanism in which ion and substrate binding facilitate conformational changes in the transporter allowing a central binding domain to be alternatively open to either side of the membrane (Jardetzky 1966; Forrest et al. 2008; Forrest and Rudnick 2009). Recently, a number of solute transporters from different families have been crystallized, providing critical details about the structural features of these carriers (Yamashita et al. 2005; Faham et al. 2008; Weyand et al. 2008; Gao et al. 2009; Ressl et al. 2009; Shaffer et al. 2009; Schulze et al. 2010; Shimamura et al. 2010; Penmatsa and Gouaux 2013). Despite these transporters possessing little to no sequence homology, all share a 5 + 5 arrangement of transmembrane helices termed the FIRL ("five-transmembrane helix-inverted topology repeat, LeuT-like") or "LeuT-fold" (Khafizov et al. 2012), where the second bundle of five helices have inverted symmetry in relation to the first group of five helices, supporting the idea of a conserved functional mechanism (Abramson and Wright 2009; Forrest and Rudnick 2009; Krishnamurthy et al. 2009). Importantly, a collection of crystal structures have been solved representing the "open-to-out",

"occluded," and "open-to-in" conformations of the carriers, suggesting mechanisms that may support substrate translocation (Yamashita et al. 2005; Zhou et al. 2007; Singh et al. 2008; Krishnamurthy and Gouaux 2012; Piscitelli and Gouaux 2012). Unfortunately, these static poses are limited in their ability to explain how ion binding is mechanistically and energetically coupled to the conformationally mediated transport of substrate.

In this study, we focus on the human serotonin transporter (hSERT), a member of the SLC6 family that plays a major regulatory role in synaptic transmission by clearing 5-HT from the synaptic cleft, thereby terminating 5-HT receptor activation (Blakely et al. 1991; Hoffman et al. 1991; Reith 2002; Beuming et al. 2006; Kristensen et al. 2011; Pramod et al. 2013). hSERT has importance in human health, being the target of a number of therapeutic and illicit drugs, including tricyclic antidepressants, selective serotonin reuptake inhibitors, cocaine, and 3,4-methylenedioxymethamphetamine ("ecstasy") (Ramamoorthy et al. 1993; Tatsumi et al. 1997; McCann et al. 1998; Pramod et al. 2013). Although SERT shares only ~21% overall sequence identity with the SLC6 bacterial amino acid transporter LeuT, the residues in the core of the two proteins, where substrate and ions bind, approach ~60% identity, suggesting that the two Na^+-binding sites in LeuT, termed Na1 and Na2 (Yamashita et al. 2005), are conserved in hSERT (Barker et al. 1999). Evidence for two Na^+-binding sites in MATs was recently bolstered by the solving of the eukaryotic Na^+/Cl^--dependent dopamine transporter from *Drosophila melanogaster* (dDAT) with sodium-binding sites comparable with those in LeuT (Penmatsa and Gouaux 2013). Crystal structures of dDAT and a LeuT Cl^--dependent mutant (E290S) (Kantcheva et al. 2013) have greatly advanced our understanding of the Cl^--binding site in these

proteins and support previous biochemical studies (Forrest et al. 2007; Zomot et al. 2007; Tavoulari et al. 2011).

Interestingly, 5-HT uptake analysis indicates that during coupled transport, only one Na^+ is translocated per cycle (Sneddon 1969), suggesting that the Na1 and Na2 sites probably have distinct but as yet unknown roles. Recent computational analysis of the Na2 binding site in proteins with the LeuT-fold predicted that transition to an inward facing conformation destabilizes Na^+ coordination at Na2, resulting in Na^+ release followed by substrate dissociation (Noskov and Roux 2008; Shi and Weinstein 2010; Yu et al. 2010; Krishnamurthy and Gouaux 2012; Zdravkovic et al. 2012; Zhao et al. 2012). Were this true in hSERT, which appears to translocate a single Na^+ per transport cycle, the cation at Na1 would not be mobile. This surmise is consistent with data from crystal structure and molecular dynamic analysis of the bacterial galactose transporter, vSGLT, because this transporter possesses the homologous Na2 site but lacks the Na1 site (Faham et al. 2008; Watanabe et al. 2010). Despite these implications, however, the distinct role of the Na1 and Na2 in hSERT remains elusive. To understand the roles that each bound Na^+ performs in hSERT, we used site-directed mutagenesis in combination with biochemical and electrophysiological analyses to characterize how alterations at either of the Na^+coordination sites affect ion dependence and selectivity as well as ion and 5-HT transport. Using a mutation that alters Na1 coordination yet retains 5-HT transport, we uncovered distinct roles for the Na1 and Na2 coordination sites as well as molecular interactions that appear to be important in the 5-HT transport mechanism.

Methodology

Site-Directed Mutagenesis

Mutagenesis of hSERT cDNA in pcDNA 3.1 was accomplished using the Change-IT multiple mutation site-directed mutagenesis kit (Affymetrix, Cleveland, OH). Mutations were verified by DNA sequencing via Northwoods DNA, Inc. (Bemidji, MN).

5-HT Uptake Analysis

All transport studies of the mutants were conducted using either HEK-293 cells transfected with Trans-IT LTI (Mirus Inc.) in Opti-MEM medium as described previously (Henry 2003) or stably expressing HEK-293 cells under G418 (800µg/ml) selection. Cell lines were plated on 24-well poly-D-lysine-coated culture plates at a density of 50,000 cells/well and maintained at 37°C, with 5% CO_2 and under high humidity. Prior to uptake, plates were washed using the appropriate buffer as follows. Standard complete buffer contained 120mM NaCl, 5.4mM KCl, 1.2mM $CaCl_2$, 10mM glucose, 7.5mM HEPES, pH 7.4. Cation-only replacement buffers were prepared by replacing NaCl with a specific cation, giving XCl, where X represents Li^+, K^+, Ca^{2+}, Mg^{2+}, Ba^{2+}, NH_4^+, N-methyl-D-glucamine ($NMDG^+$), or $choline^+$ (120mM for single valence cations or 60mM for divalent cations). When Ca^{2+} was completely removed from the buffer, 10mM mannitol was added to balance the osmolality. A small amount of cell detachment was detected when assays were conducted in buffer lacking Ca^{2+}, suggesting that could be responsible for lower uptake activity under "Na^+-only" conditions; however, cell viability studies show that the cell wash off is minimal. Furthermore, a similar decrease in activity was observed in the Na^+-only buffer supplemented with 50µM Ca^{2+}, which eliminated detachment during uptake, indicating that any cell loss had little to no impact on the decreased

activity observed in the Na$^+$-only buffers. Buffers were adjusted to pH 7.4 using KOH or NMDG. Anion replacement buffers were made similarly, with all buffer salts having Cl$^-$ replaced by Y (120mM NaY, 5.4mM KY, 1.2mM CaY, where Y represents acetate, gluconate, or sulfate). Assays measured transport of 50nM [^{3}H]5-HT (5-hydroxy[^{3}H]tryptamine-trifluoroacetate, 28.5Ci/mmol, PerkinElmer Life Sciences) as described previously (Henry 2003). Assays were conducted for 10 minutes in order to stay within the linear range of uptake, with the exception of 5-HT saturation analysis (15 minutes) and 5-HT equilibrium analysis (2–90 minutes). Saturation assays were performed as described, except [^{3}H]5-HT was diluted 50-fold with non-radiolabeled 5-HT to achieve the highest concentration of 50μM. Washing with cold assay buffer terminated transport assays. Cells were dissolved in Microscint 20 (PerkinElmer Life Sciences) scintillation fluid, and counts/minute were determined using a TopCountNXT (PerkinElmer Life Sciences). Basal activity from non-transfected (or parental) cells was subtracted from experimental wells to obtain specific activity. K_m, V_{max}, and EC$_{50}$ values were calculated by fitting non-linear curves to the data as a function of 5-HT concentration (GraphPad Software Prism 5). All experiments were conducted in triplicate and were independently replicated a minimum of three times.

Protein Expression Analysis

Transporter surface expression was determined in stably expressing HEK-293 cells plated on poly-D-lysine-coated 24-well plates at a density of 100,000 cells/well. 24–48 hours after plating, cell surface proteins were biotinylated, quantitated, and analyzed using Western blotting as described previously (Henry 2003).

Cysteine Accessibility Analysis

HEK-293 hSERT cells were plated at 50,000 cells/well and transfected as described above. Plates were washed with a cation-specific assay buffer, followed by treatment using the same buffer supplemented with 1mM (2-trimethylammonium)ethyl)methanethiosulfonate bromide (MTSET) (Toronto Research Chemicals Inc.), 1mM MTSET + 20μM 5-HT, or vehicle. In wells receiving 5-HT and MTSET, 5-HT was added 2 minutes prior to MTSET. Plates were incubated at room temperature for 10 minutes. To terminate the reaction, MTSET was removed via multiple washes with MKRH+G (120mM NaCl, 4.7mM KCl, 2.2mM $CaCl_2$, 1.2mM $MgSO_4$, 1.2mM KH_2PO_4, 10mM Glucose, 10mM HEPES, pH 7.4). The remaining transport activity was determined using 50nM [^{3}H]5-HT as described previously.

Two-Electrode Voltage Clamp Analysis

cRNA preparation. Plasmids encoding hSERT were linearized and transcribed into RNA with a T7 RNA polymerase kit mMessage mMachine (Ambion). A total of 5ng of cRNA was microinjected into each oocyte. Electrophysiological recordings were performed 3–9 days following injection.

Oocyte preparation. *Xenopus laevis* frogs (Nasco, Fort Atkinson, WI) were anesthetized with ethyl 3-aminobenzoate methanesulfonate (FLUKA A5040) (2mg/ml in H_2O). The frog was decapitated, and the ovarian lobes were removed and transferred to sterile Ca^{2+}-free OR2 solution (82.5mM NaCl, 2.5mM KCl, 2mM $MgCl_2$, 10mM HEPES, pH adjusted to 7.4 with NaOH). The lobes were manually dissected to produce groups of 5–10 oocytes and incubated in OR2, containing 1mg/ml collagenase from *Clostridium histolyticum* (Sigma). Incubation for 45–60 minutes at 18°C was sufficient to digest and remove the follicular layer. Oocytes were then

selected and transferred to a Ringer solution (100mM NaCl, 2mM KCl, 1.8mM CaCl$_2$, 1mM MgCl$_2$, 5mM Hepes, pH adjusted to 7.6 with NaOH). Oocytes were kept at 18°C for a minimum of 2 hours prior to injection. Injected oocytes were kept for 6–9 days at 18°C in a Ringer solution containing 2.5mM Na$^+$ pyruvate, 100μg/ml penicillin, 100μg/ml streptomycin. Solutions were changed daily.

Electrophysiological recordings in *X. laevis* oocytes. A CA-1B high performance oocyte clamp (Dagan Corp.) was employed for the measurements. The recorded signal was digitized with a Digidata 13222A system (Axon Instruments). pCLAMP 9.2 (Axon Instruments) was used for data acquisition. Borosilicate glass capillaries were pulled to a final resistance of 0.4–1.2 megaohms and filled with 3M KCl. Oocytes were impaled, and the membrane potential was clamped to a holding potential of −60mV. For continuous superfusion with Na$^+$ solution (120mM NaCl, 2mM KCl, 1mM BaCl$_2$, 1mM MgCl$_2$, 10mM HEPES, pH adjusted to 7.4 with NaOH) a gravity-driven superfusion system (Warner Instruments, Eight Channel Perfusion Valve Control System (VC-8)) was used. For the Ca^{2+} solutions, NaCl was replaced by CaCl$_2$. The osmolarity of all solutions was kept the same. For measurements of the substrate-independent leak current, we used 10μM paroxetine. The leak was defined by subtraction of the respective currents ($I_{Na+} - I_{paroxetine}$). Recordings were started after a stable current base line had been established. The current was sampled with 100Hz and low pass-filtered with 20Hz.

Whole Cell Patch Clamp

For patch clamp recordings, HEK293 cells stably expressing hSERT N101A were seeded at low density for 24 hours before measuring currents. To measure substrate-induced hSERT currents, cells were voltage-clamped using the whole cell patch clamp technique. Briefly, glass

pipettes were filled with a solution consisting of 133mM potassium gluconate, 5.9mM NaCl, 1mM $CaCl_2$, 0.7mM $MgCl_2$, 10mM EGTA, and 10mM HEPES adjusted to pH 7.2 with KOH. For some experiments, the internal Cl^- concentration had to be increased. In these instances, the pipette solution consisted of 133mM KCl, 5.9mM NaCl, 1mM $CaCl_2$, 0.7mM $MgCl_2$, 10mM EGTA, and 10mM HEPES adjusted to pH 7.2 with KOH. The cells were continuously superfused with external solution: 140mM NaCl, 3mM KCl, 2.5mM $CaCl_2$, 2mM $MgCl_2$, 20mM glucose, and 10mM HEPES adjusted to pH 7.4 with NaOH. In those experiments where external Na^+ was replaced by Ca^{2+}, we used the following solution: 15mM $CaCl_2$, 150mM choline chloride, 1mM $MgCl_2$, and 10mM HEPES, adjusted to pH 7.2 with KOH.

Currents were recorded at room temperature (20–24°C) using an Axopatch 200B amplifier and pClamp version 10.2 software (MDS Analytical Technologies). Cells were voltage-clamped to potentials between −100 and −10mV, and 10μM 5-HT was applied for 5 seconds once every 60 seconds. Current traces were filtered at 1kHz and digitized at 2kHz using a Digidata 1320A (MDS Analytical Technologies). The liquid junction potentials were calculated, and measurements were compensated accordingly. Drugs were applied using a DAD-12 device (Adams & List, Westbury, NY), which permits complete solution exchange around the cells within 100ms. Current amplitudes in response to 5-HT application were quantified using Clampfit version 10.2 software. Passive holding currents were subtracted, and the traces were filtered using a 100-Hz digital Gaussian low pass filter.

Molecular Dynamic (MD) Simulations of hSERT·5-HT·Ion Complexes

MD simulations were conducted using hSERT and N101A mutant homology-modeled structures complexed with 5-HT and ions. Homology models of hSERT were based on the "open

to out" conformation of the leucine transporter (Protein Data Bank code 3F3A) and built using Prime (Prime, version 3.1, Schrödinger, LLC, New York). The alignment obtained in the structure prediction module of Prime was manually edited to match the comprehensive alignment by Beuming *et al.* (Beuming et al. 2006; Kaufmann et al. 2009). The loops were modeled and refined in Prime using an *ab initio* loop prediction method. Side chain optimization and minimization was conducted on loop candidates, and the models were validated for quality based on Ramachandran plots (Ramachandran et al. 1963) by PROCHECK validation (Laskowski et al. 1993) using the ADIT site. hSERT structural models were prepared for docking in the Protein Preparation Wizard (Sastry et al. 2013) (Schrödinger Suite 2012 Protein Preparation Wizard, Epik version 2.3, Schrödinger, LLC, New York; Impact version 5.8, Schrödinger, LLC, New York; Prime version 3.1, Schrödinger, LLC, New York) using default options. Protonated 5-HT conformers generated by LigPrep (LigPrep, version 2.5, Schrödinger, LLC, New York) were docked into hSERT homology models containing various combinations of Na^+, Ca^{2+}, and Cl^- utilizing the induced fit docking protocol (Sherman et al. 2006). The best scoring 5-HT-docked hSERT and N101A complexes were placed in the center (along the z axis, coinciding with the normal of the 1-palmitoyl-2-oleoyl-phosphatidylcholine bilayer) of the pre-equilibrated 1-palmitoyl-2-oleoyl-phosphatidylcholine lipid bilayer using the VMD visualization package (Humphrey et al. 1996). The dimensions of the simulation box were $20 \times 20 \times 14$Å, containing 1 protein, 1 ligand, and ~50,340 TIP3P water molecules and 222 1-palmitoyl-2-oleoyl-phosphatidylcholine molecules. 186 Na^+ ions and 191 Cl^- counterions were added to obtain an electroneutral system with a salt concentration of 150mM. All calculations were carried out with GROMACS version 4.5.4 (Hess et al. 2008), using a CHARMM27 force field under periodic

82

boundary conditions. The topologies and parameters files for the ligand were generated by the SwissParam tool (Zoete et al. 2011) based on the Merck molecular force fields that are compatible with CHARMM and GROMACS. All simulations were performed in the NPT ensemble with velocity scaling (V-rescale) thermostat and Parrinello-Rahman barostat. For the CHARMM force field operating in GROMACS, electrostatics were calculated using particle mesh Ewald with appropriate cut-offs: rlist = 1.3, rcoulomb = 1.3, rvdw = 1.2, vdwtype = switch, rvdw_switch = 0.8. Fourier spacing of 0.12nm and a particle mesh Ewald order of 4 were employed. V-rescale thermostat with a coupling constant of 0.1 ps was used to separately couple protein, lipid, and solvent, including water and ions. The pressure was coupled using the Parrinello-Rahman algorithm at 1 bar with a coupling constant $\rho = 1$ ps and a uniform compressibility of 4.5×10^{-5} bar^{-1}. The coordinates were saved every 100ps with an integration time step of 2fs. The LINCS (linear constraint solver) algorithm was used to restrain all bond lengths (Hess et al. 1997). The steepest descent algorithm in GROMACS was used to minimize the energy of the 5-HT-docked and ion-incorporated WT and N101A mutant hSERT structures in 1-palmitoyl-2-oleoyl-phosphatidylcholine bilayer followed by the equilibration phase. At the temperature of 303K, the initial velocities were generated following a Maxwellian distribution. The system was equilibrated for 1ns at a temperature of 303 Kby fixing the position of the docked complex by applying position restraints of 1000 kJ mol^{-1} nm^{-2} on each heavy atom, whereas lipids and water were allowed to move normally. After initial equilibration for 1ns, the production runs were performed for 12ns. The pressure was maintained at 1 atmosphere using semi-isotropic pressure coupling to a Parrinello-Rahman barostat with a coupling constant of 5ps. Conformations resulting from the production phase of each simulation were stored at

intervals of 100ps and analyzed. PyMOL (DeLano 2010) was used to generate the molecular graphic diagrams.

Results

N101 Mutation Specifically Modifies Cation Dependence, Allowing Ca^{2+} to Functionally Replace Na^+ for 5-HT Transport

Previously, we demonstrated that mutation of N101 to Ala or Cys conferred Cl^--independent transport to hSERT (Henry et al. 2011) while maintaining little to no loss in transport activity. Sequence analysis between hSERT and LeuT shows that the hSERT N101 residue corresponds to N27 in LeuT and N49 in dDAT, residues that directly coordinate Na^+ at the Na1 site. Direct coordination of N101 with Na^+ at Na1 is further supported by the fact that lengthening the side chain by one carbon through a N101Q mutation yields a non-functional transporter, whereas smaller side chains are tolerated (Henry et al. 2011). We examined the impact that mutations at N101 have on Na^+ coupling to 5-HT transport in hSERT. First, we looked for alterations in cation selectivity through measurement of $[^3H]$5-HT uptake in cells stably expressing the hSERT, hSERT N101A, or hSERT N101C mutant transporters in simple buffers containing only a single cation, where the cation was either Na^+, Ca^{2+}, Li^+, Ba^{2+}, NH_4^+, choline$^+$, $NMDG^+$, K^+, or Mg^{2+} (Figure 20). Appreciable 5-HT transport was observed with hSERT in the presence of Na^+-only buffer, which was 85% ± 6.3% of the uptake observed with complete buffer (see "Methodology"). Under the same conditions, the N101A and N101C mutants yielded uptake levels of 69 ± 2.8 and 63 ± 2.3%, respectively (Henry et al. 2011). The inability of K^+, Li^+, Mg^{2+}, Ba^{2+}, NH_4^+, choline$^+$, and $NMDG^+$ to functionally replace Na^+ in the N101 mutants for 5-HT uptake revealed that cation selectivity for 5-HT uptake is relatively
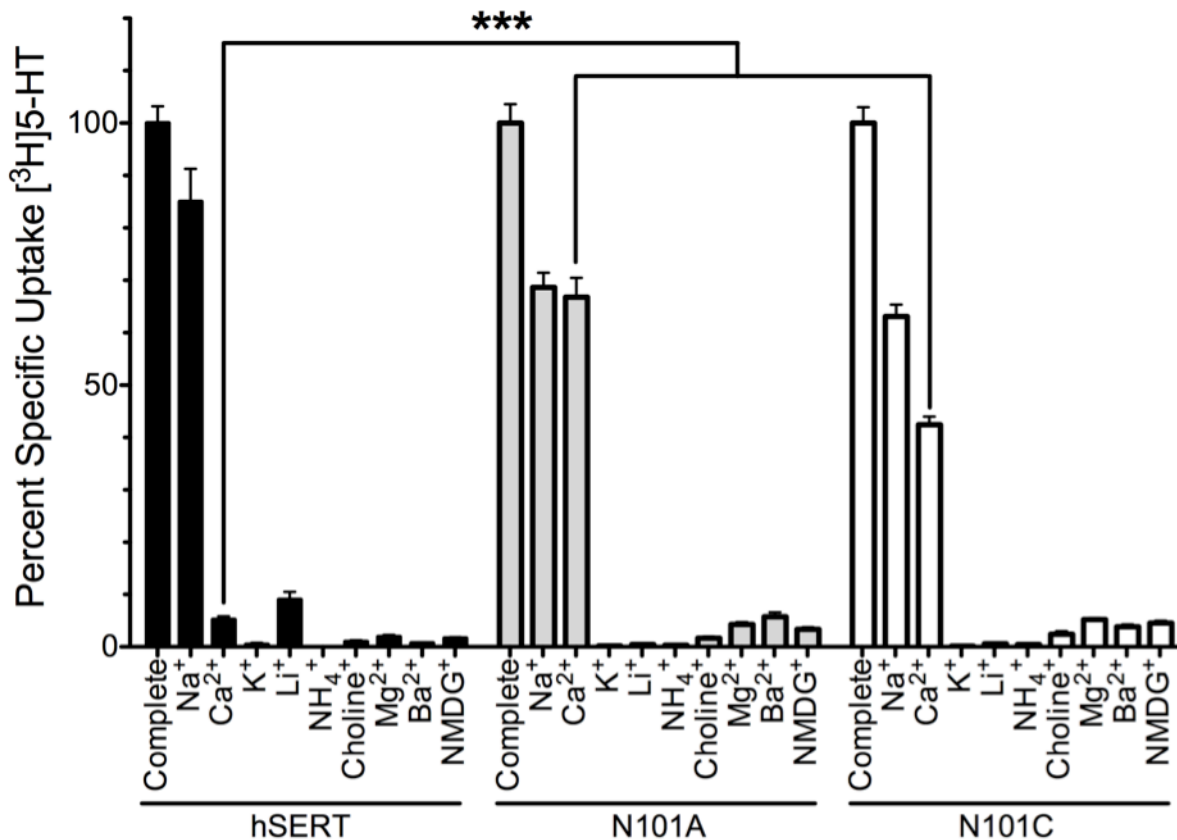
Figure 20. 5-HT uptake by N101 mutants under cation substitution reveals Ca^{2+} can functionally replace Na$^+$ in 5-HT transport. Transport activity was measured in HEK cells stably expressing hSERT, N101A or N101C. Initial transport rates (10 min.) were obtained in complete buffer or in the presence of a cation-ONLY buffer as indicated on the x-axis. Activity is given as percentage of uptake in complete buffer. A small amount of K$^+$ (5.4mM) was also added to each buffer, as transport activity was lost upon complete removal of K$^+$. Notably, K$^+$ alone is unable to support 5-HT uptake. The Ca^{2+} effect on uptake by the N101 mutants was specific, as 5-HT transport was not observed in Ca^{2+} only buffers using the parental cell line lacking hSERT. Each bar represents the mean and SEM of at least three independent experiments, each of which was performed in quadruplicate. A two-way ANOVA was performed on sample sets with a Bonferroni post-hoc test; *** = $p < 0.001$.
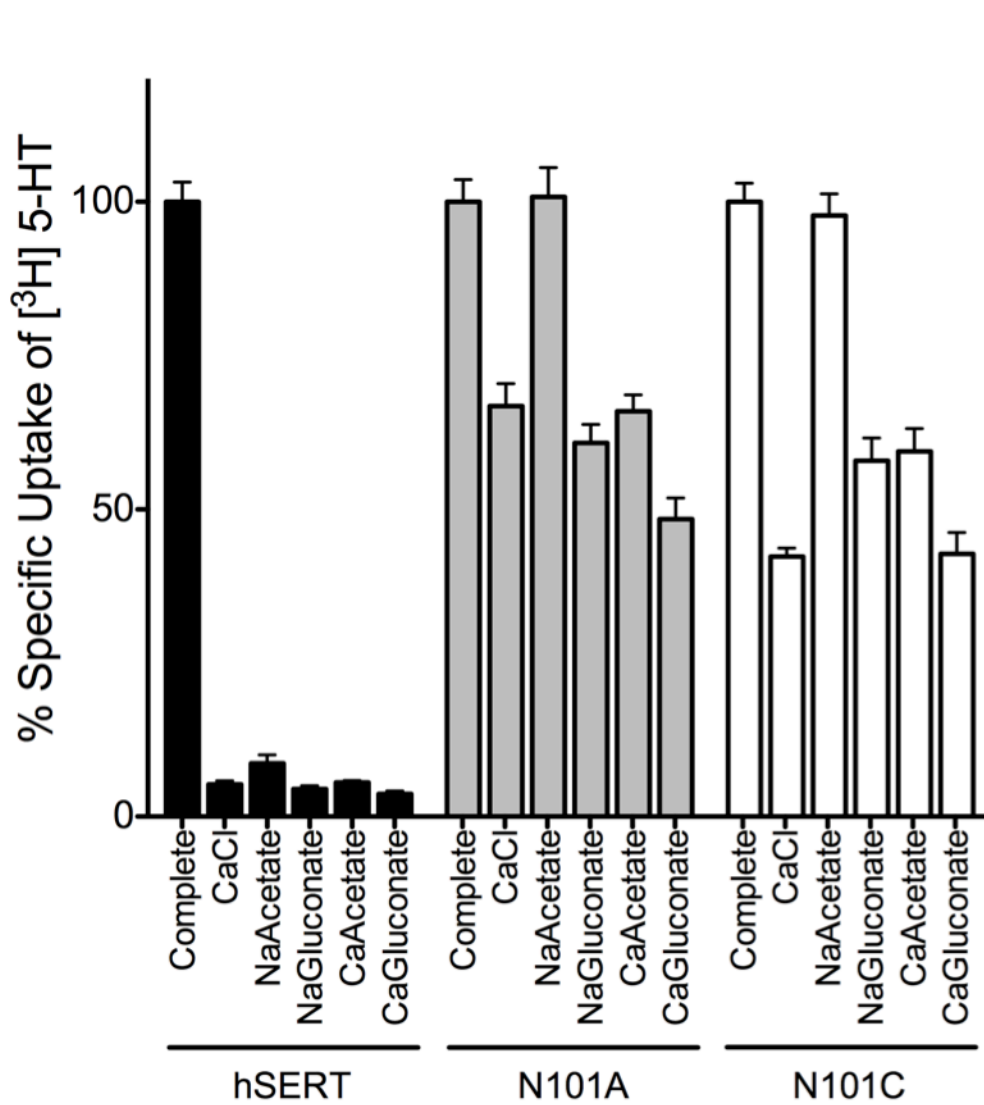
Figure 21. 5-HT uptake in N101 mutants under cation and/or anion ion replacement. Transport activity was measured in HEK cells stably expressing hSERT, N101A or N101C. Initial transport rates (10 min.) were obtained in complete buffer or in the presence of a buffer in which NaCl is replaced with 60mM $CaCl_2$, 120mM Na-acetate, 60mM Ca-acetate or 60mM Ca-gluconate. Activity was normalized to activity in complete buffer. Each bar represents the mean and SEM of three separate experiments, each performed in quadruplicate. Data were analyzed using a two-way ANOVA and Bonferroni post-hoc test.

86

intact. In fact, replacement of Na^+ with Ba^{2+} (hSERT), Li^+ (N101 mutants), and K^+ actually inhibited 5-HT uptake to levels below those observed with $NMDG^+$ (Figure 20). Remarkably, whereas native hSERT exhibited only $5.2\% \pm 0.6\%$ activity when Ca^{2+} replaced Na^+, Ca^{2+} could fully substitute for Na^+ in the N101A mutant, exhibiting the same degree of uptake observed in the Na^+-only buffer. Likewise, Ca^{2+} could substitute for Na^+ in the N101C mutant, albeit with less efficacy ($64.2 \pm 2.9\%$), suggesting that Ca^{2+} coordination may be suboptimal in the N101C mutant compared with N101A. Uptake of 5-HT under Ca^{2+}-only conditions maintained the Cl^- independence observed in Na^+-containing buffers (Figure 21).

Na^+, but Not Ca^{2+}, Imparts Conformational Changes in Native hSERT, whereas both Na^+ and Ca^{2+} Can Promote 5-HT-induced Conformational Changes in the N101A Mutant

The ability of Ca^{2+} to support 5-HT translocation by N101A and N101C mutants suggests that Ca^{2+} binding to SERT induces conformational changes similar to those obtained with Na^+. Inactivation of SERT-mediated 5-HT transport by cysteine-directed methanothiosulfanate (MTS) reagents (Chen 1997; Chen et al. 1997; Henry 2003) can be used as an indicator of conformational changes in hSERT (Androutsellis-Theotokis et al. 2001; Ni 2001; Androutsellis-Theotokis and Rudnick 2002; Henry et al. 2011). We used the membrane-impermeant (MTS) reagents MTSET to examine altered accessibility of residue C109 in the presence of Na^+, Ca^{2+}, and the large monovalent cation, $NMDG^+$, as well as the anions Cl^- and acetate$^-$. C109 is positioned on the extracellular end of TM1, a domain thought to undergo significant conformational change during substrate translocation (Krishnamurthy and Gouaux 2012). The extent of inactivation of hSERT by MTS adduction at C109 can be modulated by both cation and anion interactions with the transporter (Chen et al. 1997; Henry et al. 2011). In the presence of NaCl, hSERT was relatively insensitive to 1mM MTSET, and co-incubation with 20μM 5-HT
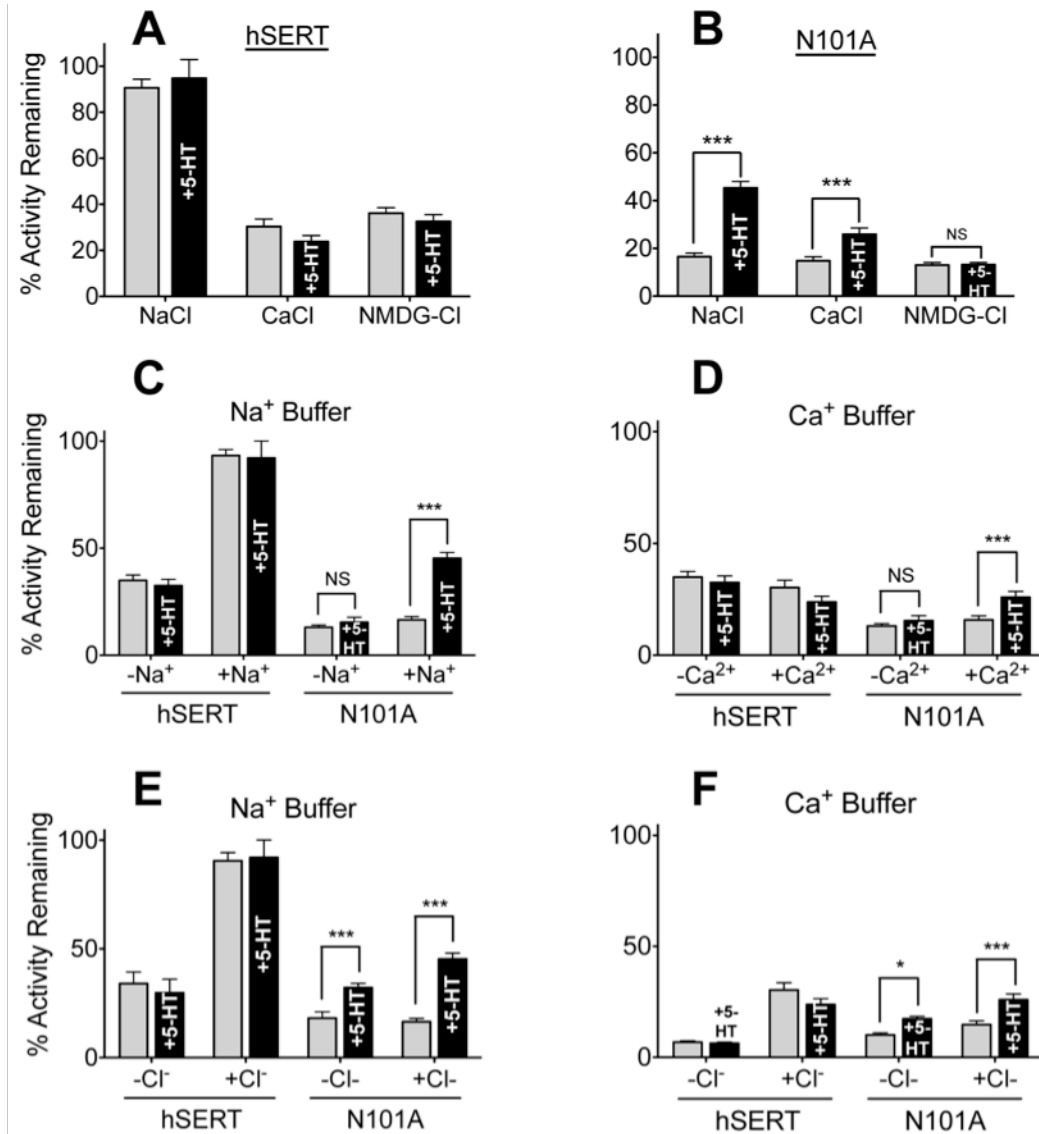
Figure 22. Ca^{2+} and Na^+ alter C109 accessibility to MTSET, suggesting these cations may promote similar conformational changes in the N101A mutant. HEK-293 cells expressing hSERT or hSERT N101A were pretreated with 1mM MTSET in the absence (*gray bars*) or presence (*black bars*) of 5-HT (20μM) and in the presence of Na^+, Ca^{2+} or $NMDG^+$. Following treatment, 5-HT uptake assays were performed in complete buffer to quantitate activity. Percent remaining activity is plotted and is defined as the amount of 5-HT uptake of MTSET-treated cells as a percent of untreated cells. Each bar represents the mean and SEM of at least three independent experiments, each of which was performed in quadruplicate. Panels (*A*) & (*B*) depict results of MTSET treatment on (*A*) WT hSERT and (*B*) hSERT N101A in each cation buffer. Panels (*C*) and (*D*) represent data from (*A*) and (*B*) replotted with respect to genetic background and the presence or absence of Na^+ (*C*) or Ca^{2+} (*D*). Panels (*E*) and (*F*) highlight the effect of Cl^- replacement under full Na^+ (*E*) or full Ca^{2+} (*F*) buffer conditions. A two-tailed *t*-test was performed on sample sets as indicated with brackets; *** = $p < 0.001$; * = $p < 0.05$; n.s = not significant.

had no detectable effect (Figure 22A). Substitution of Na^+ with either Ca^{2+} or $NMDG^+$ resulted in a significant increase in sensitivity of hSERT to MTSET, while co-incubation with 20μM 5-HT had no effect on sensitivity. In contrast, the N101A background revealed that C109 is highly sensitive to MTSET treatment, giving an $83.5 \pm 1.5\%$ loss of 5-HT transport in Na^+ buffer (Figure 22B). Importantly, a C109A/N101A mutant is insensitive to MTSET inactivation (Henry et al. 2011). Unlike in WT hSERT, co-incubation with 5-HT in the presence of Na^+ or Ca^{2+} significantly protected the N101A mutant from inactivation, yielding only a 55 ± 2.7 and $74 \pm 2.6\%$ loss of activity, respectively. Co-incubation of 5-HT with $NMDG^+$ did not afford the same protection from MTSET (Figure 22B). Thus, in the N101A mutant, Na^+ and Ca^{2+} are both capable of promoting conditions that, together with 5-HT, result in conformational changes in SERT. This effect was not observed with the larger $NMDG^+$ ion, which due to its bulk is unlikely to access the cation-binding site in hSERT (Mager et al. 1994). The data also reveal that both Na^+ and Cl^- are necessary for protection from MTS inactivation at C109 in hSERT, as removal of either ion results in a significant increase in sensitivity (Figure 22, C and E). However, Ca^{2+} cannot afford protection in WT hSERT, as the absence or presence of Ca^{2+} does not alter the sensitivity of C109 (Figure 22, D and F). In the N101A mutant, increased protection from MTS inactivation was not dependent on Cl^- but did require the presence of a cation (Na^+ or Ca^{2+}) and 5-HT (Figure 22, C–F), suggesting that conformational changes normally mediated by binding of only Na^+ and Cl^- require a cation and 5-HT in the N101A mutant.

hSERT N101 Mutants Display a Loss of Potency for Na^+ to Drive 5-HT Transport

Given that LeuT residue N27 and dDAT residue N49 are homologous to hSERT N101 and they directly coordinate Na^+ at the Na1 site (Yamashita et al. 2005; Penmatsa et al. 2013), it

is reasonable that mutations at N101 would directly impact Na^+ binding in hSERT. To evaluate this possibility, $[^3H]$5-HT uptake was measured using Na^+ dose-response assays, where Na^+ concentrations ranged from 0 to 120mM, and $NMDG^+$ or Ca^{2+} was used to compensate for the reductions in Na^+. When $NMDG^+$ was replaced by Na^+, the dose-response curves for N101A and N101C shifted rightward compared with WT, yielding increased EC_{50}^{Na+} values of 10.2 ± 3.0 and 18.3 ± 4.7mM, respectively, compared with 3.8 ± 1.2mM in hSERT (Figure 23A). The loss of N101 coordination of Na^+, due to its mutation to Ala or Cys, is consistent with the observed decrease of Na^+ potency, as well as the reduced ability of the N101 mutants to efficiently couple the Na^+ chemiosmotic gradient to 5-HT transport (Figure 23D) (Henry et al. 2011). A similar rank-order increase in the EC_{50}^{Na+} values for the N101 mutants is observed upon substitution of Na^+ with Ca^{2+} (28 ± 3.7 and 47 ± 6.1mM for N101A and N101C, respectively, compared with 16 ± 1.8mM for hSERT (Figure 23B)). Ca^{2+} has not previously been reported to modulate 5-HT transport in SERT; however, we found that at low Na^+ concentrations, Ca^{2+} was able to enhance 5-HT uptake (Figure 23B) in hSERT, whereas $NMDG^+$ did not (Figure 23A). In contrast, the presence of moderate to low levels of Ca^{2+} negatively affected 5-HT uptake as Na^+ levels increased, as evidenced by a shallower slope and increase in EC_{50}^{Na+} values compared with $NMDG^+$ replacement. Taken together, these data indicate that Ca^{2+} may act in a competitive manner to modulate the efficacy of Na^+ to support 5-HT transport in native hSERT.

Finally, equimolar replacement of $NMDG^+$ with Ca^{2+} yielded a dose-dependent increase in 5-HT transport that reached levels that were ~50% (N101A) and ~35% (N101C) of transport observed with 120mM Na^+. In contrast, the WT displayed minimal uptake (~5%) even at the highest Ca^{2+} concentration tested.
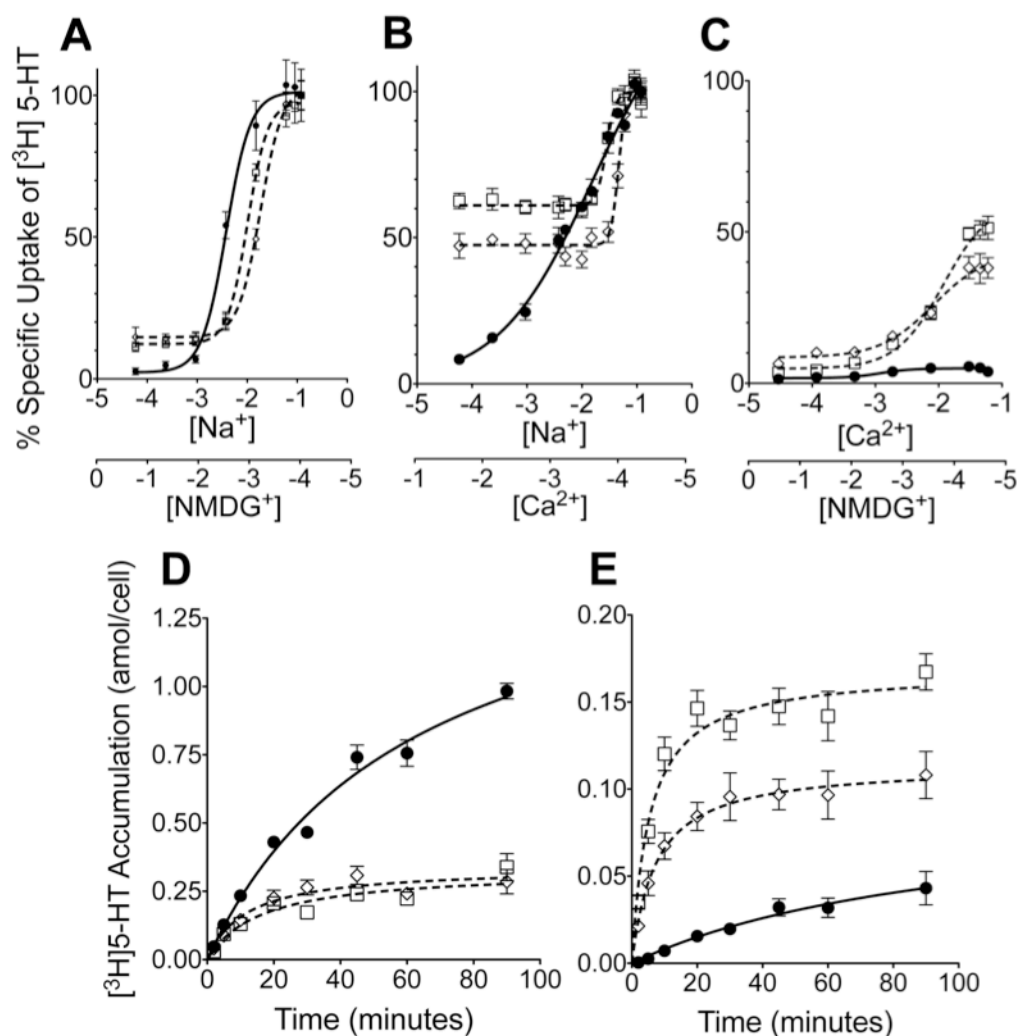
Figure 23. Cation dependency and concentrative uptake studies. Cation dependence analyses reveal N101 mutants display altered Na^+ and Ca^{2+} efficacies in driving 5-HT transport: Initial transport rates (10 min.) of [^{3}H]5-HT (50nM) were obtained for HEK cells stably-expressing hSERT (*filled circles*), N101A (*open circles*) or N101C (*open diamonds*) over a range of Na^+ concentrations (0 - 120mM) replaced with (*A*) $NMDG^+$ or (*B*) or Ca^{2+}. Uptake was also measured (*C*) using Ca^{2+} concentrations (0 - 60mM) replaced by $NMDG^+$. Transport activity is expressed relative to that at maximal Na^+ concentration. EC_{50} values were determined by fitting data to a sigmoidal dose-response curve (variable slope). Steady-state uptake kinetics reveals loss of concentrative capacity in N101 mutants: [^{3}H]5-HT uptake by HEK cells stably-expressing hSERT (*filled circles*), N101A (*open squares*) or N101C (*open diamonds*) in assay buffer containing (*D*) 120mM Na^+ or (*E*) 60mM Ca^{2+} is monitored over 120 min. Data are background subtracted using data from parental HEK cells. Data were converted to amol 5-HT accumulated per cell unit time. The data were fit to a Michaelis-Menten nonlinear regression equation using Prism 5. Each value represents the mean and SEM of a minimum of three independent experiments, each of which was performed using triplicate wells.

91

Mutation at N101 Diminishes the Ability of the Transporter to Concentrate 5-HT

Because the N101A and N101C mutants display diminished capacity to couple transport to the chemiosmotic gradients of Na^+ and Cl^-(Henry et al. 2011), we examined concentrative 5-HT uptake under both Ca^{2+} and Na^+ replacement conditions (Figure 23, D and E). As expected, concentrative transport of 5-HT by hSERT was all but eliminated (95% reduction) in Ca^{2+} buffer (Figure 23E). As previously demonstrated in chapter II (Henry et al. 2011), in Na^+-only buffer, concentrative uptake of 5-HT was significantly reduced in the N101A and N101C mutants compared with hSERT (Figure 23D). In Ca^{2+}buffer, concentrative uptake by the N101A and N101C mutants was reduced 51 and 32%, respectively, compared with equilibrium levels achieved with Na^+, suggesting that the hSERT-Ca^{2+} interaction is less efficient than Na^+ at coupling the ion gradient to 5-HT transport. Previously, we reported that the N101A and N101C mutants exhibit increased substrate efflux (Henry et al. 2011), which could account for part of the dramatic decrease in concentrative uptake. Differences were also observed for the time necessary to reach concentrative equilibrium. In Na^+, the $t\frac{1}{2}$ for hSERT was 62 ± 10 minutes compared with 16 ± 3.7 and 12 ± 3.1 minutes for N101A and N101C, respectively. The time for the mutants to reach steady state in Ca^{2+} is more rapid than in Na^+, with N101A reaching $t\frac{1}{2}$ at 5.4 ± 1.1 minutes and N101C at 7.3 ± 2.1 minutes, whereas in WT, the $t\frac{1}{2}$ is attenuated to 103 ± 59 minutes. To account for the fast saturation of the mutants, uptake assays were only 10 minutes in length.

Ca^{2+} Decreases the Apparent Affinity of 5-HT in both hSERT and the N101 Mutants

Kinetic transport analysis in Na^+ buffer yielded indistinguishable K_m values for hSERT ($1.2 \pm 0.4\mu M$), N101A ($1.6 \pm 0.5\mu M$), and N101C ($1.2 \pm 0.3\mu M$). As stated above, 5-HT uptake

by hSERT under Ca^{2+}-only conditions retains ~5% activity, which is sufficient to measure transport kinetics. Interestingly, K_m values for 5-HT transport increased in all three transporters by ~10-fold (hSERT, 14 ± 2.6μM; N101A, 18 ± 3.1μM; N101C, 11 ± 1.7μM). This equivalent increase in K_m for 5-HT in hSERT and the N101 mutants suggests that Ca^{2+} binds hSERT and the N101 mutants in a similar manner. When taken together with the fact that the Na1 site is thought to directly coordinate 5-HT, these data suggests that Ca^{2+} binds at Na1.

Mutations at Na2 Site Fail to Alter Cation Selectivity

Although the amino acid substitutions at N101 would directly implicate the Na1 site as the target for Ca^{2+} activity in the mutants, studies have suggested that an extensive ion network connects the Na1, Na2, Cl^-, and 5-HT binding sites (Forrest et al. 2007; Zomot et al. 2007; Henry et al. 2011; Zdravkovic et al. 2012). Therefore, it is possible that alterations in amino acids and their coordination at Na1 could structurally influence ionic coupling at Na2, permitting Ca^{2+} to bind at the Na2 site and activate transport. To investigate Ca^{2+} binding to Na2, amino acid substitutions were introduced at residues D437 and S438 in the Na2 site to disrupt their side chain carboxyl- and hydroxyl-mediated coordination with Na^+. The other amino acids comprising the Na2 site (G94, V97, and L434) were not mutated, because they coordinate the Na^+ion via backbone carbonyls. Functional characterization of the mutants with $[^3H]$5-HT uptake assays revealed that the conservative D437E mutant is non-functional, whereas the other substitutions showed 16–93% activity (Table 2). Activity of S438 mutants ranged from 27 to 94%, with the highest activity exhibited by the conservative S438T mutant. None of the substitutions at D437 or S438 conferred Ca^{2+}-mediated 5-HT transport (Table 2).

	% Surface Expression	Percent Activity		
		120 mM Na$^+$	60 mM Ca^{2+}	0 mM Cl$^-$
hSERT	100 ± 11	100 ± 4.7	3.23 ± 0.9	3.51 ± 0.4
N101A	77.7 ± 8.9	77.0 ± 4.2	68.9 ± 3.7	99.2 ± 8.5
N101C	62.4 ± 7.2	69.2 ± 5.3	42.5 ± 1.5	97.4 ± 5.5
D437A	115 ± 11	66.5 ± 7.8	6.53 ± 1.5	8.48 ± 2.0
D437C	109 ± 9.2	93.4 ± 5.4	6.91 ± 1.3	6.08 ± 0.8
D437E	N/A	N/A	N/A	N/A
D437T	85.7 ± 4.0	83.3 ± 5.6	5.64 ± 1.5	11.1 ± 1.6
D437V	78.7 ± 13	15.9 ± 4.3	5.93 ± 3.1	25.0 ± 6.1
S438A	101 ± 15	62.0 ± 6.5	6.08 ± 0.9	35.9 ± 3.4
S438C	105 ± 7.4	77.1 ± 4.1	1.97 ± 0.5	7.01 ± 1.4
S438T	131 ± 11	93.5 ± 5.6	4.18 ± 0.8	2.31 ± 0.3
S438V	48.0 ± 2.4	26.7 ± 5.1	5.13 ± 2.4	4.20 ± 1.3

Table 2. Determination of surface expression, transport activity and ion dependency for the Na1 and Na2 site mutants. Surface expression was calculated by performing densitometry of SERT bands from Western Blots of biotinylated surface proteins. Transport activity was measured in HEK cells expressing hSERT or indicated mutants with assays conducted in complete buffer. Activity of mutants in 120mM NaCl is expressed as percent of hSERT WT activity. Activity under Ca^{2+} or Cl$^-$ replacement conditions is expressed as percent uptake observed of the same construct in NaCl buffer. Each value represents the mean and SEM of triplicate wells from independent experiments repeated at least three times. No data is reported for D437E, as no measurable expression was present when transfected into HEK cells.
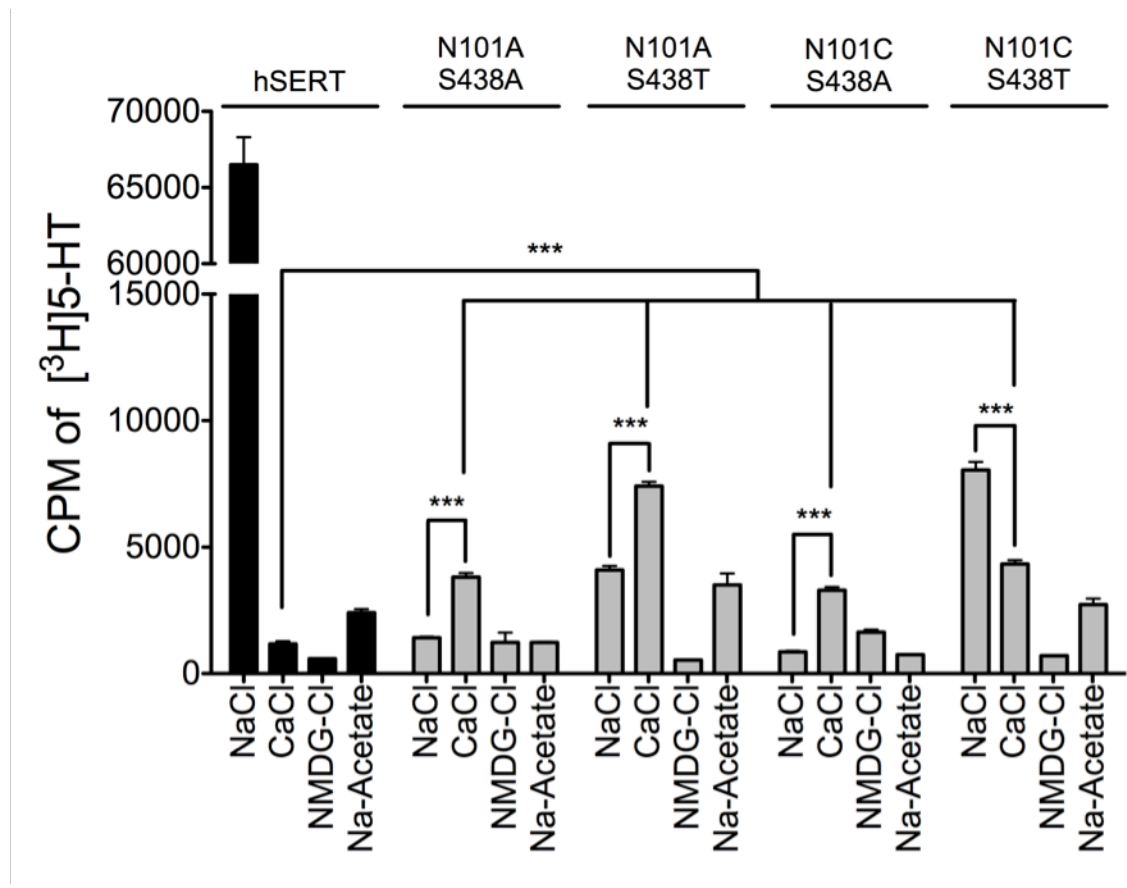
Figure 24. Introduction of the N101 mutations into the Na2 mutant backgrounds restored Ca^{2+}-dependent uptake activity. Transport activity was measured in HEK cells transiently expressing hSERT or a N101/S438 double mutant. Initial transport rates (10 min) were obtained in a Na$^+$-containing buffer (120mM) or in a buffer in which Na$^+$ was completely replaced by Ca^{2+} (60mM) or NMDG$^+$ (120mM). Each bar represents the mean and SEM for a figure representing three separate experiments, each performed in quadruplicate. Data were analyzed using a two-way ANOVA and Bonferroni post-hoc test; *** = p ≤ 0.001.

Simultaneous mutation of residues N101 and S438 was not well tolerated, resulting in a marked reduction in transport (1–12% remaining activity) (Figure 24). However, introduction of N101A or N101C into either the S438T or S438A background restored Ca^{2+}-supported translocation, which is consistent with Ca^{2+} interaction at Na1. Notably, Ca^{2+} was superior to Na^+ in supporting uptake in transporters containing the N101A/S438A, N101A/S438T, or N101C/S438A mutations. Conversely, the N101C/S438T mutant, which showed the most uptake activity of the double mutants, had greater levels of transport in Na^+ buffer compared with Ca^{2+}, but uptake in Ca^{2+} was still ∼6-fold greater than in NMDG buffer. These data further support the idea that Ca^{2+}-mediated influence on transport occurs through interaction at Na1 rather than Na2.

The Na1 Site Does Not Contribute to the Substrate-induced or Leak Currents in hSERT

SERT exhibits not only Na^+-dependent Na^+ and 5-HT flux but also 5-HT-gated suprastoichiometric current (Mager et al. 1994). Because our data support binding of Ca^{2+} at the Na1 site in hSERT, we surmised that analysis of the substrate-induced or leak currents in the N101 mutants under Ca^{2+} replacement conditions would provide insight into the contribution of the Na1-bound cation to the conductive states of hSERT. Therefore, we utilized two-electrode voltage clamping studies to examine currents generated by 5-HT transport via the N101A mutant in the presence of various concentrations of Na^+ and Ca^{2+}. Buffers containing different concentrations of Na^+, Ca^{2+}, or both cations were perfused into the system and allowed to equilibrate, after which 5-HT was added to induce transport-associated current. In the presence of only Na^+, an inward current of ∼-30nA is generated by the movement of a large amount of Na^+ ions through the WT transporter. When Na^+ is partially replaced by increasingly larger amounts of Ca^{2+}, the inward current displayed by hSERT decreases in a dose-dependent manner

(Figure 25A), whereas in the N101A mutant, the current persists; however, its magnitude is slightly decreased (Figure 25B). The large transient current observed upon the first addition of Ca^{2+} is not dependent on SERT and probably results from activation of endogenous channels because the same transient can be seen in uninjected oocytes upon the addition of Ca^{2+} (Figure 25B, *inset*). Therefore, after the initial addition of Ca^{2+} to the buffer, readings were taken only after a stable base line was reached.

Previous analysis of the N101 mutants in Na^+ buffer revealed a reversal potential of $\sim+70mV$ (Henry et al. 2011), indicating that Na^+ was the conducting ion. However, when we fully replaced Na^+ with Ca^{2+} in the N101A mutant, the reversal potential dropped to $\sim-30mV$, suggesting that Ca^{2+} does not carry the current when substituted for Na^+, because we would expect a more positive reversal potential if Ca^{2+} were now carrying the current (Figure 25C). Remarkably, this indicates that, unlike Na^+, Ca^{2+} does not seem to permeate through the transporter, which may also explain why current levels decreased when Na^+ was replaced by Ca^{2+} (Figure 25B). Under full cation replacement with 80mM Ca^{2+}, there is a prominent leak current, as defined by current block with 10μM paroxetine. This leak current also reverses at $-30mV$ (Figure 25C). A similar reversal potential for the substrate-induced current and the leak current is expected if both currents are carried by the same conformational intermediate, as recently suggested by Schicker *et al.* (Schicker et al. 2011). The fact that the reversal potential for $I_{5\text{-HT}}$ and I_{leak} occurs at $\sim-30mV$ suggests that Cl^- is the permeating ion. Unfortunately, we were unable to determine the *I*/V relationship for WT hSERT when Na^+ was replaced with 80mM Ca^{2+} because the currents were <2nA at $-60mV$.
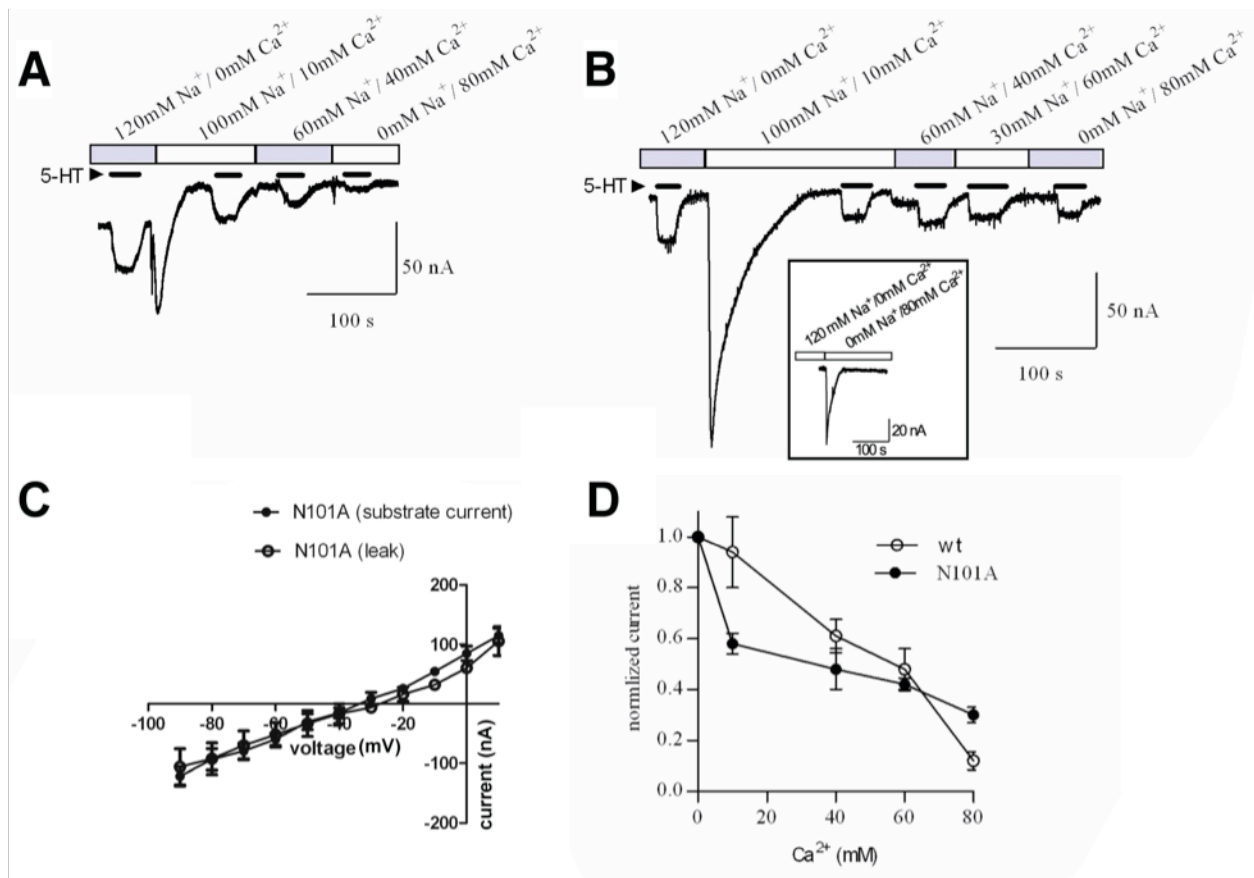
Figure 25. Whole cell clamp electrophysiology studies. Replacement of Na^+ with Ca^{2+}: Shown are representative current traces of (*A*) WT and (*B*) N101A, respectively, recorded from *Xenopus laevis* oocytes using the two-electrode voltage clamp (TEVC) technique. The cells were clamped to –60mV and currents were induced with 10μM 5-HT (*black bars*). The Ca^{2+} concentration was successively increased and the Na^+ concentration was simultaneously decreased as indicated. Upon wash in 10mM Ca^{2+}, a transient inward current was observed. The inset between panels (*A*) and (*B*) depicts bars representative of substrate-induced current from oocytes expressing N101A in the presence of Na^+ (*left bar*) or Ba^{2+} (*right bar*). (*C*) Current amplitudes elicited by 10μM 5-HT in WT (*open circles*) and N101A (*filled circles*) are plotted as a function of increasing Ca^{2+} concentrations (each data point is the average of 6 experiments). The remaining fraction of normalized current in WT and N101A at 80mM Ca^{2+} was 0.12±*0.35* and 0.30±*0.30* respectively. (*D*) The current-voltage dependence of 5-HT induced currents of the N101A mutant assessed in a solution containing 80mM Ca^{2+} are plotted (N=5). For the Ca^{2+} solutions, NaCl was replaced by $CaCl_2$. Shown are the IV for the substrate-induced current and the IV for the substrate independent leak in Na^+. The leak was defined by the application of 10μM paroxetine.
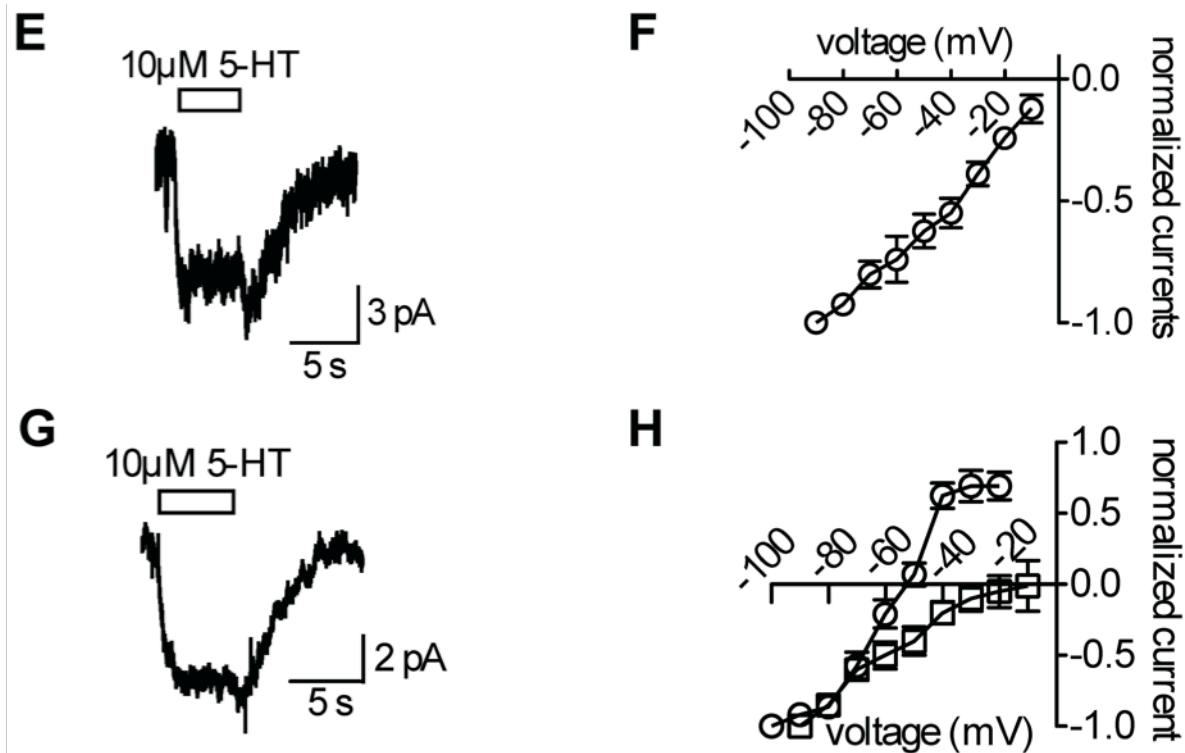
Figure 25 (continued). Whole cell clamp electrophysiology studies. (*E*) Shown is a representative current trace recorded from HEK-293 cells expressing hSERT N101A in the presence of physiological ion gradients. At –90mV, a 5 sec. application of 10μM 5-HT provoked an inwardly directed current. (*F*) Current responses to 10μM 5-HT were also measured at successively positive voltages. The currents were normalized to the maximum amplitude at –90mV and plotted as a function of the respective holding potential. (*G*) A typical trace of a current through hSERT N101A is shown in the absence of external Na^+ but in the presence of 15mM external Ca^{2+}. At –90mV the current induced by 10μM 5-HT was inwardly directed. (*H*) However, this current reversed at around –60mV, when the inner Cl^- concentration was low (5mM) (*open circles*) or around 0mV at high (140mM) inner Cl^- concentrations (*filled boxes*).

Because Ca^{2+} does not appear to be transported and carry current, we wanted to see if the addition of Ca^{2+} could inhibit Na^+-mediated currents by examining transport-mediated currents at increasing concentrations of Ca^{2+} (Figure 25D). We found that hSERT exhibited a linear, dose-dependent decrease in current as Ca^{2+} concentration increased (and Na^+ concentration decreased). In contrast, N101A displayed a hyperbolic curve, indicating that Ca^{2+} reduces the amount of Na^+-generated current.

Finally, although Ba^{2+} can often functionally replace Ca^{2+} in channels (Partridge and Leach 1991), Ba^{2+} was unable to support substrate-induced currents in the N101A mutant (data not shown). This is consistent with the failure of Ba^{2+} to promote transport in radiolabeled 5-HT uptake studies (Figure 20), revealing that Ca^{2+} binding is selective and is a prerequisite for current generation.

Whole Cell Clamp of the N101A Mutant in HEK293 Cells Suggests That Cl^- Is the Main Charge Carrier When External Na^+ Is Substituted by Ca^{2+}

In order to further test if Cl^- (and not Ca^{2+}) is the main charge carrier by the N101A mutant, we performed whole cell patch clamp analysis on HEK293 cells stably expressing hSERT N101A. This technique allowed us to control the internal ion composition, thus facilitating the interpretation of the reversal potential. When cells were recorded in the presence of an external solution containing 152mM Na^+, application of 10μM 5-HT for 5 seconds provoked an inwardly directed current at a holding potential of −90mV (Figure 25E). Current-voltage analysis in the presence of full external Na^+ was performed (Figure 25F); however, excessive noise occurred at voltages positive to −10mV (probably due to endogenous channels), precluding analysis in that voltage range. When Na^+ was removed from the external solution and replaced with 15mM Ca^{2+} and 150mM choline, 10μM 5-HT was still able to induce current

(Figure 25G). In HEK293 cells, unlike oocytes, full replacement of Na^+ by Ca^{2+} (80 mM) resulted in unstable electrical recordings. For this reason, we employed a solution containing Ca^{2+} and choline that has been used in studies of voltage-gated Ca^{2+} channels (Bock et al. 2011). Importantly, choline could not support 5-HT uptake in WT SERT or the N101A or N101C mutants (Figure 20); therefore, the data represent the contribution of extracellular Ca^{2+}. In this buffer, application of 5-HT led to currents that were absent in cells expressing WT hSERT (data not shown). Current-voltage relationships were recorded with 15mM external Ca^{2+} and two internal Cl^- concentrations. The current reversed at -55mV when the internal Cl^- concentration was 9.3mM compared with a reversal potential of ~-5mV when internal Cl^- was at 143.3mM (Figure 25H). These observed shifts in reversal potential in response to internal Cl^- concentration suggest that Cl^- mediates the current in the N101A mutant when Ca^{2+} is the supporting cation.

hSERT N101 Mutants Appear to Function as both Active and Passive Transporters

Comparison of 5-HT saturation uptake in hSERT with buffers containing either Na^+ or $NMDG^+$ reveals that, when Na^+ is completely replaced by $NMDG^+$, increasing the amount of extracellular 5-HT only marginally elevates substrate uptake in a dose-dependent manner (Figure 26). In contrast, both N101 mutants demonstrate enhanced substrate uptake in response to increasing extracellular 5-HT, suggesting that the inside/outside gradient of 5-HT is better able to drive transport in the mutants. Furthermore, the similar levels of uptake by the N101 mutants in the presence or absence of Na^+ suggest that the mutant transporters do not couple efficiently to the Na^+ gradient and may act more as passive-facilitative transporters when extracellular 5-HT levels are high.
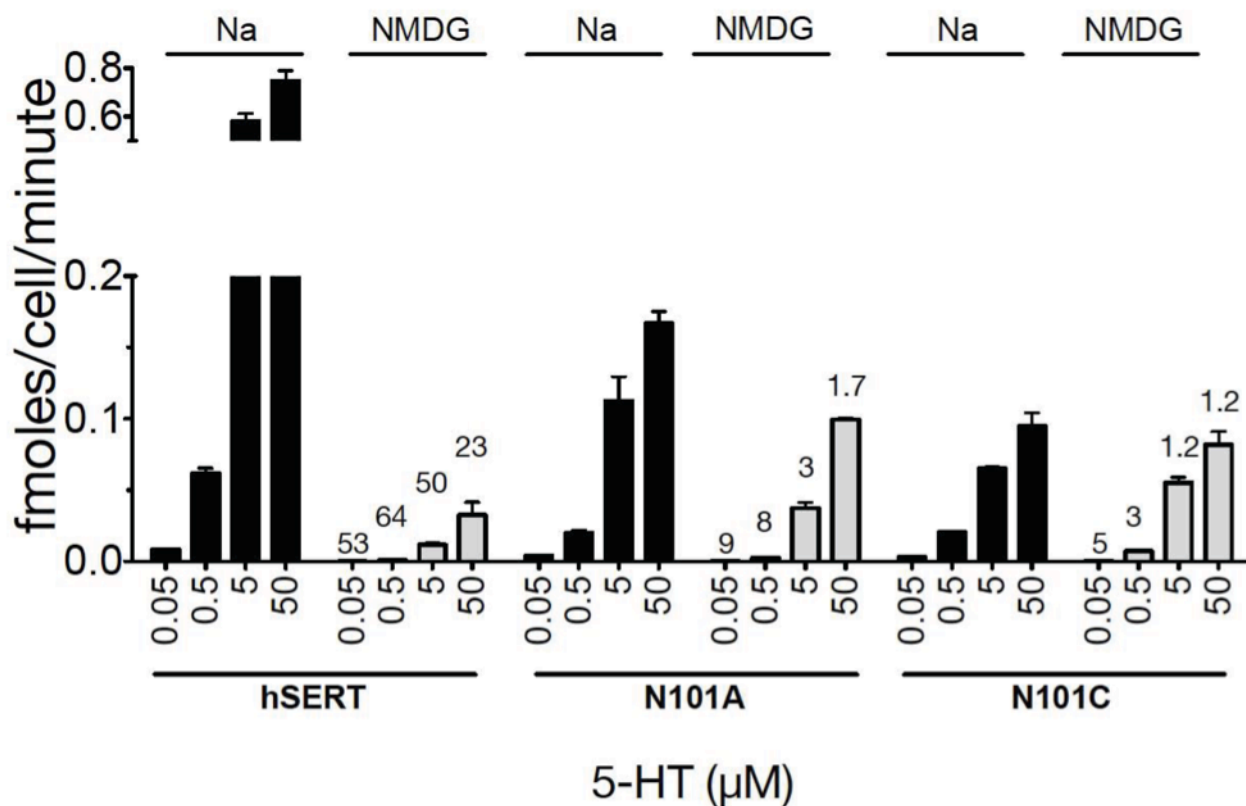
Figure 26. N101 mutants exhibit increased in 5-HT dose-dependent levels of substrate transport in the absence of Na$^+$. HEK cells stably expressing the hSERT, N101A, or N101C were evaluated for dose-dependent 5-HT uptake after 15 min in the presence (*black bars*) or absence (*gray bars*) of Na$^+$. Data was converted to fmol 5-HT transported per cell per minute. Each bar represents the mean and SEM of a data set representing at least three independent experiments, each of which was performed in triplicate. Numbers above gray bars indicate the fold-decrease in activity when comparing the corresponding experimental condition in Na$^+$ buffer. A two-way ANOVA performed on sample sets with a Bonferroni post-hoc test revealed that all mutant fold-decreases in activity were significantly different than the same experimental paradigm in WT hSERT ($p < 0.001$).

Molecular Dynamics Simulations Suggest a Mechanism for Ca²⁺ Gain-of-function Phenotype

The dramatic impact the N101 mutation has on ion- and substrate-coupled translocation suggested that mechanisms important to the translocation process could be revealed through comparison of hSERT and the N101A mutant in molecular dynamic simulations. To carry out these studies, 5-HT and ion-docked comparative models of hSERT and N101A were subjected to 12ns of MD simulations in a lipid bilayer system to investigate alterations in ion coordination (Table 3). Simulations of hSERT Na1^{Na+}, Na2^{Na+}, and Cl^{Cl-} with 5-HT bound revealed that coordination of Na$^+$ at Na1 was optimal, with a coordination number of 6 (CN:6) (Harding 2002) (Table 3) and was identical to that shown for LeuT (Yamashita et al. 2005). Likewise, coordination of Na$^+$ at Na2 was similar to that in LeuT and dDAT except that the Oγ S438 (S335 in LeuT, S421 in dDAT) interaction with Na$^+$ (expected by homology to LeuT) was varied based on the system. Cl$^-$ coordination was similar to that reported by Tavoulari *et al.* (Tavoulari et al. 2011) with the addition of Gln-332 Nε (Ben-Yona et al. 2011; Tavoulari et al. 2011). dDAT residue Gln-316, which is homologous to Gln-332, coordinates Cl$^-$ in the crystal structure (Penmatsa et al. 2013). The Cl$^-$ ion was omitted from MD simulations with the N101A mutant, because these transporters exhibit Cl$^-$ independence (Henry et al. 2011). As indicated by the reduced potency for Na$^+$ to support 5-HT uptake in the N101 mutants, the simulations reveal that coordination of Na$^+$ at Na1 in N101A is decreased to CN:5, due to the loss of the N101 Oδ interaction.

Notably, we observed a correlation between transporter function and the coordination state of the carboxyl side chain of residue D98 in Na1. 5-HT lacks the carboxyl group found on amino acid substrates, such as leucine, and this Asp at position 98, which is strictly

WT:

Na1: A_{96} O, D_{98} Oδ, N_{101} Oδ, S_{336} O Oγ, N_{368} Oδ; n=6

Na2: G_{94} O, V_{97} O, L_{434} O, D_{437} Oδ_1 Oδ_2; n=5

Cl: Y_{121} HH, Q_{332} Nε, S_{336} Hγ, N_{368} Hδ, S372 Hγ; n=5

WT: without Cl

Na1: A_{96} O, D_{98} Oδ_1 O$\delta_{2\,(0.8)}$, N_{101} Oδ, S_{336} O$_{(0.5)}$; n=5

Na2: G_{94} O, V_{97} O, L_{434} O, D_{437} Oδ_1 Oδ_2; n=5

WT: with Ca, Na, & Cl

Ca1: A_{96} O, D_{98} Oδ_1 Oδ_2, N_{101} Oδ, S_{336} O; n=5

Na2: G_{94} O, V_{97} O, L_{434} O$_{(0.9)}$, D_{437} Oδ_1 Oδ_2; n=5

Cl: Ca^{2+}, N_{101} Oδ, S_{336} H$\gamma_{(0.9)}$; L_{337} N $_{(0.5)}$; n=4

WT: without Cl, without 5HT

Na1: A_{96} O, D_{98} Oδ_1 Oδ_2, N_{101} Oδ, S_{336} O $_{(0.945)}$, n=5

Na2: G_{94} O, V_{97} O, L_{434} O $_{(0.7)}$, D_{437} Oδ_1 Oδ_2; S_{438} Oγ ; n=5.7

WT: without 5HT

Na1: A_{96} O, D_{98} Oδ_1 Oδ_2, N_{101} Oδ $_{(0.9)}$, S_{336} O $_{(0.9)}$, n=4.8

Na2: G_{94} O, V_{97} O, L_{434} O $_{(0.8)}$, D_{437} Oδ_1 Oδ_2 ; S_{438} O$\gamma_{(0.9)}$; n=5.6

Cl: Y_{121} HH, Q_{332} Nε, S_{336} Hγ, S372 Hγ; S369 Hγ $_{(0.2)}$; n=4.1

N101A: without Cl

Na1: A_{96} O, D_{98} Oδ_1 O$\delta_{2(0.2)}$, S_{336} O Oγ, N_{368} Oδ; n=5

Na2: G_{94} O, V_{97} O, L_{434} O $_{(0.5)}$, D_{437} Oδ_1 Oδ_2; n=4.5

N101A: with Ca, without Cl

Ca1: D_{98} Oδ_1 O$\delta_{2\,(0.9)}$, S_{336} O Oγ, N_{368} Oδ; n=5

Na2: G_{94} O, V_{97} O, L_{434} O, D_{437} Oδ_1 Oδ_2; n=5

N101A: with Ca, without Na, without Cl

Ca1: A_{96} O $_{(0.6)}$, D_{98} Oδ_1 Oδ_2, S_{336} O $_{(0.6)}$ Oγ $_{(0.7)}$, N_{368} Oδ; n=6

Table 3. Molecular dynamics simulation occupancies. Occupancies for atomic coordinations were calculated over 12ns of simulation and are scaled from zero to one with one being 100% occupancy within the designated distance cutoffs (Na$^+$ 3.5 Å, Ca^{2+} 3.5 Å and Cl$^-$ 4.0 Å). Occupancies that were not equal to one were notated in subscript parentheses.
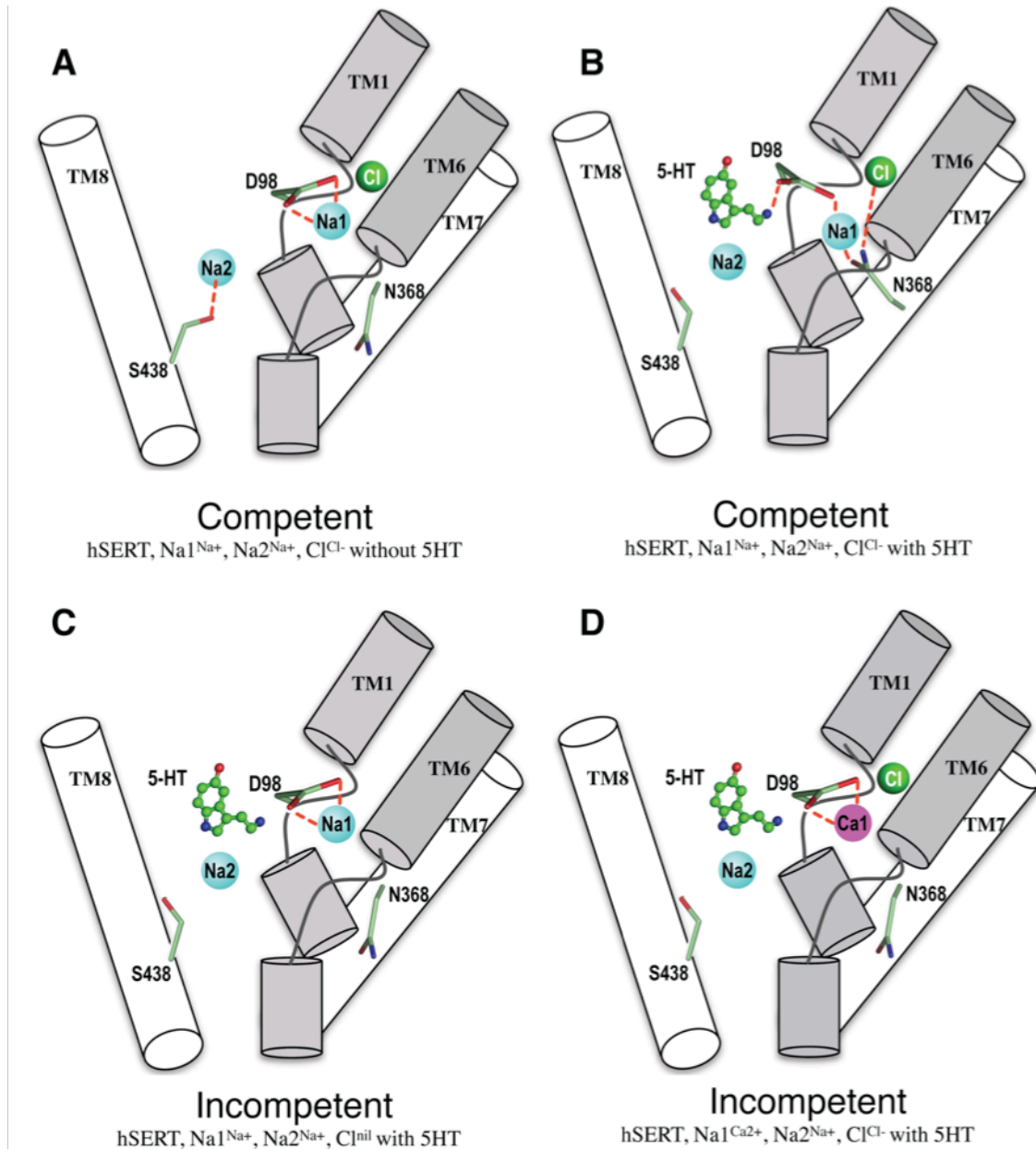
Figure 27. Proposed model for the coupling of Na1, Na2 and Cl sites to substrate transport in WT hSERT. Core regions of TMs 1, 6 (*gray*) and 7, 8 (*white*) of hSERT are displayed for clarity. Highlighted residues D98, N368 and S438 are shown as sticks. 5-HT is depicted in ball and stick representation. Na^+, Ca^{2+} and $Cl^−$ ions are represented as blue, magenta and green spheres, respectively. Red dashed lines indicate coordination. Panels demonstrate: **1.** D98 coordination determines hSERT transport competency – D98 coordinates both Na1 and 5-HT when hSERT is transport competent (*B*), while D98 exhibits bidentate coordination to Na1 when simulations lack 5-HT (*A*) or $Cl^−$ (*C*), as well as when Ca^{2+} is placed at Na1 (*D*). **2.** Bound 5-HT alters S438 coordination of Na2 – In simulations lacking 5-HT, S438 interacts with Na2 (*A*), whereas simulations with 5-HT bound reveal S438 does not coordinate Na^+ at Na2 (*B-D*). **3.** N368 does not interact with Na1 in transport incompetent hSERT (*A, C, D*).

105

conserved among MATs, is believed to serve as the functional correlate to the leucine carboxyl group in support of Na^+ and 5-HT binding. In the inhibitor bound dDAT structure, this conserved Asp (D46) indirectly coordinates Na^+ at Na1 through a water molecule (Penmatsa et al. 2013). However, it is possible that direct Na^+-Asp^- interaction may occur in substrate-bound dDAT.

In the absence of 5-HT, the side chain of D98 in WT SERT exhibits bidentate coordination ($O\partial1$, $O\partial2$) with the Na^+ at Na1 (Figure 27A). However, in 5-HT-bound models, D98 coordination to Na1 is monodendate, with one $O\partial$ from the carbonyl participating in coordination of the (+)-charged amine of 5-HT (Figure 27B). Simulations involving an empty Cl site revealed that D98 retains bidentate coordination with Na1 and, importantly, lacks coordination with 5-HT (Figure 27C). This apparent Cl^--dependent coordination of D98 to 5-HT is consistent with previously published findings, where Cl^- binding to hSERT decreased the K_m of 5-HT ~4-fold (Nelson and Blaustein 1982; Henry et al. 2011; Koldsø et al. 2011). In contrast, simulations with the N101A mutant with Na^+ reveal that D98 ($O\partial$) can coordinate the amine of 5-HT even in the absence of Cl^-. This loss of Cl^--dependent coordination of D98 in the N101A background could explain why, under Cl^--free conditions, the N101A mutant exhibits a K_m for 5-HT that is comparable with values obtained with the Cl^--bound WT hSERT (Henry et al. 2011).

Analysis of Ca^{2+} at Na1 revealed bidentate coordination between Ca^{2+} and the side chain of D98 under all simulation conditions, which precludes D98–5-HT coordination (Figure 27D). This loss of 5-HT stabilization is consistent with our finding that under Ca^{2+}-only conditions, WT hSERT as well as the N101 mutants exhibit a 10-fold increase in K_m for 5-HT compared with Na^+-containing buffers. Evaluation of the transport-competent and -incompetent complexes

with the non-functional transporters represented by hSERT without Cl⁻ and hSERT with Ca^{2+} in the Na1 site and Cl⁻ in the Cl site revealed reorganization of residues S336 and N368 in the Na1 site. These amino acids have been reported to be critical for Na^+ and Cl⁻ coordination (Forrest et al. 2007; Zomot et al. 2007; Ben-Yona et al. 2011; Tavoulari et al. 2011; Zdravkovic et al. 2012). In the non-functional transporters, the side chain of residue S336 is oriented with Hγ pointing away from the reported Cl⁻-binding site as per Forrest *et al.* (Forrest et al. 2007) (Figure 28A). In contrast, all of the transport competent structures have the Hγ directed toward the Cl⁻-binding site (Figure 28B). Likewise, N368, which normally coordinates the Na^+ at Na1, as shown in the transport-competent structures, is flipped away from the Na1 site in the non-functional models, losing contact with both the Na1 and Cl⁻-binding sites. These data suggest that the availability of S336 and N368 to participate in the Na1 and Cl coordination sites plays a critical role for transport function and provide a mechanistic explanation for 1) the inability of Ca^{2+} to substitute for Na^+ in the WT transporter, 2) the loss of function of WT transporter in the absence of Cl⁻, and 3) the gain of function by the N101A mutant to utilize Ca^{2+} or Na^+ without Cl⁻.

Finally, we evaluated ion coordination at Na2 in our MD simulations, in light of our biochemical data, to look for possible clues to the functional role of Na2 in transport. In simulations lacking 5-HT, we found that the TM8 residue S438 coordinates the Na^+ ion at Na2 (Figure 27A). However, in 5-HT-bound simulations, the S438 side chain reorients away and no longer participates in coordination of the Na2 ion, suggesting that 5-HT binding may contribute to destabilization of the Na2 site (Figure 27, B–D). Further analysis of the simulated transporter systems revealed that transporters lacking coordination between S438 and Na^+ at Na2 were functionally competent in biochemical analysis, suggesting that loss of S438/Na2 coordination
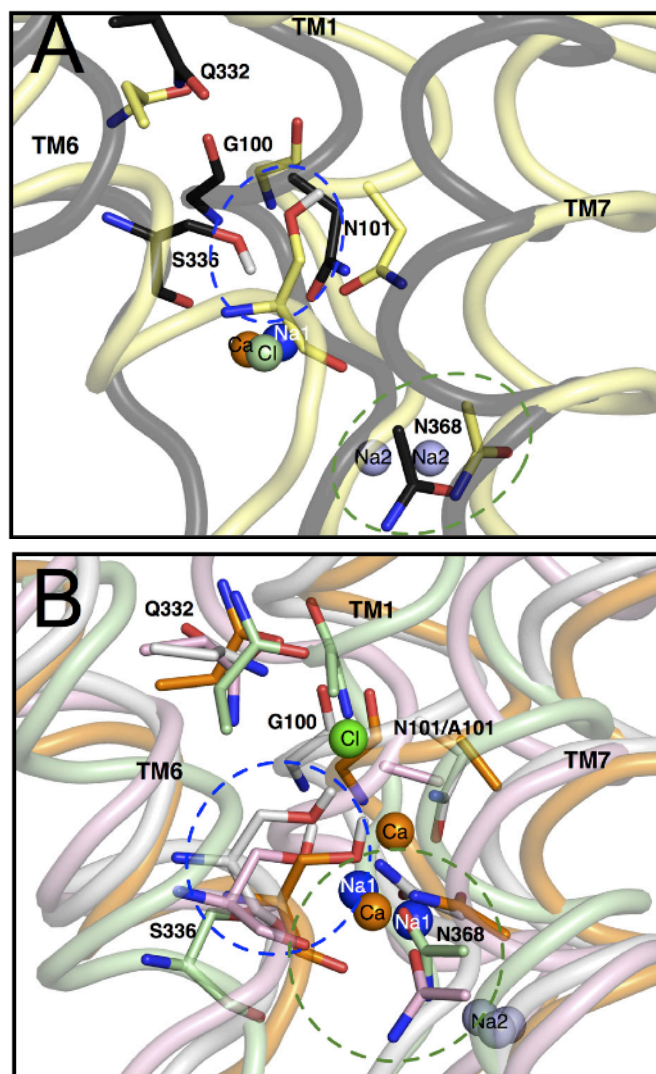
Figure 28. MD simulations of hSERT comparative models support a mechanistic role for Na1 site coordinating residues. (*Panels A and B*) 5-HT-docked comparative hSERT models were simulated in a lipid bilayer system for 12ns using GROMACS. Models were simulated with various combinations of ions representative of our biochemical analyses. The constructs were named using the convention where hSERT Na1^{Na+}, Na2 $^{Na+}$, Cl^{Cl-} represents hSERT with Na$^+$ at Na1, Na$^+$ at Na2 and Cl$^-$ at Cl. Empty ion binding sites are not listed. The peptide backbones are shown as tubes colored as follows: *[1]* hSERT Na1-Na2-Cl (*white*), *[2]* hSERT Na1-Na2 (*yellow*), *[3]* hSERT Ca1-Na2-Cl (*black*), *[4]* N101A Na1-Na2 (*orange*), *[5]* N101A Ca1-Na2 (*pink*) and N101A Ca1 (*green*). The structures were aligned using Cαs in Pymol and for clarity only TMs 1, 6 and 7 are shown. Na1^{Na+}, Na2^{Na+}, Cl$^-$ and Ca^{2+} are represented as blue, purple, green and orange spheres, respectively. Panels are representative trajectories from simulations under (*A*) transport incompetent and (*B*) competent conditions. Residues of interest are depicted as sticks. The blue and green dashed ovals highlight the orientation of the S336 and N368 side chains, respectively.

may be important for progression through the transport process (Table 3 and Figure 27, A and B). However, two simulated systems did not follow this rule. The WT hSERT, 5-HT, Na1^{Na+}, and Na2^{Na+}, which lacks Cl$^-$ (Figure 27C), and the WT hSERT, 5-HT, Na1^{Ca2+}, Na2^{Na+}, and Cl$^-$, which has Ca^{2+} bound to Na1 (Figure 27D), are both functionally inactive yet lack the S438/Na2 interaction. This discrepancy can be explained if the loss of the S438/Na2 interaction disturbs the hydrogen bond network linking Na2 to the Cl and Na1 sites, thereby disrupting their function as molecular checkpoints and preventing translocation by the WT transporter unless the appropriate ions and substrate are bound. In contrast, although the N101A transporter also exhibits Na2 destabilization due to loss of S438 interaction, substrate translocation can proceed relatively unchecked because Na2 is uncoupled from the Na1 and Cl sites (as evidenced by functionality in the absence of Cl$^-$ or when Ca^{2+} replaces Na$^+$).

Discussion

This study presents biochemical, electrophysiological, and computational analyses of mutations in a conserved Asn residue (N101) in TM1 of hSERT that is part of the proposed Na1 binding site. The findings of this work reveal that, in addition to the previously reported Cl$^-$ independence afforded by mutation of N101 (Henry et al. 2011), the N101A and N101C mutants can utilize Ca^{2+}, in addition to Na$^+$, to support 5-HT uptake. The unique properties afforded by these substitutions at N101 have allowed us to uncover distinct roles for the Na1 and Na2 sites in the 5-HT transport process.

Conformational studies based on TM1 sensitivity to MTS reagents support the Na$^+$-like behavior of Ca^{2+} in the N101 mutants, because both Na$^+$ and Ca^{2+}, but not the large cation

NMDG$^+$, impart conformational changes to the N101A mutant transporter. Also, Ca^{2+} alters the dose dependence of Na$^+$for 5-HT uptake and was able to support small but detectable 5-HT-induced currents in native hSERT. This suggests that Ca^{2+} can bind to WT hSERT but leads to a primarily non-productive coordination state, one that can be overcome in the N101 mutant background.

The functional interplay between the Na1, Na2, and Cl binding sites (Yu et al. 2010; Zdravkovic et al. 2012; Zhao et al. 2012) presented a challenge to delineate where Ca^{2+} binds to promote transport in the N101 mutants. However, we uncovered several lines of evidence indicating that Ca^{2+} binds at Na1. First, mutation at N101 resulted in Ca^{2+}-dependent transport, whereas mutations at Na2 site residues failed to yield Ca^{2+}-dependent uptake. (Interestingly, two of the Na2 mutants displayed significant Cl$^-$ independence (Table 2)). Second, introduction of N101A or N101C mutations into the Na2 mutant backgrounds yielded Ca^{2+}-mediated transport. Third, the K_m of 5-HT for hSERT, as well as the N101 mutants, increases 10-fold in Ca^{2+}-only buffers. This decrease in apparent affinity of 5-HT is consistent with our MD analyses showing that Ca^{2+} binding at Na1 results in bidentate coordination between Ca^{2+} and the conserved Asp (D98) in TM1. The nature of this interaction precludes the ability of D98 to stabilize 5-HT binding, by preventing the D98 side chain from interacting with the (+)-charged amine of 5-HT in agreement with the increased 5-HT K_m.

Remarkably, although our data suggest that Ca^{2+} binds to Na1, reversal potentials from I/V analyses suggest that Cl$^-$, and not Ca^{2+}, is the major carrier of current in the N101A mutant. Furthermore, Ca^{2+}does not appear to permeate during transport in the N101 mutant. This finding, combined with our evidence that Ca^{2+} binds at Na1, supports distinct roles for Na1 and

Na2 in the translocation process. This assertion is strengthened by sequence comparison analysis and crystal structures (Pramod et al. 2013), which reveal that Na2, in contrast to Na1, is absolutely conserved among LeuT-like transporters and therefore probably serves to couple substrate translocation to the Na^+ gradient. This essential role of Na2 is also supported by inward facing crystal structures (Krishnamurthy and Gouaux 2012) and molecular dynamic studies (Watanabe et al. 2010; Koldsø et al. 2011), which indicate that the destabilization of Na2 and release of its coordinated Na^+ ion are critical steps for substrate release. Based on this understanding, if Ca^{2+} were able to bind at Na2 in the N101 mutants, a Ca^{2+} ion would probably be released into the cytoplasm during 5-HT translocation. However, our electrophysiological data argue against contribution of Ca^{2+} to the substrate-induced or leak currents in the N101A mutant under full replacement of Na^{2+} by Ca^{2+}. Collectively, these findings support the binding of Ca^{2+} to the Na1 site, which allows us to propose that the ion bound at Na1 (*i.e.* Na^+ or Ca^{2+}) is not co-translocated during stoichiometric transport. However, we acknowledge that we may not be able to detect low level Ca^{2+} flux. Nevertheless, such a mechanism, where only the Na^+ at Na2 is co-transported, agrees with the historical $^1Na_{in}$:^{1}5-HT$_{in}$:$^1Cl_{in}$:$^1K_{out}$ stoichiometry (Rudnick and Nelson 1978; Nelson and Rudnick 1979; Quick 2003) and indicates that the Na1 site acts as a molecular checkpoint for 5-HT binding, whereas Na2 primarily functions to couple the Na^+ gradient to transport.

Schicker *et al.* (Schicker et al. 2011) showed that substrate currents in SERT are probably carried by a conducting state in equilibrium with the K^+-bound inward facing conformation. In the same study, a model was produced in which 5-HT-induced currents were explained by conformational changes that increased the fraction of transporters in the conducting state. In this

model, currents induced by 5-HT were assumed to be carried by an intermediate from which 5-HT had already dissociated. In addition, it was suggested that other known activities of SERT, such as the substrate-independent leak current of Na^+ or Li^+, might also be explained by the same conducting state. In this current study, we found that the leak current and the substrate-induced current through hSERT N101A reversed at the same potential, consistent with the hypothesis that both activities are related to the same conformational state. WT SERT cannot convert to the inward facing conformation with 5-HT when external Na^+ is absent. However, in hSERT N101A Ca^{2+} supports this conversion. Therefore, if we assume that currents through WT and N101A are mechanistically similar, hSERT N101A may serve as a resource to explore the conducting state in a solution devoid of Na^+. Additionally, our data support the idea that the conducting state is capable of carrying Cl^-, a conjecture that is difficult to test in WT SERT. However, understanding this mechanism may provide insight into DAT function where Cl^- has been identified as the primary conducting ion in the transient channel mode (Ingram et al. 2002; Carvelli et al. 2004; Meinild 2004).

The ability of the N101 mutants to utilize Ca^{2+} to support 5-HT uptake may indicate that N101 mutations alter ion selectivity at Na1. However, we found that Ca^{2+} can bind to WT SERT and promote low levels of substrate transport and ion currents. Also, although Ca^{2+} was able to functionally replace Na^+ in the N101 mutant, other mono- and divalent cations could not. These findings argue that the Ca^{2+}-mediated transport gained in the N101 mutants does not originate from altered ion selectivity. Rather, they suggest that the Na1 site has a molecular restriction that prevents Ca^{2+} from permitting transporter activation. The N101 mutants appear to disrupt this restriction by altering the ionic network connecting the Cl, Na1, and Na2 sites, revealing critical

aspects of the molecular interactions between substrate and ions necessary for transporter operation that have, until now, remained enigmatic.

Evaluation of the data from this study, in light of our previous analysis of the N101 residue (Henry et al. 2011), suggests critical mechanistic roles for a number of hSERT residues in substrate binding and transport. Uptake studies have shown that, in the absence of Cl^-, the K_m for 5-HT transport is increased significantly, indicating that Cl^- binding alters the apparent affinity of 5-HT for hSERT (Nelson and Blaustein 1982; Chang and Lam 1998; Henry et al. 2011). Our MD studies link this positive impact of Cl^- on the K_m of 5-HT to the residue D98. Under normal Na^+ and Cl^- conditions, we observed monodentate coordination of the D98 side chain carbonyl with the Na^+ at Na1 and the amine of 5-HT. However, removal of Cl^- in the simulations resulted in a loss of N368 coordination with Na1, which is replaced by a bidentate interaction of the side chain of D98 with Na1. This eliminates the D98–5-HT interaction, providing a rational explanation for the observed increase in the K_m for 5-HT. Likewise, the absence of a cation at the Na1 site does not alter 5-HT binding (Chang and Lam 1998), suggesting that, in the absence of Na^+, the carboxyl side chain of D98 is available to stabilize 5-HT binding, although it does not lead to productive transport. Therefore, we propose that upon 5-HT binding, D98 transitions from bidentate to monodentate coordination of Na^+ at Na1 and that this change in coordination is critical to initiate transport. This is supported in our MD simulations with Ca^{2+} bound at Na1, where D98 shows bidentate coordination with Na1 in both WT and N101 mutant backgrounds. This lack of interaction between D98 and 5-HT would lead to decreased stabilization of 5-HT binding. This is backed by uptake studies where Ca^{2+} replacement of Na^+ resulted in a ~10-fold increase in the K_m for 5-HT in both the WT and

N101 mutant backgrounds. Therefore, the inability of D98 to interact with 5-HT would prevent the side chain rearrangement in D98 that we speculate is important to initiate transport and provides a rationale for the inability of Ca^{2+} to functionally replace Na^+ in the WT transporter.

Given that our data reveal that Ca^{2+} can only bind to the Na1 site, this would suggest that the N101 mutant transporters can function despite having an unoccupied Na2 site. This ability of the transporter to function with Na2 in a bound or unbound state suggests at least partial uncoupling of transport to the Na^+ gradient, allowing the transporter to function in a "slippage" mode. Support for this idea comes from our MD studies, where we propose that 5-HT binding to SERT results in loss of S438 coordination of Na^+ at Na2. Normally, in the absence of Cl^- or the presence of Ca^{2+}, our proposed role for the Cl and Na1 sites as molecular checkpoints in WT SERT would keep the transporter from cycling, although Na2 is destabilized by 5-HT binding. However, in the N101A mutant, the regulatory role of the Cl and Na1 sites is uncoupled from Na2, allowing 5-HT binding to destabilize Na2 via S438 and promote transport. This uncoupling could also account for the large Na^+ leak currents and increased efflux previously reported for the N101 mutants (Henry et al. 2011) as well as the observed 5-HT dose-dependent uptake in the absence of Na^+ or Ca^{2+} described in this study. The N101A- and N101C-mediated disruption of the Na1 and Cl sites to act as a molecular switch could explain how 5-HT binding alone to these mutants can promote transport, although D98 has bidentate coordination to Na1 in absence of Cl^- or the presence of Ca^{2+}. This uncoupled state could also explain our finding that 5-HT can enhance its own uptake in a dose-dependent manner in N101 mutants, even when Na^+ is replaced by $NMDG^+$.

Additional support for uncoupling of substrate to ion binding in the N101 mutants comes from our substituted cysteine accessibility method studies, which reveal differential conformational changes proximal to C109 (extracellular vestibule end of TM1) under various ion and substrate conditions. The findings show that in hSERT, Na^+ and Cl^-, but not 5-HT, are sufficient and necessary to induce a vestibular conformational change involving TM1, indicating that this movement is coupled to ion occupancy of the Na^+- and Cl^--binding sites. In the N101A mutant, however, neither Cl^-, Na^+, nor Ca^{2+}, alone or in combination, support the vestibular conformational change. Notably, 5-HT is able to promote a vestibular conformational change, suggesting that, whereas cation and anion binding are no longer sufficiently coupled to bring about conformational changes on their own, the uncoupled state can be overcome by 5-HT coordination. Thus, 5-HT binding could act to orient TM1, -3, -6, and -8, allowing transport to proceed, albeit less efficiently. In WT SERT, the absence of Na^+ or Cl^- in their binding sites would inhibit the ability of 5-HT to engage transport, but in the uncoupled state of the mutant, the ion binding sites no longer tightly regulate initiation of the transport cycle, permitting 5-HT alone to activate transport.

The recent LeuT crystal structures supplement the collection of conformational intermediates such that we now have structures spanning from the "apo open outward" to the "apo open inward" conformations. Comparison of the findings from our study with these LeuT transporter snapshots provides support for our proposed mechanism (Yamashita et al. 2005; Singh et al. 2008; Krishnamurthy and Gouaux 2012). As LeuT transitions from the outward facing to the inward facing structures, the residues that coordinate Na^+ at Na1 (distances around 2.4Å) move further away from Na^+ (to around 3.4Å), becoming weaker, but notably still
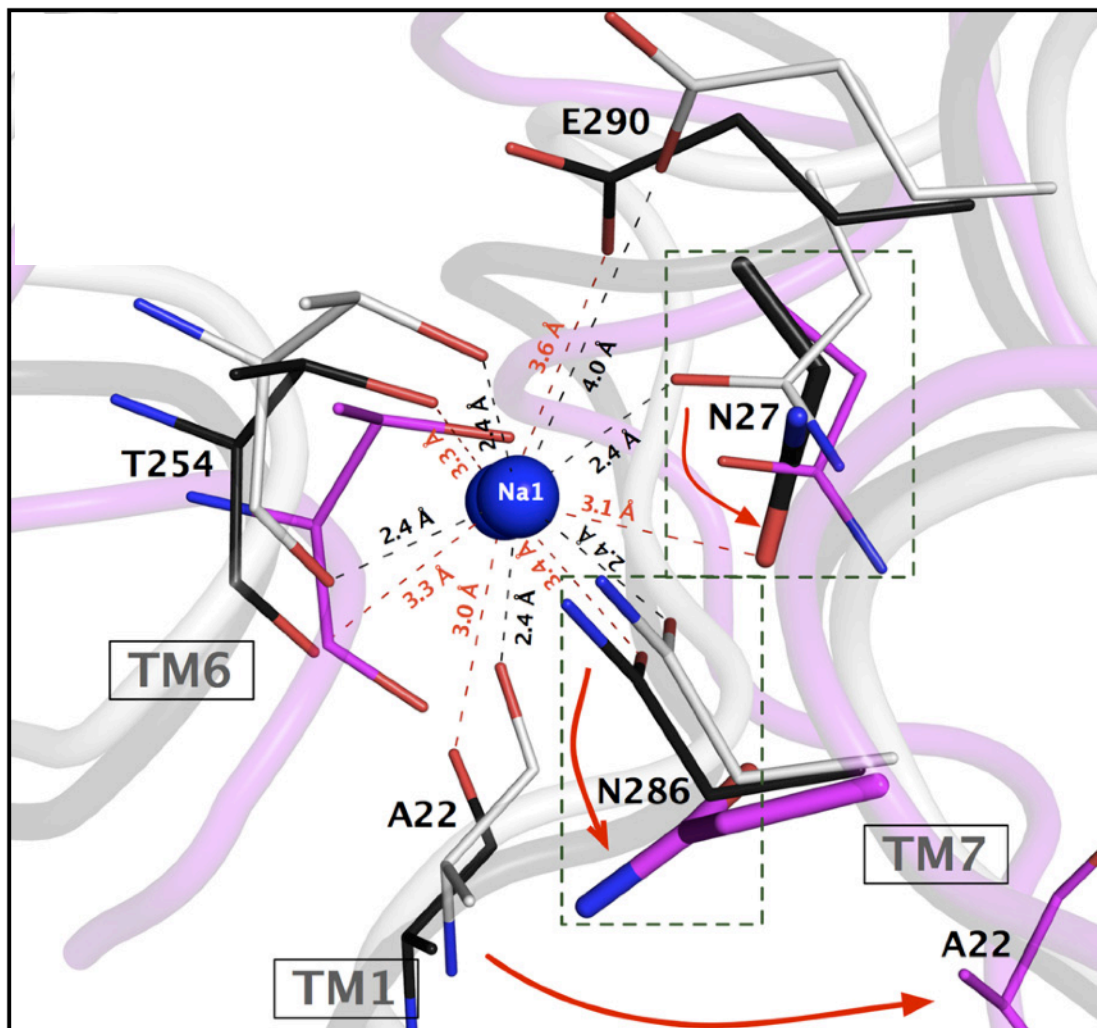
Figure 29. Alignment of LeuT crystal structures in poses associated with the translocation mechanism support the purposed roles of hSERT N101 and N368. LeuT transporter crystal structures representing "outward open" (*white*), "inward open occluded" (*black*) and "inward open" (*magenta*) conformations. Na$^+$ at Na1 is shown as blue spheres. Residues coordinating Na$^+$ are shown in lines and sticks. Dashed-line boxes depict the reorientation of N27 (*homologous to hSERT N101; black sticks*) and N286 (*homologous to N368; magenta sticks*) in "inward open occluded" (*black*) conformation lacking sodium ion at Na2 site and "inward open" (*magenta*) conformation with both Na$^+$ sites unoccupied.

116

coordinate Na^+. However, more importantly, there is a large shift in the position of the A22, N27, and N268 side chains in the Na1 site when LeuT transitions to an inward facing conformation (Figure 29). These residues correspond to A96, N101, and N368, respectively, in hSERT, which are highly conserved amino acids and may demonstrate a preserved role for these residues in facilitating coupled transport in the SLC6 family. In fact, we found it intriguing that in all of the MD simulations, N368 coordination of the cation bound at Na1 correlated with the functionally competent transporter systems, whereas a lack of N368 coordination was observed in all transporter systems that were non-functional. This is not too surprising, given that in comparative models (Forrest et al. 2007; Henry et al. 2011) and by homology to dDAT (Penmatsa et al. 2013), N368 is proposed to interact with $Na1^{Na^+}$, Cl^-, N101, and S336 (which directly coordinates Cl^-).

Finally, the ability of the mutation at N101 to affect such a large number of SERT biophysical properties emphasizes the requirement for proper communication between the ion- and substrate-binding sites to provide efficient coupling of transport to the ionic gradients. To that end, mutations such as N101 will offer powerful tools for future studies to gain a better understanding of the molecular features necessary for secondary active transport.

CHAPTER IV

ANTAGONIST-INDUCED CONFORMATIONAL CHANGES IN DOPAMINE TRANSPORTER EXTRACELLULAR LOOP TWO INVOLVE RESIDUES IN A POTENTIAL SALT BRIDGE

Introduction

DAT, like its MATs homologues SERT and NET, is composed of 12 transmembrane spanning domains (TMs) connected by extracellular and intracellular loops (ELs and ILs) (Figure 30) (Kristensen et al. 2011; Pramod et al. 2013). Substrates are translocated by an alternating access mechanism in which the protein cycles through outwardly and inwardly facing states that allow solutes to enter or exit the permeation pathway from opposite sides of the membrane (Jardetzky 1966; Forrest and Rudnick 2009). These forms are generated by the coordinated opening and closing of extracellular and intracellular gates that control substrate access and direction of movement (Kniazeff et al. 2008). The structures of some of these conformations have been captured through crystallization of LeuT in different phases of the cycle, providing templates for computational modeling of DAT and other homologous mammalian transporters (Yamashita et al. 2005; Singh et al. 2008; Zhou et al. 2009; Krishnamurthy and Gouaux 2012). Recently, Drosophila DAT (dDAT) complexed with the antidepressant nortriptyline was crystallized in an 'outward-open' conformation (Penmatsa et al. 2013), although stabilization of the protein for crystal formation required deletion of 43 amino acids from EL2 and inclusion of five thermostable mutations. The modified dDAT was inactive

118
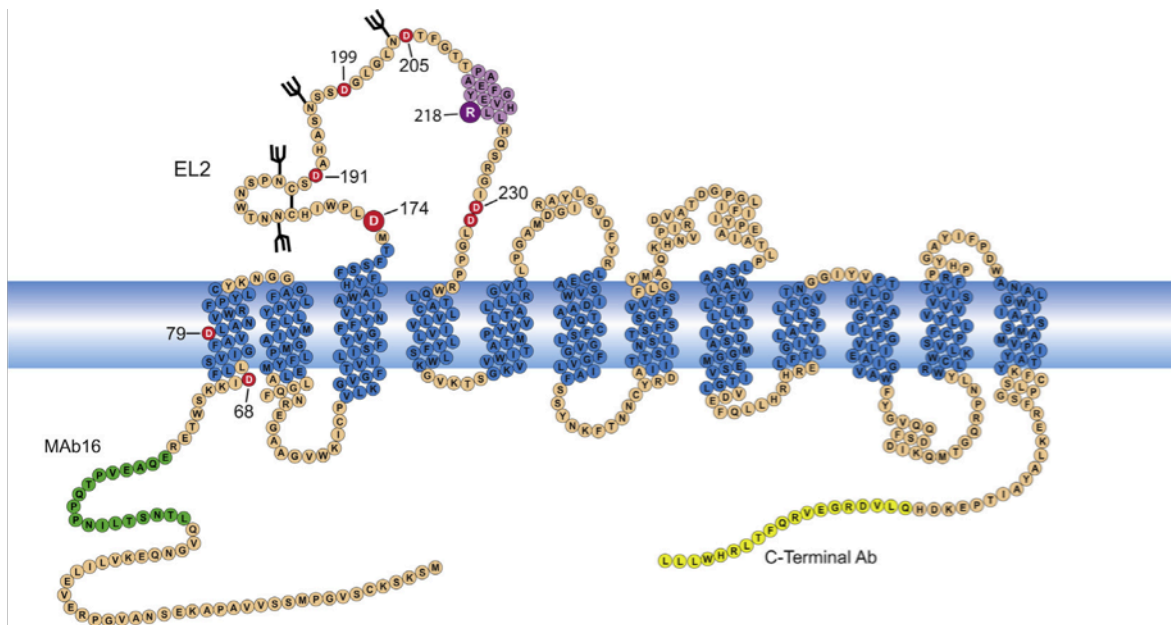
Figure 30. Two-dimensional diagram of DAT. (*A*) Schematic diagram of rDAT illustrating 12 transmembrane spanning domains, epitopes for N- and C-terminal tail antibodies (*green and yellow*), and EL2 components including N-linked glycosylation (*branched structures*), disulfide bond (*solid line*), Asp residues (*red circles*), D174 (*large red circle*) and R218 (*large purple circle*). The full rDAT sequence was analyzed by PsiPred and JUFO secondary structure prediction algorithms, which predicted the region surrounding and including R218 is likely a helical structure (*purple*).

for transport and lacked the functionally relevant zinc binding site present in mammalian DATs formed by residues from EL2 and EL4 (Norgaard-Nielsen et al. 2002; Stockner et al. 2013), which may limit the application of its structure to mammalian DAT. Recently, a valid computational model of hDAT EL2 in the outward-facing transporter conformation has been constructed using the molecular constraints provided by the zinc binding site and conserved disulfide bond (Stockner et al. 2013).

Substrate binding in LeuT occurs in a pocket referred to as S1 that is formed between the extracellular and intracellular gates (Yamashita et al. 2005). This site is formed from residues in TMs 1, 3, 6, and 8, and similar regions of DAT, NET, and SERT have been implicated in substrate binding and transport. Some findings also support the presence of an S2 substrate site on the extracellular side of the extracellular gate in both LeuT and mammalian transporters (Singh et al. 2007; Shi et al. 2008; Zhou et al. 2009; Piscitelli et al. 2010; Plenge et al. 2012; Wang and Gouaux 2012). Findings obtained from mutagenesis approaches showing interaction of DAT and SERT inhibitors with residues in TM1, TM3, TM6, and TM8 (Kitayama et al. 1992; Chen et al. 1997; Henry 2003; Henry et al. 2006b; Beuming et al. 2008; Andersen et al. 2009; Field et al. 2010), adduction of irreversible cocaine analogs to DAT near S1 residues in TM1 and TM6 (Vaughan et al. 2005; Parnas et al. 2008), and molecular modeling of cocaine analog binding (Beuming et al. 2008), strongly support the binding of neurotransmitter transport inhibitors in S1. Further support for high-affinity antagonist binding to S1 comes from recent crystal structures of a LeuT engineered with SERT residues in the central substrate binding pocket (Wang et al. 2013) and from dDAT complexed with nortriptyline and cocaine (Penmatsa et al. 2013; Wang et al. 2015). Some computational studies however, suggest that inhibitors can

also bind at S2 (Plenge and Wiborg 2005; Shi et al. 2008; Huang et al. 2009; Hill et al. 2011; Plenge et al. 2012).

The conformational changes that occur in DAT during the transport cycle establish the transport kinetic rate, overall level of DA clearance, and strength of neurotransmission, and are affected by regulatory mechanisms that may become disrupted in dopaminergic disorders and drug abuse (Pramod et al. 2013; Vaughan and Foster 2013). These events are not fully explained by information gleaned from static transporter crystal structures, and their elucidation remains an important area of research. Biochemical and molecular approaches used to probe structural rearrangements of neurotransmitter transporters include protease- and alkylation-protection analyses and the substituted cysteine accessibility method (SCAM), (Reith et al. 1996; Ferrer and Javitch 1998; Chen and Rudnick 2000; Reith 2001; Hastrup et al. 2003; Norregaard et al. 2003; Chen et al. 2004; Loland et al. 2004; Wenge and Bönisch 2013). Our lab previously described a pronounced reduction in the sensitivity of rat (r)DAT EL2 residue R218 to proteolysis by the arginine/lysine specific protease trypsin in response to binding of uptake blockers that we attributed to conformational movements generated during transport inhibition (Gaffaney 2004).

Here we continue our analysis of uptake blocker-induced changes in EL2 using the aspartic acid specific enzyme endoproteinase Asp-N and identify ligand-induced conformational sensitivity of D174, a residue just C-terminal to the extracellular end of TM3. Comparative modeling of DAT and LeuT places D174 and R218 in close proximity, suggesting a structural basis for their similar uptake inhibitor sensitivities and indicating their potential to form a salt bridge. Using SCAM we examine the regions around rDAT D174 and human (h) DAT R219 and identify conformational activity of hDAT V221. Similar to previous findings obtained with

trypsin, we show that DA transport and cocaine analog binding activities are decreased after Asp-N cleavage of EL2, suggesting a role for this domain in these functions. These findings suggest that conformational changes in this region of EL2 following antagonist binding may represent part of the transport inhibition mechanism and add to our understanding of an under-characterized region of DAT.

Methodology

Tissue Preparation and Proteolysis

Male Sprague Dawley rats (175–300g) were decapitated and the striatum was quickly removed, weighed, and placed in ice-cold sucrose phosphate buffer (SP) consisting of 0.32M sucrose, 10mM sodium phosphate, pH 7.4. The tissue was disrupted with a Polytron homogenizer and centrifuged at 20,000xg for 10 minutes at 4°C. The resulting membranes were washed twice and resuspended to 20mg/ml original wet weight (o.w.w.) in ice-cold SP buffer. Equal volumes of membranes and endoprotease Asp-N (1–5µg/ml final) prepared in SP buffer were gently mixed and incubated for 45 minutes at room temperature. Proteolysis was stopped by addition of 500 µl of ice-cold SP buffer, membranes were centrifuged at 15,000xg for 8 minutes at 4°C and the supernatant was removed. The resulting pellet was solubilized in sample buffer (2% SDS, 10% glycerol, 100mM DTT, 60mM Tris–HCl, pH 6.8) at 20mg/ml o.w.w. and subjected to electrophoresis and immunoblotting. For experiments testing the effects of ligands on proteolysis, striatal membranes were incubated on ice for 1 hour in the presence or absence of DAT uptake inhibitors (2µM), substrates (30µM), or $ZnCl_2$ (10µM) followed by addition of Asp-N. For sodium replacement studies SP buffer was prepared with 10mM monobasic/dibasic

potassium phosphate. Proteolysis of DAT was quantified as described below, with statistical evaluation of proteolysis performed using ANOVA with significance set at $p < 0.05$. All experiments were performed three or more times.

Immunoblot Analysis

Solubilized striatal membranes (25μl) were electrophoresed on 4–20% Tris/glycine polyacrylamide gels and transferred to 0.2μm PVDF membranes. DAT and its proteolytic fragments were detected by immunoblotting as previously described (Gaffaney 2004) with mouse monoclonal antibody 16 (mAb16; EMD Millipore; 1:1000 dilution) generated against rDAT N-terminal tail amino acids 42–59 or goat polyclonal antibody raised against rDAT C-terminal tail amino acids 601–619 (Research Diagnostic Inc.; 1:100 dilution). Bound antibodies were detected with anti-mouse or anti-goat IgG 2°antibodies linked to alkaline phosphatase (1:5000 dilution) and membranes were developed with the alkaline phosphatase substrate, 5-bromo-4-choloro-3-indolyl phosphate/nitro blue (BCIP/NBT). Blots were dried, scanned, and quantified using LumiAnalyst software (Roche/Boehringer- Mannhiem). Specificity of mAb16 immunostaining was verified by preabsorbing antibody with 30μg/ml peptide 16, using 30μg/ ml peptide 5 (a.a. 225–236) as a negative control. Tissue linearity experiments verified that mAb16 signal intensity was linear between 0.1 and 10mg/ml tissue (not shown).

Quantification of DAT Proteolysis

Immunoblots were scanned at 600dpi with an Epson Perfection 12000U scanner and saved as grey-scale images. Grey scale values were converted to Boehringer light units by LumiAnalyst 3.0 software. Proteolysis of DAT was quantified dividing the immunoreactivity of the 80kDa DAT form by the combined immunoreactivity of all DAT bands (full length protein

and proteolytic fragments), with results converted to percent and subtracted from 100%. This allowed for correction of low amounts of endogenous proteolysis observed in some experiments, and served as an internal loading and transfer control. PeptideCutter (Expasy) was used to determine the calculated M_r of peptide fragments.

Deglycosylation Analysis

DAT and DAT Asp-N fragments were immunoprecipitated with polyclonal antibody 16 as described previously (Foster et al. 2002). Protein A Sepharose beads containing the immune complex were incubated with 1.5 units of glycopeptidase-F (PNGF) for 18 hours at 22°C to deglycosylate DAT (Vaughan and Kuhar 1996). Beads were washed twice with immunoprecipitation buffer (50mM Tris–HCl, 0.1% Triton X-100) and proteins were eluted with sample buffer followed by immunoblotting with mAb16.

Asp-N Activity Assay

The Asp-N peptide substrate Azocoll® which generates a blue product when cleaved was used to determine the activity of Asp-N in the presence or absence of 5μM cocaine, GBR 12909, mazindol, benztropine, $ZnCl_2$, dopamine, or amphetamine. Azocoll® was incubated with 1–5μg/ml Asp-N at 37°C for 15 minutes in the presence of ligands, particulates were removed by filtration through a Whatman No. 1 filter and the absorbance of the filtrate was measured at 520nm in a Molecular Devices SpectraMax 190 spectrometer. Absorbance was linear with enzyme concentration and activity was not affected by any of the DAT compounds tested (not shown).

[3H]CFT Binding and [3H]DA Uptake

For binding assays rat striatal membranes were treated with or without 5μg/ml Asp-N for

45 minutes at 22°C, followed by addition of ice-cold SP buffer, centrifugation, and removal of

supernatant. Membrane pellets were resuspended in SP buffer to a concentration of 6mg/ml

o.w.w. and triplicate samples were incubated on ice with 2nM [^{3}H]2b-carbomethoxy-3b-(4-

fluorophenyl)tropane ([^{3}H]CFT) for 2 hours with non-specific binding determined by addition of

100µM (–)-cocaine. Reactions were terminated by rapid vacuum filtration using a Brandel tissue

harvester over Whatman GF/B glass fiber filters soaked in 0.1% BSA for 2 hours. Filters were

counted in a Beckman model 1600 scintillation counter. For uptake assays P_2 synaptosomal

fractions were prepared in SP buffer from freshly dissected rat striatum (Krueger 1990), and

resuspended at 6mg/ml o.w.w. in ice-cold SP buffer. Aliquots were treated with or without

1µg/ml of Asp-N for 45 minutes and dispensed into assay tubes. Dopamine uptake assays were

performed in triplicate in modified Krebs phosphate buffer (16mM KPO_4, 126mM NaCl, 4.8mM

KCl, 1.4mM MgSO4, 10mM glucose, 1.1mM ascorbic acid, and 1.3mM $CaCl_2$, pH 7.4)

containing 10nM [^{3}H]dopamine plus 100nM dopamine (Vaughan et al. 1997) with non-specific

uptake determined by addition of 100µM (–)-cocaine. Uptake assays were initiated by addition

of 100µl of synaptosomes to the reaction tube and conducted for 5 minutes at 30°C. Uptake was

stopped by addition of 5ml of ice-cold SP buffer and immediate vacuum filtration using a

Brandel tissue harvester over a Whatman GF/B filter soaked for 2 hours in 0.1% BSA. Filters

were counted using a Beckman model 1600 liquid scintillation counter. Aliquots of each sample

were subjected to immunoblotting to determine the extent of DAT proteolysis. Results were

analyzed by Student's t-test with significance set at $p < 0.05$.

SCAM Analysis

The expression plasmid for hDAT E2C with two extracellularly facing Cys residues (C90

and C306) mutated to Ala was the generous gift of Dr. Jonathan Javitch, Columbia University and was used for analysis of R219 and flanking residues. The homologous rDAT E2C (C90A, C305A) was generated in our lab for analysis of D174 and flanking residues. E2C and Cys mutations in the E2C background were made using the Stratagene QuikChange kit with codon substitution verified by sequencing (Alpha Biolabs; Northwoods DNA). For production of human stable transformants, GripTight cells™ (Invitrogen) were transfected using FuGENE, (Roche Applied Bioscience) and pooled lines were maintained under selection with 250μg/ml Hygromycin. For production of stable rat transformants, Lewis Lung Carcinoma Porcine Kidney (LLC-PK$_1$) cells were transfected using X-tremeGENE, (Roche Applied Bioscience) and pooled lines were maintained under selection with 800μg/ml G418. For Western blotting, cells were lysed with solubilization buffer (25mM Tris–HCl, 150mM NaCl, 1mM EDTA, 5mM NEM, and 1% Triton X-100), protein content was determined using the BCA method and 10μg of total protein was immunoblotted with mAb16 for rDAT or mAb369 (Chemicon; Temecula, CA) for hDAT.

For activity assays cells expressing h/rDAT E2C or E2C Cys mutants were grown on 12- or 48-well plates to 90–95% confluency. Cells were washed 2x with Krebs–Ringer HEPES buffer (25mM HEPES, 1.2mM KH$_2$PO$_4$, 125mM NaCl, 4.8mM KCl, 1.2mM MgS0$_4$, 5.6mM glucose, and 1.3mM CaCl$_2$, pH 7.4). For binding assays cells were incubated with 1nM (12-well) or 10nM (48-well) [^{3}H]CFT for 2 hours on ice, rinsed twice with ice-cold KRH, and solubilized in 1% SDS. For uptake assays, cells were incubated for 10 minutes at 37°C with 10nM [^{3}H]DA plus 3μM DA. Non-specific binding and transport were determined using 100μM (–)-cocaine. Cells were washed twice with ice-cold KRH, solubilized in 1% SDS, and analyzed for

126

radioactivity by scintillation counting. Uptake and binding values were normalized for protein content and results for mutants are indicated as percent of E2C activity set to 100%. For SCAM analysis MTSET, MTSES, or MTSEA (Biotium; Hayward, CA) were prepared immediately prior to use, and added to the cells (1mM final) for 10 minutes at room temperature. For cocaine protection assays cells were incubated with 10μM (–)-cocaine for 10 minutes prior to MTSET addition. Following incubation the cells were washed 3 times with KRH and assayed for [³H]CFT binding or [³H]DA transport.

Molecular Modeling

To determine distance between residues L126 and S150 that are homologous to D174 and R218 in rDAT, the X-ray coordinates for the second extracellular loop (EL2) of LeuT were analyzed from the crystal structures representing the 'apo-out' (PDBID: 3TT1), 'open-to-out' (3F3A), 'outward-occluded' (2A65), 'outward-occluded' (3TU0), 'apo-in' (3TT3), and 'occluded with sertralinebound' (3GWU). With the exception of the apo-inward structure, residues 132 through 135 were unresolved and were therefore re-built using Prime 3.1 in Schrödinger suite (Schrödinger LLC), with the native crystal structures as templates. The resulting structures differed only 0.000–0.005 RMSD from their respective templates. The mutations L126D and S150R were introduced and EL2 structures modeled using Rosetta Backrub which allows for focused flexible backbone modeling (Smith and Kortemme 2008). The top scoring Backrub models were analyzed for distances between D126 and R150. Possible backbone-dependent rotamers for D126 and R150 were analyzed in PyMol. Figures were generated using PyMol. (The PyMOL Molecular Graphics System (Schrödinger, LLC)).

Results

Endoproteinase Asp-N Digestion of rDAT

In a previous study we found that in situ proteolysis of $^{32}PO_4$-labeled rat striatal membranes with Asp-N generated a phosphorylated 19kDa DAT fragment that precipitated with N-terminal polyclonal Ab16 (Foster et al. 2002), suggesting that Asp-N could provide a suitable enzyme for analysis of DAT proteolysis. In the N-terminal region of the protein rDAT contains two Asp residues (D68 and D79) that are embedded in TM1 and inaccessible to protease during in situ treatments, and six that are in EL2 (D174, D191, D199, D205, D230 and D231) (Figure 30). To develop an immunoblot assay for detection of Asp-N fragments that could be used to test effects of ligands we examined the overall Asp-N digestion pattern using both N-terminal (mAb 16) and C-terminal (a.a. 601–619) antibodies (Figure 31, left). In control membranes both antibodies detected full length DAT migrating at ~80kDa (arrow a). In Asp-N treated membranes the primary N-terminal proteolysis product was a 19kDa fragment (arrow d) that corresponded to the phosphorylated peptide we identified by immunoprecipitation, and a lower intensity 32kDa cleavage product (arrow b) was also produced in some but not all experiments. Because there are no Asp residues in EL1, IL1, or the N-terminal tail and those in TM1 are protected from proteolysis, these fragments extend from the transporter N-terminus to the cleavage site. The mass of the 19 kDa band is thus consistent with proteolysis at D174 (calculated M_r 19,243), while that of the 32 kDa band is consistent with proteolysis at D191 or D199, which would generate fragments of calculated protein M_r 21,244 and 22,032 with the remaining mass contributed by N-linked carbohydrates on N181, N188, or N196 (Figure 31). The 32 kDa fragment was not more prominent than the 19kDa fragment at lower Asp-N doses or

128
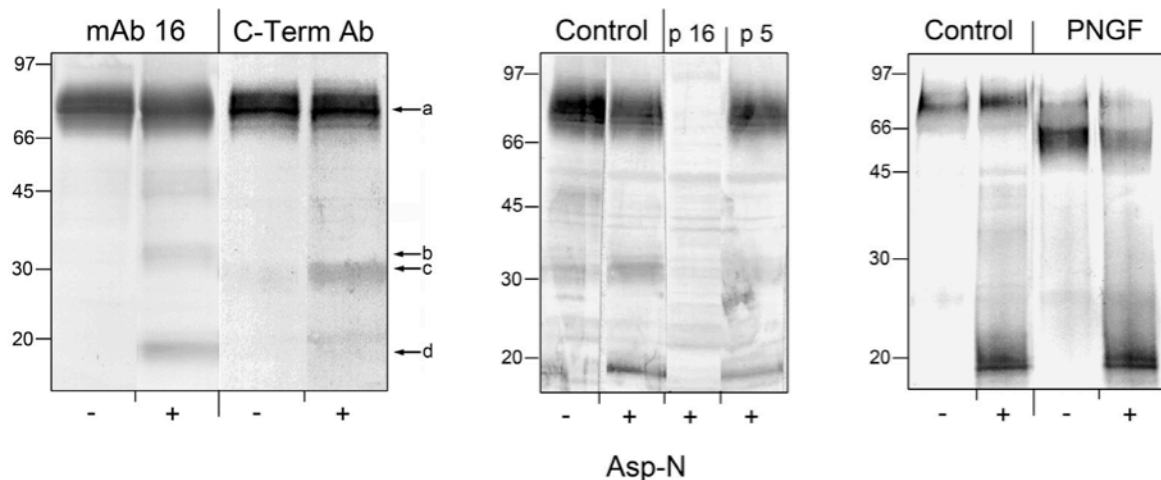
Figure 31. Characterization of DAT Asp-N fragments. Rat striatal membranes were treated with (+) or without (−) 1µg/ml Asp-N and analyzed as indicated. Left panel, immunoblotting of samples with N- and C-terminal specific DAT antisera: (*arrow a*) full-length DAT; (*arrows b and d*) 32 and 19kDa fragments detected by mAb 16; (*arrow c*) 30kDa fragment detected with C-terminal antibody. Middle panel, immunoblotting of Asp-N treated samples with mAb16 containing no addition (*control*), 30µg/ml peptide 16 (*p16*), or 30µg/ml peptide 5 (*p5*). Right panel, DAT and DAT Asp-N fragments were immunoprecipitated with polyclonal antibody 16 and treated with or without 1.5 units PNGF, followed by immunoblotting with mAb16.

129

treatment times, or seen in its absence, suggesting that D174 is the preferred site of proteolysis with occasional missed cleavages producing the larger peptide. Immunoblotting of Asp-N digests with the C-terminal mAb detected a 30kDa fragment (arrow c) that is similar in mass to a 32kDa C-terminal fragment produced by cleavage of R218 (Vaughan and Kuhar 1996; Gaffaney 2004), and is thus consistent with proteolysis of D205, D230, or D231.

The specificity of N-terminal fragment immunoreactivity was confirmed by preabsorbing mAb16 with its antigenic peptide (peptide 16), which blocked staining of full-length DAT and all fragments (Figure 31, middle), while inclusion of peptide 5 (rDAT a.a. 225–236) had no effect. To further characterize the fragments we treated control and Asp-N proteolyzed DATs with glycopeptidase-F to remove N-linked carbohydrates (Figure 31, right). This reduced the mass of the full-length protein by ~20–25kDa as previously shown (Vaughan 1995; Li et al. 2004), but did not affect the mass of the 19kDa fragment. This result strongly indicates that the 19kDa fragment is produced by cleavage of D174, which is the only Asp residue in EL2 that is N-terminal to all glycosylation sites. We note that we have been unable to drive in situ proteolysis of heterologously expressed DATs and thus have not been able to confirm usage of protease sites by site-directed mutagenesis.

Uptake blockers reduce Asp-N proteolysis

To determine if uptake blockers or substrates affect the Asp-N sensitivity of DAT, rat striatal membranes were incubated with various DAT ligands during protease treatment (Figure 32). In control membranes, Asp-N treatment caused robust production of the 19kDa fragment (Figure 32A), with DAT proteolysis levels averaging 62 ± 4% (Figure 32B). Incubation of membranes with the DA uptake inhibitors (–)-cocaine, GBR 12909, mazindol, nomifensine, or b-
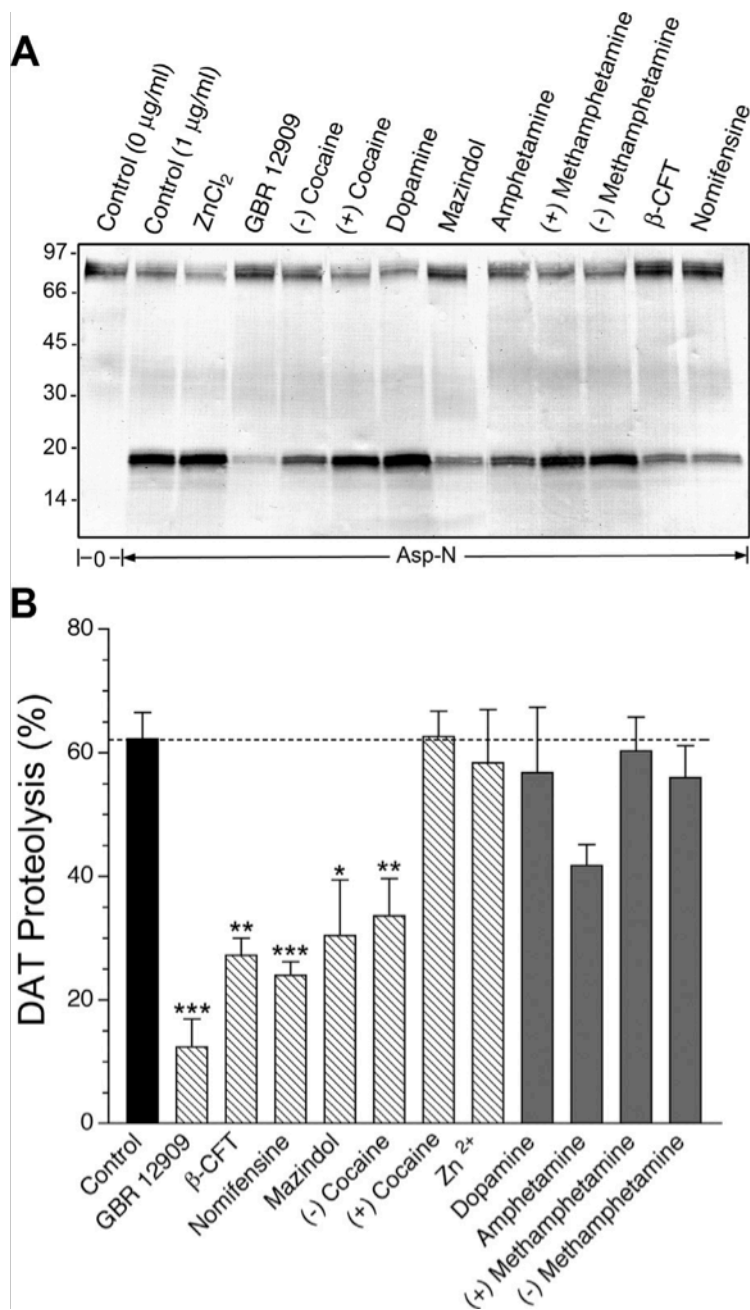
Figure 32. Effect of ligand binding on Asp-N proteolysis. Rat striatal membranes incubated in the absence (*control*) or presence of 2μM uptake blockers, 30μM substrates, or 10μM Zn^{2+}, were treated with vehicle or 1μg/ml Asp-N and immunoblotted with mAb16. (*A*) Representative immunoblot showing full-length DAT and 19kDa Asp-N fragments produced in indicated conditions. (*B*) Quantification of DAT proteolysis in the presence of tested compounds. Bars indicate the fraction of DAT digestion in the presence of vehicle (*black bar*), uptake blockers or Zn^{2+} (*hatched bars*), or substrates (*gray bars*). Values shown are means ± S.E.M. of three independent experiments. * = $p < 0.05$, ** = $p < 0.01$, *** = $p < 0.001$ relative to control by ANOVA with a Dunnett's multiple comparison post hoc test.

131

CFT strongly inhibited production of the 19kDa fragment, with proteolysis levels ranging from $12 \pm 5\%$ to $33 \pm 6\%$ (all $p < 0.05$ to $p < 0.001$ relative to control). Proteolysis was not affected by the inactive cocaine stereoisomer (+)-cocaine or by the NET inhibitor desipramine (not shown), demonstrating the pharmacological specificity of the effect. In contrast to the effects of transport inhibitors, incubation of membranes with the substrates DA, AMPH, or METH, or with Zn^{2+}, did not affect DAT proteolysis (all $p > 0.05$ relative to control) (Figure 32, A and B).

To further verify that the reduced proteolysis of DAT was due to ligand binding, we tested for the effects of Asp-N in the absence of Na^+ (Figure 33), which significantly reduces the affinity of DAT for cocaine (Wang et al. 2003). In Na^+-containing buffer, DATs showed robust proteolysis that was strongly inhibited by uptake blockers (Figure 33, A and B). However, when K^+ was substituted for Na^+, uptake blockers did not prevent proteolysis, consistent with reduced ligand affinity resulting in lack of transporter conformational change. No difference was found in the levels of control DAT proteolysis in the presence or absence of Na^+, indicating that Na^+ binding alone does not induce transporter conformational changes detectable with this assay. Finally, as an additional control, we determined that none of the DAT blockers or substrates tested affected Asp-N cleavage of a synthetic substrate (not shown), indicating that reduced production of DAT fragments by ligands was not the result of Asp-N inhibition. Together these results demonstrate that binding of uptake blockers but not substrates or Zn^{2+} leads to reduced proteolysis of D174.

Asp-N treatment disrupts DAT function

To determine if proteolysis of EL2 affects DAT function, rat striatal membranes or synaptosomes were treated with Asp-N followed by assessment of [^{3}H]CFT binding
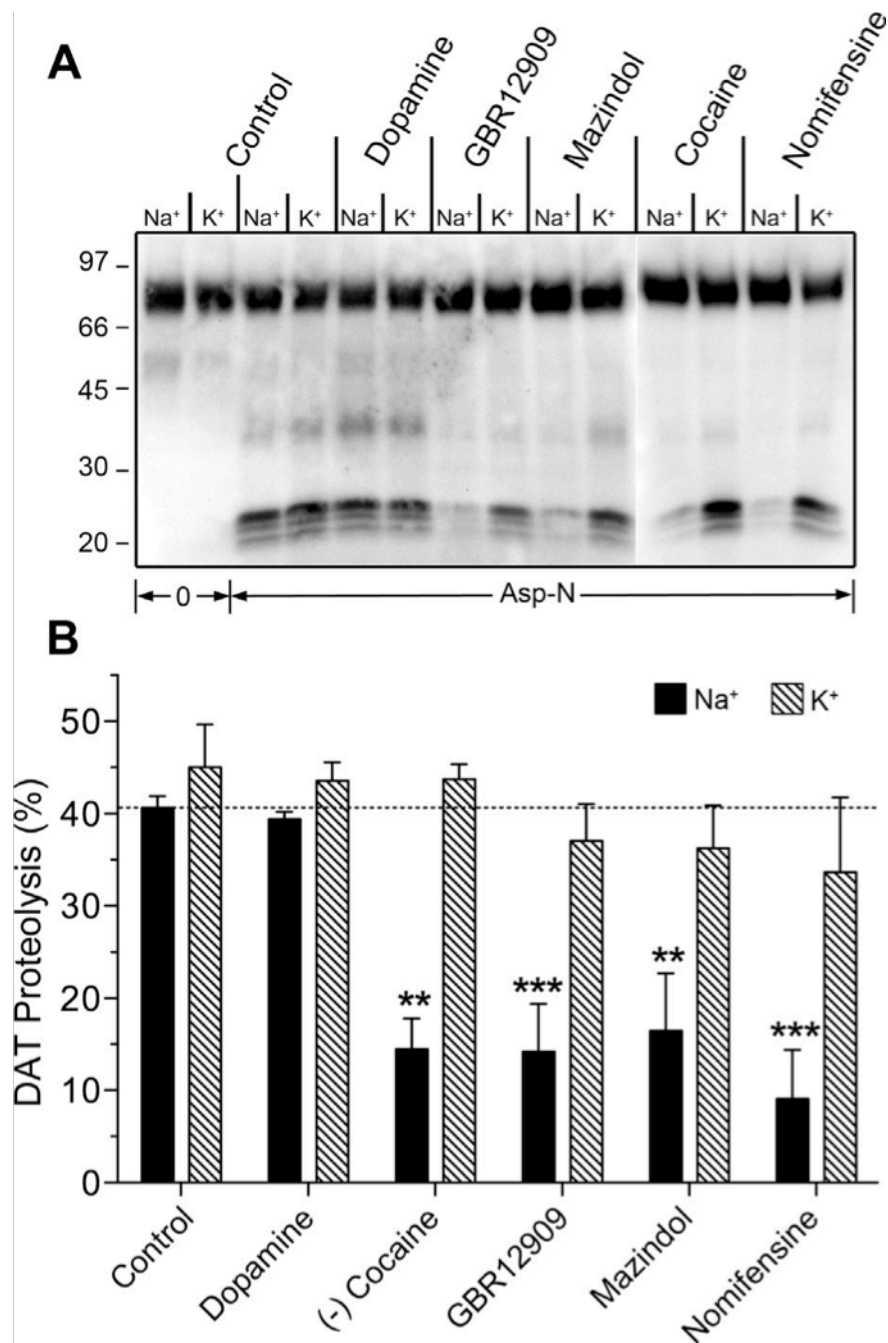
Figure 33. Uptake ligand-induced protease resistance requires Na$^+$. Rat striatal membranes suspended in buffer containing either Na$^+$ or K$^+$ were incubated with uptake blockers (2μM) or substrates (30μM) and treated with vehicle or Asp-N followed by immunoblotting with mAb16. (*A*) Representative immunoblot. (*B*) Quantification of DAT proteolysis (*means ± S.E.M.*) in the presence of Na$^+$ (*black bars*) or K$^+$ (*hatched bars*). ** = $p < 0.01$, *** = $p < 0.001$ relative to control by ANOVA with a Dunnett's multiple comparison post hoc test.

133

(Figure 34A) or [^{3}H]DA transport (Figure 34B). Immunoblotting of membranes and synaptosomes confirmed production of Asp-N fragments with proteolysis levels averaging 18 ± 3%. After Asp-N treatment, binding and transport activities of DAT were reduced by 31 ± 6% and 20 ± 4%, respectively, roughly correlating with the extent of digestion, and suggesting that loss of EL2 integrity leads to reduction of DAT transport and binding functions.

SCAM analysis of EL2 residues

We then performed SCAM analysis of the regions around rDAT D174 and hDAT R219 to further assess the conformational sensitivity of these residues and to examine flanking sequences. For analysis of the N-terminal side of EL2 we generated an rDAT E2C construct as the background for insertion of Cys mutations at residues 171–177 (F171, T172, M173, D174, L175, P176, and W177) (Figure 35). The corresponding human sequence (FTTELPW) differs slightly but retains conservation of the negative charge at Glu174. rDAT E2C displayed uptake and binding activities that were similar to those of the WT protein (not shown). Immunoblotting showed that all mutants expressed full-length DAT at ~20–100% of E2C levels except for W177C, which showed no mature protein (Figure 35A). A pronounced band that migrated at ~200 kDa was present in T172C, M173C and D174C forms. As surface projections indicate that these residues are at the transporter surface (not shown), this suggests the possibility for disulfide bond formation to occur between DAT monomers via the inserted cysteines. [^{3}H]DA uptake and [^{3}H]CFT binding activities of these mutants roughly paralleled their expression levels, suggesting that kinetic properties were not strongly altered by the mutations. Consistent with its lack of expression, W177C showed ≤5% of E2C levels of transport and binding activity (Figure 35B), and could not be further analyzed. The remaining mutants were analyzed by SCAM using

134
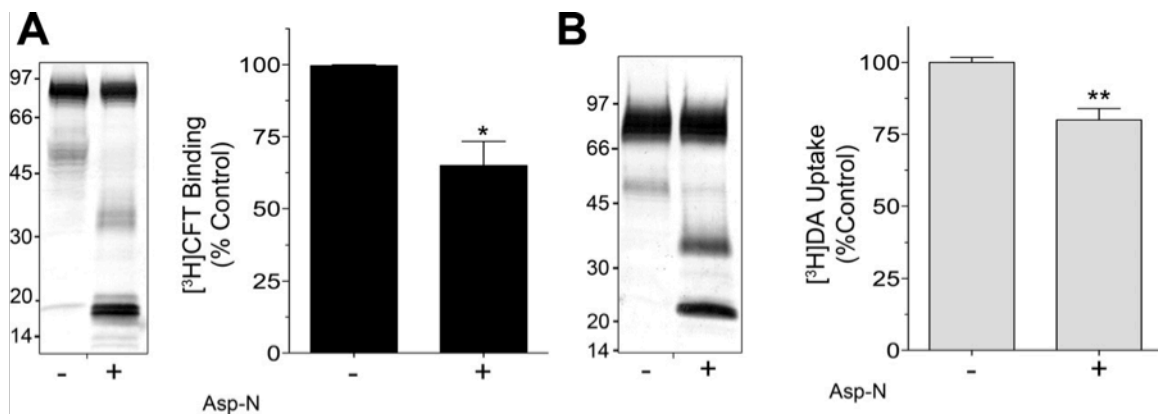
Figure 34. Asp-N treatment disrupts binding and transport activities. (*A*) Rat striatal membranes or (*B*) rat striatal synaptosomes were treated with (+) or without (−) 5µg/ml Asp-N followed by assessment of (*A*) [^{3}H]CFT binding or (*B*) [^{3}H]DA uptake. Left panels show verification of proteolysis by immunoblotting. Histograms show quantification of uptake or binding (*means ± S.E.M.*). * = p < 0.05, ** = p < 0.01 relative to control by Student's t-test.
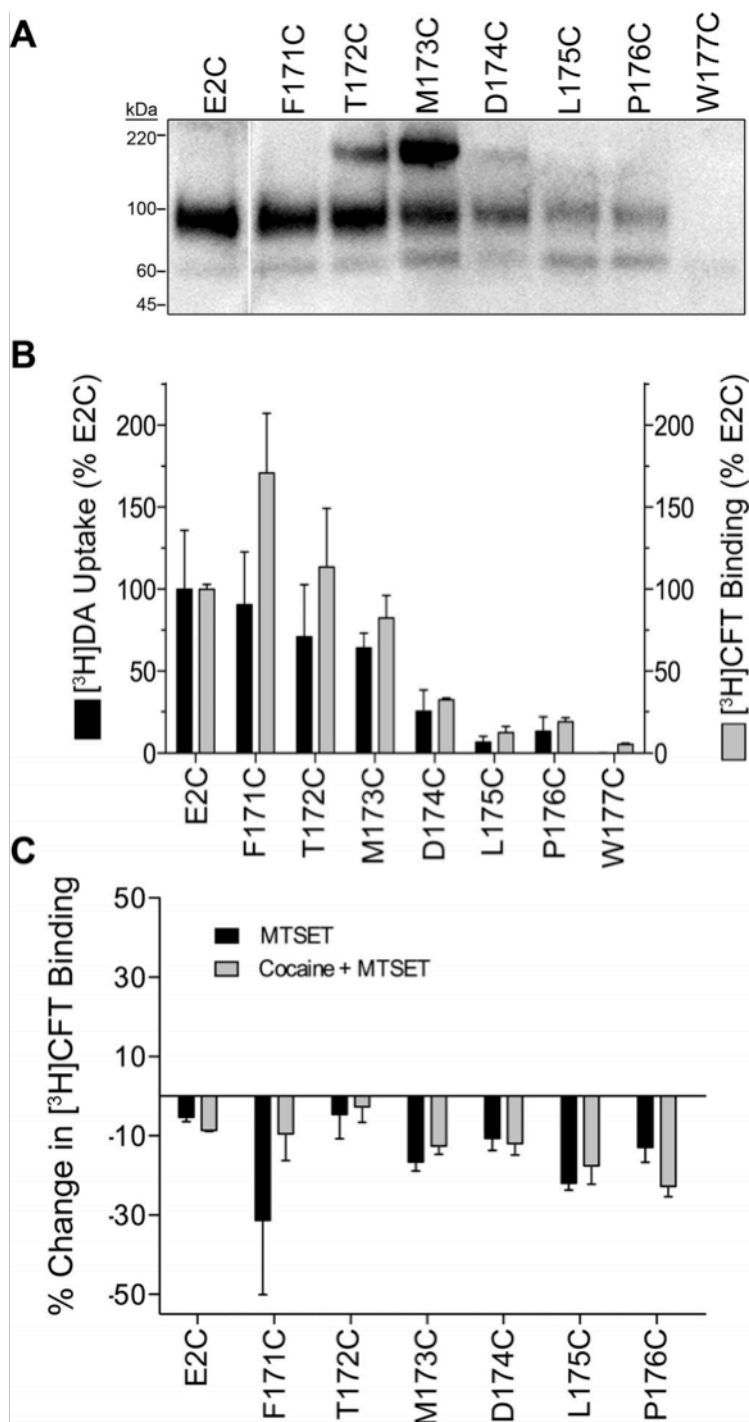
Figure 35. SCAM analysis of the N-terminal region of EL2. Cells expressing the indicated rDAT mutants were analyzed by (*A*) immunoblotting or (*B*) [^{3}H]DA transport (*black bars*) and [^{3}H]CFT binding (*gray bars*). (*C*) Cells were incubated with vehicle (*black bars*) or 10μM (−)-cocaine (*gray bars*) followed by addition of 10mM MTSET prior to binding analysis. The histogram shows percent changes in [^{3}H]CFT binding for each form (*means ± S.E.M, n = 3*). Treated and untreated samples were not significantly different.

[^{3}H]CFT binding as the functional read-out. Treatment of cells with the positively charged MTS reagent MTSET caused only slight (~5–20%) reductions in binding for mutants at positions 172–176 and larger but more variable reduction (31 ± 19%) for F171C, none of which were significantly different from E2C (all p > 0.05), and inclusion of (–)-cocaine during the treatment did not alter these effects (Figure 35C). [^{3}H]DA transport activity of D174C was also not affected by MTSET, and [^{3}H]CFT binding activity for D174C was not significantly affected by the negatively and positively charged MTS reagents MTSES and MTSEA (not shown). Pull down experiments showed that MTSEA biotin reacted with D174C (not shown) indicating that the residue was accessible to the reagent. These results thus suggest that binding and transport activities of these DAT forms were not affected by modification of the inserted cysteines.

For analysis of the C-terminal side of EL2 we used the hDAT E2C construct (Loland et al. 2004) as the background for insertion of Cys mutations at residues 210–226 (Figure 36). This sequence is identical in hDAT and rDAT. The mutants were analyzed by immunoblotting and [^{3}H]CFT binding, and in some cases for [^{3}H]DA transport (Figure 36, A and B). E215C, Y216C and F217C forms showed little to no expression, [^{3}H]DA uptake, or [^{3}H]CFT binding, and could not be analyzed by SCAM. The remaining mutants showed ~15–100% of E2C levels of [^{3}H]CFT binding (Figure 36B), which roughly corresponded to the protein expression levels, suggesting that the mutations did not strongly impact binding characteristics. The proportionally lower uptake levels for E218C and R219C compared to binding could be consistent with impairments in transport or surface expression, although further work will be necessary to confirm the mechanism. Using [^{3}H]CFT binding as the functional read-out, we found that MTSET caused ~60% reduction in binding for A213C; ~20–30% reductions in binding for R219C, G220C,
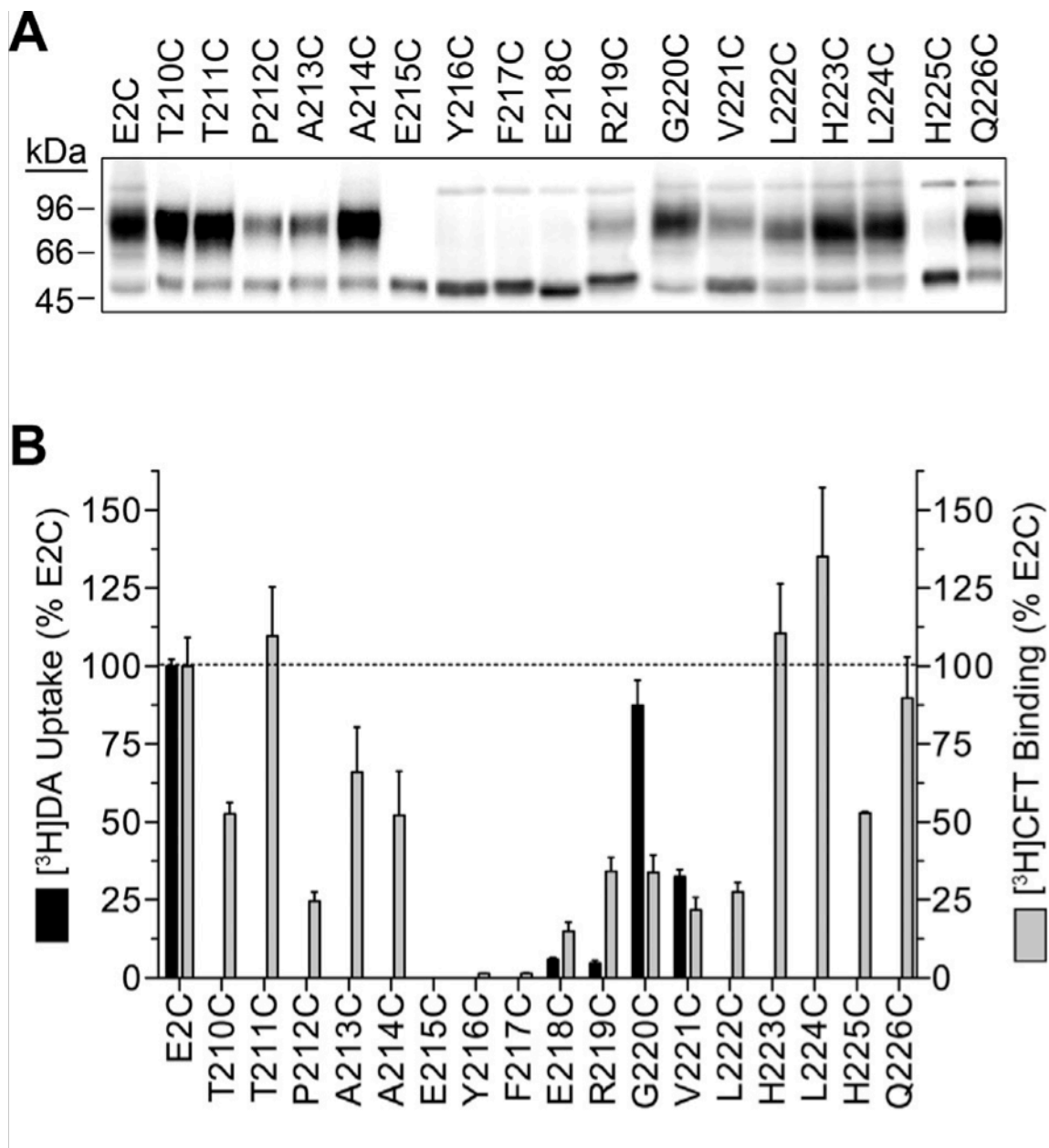
Figure 36. SCAM analysis of the C-terminal region of EL2. Cells expressing the indicated hDAT mutants were analyzed by (*A*) immunoblotting or (*B*) [³H]DA transport (*black bars*) and [³H]CFT binding (*gray bars*).
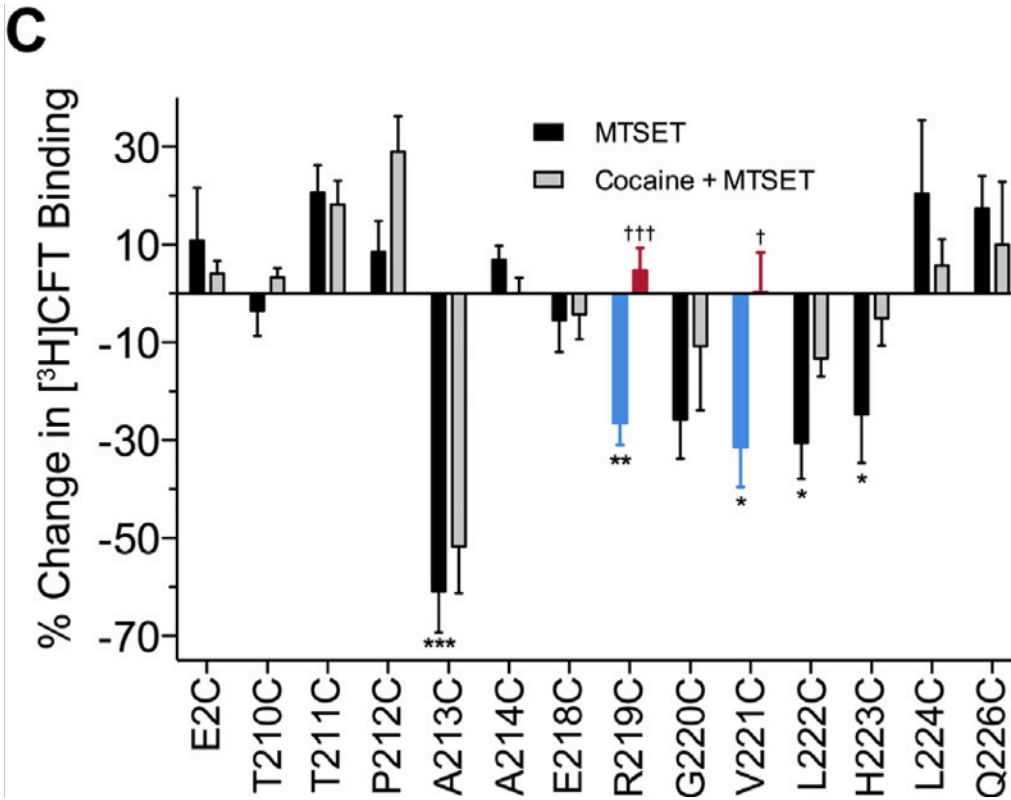
Figure 36 (continued). SCAM analysis of the C-terminal region of EL2. (*C*) Cells were incubated with vehicle (*black bars*) or 10μM (−)-cocaine (*gray bars*) followed by addition of 10mM MTSET prior to binding analysis. Responses for R219C and V221C are indicated in blue (*vehicle*) or red (*cocaine*) for clarity. Results show percent changes in [^{3}H]CFT binding for each form (*means ± S.E.M.*). * = $p < 0.05$, ** = $p < 0.01$, *** = $p < 0.001$ relative to E2C by ANOVA with a Dunnett's multiple comparison post hoc test; † = $p < 0.05$, ††† = $p < 0.001$ for indicated forms relative to the absence of cocaine by Student's t-test. $n = 3–5$ for all forms except T211C (6), P212C (6), A213C (6), E218C (8), R219C (10), and H223C (6).

V221C, L222C, and H223C; ~10–15% increases in binding for T211C, P212C, L224C, and Q226C; and lesser changes for the remaining residues (Figure 36C). Statistically different changes relative to that of E2C were seen for A213C ($p < 0.001$), R219C ($p < 0.01$), and V221C, L222C, and H223C ($p < 0.05$), indicative of modifications that altered binding. Inclusion of (–)-cocaine during the MTSET treatment did not alter the binding changes at most of these residues, but significantly reduced the inhibition of binding at R219C ($p < 0.001$) and V221C ($p < 0.05$) (Figure 36C), confirming the conformational sensitivity of R218/219 to cocaine and identifying cocaine-induced conformational changes at V221.

Molecular modeling

To further understand the significance of these findings we performed molecular modeling of D174 and R218 using homology to LeuT structures solved in the 'apo-out', 'open-to-out', 'outward-occluded', 'apo-in', and 'occluded with sertraline-bound' forms that represent different states of the transport cycle (Yamashita et al. 2005; Singh et al. 2008; Zhou et al. 2009; Krishnamurthy and Gouaux 2012) (Figure 37). The LeuT residues homologous to D174 and R218 are L126 and S150, and their positions have been solved in all LeuT crystal structures, providing a reasonable template for low level modeling of D174 and R218. The results revealed that L126 and S150 were present within ~11Å of each other (Figure 37A), but showed no significant differences in proximity or orientation in any of the transporter forms (Figure 37B), consistent with a lack of movement during transporter cycling or ligand binding in LeuT. We then substituted LeuT residues L126 and S150 *in silico* with D and R to model D174 and R218 positions. The structures were subjected to refinement using Rosetta Backrub, which is designed to sample and energy-minimize local backbone and side chain conformations following residue

140
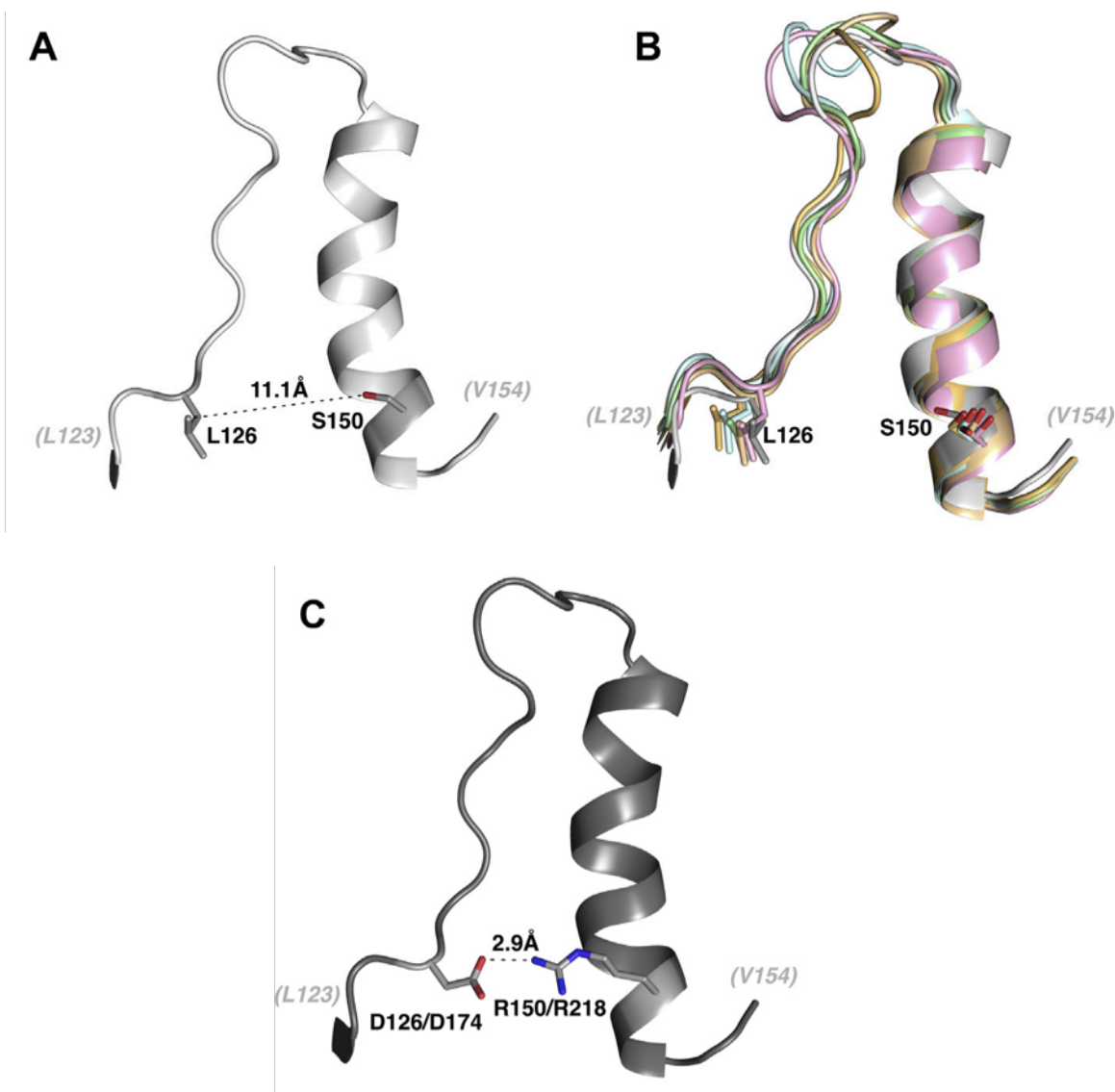
Figure 37. Comparative modeling of D174 and D218 from LeuT EL2 crystal structures. (*A*) Ribbon diagram of LeuT EL2, highlighting positions and calculated distance between L126 and S150 (*dashed line*). (*B*) Superimposed ribbon diagrams of EL2 coordinates from LeuT forms 'apo-out' (*pink*); 'open-to-out' (*orange*); 'outward-occluded' (*brown, green*); 'apo-in' (*gray*); and 'sertraline-bound' (*cyan*), show minimal changes in overall domain structure or L126 and S150 distances. (*C*) Ribbon diagram of LeuT with *in silico* mutation of L126 and S150 side chains to D and R. Energy minimization using Rosetta Backrub revealed several conformations in which the residues are close enough to form a salt bridge (*dashed line*).

141
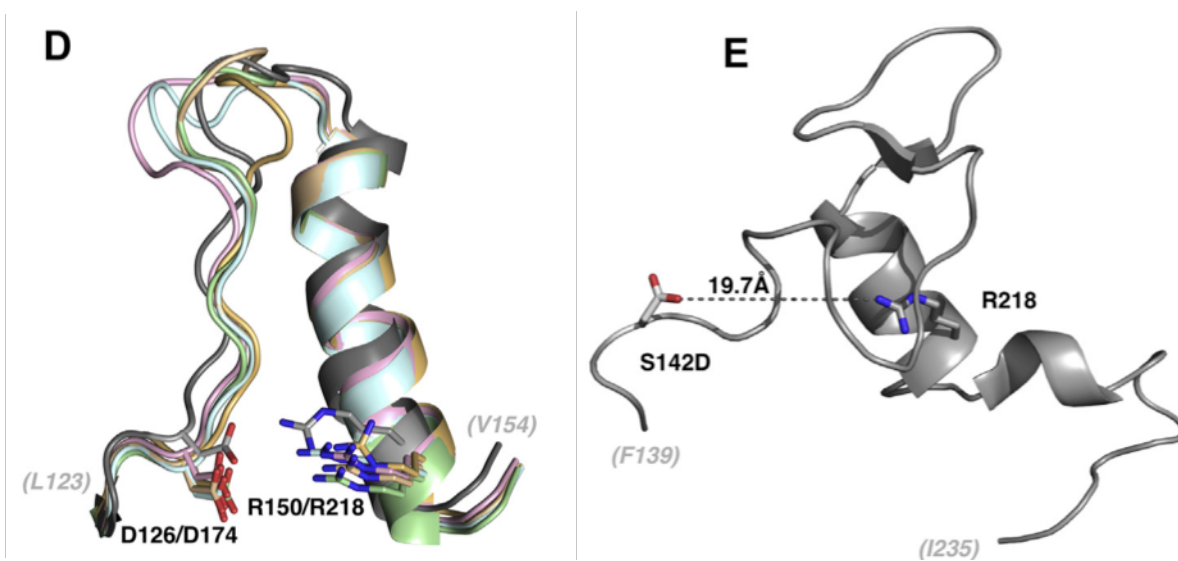
Figure 37 (continued). Comparative modeling of D174 and D218 from LeuT EL2 crystal structures. (*D*) Superimposed ribbon diagrams of EL2 from LeuT forms listed above with DAT substitutions reveal no significant alteration in D174/R218 side chain orientation or distance. (*E*) Ribbon diagram of dDAT EL2 with *in silico* mutation S142D. Manual rotamer search of D142 and R218 were chosen in PyMol. Measured distance between the side chains is indicated (*dashed line*).

142

substitution (Smith and Kortemme 2008). A manual backbone-dependent rotamer search revealed that the longer R and D side chains can come within 2.9Å of one another (Figure 37C), suggesting the possibility of an ionic interaction between these two residues in DAT. Similar to the endogenous LeuT residues, however, the relative positions of D174 and R218 side chains showed no significant variations across the *in silico* mutated models (Figure 37D).

Discussion

Our findings from protease and SCAM analyses suggest that rDAT/hDAT EL2 residues D174, R218/219, and V221 undergo conformational changes in response to binding of uptake blockers or achieve protection indirectly through conformational changes of nearby residues. Because the effects were not obtained with substrates, it is possible that the changes may contribute to the mechanism of transport inhibition, for instance by promoting outward conformations thought to bind to or be stabilized by cocaine (Loland et al. 2004), or by otherwise impacting structural rearrangements needed for transport. Comparative modeling places these residues in close three-dimensional proximity, which could provide a structural basis for their similar sensitivities to uptake blockers, and indicates the potential for D174 and R218 to form a salt bridge. We found no ability of substrates to induce protease resistant forms, but because substrates were analyzed in binding rather than transport conditions, it cannot be excluded that these states might exist during post-binding phases of the transport cycle. Similar to our previous results with tryptic proteolysis of R218, we found no induction of D174 resistance to Asp-N by Zn^{2+}, which slows DA transport by suppressing conformational movements needed for substrate translocation (Norregaard et al. 1998; Stockner et al. 2013). This suggests that inhibition of

transport induced by Zn^{2+} and by pharmacological blockers occurs via distinct mechanisms that might be therapeutically exploited if more fully understood.

It is not known how the conformational information from ligand binding is transmitted to these residues or if the D174 and R218 changes occur independently or via charge interactions. TM3 directly interacts with uptake blockers (Chen et al. 1997; Henry 2003; Penmatsa et al. 2013), suggesting the likelihood for direct transmission of ligand-induced conformational changes to D174, although the specific nature of these changes is unknown. R218 and V221 are predicted by PsiPred and JUFO to be present in an a-helical conformation (Figure 30). In LeuT crystal structures, the homologous helical domain undergoes significant compression and rotation during the 'apo-out' to 'apo-in' transitions (Krishnamurthy and Gouaux 2012) that could alter accessibilities of constituent residues. Although modeling in LeuT templates supports D174–R218 salt bridge interactions in all transporter states, leak conductance (Mager et al. 1994) and SCAM studies of SERT (Chen et al. 1997) indicate the occurrence of dynamic conformational changes in the absence of substrate. Similar reorientations in resting DATs could intermittently alter D174 and R218 interactions to allow protease access, while inhibitors that block transport may stabilize a conformation that locks the D174–R218 interaction. Because Asp-N and trypsin require binding of the charged side chains to position the scissile bond in the catalytic site, formation of the salt bridge could suppress enzyme recognition. Such alterations in trypsin resistance and sensitivity in response to salt bridge formation and disruption have been reported (Rajabi et al. 2008).

Whatever the mechanism responsible for D174 and R218 protease resistance, our findings indicate that molecular modeling of D174 and R218 in LeuT templates, which identifies

no significant structural alterations of these residues, does not accurately represent the properties of DAT, in which these residues clearly undergo either direct or indirect ligand-induced alterations. These inconsistencies may result from differences between DAT and LeuT in EL2 structure and/or ligand binding site. EL2 of DAT differs considerably from that of LeuT by containing 21 additional residues, a disulfide bond, multiple N-linked glycosylation sites, and Zn^{2+}-coordinating residues (Norgaard-Nielsen et al. 2002; Li et al. 2004; Meinild 2004; Chen et al. 2007; Stockner et al. 2013). Few of these elements have been solved at high resolution, and their contributions to EL2 structure are incompletely understood. It is conceivable that given these large differences, EL2 of DAT may undergo distinct or greater conformational changes than that of LeuT and that even small rotations in connecting elements could alter D174–R218 interactions. Such conformational changes in EL2 are supported by computational models of this domain based on well-defined molecular constraints which show that the zinc binding site present in the outward-facing form of DAT is destabilized in the inward-facing structure, due in part to movement of EL2 (Stockner et al. 2013). In addition, in the sertralinebound form of LeuT the ligand is complexed at low affinity in the S2 site, which may not accurately represent structures produced by high affinity and/or S1 binding of cocaine or other inhibitors in DAT. Dose–response studies of antagonist-induced R218 protease resistance showed strong agreement with published ligand affinities, indicative of responses to high affinity binding (Gaffaney 2004). Previously the only insight into competitive binding at S1 was the Trp-bound LeuT co-crystal (Singh et al. 2008), presenting the possibility that binding of larger molecules such as cocaine at S1 could induce distinct conformational changes in EL2. In fact, in the dDAT-nortriptyline co-crystal (Penmatsa et al. 2013) the residues homologous to D174 and R218 are almost twice as far

apart (19.7Å) as compared to LeuT (11.1Å) (Figure 37E), suggesting differences between DAT and LeuT in EL2 structure or conformational responsiveness. While the distance between D174 and R218 in this inhibitor-bound dDAT structure is too great to allow salt bridge interactions, it is possible that the native EL2 structure is not accurately represented due to the removal of 43 residues needed to crystalize the protein. In addition, the dDAT residue homologous to rDAT D174 is Ser, which may also impact the final loop structure and the potential for this site to interact with R218. Thus many questions remain to be addressed with respect to these issues.

Our current and previous findings that conditions that cleave EL2 but leave the resulting N- and C-terminal segments of the protein largely intact lead to reductions of DA transport and CFT binding suggest that EL2 is important for overall transporter structure and/or contributes a functional property that is lost after proteolysis. A connection between EL2 and transport inhibitor binding was also recently identified in hNET (Wenge and Bönisch 2013). Alkylation of hNET EL2 residue His222 suppressed binding of the uptake inhibitor [^{3}H]nisoxetine, although mutation of this residue was without effect. This suggested that the residue was not directly involved in binding but that its alkylation sterically blocked access of nisoxetine to its binding pocket, implicating its proximity to the binding pathway or the binding site. This residue is conserved in r/hDAT (H224/225) and is just downstream of R218/219 in the EL2 α-helix, suggesting a potential structural similarity and further supporting a mechanistic connection between this region of EL2 and uptake inhibitor binding.

High-resolution insight into neurotransmitter transporter molecular mechanisms has been obtained by homology comparison to the LeuT and dDAT ligand binding sites, but lack of information on EL and IL structures has delayed progress in understanding the roles of these

146

domains. Though EL2 has typically been thought to serve a supportive structural role rather than being directly involved in transport or ligand binding functions (Koldsø et al. 2013), our results now begin to identify functional properties associated with the region. In addition, because our protease resistance findings differentiate responses of these residues to antagonists and substrates, they suggest this region as a possible target for development of reagents to reduce inhibitor binding without directly impacting the substrate site.

CHAPTER V

THE FORMATION OF A PUTATIVE SALT BRIDGE AT THE EXTERNAL GATE OF THE SEROTONIN TRANSPORTER IS IMPORTANT FOR AMPHETAMINE TRANSLOCATION AND THE INDUCTION OF SUBSTRATE EFFLUX

Introduction

The serotonin (5-HT) transporter (SERT) is a twelve transmembrane á-helical protein responsible for the termination of serotonergic signaling by removing 5-HT from the synaptic cleft (Gu et al. 1994). Serotonergic signaling is involved in a number of physiological functions including the regulation of appetite, mood, libido, and memory (Amara 1993; Kristensen et al. 2011; Pramod et al. 2013). Alterations in serotonergic signaling have been implicated in disorders like addiction, autism and depression (Owens and Nemeroff 1994; Hahn and Blakely 2002; Veenstra-VanderWeele et al. 2012). Moreover, SERT is the target of many illicit and therapeutic substances, including cocaine, amphetamine (AMPH), and most antidepressants (Tatsumi et al. 1997; Amara and Sonders 1998; Owens et al. 2001).

Like 5-HT, AMPH is a substrate for human SERT and induces an outward movement, or efflux, of 5-HT from the cytoplasm through SERTs (Rudnick and Wall 1992a; 1992b; Sitte et al. 1998). This AMPH-induced substrate efflux is also seen *in vivo*, as AMPHs are known to increase extracellular levels of 5-HT, dopamine, and norepinephrine, resulting in the euphoric effects observed with amphetamine use (Rudnick and Wall 1992a; 1992b). The increase in synaptic 5-HT is thought to be prompted by the transport of AMPH into synaptic vesicles by vesicular monoamine transporters (VMAT), whereby increased vesicular AMPH concentration

148

results in the dissipation of the vesicular proton gradient causing VMAT transport to reverse direction and precipitating the emptying of 5-HT from the synaptic vesicles into the cytoplasm. Once in the cytoplasm, 5-HT is then reverse transported by SERT back into the synaptic cleft, a process termed efflux (Wall et al. 1995; Petersen and DeFelice 1999; Sulzer et al. 2005; Sitte and Freissmuth 2015). Currently, the molecular mechanism by which AMPH promote this non-vesicular, SERT-mediated 5-HT efflux is not well understood (Scholze et al. 2000; Sitte et al. 2000; 2001).

Previous studies in our laboratory demonstrated dramatic differences in the efflux properties between *Drosophila* SERT (dSERT) and human SERT (hSERT) (Rodriguez et al. 2003). dSERT has an increased rate of basal 5-HT efflux in the absence of efflux-inducing AMPH, in contrast to hSERT which exhibits little to no basal efflux activity. However, 5-HT release via hSERT occurs readily upon exposure to AMPH. Notably, AMPH-induced efflux is not observed with dSERT (Rodriguez et al. 2003), suggesting that variation in the primary amino acid sequence of hSERT and dSERT results in this different phenotypic response to AMPH. Electrophysiological studies in *Xenopus* oocytes revealed that upon perfusion with AMPH, currents are elicited through hSERT similar to those that are classically observed upon challenge with substrates. However, these currents were not observed when dSERT was challenged with AMPH, suggesting AMPH acts as a substrate at hSERT but not dSERT (Rodriguez et al. 2003).

In the MATs, the outer gate is an important structure which, when open, allows substrate and ions to enter and bind to the transporter. Binding of the ions and substrate results in closure of the gate to an occluded state necessary for the translocation step. Analysis of a multiple sequence alignment of the Na^+-dependent neurotransmitter transporters revealed that an acidic

residue is highly conserved at the extracellular and intracellular gates. For example, the extracellular gate of hSERT is composed of Arg 104 and Glu 493. However, in dSERT the acidic gating residue is replaced with the polar amino acid Asn yielding an Arg 99 and Asn 484 pair, which would be unable to form a salt bridge interaction. We hypothesized that the loss of a strong charge/charge interaction at the extracellular gate could contribute to the observed differences in the efflux properties of hSERT and dSERT and the transporters recognition of AMPH as a substrate.

Further analysis of the sequence alignment of the SLC6 family of proteins revealed that a vast majority (nearly 90%) of transporters contain an Asp at the external gate position on TM10 (Beuming et al. 2006). Conversely, only ~4% of SLC6 proteins have a Glu at this same position in TM10, most of which (~80%) are species variants of SERT, and even less, ~2% of the SLC6 proteins, possess an Asn. Based on the 90% prevalence of Asp in the outer gate of SLC6 proteins, we also characterized the SERT from *C. elegans* (ceSERT), as it has an Asp (D517) across from the Arg (R125) at the extracellular gate. Consistent with our hypothesis that the presence of residues capable of forming a salt bridge at the outer gate are important for AMPH-induced efflux by SERT, we found that ceSERT is capable of mediating AMPH-induced efflux.

Here we utilized species scanning mutagenesis, a process by which two outer gate mutants were generated for each SERT background that structurally mimic the outer gate composition found in the other respective SERT species variants. This allowed us to examine how the size and charge of the outer gate residue in TM10 effects MDMA interaction with the transporter, which could provide evolutionary and functional significance for both the presence and the identity of an acidic residue at the extracellular gate of SERT. This study reveals that the

150

molecular composition of the extracellular gate impacts the interaction of the transporter with MDMA, whereby recognition of MDMA as a substrate and subsequent efflux promotion are largely inhibited without the presence of the residues capable of forming a putative salt bridge at the outer gate. This may suggests that the presence of a salt bridge at the outer gate could be important in initiating or stabilizing key mechanistic steps needed during transport of and efflux induced by MDMA.

Methodology

Site-Directed Mutagenesis

hSERT, dSERT and ceSERT mutants were constructed using the QuikChange mutagenesis kit (Stratagene, La Jolla, CA). Additionally, an HA-tag was added to the C-terminal tail of the ceSERT plasmid for detection in Western blots. Analysis of the effect of HA-tag addition revealed no significant alterations in transporter function or expression (data not shown). Site-directed mutants were identified by screening for co-introduction of a silent restriction site verified by sequencing of the entire open reading frame (Eurofins MWG Operon).

[^{3}H]5-HT Uptake Assay

HEK-GripTite® cells (Invitrogen) were plated on 24-well culture plates and transiently transfected 24 hours later using the Genecellin DNA transfection reagent (Bulldog BioCells). A group of untransfected parental cells served as a negative control. 24-36 hours after transfection, cells were washed with a modified Krebs-Ringer-HEPES buffer (MKRH) (120mM NaCl, 4.7mM KCl, 2.2mM CaCl$_2$, 10mM HEPES, 1.2mM KH$_2$PO$_4$, 1.2mM MgSO$_4$ 10mM D-glucose, pH 7.4). For competition assays, drugs were added and allowed to equilibrate. 50nM [^{3}H]5-HT

(Perkin Elmer, Waltham, MA) was added to sample wells and incubated for 10 minutes at 37ºC. Cells were washed three times with ice-cold MKRH, solubilized with Microscint-20 (Perkin Elmer), and counted on a PerkinElmer TopCount NXT scintillation counter to quantitate the accumulated [^{3}H]5-HT.

For saturation transport assays, transiently transfected cells were challenged with a range of concentrations from a mixture of [^{3}H]5-HT and non-labeled 5-HT (0.001 – 5µM) at 37ºC for 12 minutes. Cells were washed and accumulated [^{3}H]5-HT was determined as described above.

For amphetamine-and substrate-induced exchange assays, transiently transfected HEK-GripTite® cells were prepared as previously described. Cells were washed once with MKRH and then preloaded with 50nM [^{3}H]5-HT for 20 min at 37ºC. Preloaded cells were washed twice with MKRH and challenged with a concentration range of cold 5-HT or MDMA. Efflux proceeded for 10 minutes at 37ºC before being terminated by washing 3X with ice-cold MKRH buffer. Cells were solubilized and remaining [^{3}H]5-HT was counted as previously described. Amphetamine- or substrate-induced efflux was calculated by determining the amount of efflux in terms of percent 5-HT remaining in pre-loaded cells treated with a substrate compared with those treated with 10µM paroxetine.

Basal efflux was determined in 24-well plates with transiently transfected GripTite® cells. Cells were preloaded with 50nM [^{3}H]5-HT for 30 minutes. Cells were washed twice with MKRH to remove excess [^{3}H]5-HT and incubated in MKRH from 0.5 to 10 minutes. The assay was terminated by two washes with ice cold MKRH. The [^{3}H]5-HT remaining in the cell was determined by scintillation counting. Results were evaluated as the percentage of [^{3}H]5-HT remaining after incubation compared with cells treated with 10µM paroxetine.

Surface Expression Analysis via Surface Biotinylation

To determine transporter surface expression transiently transfected HEK-GripTite® cells were plated on 24-well plates at a density of 100,000 cells/well. 24–48 hours later, cell surface proteins were labeled with NHS-SS-biotin (Thermo Scientific) and affinity purified using neutravidin agarose beads (Thermo Scientific). A BCA protein assay was used to determine total protein concentrations. Equal amounts of protein were processed by SDS-PAGE and Western blotting to determine the relative amount of surface and total transporter pools(Henry 2003). hSERT, dSERT, and ceSERT were detected using the ST51-2 monoclonal antibody (MAb Technologies), an anti-Drosophilla-SERT polyclonal antibody (Alpha Diagnostic International), and an anti-HA-tag monoclonal antibody (Thermo Scientific), respectively.

Whole-Cell Radioligand Binding Assay

HEK-GripTite® cells were plated in 24-well plates and were transiently transfected with SERT cDNA using Genecellin. 48 hours post-transfection, cells were washed once with MKRH. The assay was then carried out in MKRH using 10 μM paroxetine to define nonspecific binding. Equilibrium binding was carried out by incubating with 10nM [^{3}H](S)-citalopram (hSERT and ceSERT backgrounds) or 20nM [^{3}H]mazindol (dSERT background) binding at 4ºC for 1 hour. Cells were washed twice with ice-cold MKRH and accumulated [^{3}H](S)-citalopram or [^{3}H]mazindol was determined using scintillation counting as described above.

Two-electrode Voltage Clamping of *Xenopus* Oocytes

cRNA preparation. Plasmids were linearized and transcribed into RNA with a T7 RNA polymerase kit mMessage mMachine (Ambion). A total of 5-50ng of cRNA was microinjected into each oocyte. Electrophysiological recordings were performed 4–8 days following injection.

Oocyte preparation. *Xenopus laevis* frogs (Nasco, Fort Atkinson, WI) were anesthetized with ethyl 3-aminobenzoate methanesulfonate (FLUKA A5040) (2mg/ml in H_2O). The frog was decapitated, and the ovarian lobes were removed and transferred to sterile Ca^{2+}-free ND-96 solution (96mM NaCl, 2mM KCl, 5mM $MgCl_2$, 5mM HEPES, pH adjusted to 7.5 with NaOH). The lobes were manually dissected to produce groups of 5–10 oocytes and incubated in ND-96, containing 1-2mg/ml collagenase from *Clostridium histolyticum* (Sigma). Incubation for 60-90 minutes at room temperature was sufficient to digest and remove the follicular layer. Defoliculated ocytes were selected and transferred to a fortified ND-96 buffer (96mM NaCl, 2mM KCl, 0.6mM $CaCl_2$, 5mM $MgCl_2$, 5mM HEPES 1mM Na-pyruvate, 100μg/ml streptomycin, 50μg/ml tetracycline, 3% dialyzed horse serum, pH adjusted to 7.5 with NaOH). Oocytes were kept at room temperature for a minimum of 2 hours prior to injection. Injection was completed using the Nanoject II (Drummond Scientific). Injected oocytes were kept for 4–8 days at 18°C the fortified ND-96 buffer. Solutions were changed daily.

Electrophysiological recordings in *X. laevis* oocytes. A high performance oocyte clamp OC-725C (Warner Instruments) was employed for the measurements. The recorded signal was digitized with a PowerLab 8/35 system (AD Instruments). LabChart (AD Instruments) was used for data acquisition. Borosilicate glass capillaries (Drummond Scientific) were pulled (Sutter Instruments, model P-87) to a final resistance of 0.4–1.2 megaohms and filled with 3M KCl. Oocytes were impaled, and the membrane potential was clamped to a holding potential of −60mV. For continuous superfusion with unfortified ND-96 solution (96mM NaCl, 2mM KCl, 0.6mM $CaCl_2$, 5mM $MgCl_2$, 5mM HEPES, pH adjusted to 7.5 with NaOH) a gravity-driven superfusion system (Warner Instruments, Eight Channel Perfusion Valve Control System) was

used. The osmolarity of all solutions was kept equal by supplementation with mannitol. Recordings were initiated after a stable current base line had been established. The current was sampled with 100Hz and low pass-filtered with 20Hz.

Results

Disruption of hSERT External Gate Abolishes Transport

To determine the role of the external hSERT gating residues R104 and E493 in amphetamine-induced efflux, a double mutant (R104E/E493R) was engineered to determine if swapping the position of the charge could restore function. However, this reciprocal mutant completely disrupted substrate transport (Figure 38) suggesting these residues likely participate in interactions with other residues that are important in structure and/or function of the transporter. Notably, the single mutants hSERT R104E and hSERT E493R were also non-functional. Expression of the single and double mutants at the cell surface were confirmed using Western blotting and radioligand binding analysis (data not shown).

Species-Scanning Mutagenesis of the External Gate Yields Little Effect on 5-HT Transport or Protein Trafficking

As swapping the two charged residues of the outer gate was unsuccessful, we performed species-scanning mutagenesis with dSERT and ceSERT to introduce less disruptive mutations at the external gate. Species-scanning mutagenesis is a strategy whereby species variants of a protein are analyzed by multiple sequence alignment to identify alternative residues that naturally occur at a specific position (Henry et al. 2006b). The native residues identified through this technique are: hSERT, hE493D and hE493N, dSERT, dN484D and dN484E and ceSERT ceD517E and ceD517N. These mutations were engineered and examined for changes in transport

155
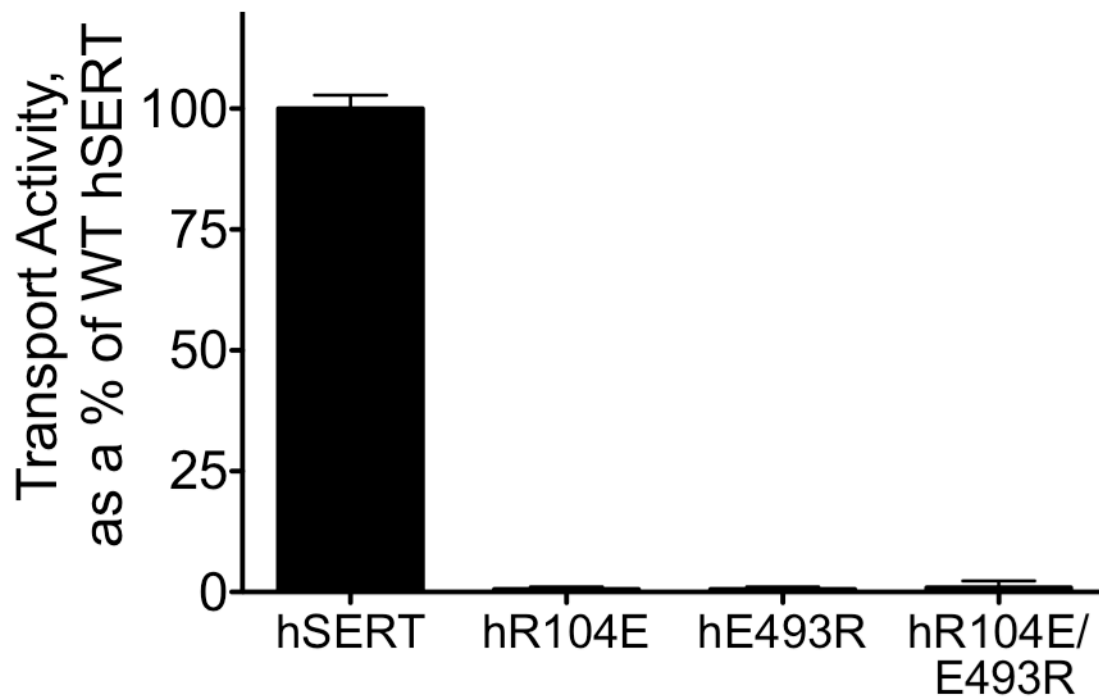
Figure 38. 5-HT transport activity of hSERT gating mutants. HEK-293 cells transiently expressing hSERT or an hSERT gating mutant were assayed for [^{3}H]5-HT uptake. Here, results are graphically represented as the amount of [^{3}H]5-HT uptake normalized to the level of uptake in WT hSERT. Data represent mean ± SEM for at least three independent experiments performed in triplicate.

	% Transport Activity of WT	Surface Expression, (% of WT)	K_M, (µM)	V_{max}, (amol/cell/min)
hSERT	100 ± 4.7	100 ± 9.4	1.02 ± 0.28	62.4 ± 5.9
hE493D	94.3 ± 6.9	108 ± 11.2	1.13 ± 0.34	49.6 ± 6.2
hE493N	91.8 ± 5.3	87 ± 7.9	1.94 ± 0.97	53.2 ± 9.5
dSERT	100 ± 7.8	100 ± 18.9	0.85 ± 0.48	39.4 ± 3.7
dN484D	93.4 ± 5.4	139 ± 17.1	2.15 ± 0.60	46.3 ± 5.8
dN484E	103 ± 6.2	122 ± 11.6	2.99 ± 0.42	37.1 ± 4.5
ceSERT	100 ± 5.6	100 ± 9.3	1.14 ± 0.51	31.7 ± 4.2
ceD517E	95.9 ± 8.3	98 ± 8.0	2.19 ± 0.76	27.0 ± 6.1
ceD517N	71.1 ± 6.5	91 ± 10.4	5.27 ± 1.02	37.5 ± 3.4

Table 4. Summary of transporter kinetics, activity and surface expression levels for each SERT species variant and their respective outer gate mutants. Shown are relative transport activity, surface expression, K_M and V_{max} values for each SERT species and their respective external gate mutants. Transport activity values and surface expression are normalized to the WT value in each respective species grouping.

activity or kinetics and surface expression (Table 4). Only the ceD517N mutant exhibited a change in functional activity compared to wild type (~29% decrease in transport activity and a ~3 fold increase in K_M) indicating the naturally occurring variations at the TM10 gating residue were well tolerated.

The Acidic TM10 Gating Residue is Important for the Ability of the Transporter to Mediate MDMA-Induced Exchange

5-HT efflux occurs readily through hSERT and ceSERT in response to AMPH application, whereas in dSERT, AMPHs elicit little or no efflux (Rodriguez et al. 2003). One of the hallmarks of a SERT substrate is its ability to induce the efflux of preloaded substrate in neurons or cultured cells (Fuller 1980; Rudnick and Wall 1992a; 1992b; Sitte et al. 1998). Thus, the ability of MDMA to evoke 5-HT efflux was accessed in order to explore the importance of the acidic amino acid at the outer gate in the recognition of AMPH as a substrate (and thus its capacity to induce efflux) (Rudnick and Wall 1992a; 1992b). When HEK-GripTite® cells expressing either hSERT, dSERT, ceSERT or one of their respective outer gate mutants were preloaded with [^{3}H]5-HT and challenged with non-labeled 5-HT to induce substrate-mediated efflux there was significant release of [^{3}H]5-HT (Figure 39).

Similarly, when the cells were challenged with MDMA, robust release of [^{3}H]5-HT was observed consistent with the properties of a substrate. However, little to no exchange was observed in either dSERT or hSERT E493N (Figure 40, A and B). This suggests that the presence of a negative charge at the outer gate is critical for the proper recognition and induction of the MDMA transport mechanism. Notably, the ceD517N mutant (Figure 40C) also displayed significant loss of MDMA-induced exchange (~41% decrease when compared with wild-type ceSERT). However, unlike with dSERT or hSERT E493N, lack of a negative charge at the
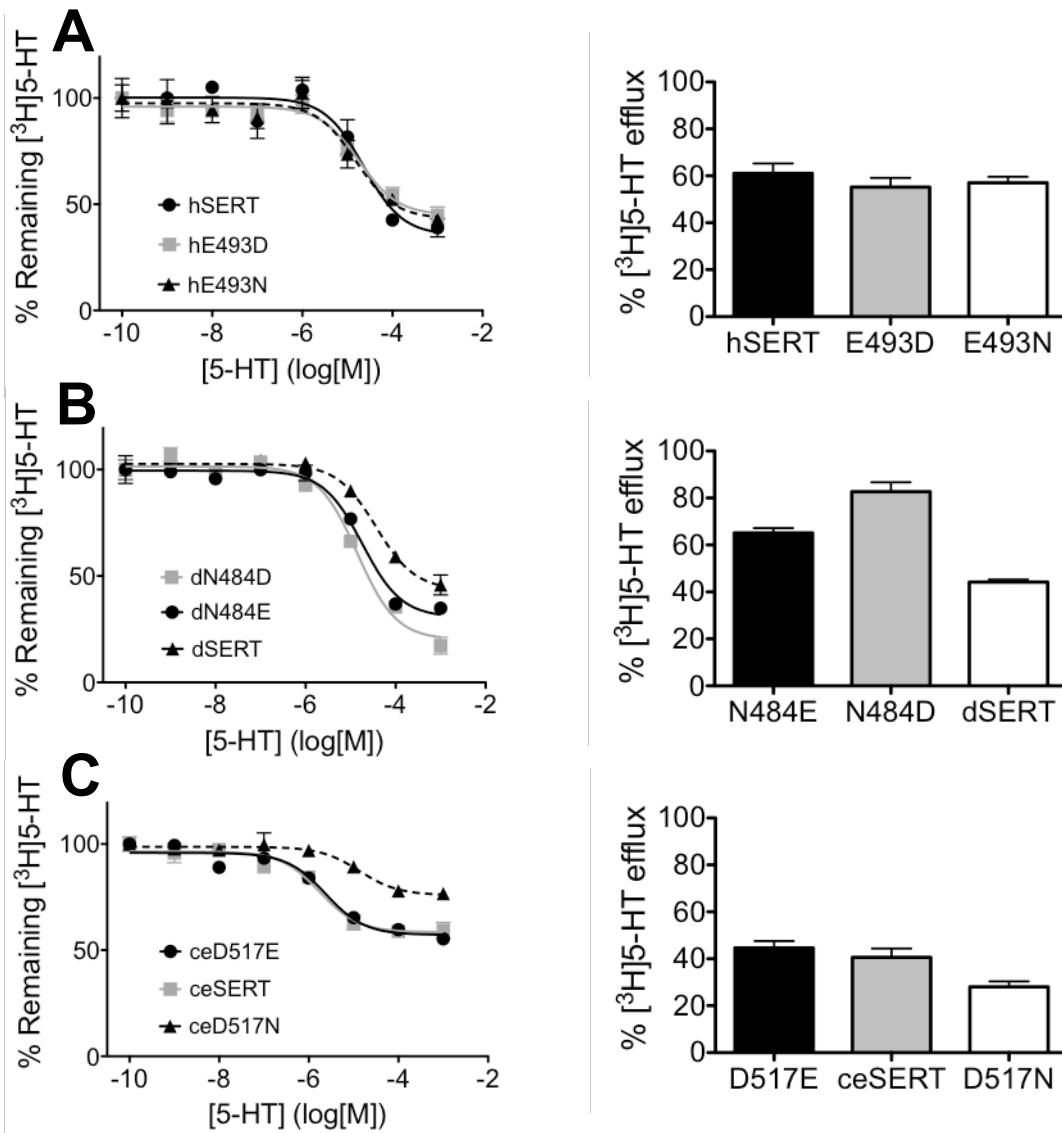
Figure 39. 5-HT can induce substrate efflux in transporters with either a negative charge or a polar Asn at the external gating position on TM10. Substrate efflux assay: HEK-GripTite® cells transiently expressing a SERT species variant or a SERT external gate mutant were preloaded with [³H]5-HT. Loaded cells were challenged with various concentrations of cold 5-HT in order to induce substrate-mediated efflux. After 10 minutes, the assay was terminated by washing with ice-cold buffer and the amount of [³H]5-HT remaining in the cell was quantified. Results for (*A*) hSERT, (*B*) dSERT and (*C*) ceSERT, along with each set of respective external gate mutants for each, are represented in two ways: (left) as a dose-response curve and (right) as a bar graph of results when 1mM 5-HT was used to induce substrate efflux; n = 2.
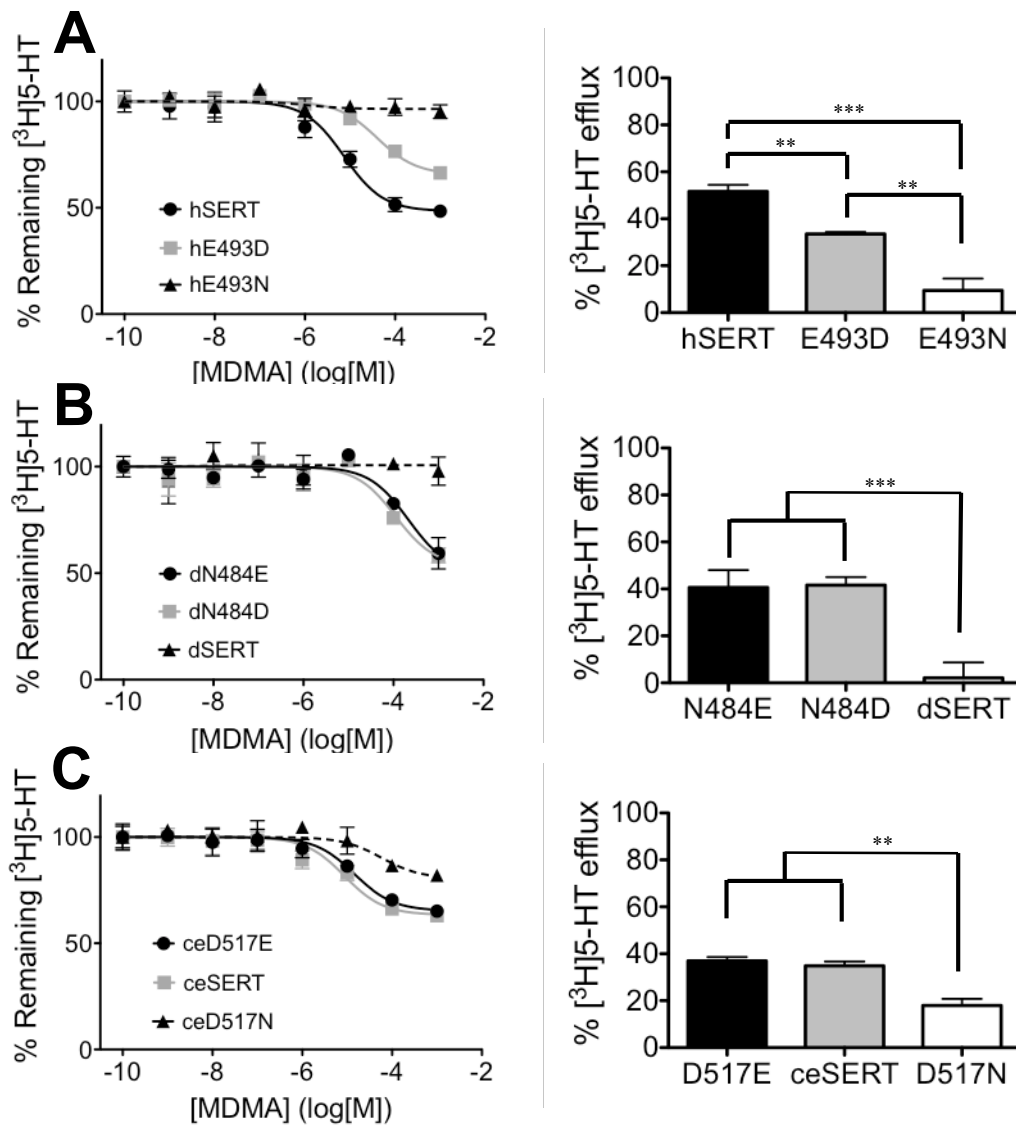
Figure 40. The presence of an Asn at the external gate of SERT results in diminished MDMA-induced substrate efflux when compared with transporters that contain an acidic amino acid at the homologous position. Substrate efflux assay: HEK-GripTite® cells transiently expressing a SERT species variant or a SERT external gate mutant were preloaded with [³H]5-HT. Loaded cells were challenged with various concentrations of MDMA in order to induce substrate-mediated efflux. After 10 minutes, the assay was terminated by washing with ice-cold buffer and the amount of [³H]5-HT remaining in the cell was quantified. Results for (*A*) hSERT, (*B*) dSERT and (*C*) ceSERT, along with each set of respective outer gate mutants for each, are represented in two ways: (left) as a dose-response curve and (right) as a bar graph of results when 1mM MDMA was used to induce substrate efflux. A one-way ANOVA was performed for each SERT grouping; ** $p < 0.01$, *** $p < 0.001$; n = 4.

160

TM10 outer gate residue did not abolish MDMA-induced exchange suggesting there may be other yet to be identified residues that are also important for MDMA recognition as a substrate.

If the presence of an acidic amino acid at the outer gate is important for AMPH-induced exchange, introduction of an acidic residue into the TM10 gating residue in dSERT would likely result in a gain-of-function, such that MDMA could induce release of internal substrate. To evaluate this prediction, [^{3}H]5-HT pre-loaded HEK Griptite culture cells expressing the dSERT N484D or dSERT N484E mutants were exposed to MDMA (Figure 40B) 5-HT release was observed at levels similar to wild-type hSERT (Figure 40A). Decreasing the bulk of the acidic residue in hSERT by engineering an hSERT E493D mutant resulted in a ~38% loss of MDMA-induced exchange when compared to wild-type hSERT (Figure 40A) suggesting that the positional length of the negative charge may be of importance. In ceSERT, where the presence of an acidic residue was not absolutely required, altering the identity of the acidic residue in ceSERT (D517E) yielded no effect on MDMA-induced exchange (Figure 40C), again suggesting the substrate recognition mechanism in ceSERT may be partially or fundamentally different than in hSERT and dSERT. These observations support our hypothesis, that the presence of an acidic amino acid at the outer gate is important, and even critical to hSERT and dSERT critical for propagating AMPH transport and promoting efflux.

Mutation at the Outer Gate does not Significantly Alter MDMA Potency

The inability of MDMA to induce substrate-like effects in dSERT could occur if lack of an acidic residue significantly reduces or completely eliminates the binding of MDMA to the transporter. Therefore, we performed [^{3}H]5-HT competition uptake analysis to determine if mutation of the acidic residue at the extracellular gate impacted the ability of MDMA to bind to
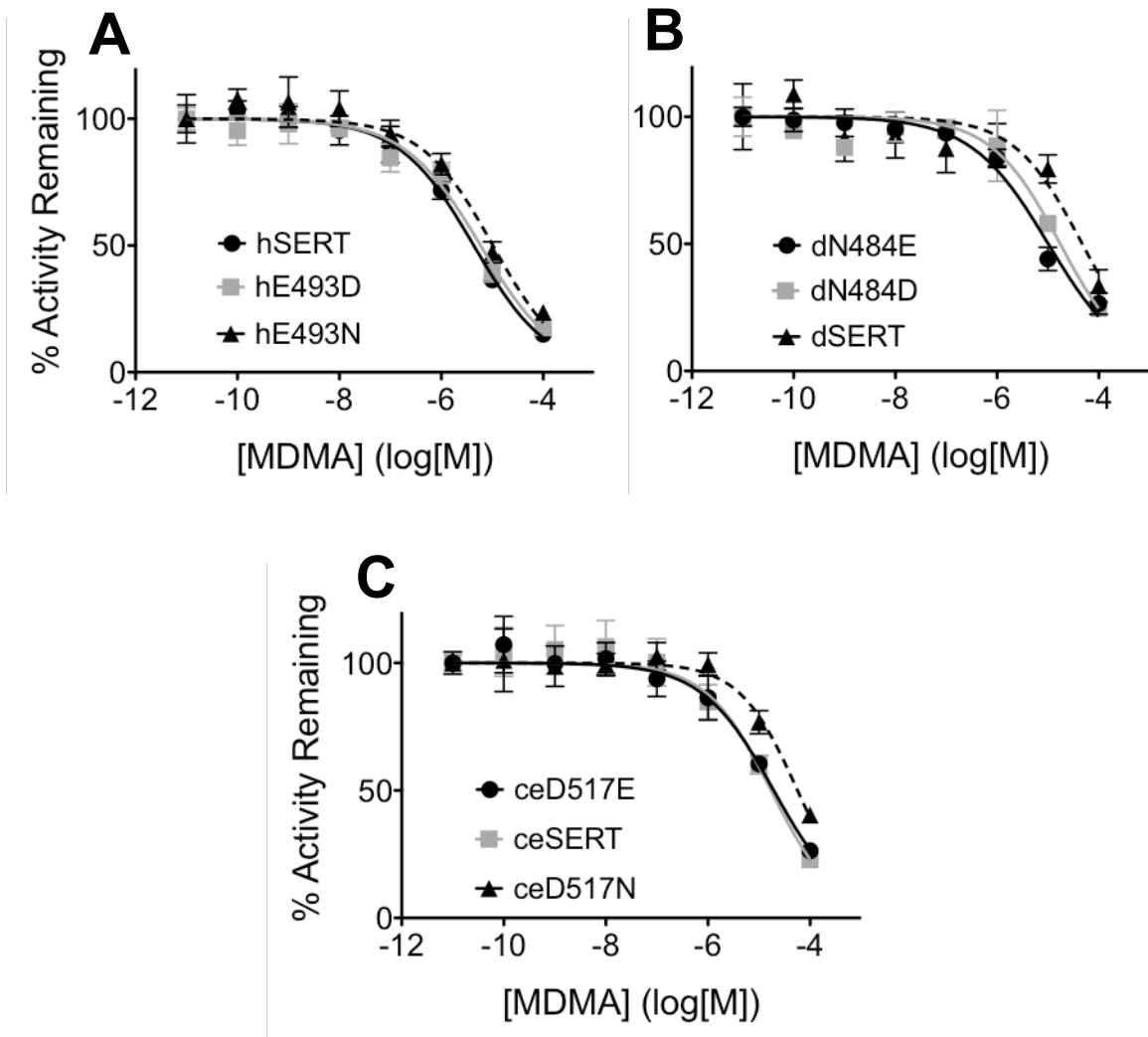
Figure 41. The ability of MDMA to block 5-HT transport is not significantly different when comparing transporters with an acidic amino acid at the outer gate to those that have an Asn. Competitive uptake assay: HEK-GripTite® cells transiently expressing a SERT or SERT outer gate mutant are simultaneously challenged with [^{3}H]5-HT (50nM) and concentrations of MDMA ranging from 10pM – 100μM. After 10 minutes, the assay was terminated by washing with ice-cold buffer and results were quantified. Results are depicted as a dose-response curve for (*A*) hSERT, (*B*) dSERT and (*C*) ceSERT, along with the external gate mutants for each SERT; n ≥ 3.

	MDMA EC$_{50}$ (µM)
hSERT	4.35 ± 1.9
hSERT E439D	5.91 ± 2.4
hSERT E439N	10.3 ± 2.8
dSERT	47.5 ± 8.1
dSERT N484D	17.5 ± 5.9
dSERT N484E	10.2 ± 5.2
ceSERT	17.3 ± 4.4
ceSERT D517E	19.5 ± 6.8
ceSERT D517N	56.8 ± 9.6

Table 5. Estimated EC$_{50}$ values from [^{3}H]5-HT competition uptake analysis. Relative MDMA potency (EC$_{50}$) values for hSERT, dSERT, ceSERT or an external gate mutant from one of the respective SERT species variant backgrounds. EC$_{50}$ values represent mean $\pm$ S.E.M. of a minimum of three separate experiments performed in triplicate.

the transporter, and thus account for the inability of MDMA to act as a substrate (Figure 41).

Transporters possessing an Asn at the external gating position on TM10 demonstrated a trend

toward decreased MDMA potency, with the wild-type dSERT and the ceSERT D517N mutant

exhibiting a ~3.5- and ~3.1-fold decrease in their ability to block [^{3}H]5-HT uptake, respectively,

when compared to the transporters from the same background with acidic amino acids at their

outer gate (Table 5). For the hSERT E493N mutation, this effect was less pronounced (~2.1-fold

decrease in MDMA potency). Despite a trend towards reduced MDMA potency in transporters

with an Asn at the outer gate, these transporters remain capable of binding and blocking [^{3}H]5-

HT uptake. This does not completely rule out the presence of an acidic amino acid being

important for the composition of the MDMA binding site, however it does suggest that MDMA

still binds to transporters with an Asn at the outer gate, but that these transporters are

mechanistically incapable of transporting MDMA.

The Generation of MDMA-Induced Current by SERT is Dependent on the Presence of the Acidic TM10 Gating Residue

Along with inducing efflux, substrates are known to elicit currents when applied to cells

expressing SERT. To measure this effect, two-electrode voltage-clamp (TEVC) studies in

Xenopus laevis oocytes injected with SERT cRNA are used, whereby SERT-expressing oocytes

challenged with 5-HT or MDMA exhibit substrate-induced currents if the ligand is recognized as

a substrate. Previously, we have shown that, for hSERT, similar current amplitudes are observed

for 5-HT and the AMPH-like derivative 5-Methoxy-6-methyl-2-aminoindane (MMAI); however,

for dSERT, current is observed only in response to 5-HT (Rodriguez et al. 2003).

Using the TEVC methodology, we examined hSERT, dSERT, ceSERT and the two

respective outer gate mutants in each background (hSERT E493D and E493N; dSERT N484D

164

and N484E; ceSERT D517E and D517N) to determine the ability of each to mediate 5-HT and/or MDMA-induced current (Figure 42 and Table 6). In direct support of the results from the [³H]5-HT efflux studies, both the wild-type dSERT and the hSERT E493N mutant exhibited 5-HT-induced current but were unable to mediate significant MDMA-induced currents, even at high MDMA concentrations (MDMA-induced currents in hSERT E493N and dSERT were not significantly different than the response to equal MDMA concentrations in water-injected control oocytes). Similarly, the ceSERT D517N mutant showed a sizable decrease (~45%) when comparing its respective MDMA:5-HT-induced current ratio with wild-type ceSERT, however this was not the complete lack of MDMA-induced current that was found with wild-type dSERT or the hSERT E493N mutant, further supporting a difference in the role of the outer gate in each SERT background.

Also in direct support of the [³H]5-HT exchange studies, both dSERT N484D and dSERT N484E demonstrate a gain of function compared to the wild-type dSERT, where both mutants exhibit MDMA-induced currents for which the wild-type dSERT is unable to mediate (Figure 42). Moreover, while the identity of the acidic amino acid does not alter the generation or magnitude of MDMA currents induced in the dSERT or ceSERT mutants, hSERT demonstrates a distinct preference for the presence of a Glu residue over an Asp as MDMA-induced current for hSERT E493D is reduced by ~58% compared with the wild-type hSERT (after first being normalized to each 5-HT-induced current, respectively, to control for differences in expression).

Our competitive binding data revealed that MDMA maintains the ability to bind and inhibit 5-HT uptake in dSERT or hSERT E493N transporters that possess a polar Asn rather than an acidic amino acid at the outer gate (Figure 41). Furthermore, MDMA should inhibit 5-HT-
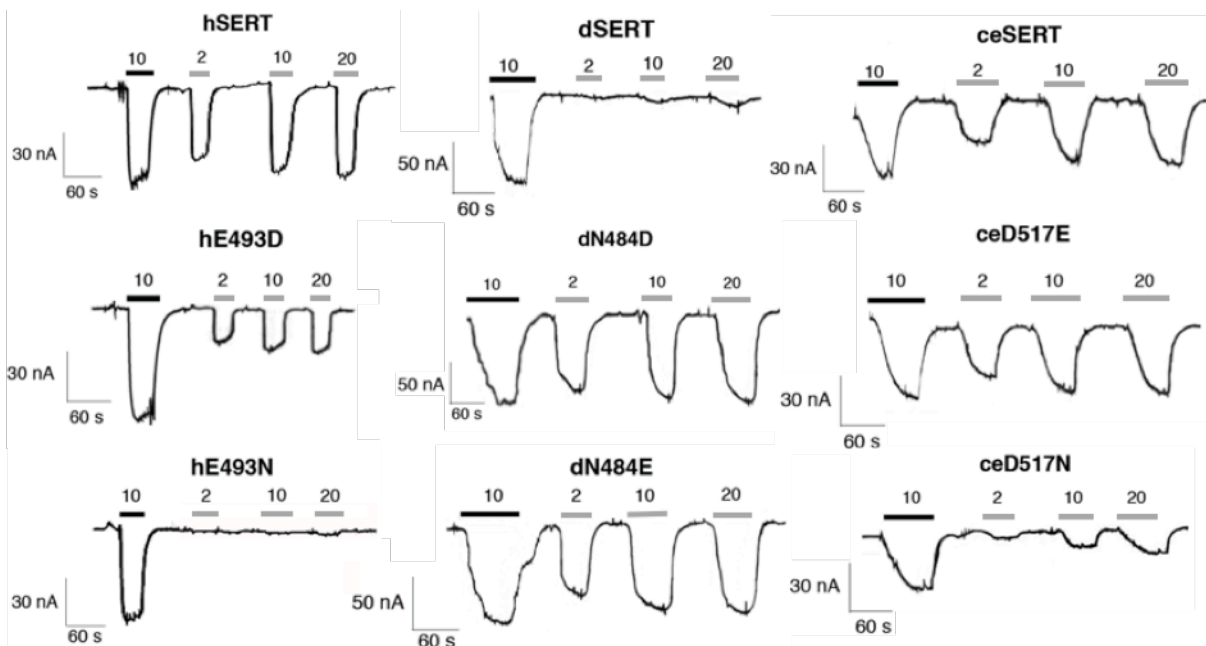
Figure 42. The effect of outer gate composition on 5-HT and MDMA-induced currents. *Xenopus* oocytes injected with mRNA transcripts that code for hSERT, dSERT, ceSERT or one of each species' respective outer gate mutants were examined for substrate-induced currents four-seven days post-injection. Oocyte membranes were held at –60mV and were challenged with either 10μM 5-HT (*black bars*) or 2, 10 or 20μM MDMA (*gray bars*). Traces were smoothed and analyzed using LabChart (AD Instruments). Each trace is representative of a much larger data set, where n ≥ 11. A summary of the average results for each construct can be found in table 6.

Summary table for 5-HT and MDMA-induced currents

	I_{5-HT} [10 µM] (nA ± SEM)	I_{MDMA} [2 µM] (nA ± SEM)	I_{MDMA} [2 µM], as a % of I_{5-HT} [10 µM]	I_{MDMA} [10 µM] (nA ± SEM)	I_{MDMA} [10 µM], as a % of I_{5-HT} [10 µM]	I_{MDMA} [20 µM] (nA ± SEM)	I_{MDMA} [20 µM], as a % of I_{5-HT} [10 µM]	N
hSERT	67.1 ± 8.1	53.1 ± 6.3	79.1	62.9 ± 8.5	93.7	64.6 ± 7.7	96.3	17
hE493D	64.5 ± 7.4	17.9 ± 5.9	27.8	22.2 ± 6.2	34.4	27.6 ± 7.4	42.8	12
hE493N	60.6 ± 6.3	1.0 ± 0.6	1.7	2.2 ± 0.9	3.6	4.8 ± 1.1	7.9	11
dSERT	105.8 ± 9.2	1.7 ± 0.5	1.6	4.4 ± 1.8	4.2	8.2 ± 2.2	7.8	19
dN484D	103.8 ± 11.5	87.0 ± 9.6	83.8	94.1 ± 11.1	90.7	99.5 ± 10.5	95.9	12
dN484E	97.1 ± 9.8	74.9 ± 12.3	77.1	87.4 ± 11.4	90.0	91.8 ± 12.7	94.5	12
ceSERT	46.0 ± 5.5	22.2 ± 4.7	48.3	33.9 ± 5.1	73.7	39.1 ± 4.7	85.0	16
ceD517E	50.4 ± 5.9	36.5 ± 4.1	72.4	43.1 ± 4.4	85.5	45.3 ± 5.8	89.9	11
ceD517N	31.6 ± 4.5	3.1 ± 1.9	9.8	9.4 ± 2.8	29.7	11.7 ± 3.7	37.0	12

Table 6. Summary table for TEVC analysis of 5-HT and MDMA-induced currents. Listed are the average magnitudes of currents generated under each listed condition when *Xenopus* oocytes expressing a SERT or SERT outer gate mutant were challenged with 5-HT or MDMA. Each I_{MDMA} value is listed and is also normalized to the average I_{5-HT} produced by that same transporter (column to the right of each I_{MDMA} column). The N value listed for each transporter is the number of individual oocytes tested under each condition. These oocytes are all taken from a single *Xenopus* frog, but are representative of data from three frogs in total.

induced current in transporters that either lack or exhibit reduced MDMA-induced current. To address this prediction, we used the TEVC method while simultaneously perfusing 0.5µM 5-HT and a range of MDMA concentrations (Figure 43).

Whereas transporters containing an acidic amino acid at the outer gate all demonstrated substrate-induced currents under all the tested conditions, with wild-type dSERT and the hSERT E493N mutant we observe that higher concentrations of MDMA are capable of blocking the 5-HT-induced current (Figure 43). Similarly, the ceSERT D517N mutant exhibits greatly reduced 5-HT-induced currents in the presence of increased MDMA concentrations, although the substrate-induced current is not completely eliminated, as a small but significant MDMA-induced signal can be detected. A similar effect is seen with the hSERT E493D mutant, whereby increasing the concentration of MDMA results in a decrease in the magnitude of the induced current due to the decreased capacity of the hSERT E493D transporter to transport MDMA. Overall though, increased concentrations of MDMA are capable of diminishing or even eliminating the 5-HT-induced current in transporters with reduced MDMA transport capacities, suggesting that MDMA remains capable of binding to transporters with and Asn at the outer gate but that once bound the transporter is unable to initiate or complete the translocation mechanism.

Discussion

The use of species variants in the primary amino acid sequence of MATs to discern the functions of individual residues has been a well-utilized and beneficial methodology (Barker et al. 1994; 1999; Adkins et al. 2001; Henry et al. 2006b). Here, we demonstrate that the presence of an acidic amino acid at the outer gate is vital for the ability of SERT to transport MDMA and
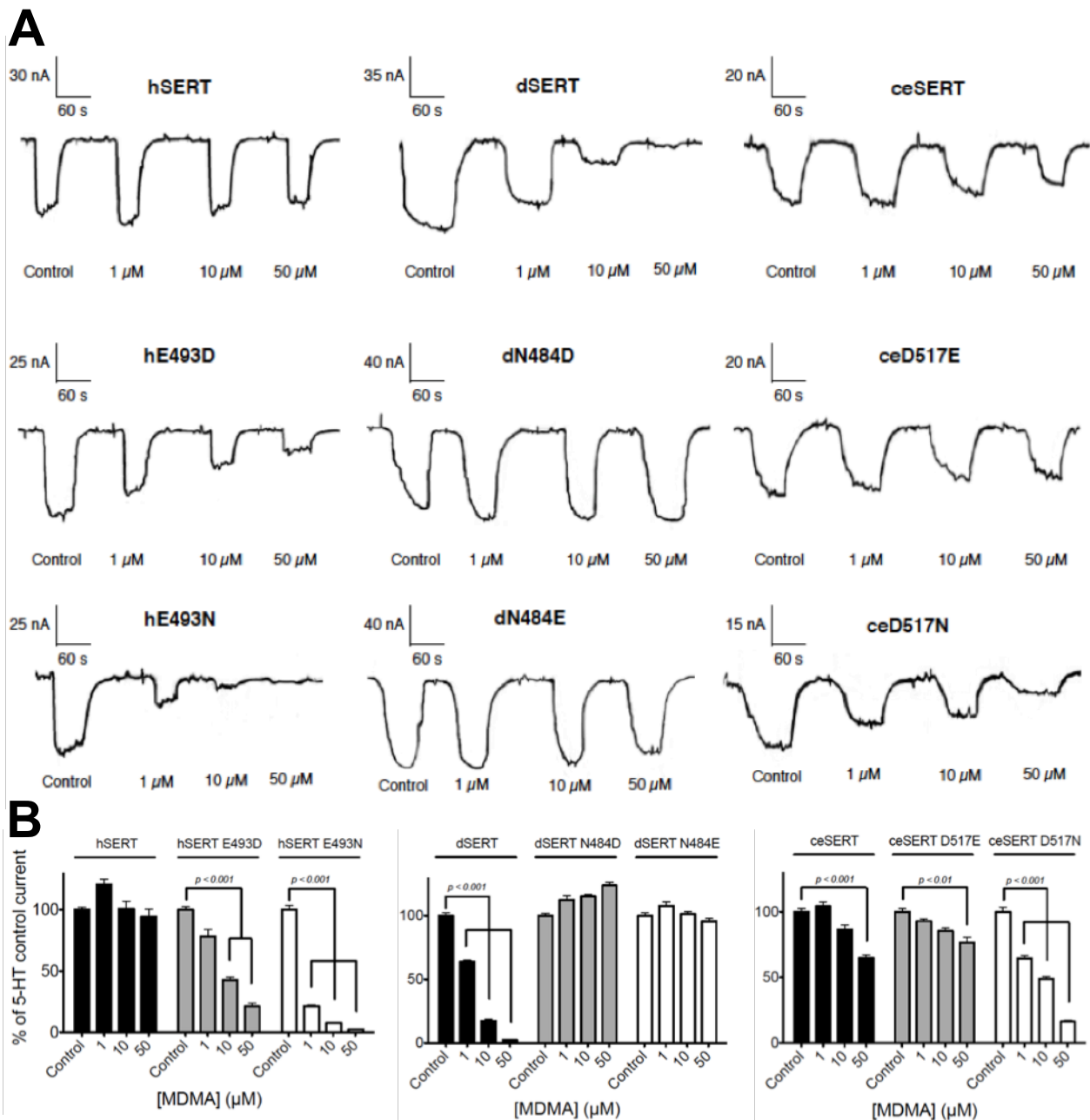
Figure 43. MDMA binds and blocks 5-HT transport in transporters with an Asn at the TM10 external gating position – (*A*) TEVC analysis, where the cell membrane was held at –60mV and oocytes were simultaneously challenged with 1μM 5-HT and the amount of MDMA labeled under each respective trace. Curves labeled control were only challenged with 5-HT. Each trace is a representation of a much larger data set, where n ≥ 8. (*B*) Graphical representation of TEVC data in (*A*), where each bar denotes the magnitude of the average current induced at each tested condition as a percentage of the average magnitude generated under the control (5-HT only) condition. A one-way ANOVA was performed for each construct, and significant differences from the control are denoted with brackets above the bars.

to mediate the process of MDMA-induced efflux.

The acidic amino acid found in the external gating position in TM10 of hSERT (E493) is highly conserved throughout the SLC6 family (Beuming et al. 2006). Crystal structures from a bacterial homolog of the MATs, LeuT, as well as a crystal structure of the dDAT provide direct evidence that this acidic residue (an Asp in both LeuT and dDAT) forms an important interaction with an Arg (homologous to R104 in hSERT) located at the cytoplasmic end of TM1, which aids in stabilizing the formation of an outer gate (Yamashita et al. 2005; Singh et al. 2008; Penmatsa et al. 2013). In most crystal structures, interaction between D404 (LeuT numbering) and R30 (LeuT) is shown to be water mediated, however in an inward-facing conformation of LeuT, there is a direct ionic interaction between the two residues (Krishnamurthy and Gouaux 2012). This provides strong evidence that the R30-D404 salt bridge produces a stronger and/or tighter seal to effectively block access between the extracellular milieu the inside of the cell during the translocation process. In addition, such a bond would likely stabilize the inward-facing conformation. The findings we present here indicate the importance of a negative charge at the TM10 external gating position to the mechanism of MDMA transport in SERT (Figures 42 and 40), and therefore it is tempting to speculate that the formation of a salt bridge with R104 (hSERT) at the outer gate is a critical step of the MDMA translocation process.

Both charged gating residues form multiple interactions that are highly important to the translocation mechanism. For instance, the well conserved gating residue R30 (LeuT numbering) has been reported to form two additional hydrogen bonds with TM10 mediated through the polar side chain of T409 and the backbone carbonyl of G408 (LeuT numbering; T497 and G498 in hSERT), along with the salt bridge with the acidic residue on TM10 when the external gate is

closed. Therefore, our substitution of this Arg with an acidic amino acid (Figure 37) likely resulted in a disruption of the interactions that are necessary for the composition of the extracellular gate, thereby destroying proper functionality of the transport mechanism. Our findings are consistent with work on the GABA transporter GAT-1, where even the conservative replacement of this TM1 Arg with a Lys completely eliminating substrate uptake activity (Pantanowitz et al. 1993). This same conservative mutation in hSERT (R104K) retains functionality, though it does impart a ~5-fold decrease in the V_{max} for 5-HT transport and causes a drastic decrease in allosteric potency of both the SSRI (*S*)-citalopram and the TCA clomipramine (Plenge et al. 2012).

Analysis of the inward-facing crystal structure of LeuT suggests that, in addition to preventing the access of extracellular milieu to the binding region when the transporter is facing the cytoplasm, the salt bridge at the extracellular gate may also be important in the stabilizing of TM1b during the process of structural rearrangement when moving to the inward-facing conformation. This is consistent with the "rocking bundle" mechanism purposed by Forrest and Rudnick, where TMs 1, 2, 6 and 7 act as a moving bundle against the stationary scaffold composed of TMs 3, 4, 5, 8, 9 and 10, allowing the transporter to modulate through the outward, occluded and inward states (Forrest and Rudnick 2009). In this way, the extracellular salt bridge acts as an anchor, which tethers TM1b to TM10 (Figure 8) and keeps their position relatively stable. This allows TM1a to pivot outward at a specific hinge point in the unwound region of TM1 (Krishnamurthy and Gouaux 2012). The position of these hinge structures has profound consequences for the substrate and both Na^+ ion sites (termed Na1, the site adjacent to the substrate binding site, and Na2, the site that is slightly more distal from the bound substrate)

171

when the transporter is in the inward-open state. The hinge for TM1a is located at Leu25, which is considerably more central than the Na2 binding site, leading to separation of residues on TM1a from the static TM8 as TM1a undergoes a large shift away from the scaffold domain in order to open the permeation pathway to the cytoplasm. This dramatic shift in the position of TM1a relative to the scaffold domain effectively destroys the Na2 site and demonstrates how the release of this Na^+, the movement of TM1a and the opening of the transporter to the cytoplasm are coupled. A similar mechanism has been suggested for the *V. parahaemolyticus* sodium/galactose transporter (vSGLT) (Shimamura et al. 2010) and supported through both biochemical and computational studies of SERT (Koldsø et al. 2011; Felts et al. 2014).

Likewise, there are two hinge residues in TM6, S256 in TM6a and F259 in TM6b. During dynamic movement to the inward-facing conformation, these hinge regions remain relatively static by comparison to residues at the ends of TMs 1 and 6. Therefore, because the hinge residues undergo little displacement during the transition to the inward facing conformation, many of the substrate binding residues on TMs 3 and 8 that are in close proximity to these hinge regions remain unperturbed, maintaining the structural integrity of the aliphatic portion of the substrate-binding pocket. Thus, although dramatic movements in positioning of TM1 and TM6 affect residues coordinating the amino group of the substrate (allowing for the dissociation of substrate into the cytoplasm), a considerable portion of the substrate-binding pocket is retained in the inward-open state, possibly preserving the ability of the transporter to bind substrate under conditions of reversed substrate flux.

Similarly, the tethering of TM1b to the scaffold domain during the MDMA translocation process may be crucial for the conformational shift to an inward facing pose. In fact, the overall

172

stabilization of TM1b that is brought about by formation of the salt bridge at the outer gate could have conformational consequences in the N-terminal tail, thereby allowing kinases to access specific phosphorylation sites whose modification have been linked to the efflux mechanism (Khoshbouei et al. 2004; Sucic et al. 2010; Cremona et al. 2011; Pizzo et al. 2013). Changes to the conformation of the N-terminal tail could be substrate-dependent, as molecules of different sizes and chemical groups could impart distinct inward-facing conformations, which may impact the ability of the transporter to be post-translationally modified (ie phosphorylation). Likewise, increased stability of the inward-facing conformation mediated by the external salt bridge or alternative states resulting from MDMA transport could alter the conformational equilibria of the transporter, resulting in an increase in the population of transporters facing the cytoplasm. Such changes in the conformational equilibria of the transporter have previously been associated with the uncoupled flux of Na^+ ions, as it is the presence of these suprastoichiometric Na^+ ions in the cytoplasm that are thought to thermodynamically drive efflux (Scholze et al. 2000; Sitte et al. 2000; Schicker et al. 2011). Furthermore, changes in the conformational equilibria of the transporter are altered by interaction of the phospholipid PIP_2 with the N-terminus, a connection that, when impeded, modifies the magnitude of uncoupled current flux through SERT (Buchmayer et al. 2013) and eliminates the ability of DAT to mediate efflux (Hamilton et al. 2014).

Recently, Blakely and colleagues described a DAT mutation, A559V, which is found in a small population of humans diagnosed with attention deficit hyperactivity disorder (ADHD) (Mazei-Robison et al. 2008). Studies revealed that DAT A559V exhibits enhanced non-vesicular, DAT-dependent DA release and unexpectedly DA efflux is actually blocked by AMPH as

173

opposed to enhancing efflux as seen with wild-type hDAT. Likewise, the presence of an Asn at the TM10 gating position in dSERT and the hSERT E493N mutant (rather than an acidic amino acid), yielded a transporter where MDMA functions as an antagonist rather than a substrate. In addition, we found that Asn at the outer gate increases the rate of basal efflux through SERT to a level comparable to the hDAT A559V mutant (data not shown). Therefore, it is possible that the effect of the DAT A559V mutation on the overall structural dynamic of the transporter may result in a similar alteration of conformational equilibria, thereby producing a similar phenotype.

Currently, the molecular components and interactions necessary to engage the translocation mechanism remain poorly understood and even controversial. Evidence from Shi *et al*. that suggests that an additional molecule of substrate may be requisite to trigger the completion of the translocation mechanism of SLC6 transporters (Shi et al. 2008). This study in LeuT employed biochemical techniques in concert with molecular dynamic simulations to propose the existence a second substrate-binding site (termed S2) just above where the salt bridge divides the extracellular vestibule from the core-binding region of the transporter (S1). Although a crystal structure showing substrate bound to this S2 site has not been discovered and these claims of an S2 site are contested by studies from the Goaux lab, several studies from the Javitch group have presented compelling evidence for its existence (Zhou et al. 2007; Singh et al. 2008; Zhou et al. 2009). Javitch and colleages suggest that the S2 site is obstructed from substrate binding during crystallography by requisite detergents used in the process of crystal formation, which occupy the S2 site and outcompete leucine binding (Quick et al. 2009; 2012). However, this putative S2 site shares many of the same attributes as S1, such as the hydrophobic pocket, which accommodates the aliphatic substrate side chain, and an "ionic cleft" formed by

the gating residues D404 and R30, which coordinate with the carboxyl and amine groups of the substrate (Shi et al. 2008). Reportedly, binding of substrate at S2 occurs once the outer gate is closed and the transporter is in an occluded conformation. MD simulation data, as well as several eloquent biochemical assays, demonstrated that the two molecules of substrate are capable of binding to LeuT at the same time and that occupancy of the S2 site by leucine is critical for substrate translocation. These data lead the authors to purpose a mechanism, whereby the binding of substrate to S2 is critical for triggering the release of one of the Na^+ ions (Na1) and the substrate bound at S1 into the cytoplasm. To our knowledge, no one has looked to determine if such a model holds true with MDMA or AMPH.

Nevertheless, assuming that the two-site model is correct, 5-HT can bind to both S1 and S2 and act as a substrate even if the TM10 gate residue is Asn (Table 4). However, it is possible that the size or chemical makeup of MDMA prohibits it from binding to the S2 site without an acidic residue to support its coordination. Under these conditions, 5-HT would bind both sites and promote translocation but MDMA would be incapable of engaging the transport process, as it could only bind the S1 site. Our [^{3}H]5-HT competitive uptake data demonstrates that MDMA acts as an antagonist at dSERT and hSERT E493N, which lack the acid gate residue (Figures 41 and 43). This would explain why AMPH remains capable of binding with relatively high potency to transporters containing an Asn at the external gate, as the S1 site would be unperturbed by alterations at the outer gate. However, our current analysis lacks the resolution to determine if MDMA is biding to S1, S2 or both. Future work will involve targeting the S2 site to characterize its involvement in the recognition of MDMA as a substrate.

In summary, our work demonstrates that the presence of an acidic amino acid at the outer

gate is critical for the recognition of MDMA as a substrate and the induction of the efflux machinery. This study is the first, to our knowledge, in eukaryotic transporters to demonstrate how a single mutation can completely alter the ability of the transporter to recognize a ligand as either an agonist or antagonist. Previous work by Piscitelli et al also characterize a single mutation that alters ligand recognition, whereby the introduction of the I359Q mutation in the binding site of LeuT resulted in the recognition of the classical LeuT antagonist tryptophan as a functional substrate (Piscitelli and Gouaux 2012). Both of our studies emphasize how even a single mutation can completely alter the functionality of the transporter, highlighting the intricate nature of the transport machinery. In the case of the acidic residue on TM10 that we characterize here, we speculate that the presence of a negative charge at the external gate is likely important because it allows for the formation of a salt bridge with an Arg on TM1, which is critical for the maintenance of a closed outer gate. The formation of this salt bridge may also be mechanistically important for the stabilization of a critical intermediary step in the MDMA translocation process, and play a role in mediating other SERT functions, such as the uncoupled flux of Na^+ ions and the AMPH-induced efflux of substrate.

CHAPTER VI

NOVEL AZIDO-IODO PHOTOAFFINITY LIGANDS FOR THE SEROTONIN TRANSPORTER BASED ON THE SELECTIVE SEROTONIN REUPTAKE INHIBITOR (*S*)-CITALOPRAM

Introduction

The serotonin transporter (SERT) is a member of the solute carrier 6 (SLC6) family of transporters that functions to regulate serotonin neurotransmission and homeostasis(Kristensen et al. 2011; Pramod et al. 2013; Rudnick et al. 2014). In particular, selective serotonin reuptake inhibitors (SSRIs) and tricyclic antidepressants (TCAs), widely prescribed medications for treatment of anxiety and major depressive disorders, principally work by binding to SERT and inhibiting serotonin reuptake into presynaptic neurons (Gillman 2007; Pastoor and Gobburu 2014). Notably, (*S*)-citalopram (Escitalopram, Figure 44) binds with high affinity and selectivity to hSERT. However, despite its well-documented clinical success, the molecular interactions between (*S*)-citalopram and hSERT that determine its reuptake inhibition potency and selectivity over other monoamine transporters (i.e., the norepinephrine transporter (NET) and dopamine transporter (DAT)) remain poorly understood.

The 3-D structure of SERT, as well as its structure, function, and regulation, including oligomerization and distribution in cells or brain tissue, have been studied with small molecular probes containing electrophiles (e.g. N_3, NCS) and radiolabels (e.g. ^3H, ^{125}I) (Smith and Collins 2015). In particular, the well-known technique of photoaffinity labeling utilizes molecular probes that contain a functional group capable of forming a covalent bond to a biological target upon
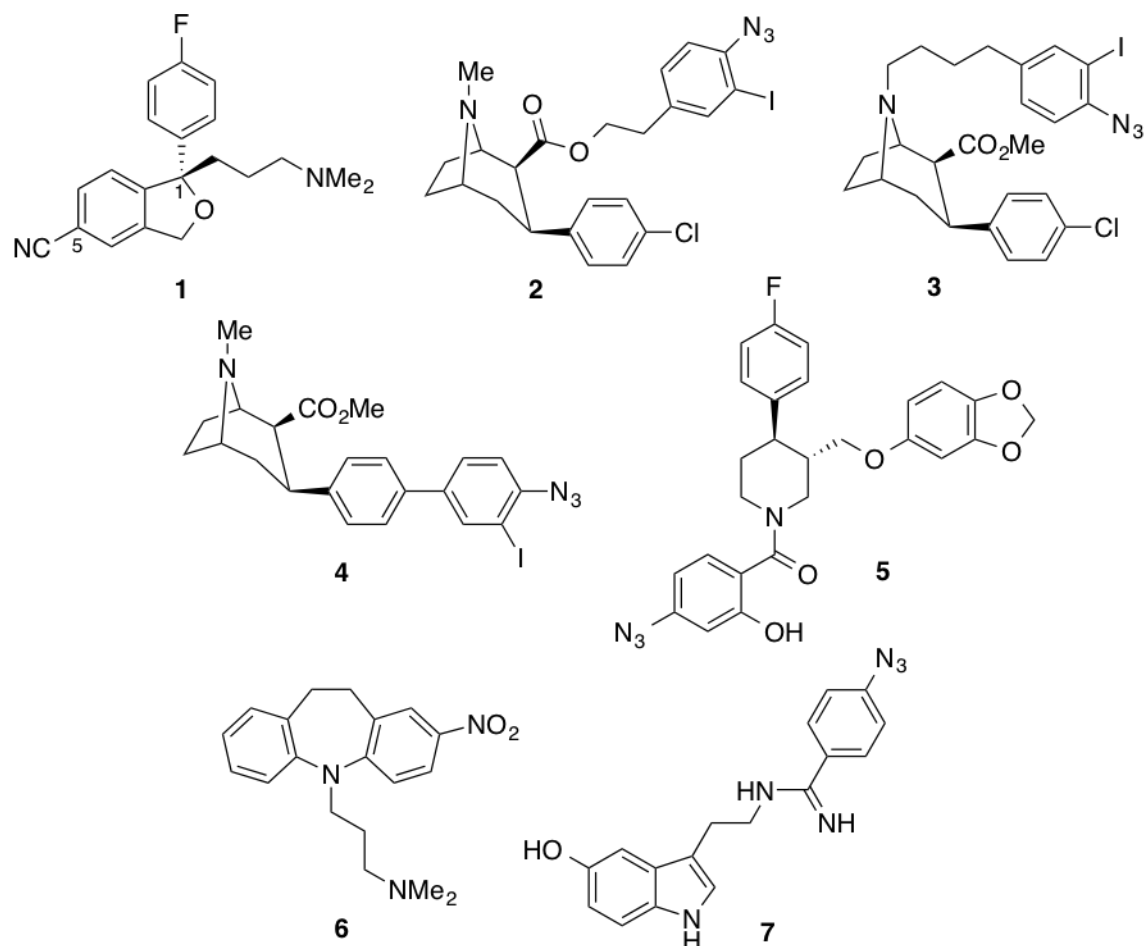
Figure 44. Chemical structures of (*S*)-citalopram and known DAT and/or SERT inhibitor PALs. Depicted are a two-dimensional representation of the chemical structures for (*1*) (*S*)-citalopram, (*2*) RTI-82, (*3*) MFZ 2-24, (*4*) JHC 2-48, (*5*) paroxetine, (*6*) 2-nitroimipramine and (*7*) the arylazido derivative of serotonin, 3-(fl-(4-azidobenzami- dino)ethyl)-5-hydroxyindole (SABA).

photoactivation (Chuang and Otagiri 2013). Of the numerous photoreactive functional groups that can be employed in the design of photoaffinity ligands (PALs) (e.g., benzophenones, aliphatic and aromatic diazirines, etc.), aryl azides are most effectively used given their relatively small size, ease of synthetic incorporation, and chemical stability (Lochner 2010).

Numerous [125I]-radiolabelled-arylazido analogs of dopamine transporter (DAT) inhibitors including cocaine (Carroll et al. 1992; Zou et al. 2001; Lever et al. 2005; Newman et al. 2006), GBR12909 (Grigoriadis et al. 1989; Sallee et al. 1989; Dutta et al. 2001; Cao et al. 2004), benztropine (Agoston et al. 1997; Zou et al. 2001; 2003), pyrovalerone (Lapinsky et al. 2009; 2012), bupropion (Lapinsky et al. 2012), and methylphenidate (Lapinsky et al. 2011) have been developed to elucidate molecular components of the ligand-binding site and mechanisms underlying uptake inhibition. The 4'azido, 3'-iodo-substituted phenyl ring is a common structural motif found in many PALs that bind DAT irreversibly upon photoactivation (e.g., RTI 82, MFZ 2-24 and JHC 2-48; Figure 44) (Carroll et al. 1992; Zou et al. 2001; Lever et al. 2005; Newman et al. 2006). Specifically, the tropane-based PALs RTI-82 and MFZ 2-24 have been instrumental in defining drug-protein interactions at the molecular level and thus further defining the structural components of DAT that are critical for transport inhibition by cocaine (Vaughan et al. 1999; Parnas et al. 2008; Dahal et al. 2014).

In contrast to DAT PALs, the development of SERT selective PALs has been more limited. To the best of our knowledge, only a few PALs have been synthesized and experimentally validated to label SERT (Figure 44). Although the tropane-based PALs bind to SERT as well as DAT, to date, only MFZ 2-24 has been used to photolabel the hSERT
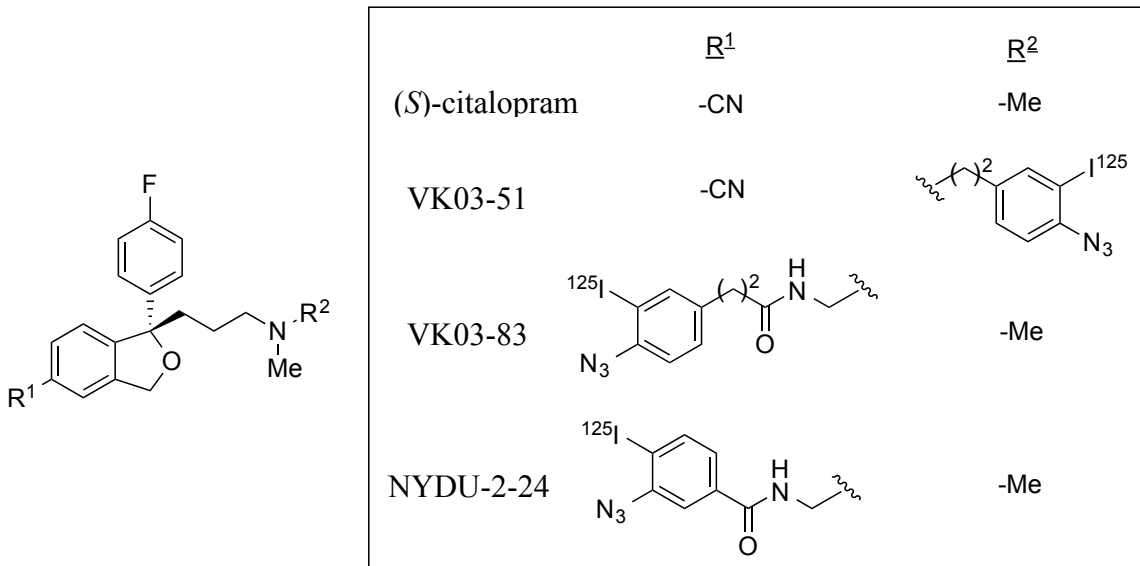
Figure 45. Substitutions at the C-1 and C-5 position on the (*S*)-citalopram structure for the PALs VK03-51, VK03-83 and NYDU-2-24. Shown is the basic parental structure of (*S*)-citalopram (*left*) and a table that defines the chemical constituents found at the C-5 (R^1) and C-1 (R^2) positions for (*S*)-citalopram, VK03-51, VK03-83 and NYDU-2-24, respectively.

(Zou et al. 2001; Lever et al. 2005; Henry et al. 2006b). Other inhibitor-based ligands that photolabel SERT include the aryl-azido derivative of the SSRI paroxetine (Chudzik et al. 1995) and a tricyclic antidepressant-based PAL, [^{3}H]-2-nitroimipramine that showed covalent incorporation into SERT present in membrane homogenates of rat brain and liver, and human platelets (Rehavi et al. 1983; Wennogle et al. 1985). Finally, photoinactivation of serotonin uptake has been demonstrated by an azidobenzamidine derivative of serotonin (Ransom et al. 1985). However, to date none of these SERT PALs have been used to define the structural basis of their binding interactions at the hSERT.

Based on the successful application of PALs (Vaughan et al. 1999; Parnas et al. 2008; Dahal et al. 2014) in elucidating drug-binding site interactions at DAT our concept for the present study was that appending the 4'-azido, 3'-iodo aryl moiety onto different positions of the (*S*)-citalopram base might reveal different sites of adduction on hSERT that would enable a clearer understanding of the (*S*)-citalopram binding mechanism. Extensive structure-activity relationships have been described with analogs of citalopram that suggest positions C-1 and C-5 can accommodate significant steric bulk without appreciable loss in hSERT binding affinity (Zhang et al. 2010; Banala et al. 2013; Kumar et al. 2014). Herein, described is the pharmacological evaluation of three novel C-1 or C-5 substituted 4'-azido, 3'-iodo- analogues of (*S*)-citalopram (named NYDU-2-24, VK03-51 and VK03-83; Figure 45) and demonstrated is their ability to covalently label hSERT upon photoactivation.

Methodology

Whole-cell Competition Uptake Assay

HEK-293 GripTite™ cells (Invitrogen) were plated in 24-well Culturplates (PerkinElmer) at 50,000 cells/well and transiently transfected with wild-type hSERT or hSERT S438T-conttaining pcDNA3 based plasmid constructs using the Trans-IT LTI transfection system (Mirus Bio). Assays were conducted 36-48 hours after transfection where cells were washed using MKRHG buffer (5mM Tris, 7.5mM HEPES, 120mM NaCl, 5.4mM KCl, 1.2mM CaCl$_2$, 1.2mM MgSO$_4$, 10mM Dextrose, pH 7.4), preincubated with the competitor compounds for 5 minutes followed by addition of [^{3}H]5-HT at a final concentration of 50nM. Uptake was allowed to proceed for 10 minutes and then terminated by washing twice with ice-cold MKRHG. [^{3}H]5-HT uptake was quantified by dissolving cells in Microscint-20 (PerkinElmer) and using the Packard TopCount NXT (PerkinElmer) to measure radioactivity (CPM). Data were normalized to percent activity in the absence of a drug competitor for each form. Assays were carried out in triplicate and were repeated at least four times. K$_i$ values were determined using Prism 5 (GraphPad).

hSERT Photoaffinity Labeling

Photoaffinity labeling of hSERT was performed using methods that have been verified previously for assessing irreversible adduction of a variety of ligands for both DAT and SERT (Agoston et al. 1997; Vaughan et al. 1999; Lever et al. 2005; Newman et al. 2006; Henry et al. 2006b; Parnas et al. 2008; Lapinsky et al. 2009; 2011; 2012; Dahal et al. 2014). These procedures were performed using LLCPK$_1$ cells stably expressing HA-hSERT (generous gift of Dr. James Foster) and with untransfected parent LLCPK$_1$ cells for negative controls. Cells were

grown to 90% confluence in 12-well plates and washed with KRH buffer. $[^{125}I]$VK03-51, $[^{125}I]$VK03-83 and $[^{125}I]$NYDU-2-24 were added to a final concentration of 10nM and incubated for 1.5 hours at 4ºC. In some experiments, hSERTs were irreversibly labeled in parallel with $[^{125}I]$MFZ 2-24 as a positive control (Henry et al. 2006b). For pharmacological displacement, 10µM (*S*)-citalopram was added 30 minutes prior to addition of the radioligands. Cells were irradiated with shortwave ultraviolet light (254nm, Fotodyne UV Lamp model 3-6000) for 5 minutes at a distance of 15–20mm to photoactivate the radioligand, washed twice with 1mL of ice-cold KRH buffer and lysed by addition of 0.5mL of RIPA buffer (50mM NaF, 2mM EDTA, 125mM Na_3PO_4, 1.25% Triton X-100, and 1.25% sodium deoxycholate) containing protease inhibitors for 30 minutes on ice. Lysates were centrifuged at 20,000 x g for 15 minutes at 4ºC to remove insoluble material and subjected to immunoprecipitation and immunoblotting using anti-HA monoclonal antibody (Covance) or anti-SERT antibody ST51 (mAB Technologies) as previously described (Henry et al. 2006b). Immunoprecipitated samples were separated on 4-20% SDS-polyacrylamide gels followed by autoradiography (Hyperfilm MP film; GE Healthcare) for 1-3 days at –80ºC. For immunoblotting, cell lysates were separated on 4–20% SDS-polyacrylamide gels transferred to 0.45mm polyvinylidene difluoride membranes and probed for hSERT with anti-HA antibody.

Results

Pharmacological properties of NYDU-2-24, VK-03-51 and VK-03-83

Inhibition of $[^3H]$5-HT uptake by WT hSERT and the hSERT S438T mutant was evaluated to determine inhibitory constants for NYDU-2-24, VK03-51, VK03-83, and (*S*)-

citalopram. When tested against WT hSERT the C-5 substituted PALs NYDU-4-24 and VK03-83 showed affinities of 24nM and 38nM, respectively, values that were reduced by 11-fold and 17-fold compared to that of (*S*)-citalopram (K_i = 2.2nM) (Figure 46, Table 7). In contrast, the C-1 substituted PAL VK03-51 showed a greater reduction in affinity (K_i = 227nM, 100-fold) compared to (*S*)-citalopram, which is in accord with structure-activity relationships previously described (Banala et al. 2013). When tested against hSERT S438T, all four compounds showed dramatic rightward shifts in inhibitory potency (Figure 46, dashed lines) with K_i values ranging from 3.8 to 9.9μM (Table 7). These findings are consistent with previous reports that S438 is a key residue for high-affinity binding of many hSERT antagonists and that its mutation to Thr results in significant loss in potency for (*S*)-citalopram and many other hSERT inhibitors (Andersen et al. 2009). Interestingly, the C-1-substituted PAL VK03-51 demonstrated significantly lower affinity than (*S*)-citalopram or the other PALs for WT hSERT, but an affinity that trended higher for the S438T mutant. Moreover, the difference in binding affinities between the mutant and WT hSERT for VK03-51 was only 17-fold, as compared to the significantly more dramatic shift for the parent ligand, (*S*)-citalopram (~3600-fold).

Photoaffinity labeling experiments with hSERT

Next, we tested [^{125}I]VK03-51, [^{125}I]VK03-83 and [^{125}I]NYDU-2-24 for irreversible labeling of HA-hSERT upon photoactivation (Figure 47). For these studies, HA-hSERT LLCPK1 cells were incubated with the PALs in the presence or absence of (*S*)-citalopram as indicated, and irradiated with UV light to cross link the ligand to the protein. Lysates were immunoprecipitated with anti-HA or anti-hSERT antibodies, and samples analyzed by SDS-PAGE and autoradiography. These methods, have been used to verify photolabeling of DAT and SERT by numerous structurally
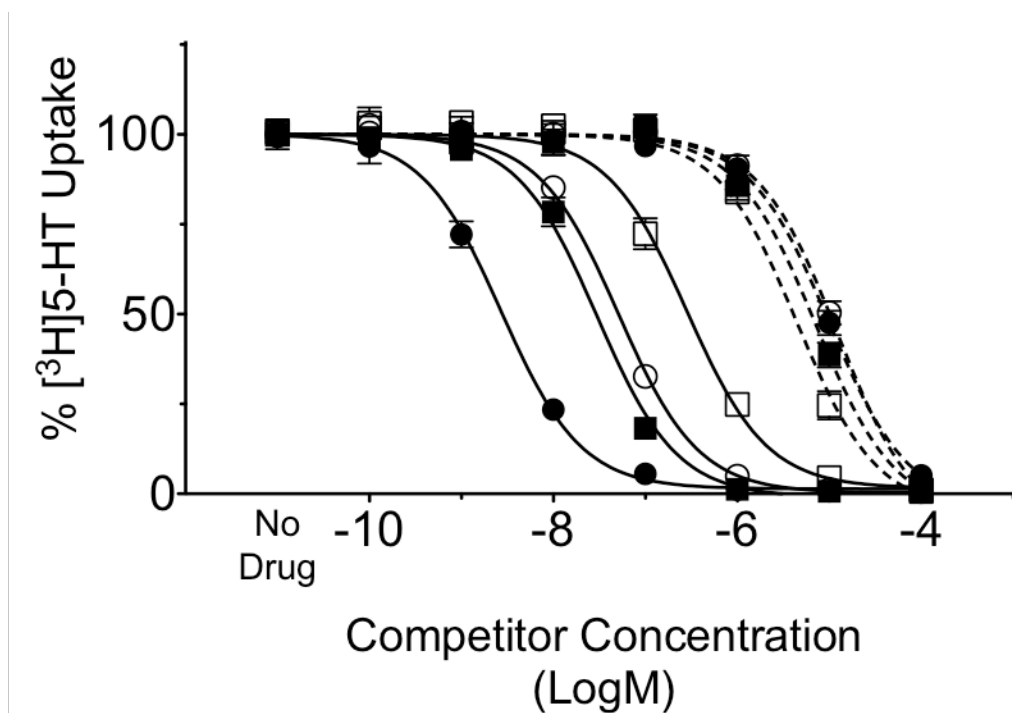
Figure 46. [³H]5-HT uptake inhibition analysis for *(S)*-citalopram, VK03-51, VK03-83 and NYDU-2-24. HEK-293 Griptite™ cells expressing hSERT (solid lines) or hSERT S438T (dashed lines) were assayed for [³H]5-HT uptake in the presence of the indicated concentrations of *(S)*-citalopram (*filled circles*), VK03-51 (*open squares*), VK03-83 (*open circles*) or NYDU-2-24 (*filled squares*). Data shown are means ± SEM of transport activity for each form in the absence of competitor, set to 100%. Assays were conducted in triplicate and were repeated at least four times.

	hSERT (K_i,nM)	hSERT S438T (K_i,nM)
(S)-citalopram	2.2 ± 0.17	7879 ± 1300[*]
VK03-51	227 ± 23[#]	3811 ± 590[*]
VK03-83	38 ± 2.9[#]	9879 ± 1200[*]
NYDU-2-24	24 ± 2.2[#]	5697 ± 745[*]

Table 7. Inhibitory constants of *(S)*-citalopram, VK03-51, VK03-83 and NYDU-2-24 for [3H]5-HT transport by hSERT and hSERT S438T. Data are K_i values (*nM*) (*means ± SEM*) for the ability of the (*S*)-citalopram-based PALs to inhibit uptake of [3H]5-HT as shown in Figure 6.3. K_i values were calculated using the Cheng-Prusoff equation in GraphPad Prism 5. Data were analyzed by paired *t*-tests for statistical significance where ***** denotes the K_i value obtained with the hSERT S438T mutant is significantly different than the K_i for WT hSERT (p < 0.001) and **#** indicates that the K_i value for the analog is significantly different than the K_i for (*S*)-citalopram obtained with WT hSERT (p < 0.001). The K_i values obtained with hSERT S438T for the analogs and *(S)*-citalopram were not statistically different from one another.
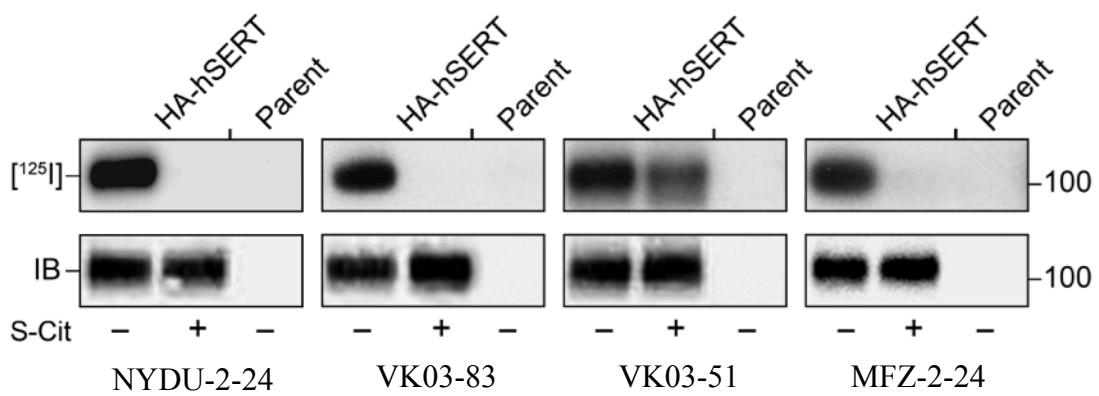
Figure 47. Photoaffinity labeling of hSERT. HA-hSERT LLCPK$_1$ cells or nontransfected (parent) LLCPK$_1$ cells were incubated with the indicated ligands in the absence (−) or presence (+) of 10μM *(S)*-citalopram (*S-Cit*). Cell lysates were immunoprecipitated with Anti-HA antibodies followed by SDS-PAGE and autoradiography to detect [^{125}I] radiolabeled proteins (*upper panels*) or were analyzed by immunblotting (*IB*) with anti-HA to detect total hSERT (*lower panels*). Results are representative of three independent experiments.

diverse tropane and non-tropane based ligands (Agoston et al. 1997; Vaughan et al. 1999; Lever et al. 2005; Newman et al. 2006; Henry et al. 2006b; Parnas et al. 2008; Lapinsky et al. 2009; 2011; 2012; Dahal et al. 2014). The results show that $[^{125}I]VK03-51$, $[^{125}I]VK03-83$ and $[^{125}I]NYDU-2-24$ all covalently label a protein of the expected hSERT molecular mass of ~100 kDa when using HA-hSERT cells, but that this band was not obtained from non-transfected hSERT-null parent cells (upper panels), supporting the identity of the band as hSERT. Immunoblotting (lower panels) verified the presence and absence of hSERT in transfected and untransfected cells, respectively. The photoaffinity labeled proteins were immunoprecipitated using anti-HA antibody (Figure 47), as well as with the anti-hSERT antibody ST-51 (not shown), but were not precipitated with non-immune IgG (not shown), also supporting the identity of the bands as hSERT. Similar results were obtained using the tropane PAL MFZ 2-24, which was previously demonstrated to photolabel hSERT (Henry et al. 2006b). Together these results demonstrate that hSERT protein is irreversibly labeled with $[^{125}I]VK03-51$, $[^{125}I]VK03-83$ and $[^{125}I]NYDU-2-24$, providing the first demonstration of photoaffinity labeling of hSERT by analogs of (*S*)-citalopram.

For pharmacological characterization of irreversible labeling, HA-hSERT-LLCPK$_1$ cells were incubated with either vehicle or 10μM (*S*)-citalopram prior to addition of the radioiodinated PALs. Incorporation of $[^{125}I]VK03-83$ and $[^{125}I]NYDU-2-24$ was blocked by >99% (Figure 47, left and center-left panels), demonstrating that (*S*)-citalopram fully displaces these C-5 substituted radioligands prior to photoactivation, further supporting the identity of this protein as hSERT. Similar results were obtained for displacement of hSERT labeling by $[^{125}I]MFZ$ 2-24**,** as we previously demonstrated (Henry et al. 2006b). In contrast, 10μM (*S*)-citalopram inhibited

[^{125}I]VK03-51 labeling of hSERT by only ~30%, suggesting that this C-1-substituted PAL possesses a different pharmacological profile than the two C-5-substituted ligands. In a previous SAR study wherein (*S*)-citalopram was modified by *N*-substitution at the C-5 position with a second molecule of (*S*)-citalopram to create a homobifunctional ligand, binding data suggested simultaneous interaction of the ligand with the S1 and S2 binding sites (Banala et al. 2013). (*S*)-citalopram binds to both S1 and S2 sites, however, its affinity for S2 is much lower than for S1 (Plenge et al. 2012). Thus it is conceivable that [^{125}I]VK03-51 may be binding to both S1 and S2 sites and the latter might not be fully inhibited by 10μM (*S*)-citalopram (Plenge et al. 2012; Banala et al. 2013).

Discussion

So far, two binding sites have been identified in the crystal structures of inhibitor-bound LeuT: the centrally located substrate S1 binding pocket and the extracellular vestibule, which contains the putative S2 binding site (Singh et al. 2007; Zhou et al. 2007; Singh et al. 2008; Zhou et al. 2009). The equivalent regions in SERT are natural candidates for harboring ligand-binding sites. Indeed, re-evaluation of extensive mutational analysis shows that the majority of residues that are critical for recognition of inhibitors are located in the TM and loop regions that contribute to the formation of the extracellular permeation pathway and the substrate binding pocket (Chen and Rudnick 2000; Goldberg et al. 2003; Neubauer 2006; Henry et al. 2006b; Andersen et al. 2009; 2010; Koldsø et al. 2010; Sinning et al. 2010).

Since the co-crystallization of LeuT with a set of noncompetitive inhibitors, including TCAs and SSRIs (Singh et al. 2007; Zhou et al. 2007; 2009), we now know that antagonists may

function in a more non-competitive mechanism as well as in a classic competitive manner (Zhou et al. 2007; 2009). Despite this, the majority of biochemical evidence indicates that the primary high-affinity binding site for TCAs and SSRIs, including those co-crystallized with LeuT, likely occurs in the S1 site of SERT (Henry et al. 2006a; Gouaux 2009). However, some studies have found that TCAs and SSRIs, in addition to binding to a high-affinity binding site, may also bind to a low-affinity allosteric site in SERT (Sette et al. 1983; Plenge and Mellerup 1985; Segonzac et al. 1985; Wennogle et al. 1985; O'Riordan et al. 1990; Plenge et al. 1991; Chen et al. 2005a). Binding to this allosteric site markedly increases the off-rate of the inhibitor bound to the high-affinity binding site. It has been suggested that the allosteric site is situated corresponding to a suggested oligomeric interface in the transporter (Neubauer 2006); however, it is tempting to speculate that the allosteric site could be situated in the S2 vestibule outside the primary S1 binding pocket.

While irreversible labeling by the C-5 substituted [^{125}I]VK03-83 and [^{125}I]NYDU-2-24 was completely eliminated by pre-incubation with *(S)*-citalopram, irreversible labeling by the C-1 substituted [^{125}I]VK03-51 was reduced by only ~30% with *(S)*-citalopram pre-incubation. The inability of (*S*)-citalopram to completely block [^{125}I]VK03-51 hSERT photolabeling indicates that this PAL has complex hSERT binding properties compared to the C-5-substitituted PALs, [^{125}I]VK03-83 and [^{125}I]NYDU-2-24. Indeed, one explanation for this nuance between the C-1 and C-5 analogue binding profiles could be a preference by the C-1 substituted VK03-51 for the S2 site over the high-affinity S1 site. This concept is further supported by the fact that VK03-51 exhibits a ten-fold increase in K_i when compared with the C-5 substituted VK03-83 and NYDU-4-24. If VK03-51 does preferentially coordinate within the S2 site, this would mean that

characterization of the point of covalent attachment following photolabeling could provide the first direct evidence of an antagonist coordinating with a residue in the extracellular vestibule when bound. Likewise, use of the two C-5 substituted photolabeled analogues could also help determine the orientation of bound citalopram in the S1 site. Together, these findings would represent a huge step forward in our understanding of the inhibitory mechanisms, both competitive and non-competitive, employed by the highly SERT selective inhibitor (*S*)-citalopram.

REFERENCES

Abramson J, Wright EM. Structure and function of Na(+)-symporters with inverted repeats. Curr Opin Struct Biol. England; 2009 Aug;19(4):425–32.

Adams SV, DeFelice LJ. Flux coupling in the human serotonin transporter. Biophys J. 2002 Dec;83(6):3268–82.

Adams SV, DeFelice LJ. Ionic Currents in the Human Serotonin Transporter Reveal Inconsistencies in the Alternating Access Hypothesis. Biophysical Journal. 2003 Sep;85(3):1548–59.

Adkins EM, Barker EL, Blakely RD. Interactions of tryptamine derivatives with serotonin transporter species variants implicate transmembrane domain I in substrate recognition. Molecular Pharmacology. ASPET; 2001;59(3):514–23.

Adragna NC, Fulvio MD, Lauf PK. Regulation of K-Cl Cotransport: from Function to Genes. J Membr Biol. Springer-Verlag; 2004 Nov;201(3):109–37.

Agoston GE, Wu JH, Izenwasser S, George C, Katz J, Kline RH, et al. Novel N-substituted 3 alpha-[bis(4'-fluorophenyl)methoxy]tropane analogues: selective ligands for the dopamine transporter. J Med Chem. 1997 Dec 19;40(26):4329–39.

Amara S. Neurotransmitter transporters: recent progress. Annu Rev Neurosci. 1993.

Amara SG, Sonders MS. Neurotransmitter transporters as molecular targets for addictive drugs. Drug Alcohol Depend. 1998 May;51(1-2):87–96.

Andersen J, Olsen L, Hansen KB, Taboureau O, Jørgensen FS, Jørgensen AM, et al. Mutational mapping and modeling of the binding site for (S)-citalopram in the human serotonin transporter. J Biol Chem. 2010 Jan 15;285(3):2051–63.

Andersen J, Taboureau O, Hansen KB, Olsen L, Egebjerg J, Strømgaard K, et al. Location of the antidepressant binding site in the serotonin transporter: importance of Ser-438 in recognition of citalopram and tricyclic antidepressants. J Biol Chem. 2009 Apr 10;284(15):10276–84.

Androutsellis-Theotokis A, Ghassemi F, Rudnick G. A conformationally sensitive residue on the cytoplasmic surface of serotonin transporter. J Biol Chem. 2001 Dec 7;276(49):45933–8.

Androutsellis-Theotokis A, Rudnick G. Accessibility and conformational coupling in serotonin transporter predicted internal domains. J Neurosci. 2002 Oct 1;22(19):8370–8.

Anisimov VM, Lamoureux G, Vorobyov IV. Determination of electrostatic parameters for a polarizable force field based on the classical Drude oscillator. Journal of Chemical Information and Modeling. 2005.

Anne C, Gasnier B. Chapter Three - Vesicular Neurotransmitter Transporters: Mechanistic Aspects. Current Topics in Membranes. 2014 pp. 149–74.

Banala AK, Zhang P, Plenge P, Cyriac G, Kopajtic T, Katz JL, et al. Design and Synthesis of 1-(3-(Dimethylamino)propyl)-1-(4-fluorophenyl)-1,3-dihydroisobenzofuran-5-carbonitrile (Citalopram) Analogues as Novel Probes for the Serotonin Transporter S1 and S2 Binding Sites. J Med Chem. American Chemical Society; 2013 Dec 12;56(23):9709–24.

Barker EL, Kimmel HL, Blakely RD. Chimeric human and rat serotonin transporters reveal domains involved in recognition of transporter ligands. Mol Pharmacol. 1994 Nov;46(5):799–807.

Barker EL, Moore KR, Rakhshan F, Blakely RD. Transmembrane domain I contributes to the permeation pathway for serotonin and ions in the serotonin transporter. J Neurosci. 1999 Jun 15;19(12):4705–17.

Barker EL, Perlman MA, Adkins EM. High Affinity Recognition of Serotonin Transporter Antagonists Defined By Species-Scanning Mutagenesis An Aromatic Residue in Transmembrane Domain I Dictates …. Journal of Biological …. 1998.

Baumann MH, Solis E, Watterson LR, Marusich JA, Fantegrossi WE, Wiley JL. Baths Salts, Spice, and Related Designer Drugs: The Science Behind the Headlines. J Neurosci. 2014 Nov 12;34(46):15150–8.

Bayly CI, Kollman PA. Molecular dynamics and free energy calculations on the peculiar bimodal alkali ion selectivity of an 8-subunit cavitand. J Am Chem Soc. 1994.

Ben-Yona A, Bendahan A, Kanner BI. A glutamine residue conserved in the neurotransmitter:sodium:symporters is essential for the interaction of chloride with the GABA transporter GAT-1. J Biol Chem. United States; 2011 Jan 1;286(4):2826–33.

Beuming T, Kniazeff J, Bergmann ML, Shi L, Gracia L, Raniszewska K, et al. The binding sites for cocaine and dopamine in the dopamine transporter overlap. Nat Neurosci. 2008 Jun 22;11(7):780–9.

Beuming T, Shi L, Javitch JA, Weinstein H. A Comprehensive Structure-Based Alignment of Prokaryotic and Eukaryotic Neurotransmitter/Na+ Symporters (NSS) Aids in the Use of the LeuT Structure to Probe NSS Structure and Function. Mol Pharmacol. 2006 Aug 3;70(5):1630–42.

Binda F, Dipace C, Bowton E, Robertson SD, Lute BJ, Fog JU, et al. Syntaxin 1A Interaction with the Dopamine Transporter Promotes Amphetamine-Induced Dopamine Efflux. Mol Pharmacol. 2008 Jul 10;74(4):1101–8.

Blakely RD, Berson HE, Fremeau RT Jr, Caron MG, Peek MM, Prince HK, et al. Cloning and expression of a functional serotonin transporter from rat brain. Nature. 1991 Nov 7;354(6348):66–70.

Bock G, Gebhart M, Scharinger A, Jangsangthong W, Busquet P, Poggiani C, et al. Functional Properties of a Newly Identified C-terminal Splice Variant of Cav1.3 L-type Ca2+ Channels. Journal of Biological Chemistry. 2011 Dec 2;286(49):42736–48.

Brill H, Patton RE. Analysis of 1955-1956 Population Fall in New York State Mental Hospitals in First Year of Large-Scale use of Tranquilizing Drugs. American Journal of Psychiatry. 1957 Dec;114(6):509–17.

Brooks BR, Brooks CL, MacKerell AD, Nilsson L, Petrella RJ, Roux B, et al. CHARMM: the biomolecular simulation program. J Comput Chem. 2009 Jul 30;30(10):1545–614.

Buchmayer F, Schicker K, Steinkellner T, Geier P, Stübiger G, Hamilton PJ, et al. Amphetamine actions at the serotonin transporter rely on the availability of phosphatidylinositol-4,5-bisphosphate. Proc Natl Acad Sci USA. 2013 Jun 24.

Canutescu AA, Shelenkov AA, Dunbrack RL. A graph‑theory algorithm for rapid protein side-chain prediction. Protein Sci. 2003.

Cao J, Lever JR, Kopajtic T, Katz JL, Pham AT, Holmes ML, et al. Novel Azido and Isothiocyanato Analogues of [3-(4-Phenylalkylpiperazin-1-yl)propyl]bis(4-fluorophenyl)amines as Potential Irreversible Ligands for the Dopamine Transporter. J Med Chem. 2004 Dec;47(25):6128–36.

Cao Y, Li M, Mager S, Lester HA. Amino acid residues that control pH modulation of transport-associated current in mammalian serotonin transporters. J Neurosci. 1998 Oct 1;18(19):7739–49.

Caplan DA, Subbotina JO, Noskov SY. Molecular mechanism of ion-ion and ion-substrate coupling in the Na+-dependent leucine transporter LeuT. Biophys J. United States; 2008 Nov 11;95(10):4613–21.

Carroll FI, Gao Y, Abraham P, Lewin AH, Lew R, Patel A, et al. Probes for the cocaine receptor. Potentially irreversible ligands for the dopamine transporter. J Med Chem. 1992 May 15;35(10):1813–7.

Carvelli L, Blakely RD, Defelice LJ. Dopamine transporter/syntaxin 1A interactions regulate transporter channel activity and dopaminergic synaptic transmission. Proc Natl Acad Sci USA. 2008 Sep 9;105(37):14192.

Carvelli L, McDonald PW, Blakely RD, Defelice LJ. Dopamine transporters depolarize neurons by a channel mechanism. Proc Natl Acad Sci USA. 2004 Nov 11;101(45):16046–51.

Celik L, Schiøtt B, Tajkhorshid E. Substrate Binding and Formation of an Occluded State in the Leucine Transporter. Biophysical Journal. 2008 Mar;94(5):1600–12.

Chang AS, Lam DM. Mechanistic analyses of ion dependences in a high-affinity human serotonin transport system in transfected murine fibroblast cells. J Physiol (Lond). 1998 Aug 1;510 (Pt 3):903–13.

Chen F, Larsen MB, Neubauer HA, Sánchez C, Plenge P, Wiborg O. Characterization of an allosteric citalopram-binding site at the serotonin transporter. J Neurochem. 2005a Jan;92(1):21–8.

Chen F, Larsen MB, Sánchez C, Wiborg O. The S-enantiomer of R,S-citalopram, increases inhibitor binding to the human serotonin transporter by an allosteric mechanism. Comparison with other serotonin transporter inhibitors. Eur Neuropsychopharmacol. 2005b Mar;15(2):193–8.

Chen J-G, Rudnick G. Permeation and gating residues in serotonin transporter. Proc Natl Acad Sci USA. 2000 Feb 1;97(3):1044–9.

Chen JG. The Third Transmembrane Domain of the Serotonin Transporter Contains Residues Associated with Substrate and Cocaine Binding. Journal of Biological Chemistry. 1997 Nov 7;272(45):28321–7.

Chen JG, Liu-Chen S, Rudnick G. External cysteine residues in the serotonin transporter. Biochemistry. 1997 Feb 11;36(6):1479–86.

Chen N, Rickey J, Berfield JL, Reith MEA. Aspartate 345 of the Dopamine Transporter Is Critical for Conformational Changes in Substrate Translocation and Cocaine Binding. Journal of Biological Chemistry. 2004 Feb 6;279(7):5508–19.

Chen R, Tilley MR, Wei H, Zhou F, Zhou FM, Ching S, et al. Abolished cocaine reward in mice with a cocaine-insensitive dopamine transporter. Proc Natl Acad Sci USA. 2006 Jun 13;103(24):9333–8.

Chen R, Wei H, Hill ER, Chen L, Jiang L. Direct evidence that two cysteines in the dopamine transporter form a disulfide bond. Molecular and cellular …. 2007.

Chuang V, Otagiri M. Photoaffinity Labeling of Plasma Proteins. Molecules. Multidisciplinary Digital Publishing Institute; 2013 Nov;18(11):13831–59.

Chudzik J, McCarthy D, Bakish D, Ravindran A, Hrdina PD. Synthesis and characterization of an aryl-azidoparoxetine. Biochem Pharmacol. 1995 Oct;50(8):1211–5.

195

Corey JL, Quick MW, Davidson N, Lester HA, Guastella J. A cocaine-sensitive Drosophila serotonin transporter: cloning, expression, and electrophysiological characterization. Proc Natl Acad Sci USA. 1994 Feb 1;91(3):1188–92.

Cremona ML, Matthies HJG, Pau K, Bowton E, Speed N, Lute BJ, et al. Flotillin-1 is essential for PKC-triggered endocytosis and membrane microdomain localization of DAT. Nature Neuroscience. 2011 Mar 13;14(4):469–77.

Dahal RA, Pramod AB, Sharma B, Krout D, Foster JD, Cha JH, et al. Computational and Biochemical Docking of the Irreversible Cocaine Analog RTI 82 Directly Demonstrates Ligand Positioning in the Dopamine Transporter Central Substrate-binding Site. Journal of Biological Chemistry. 2014 Oct 24;289(43):29712–27.

DeLano WL. The PyMOL Molecular Graphics System. 1st ed. 2010.

Dutta AK, Fei XS, Vaughan RA, Gaffaney JD, Wang N, Lever JR, et al. Design, synthesis, and characterization of a novel, 4-[2-(diphenylmethoxy)ethyl]-1-benzyl piperidine-based, dopamine transporter photoaffinity label. Life Sci. 2001 Mar 9;68(16):1839–49.

Erreger K, Grewer C, Javitch JA, Galli A. Currents in response to rapid concentration jumps of amphetamine uncover novel aspects of human dopamine transporter function. J Neurosci. 2008 Jan 23;28(4):976–89.

Faham S, Watanabe A, Besserer GM, Cascio D, Specht A, Hirayama BA, et al. The crystal structure of a sodium galactose transporter reveals mechanistic insights into Na+/sugar symport. Science. 2008 Aug 8;321(5890):810–4.

Felts B, Pramod AB, Sandtner W, Burbach N, Bulling S, Sitte HH, et al. The two Na+ sites in the human serotonin transporter play distinct roles in the ion coupling and electrogenicity of transport. Journal of Biological Chemistry. 2014 Jan 17;289(3):1825–40.

Ferrer JV, Javitch JA. Cocaine alters the accessibility of endogenous cysteines in putative extracellular and intracellular loops of the human dopamine transporter. Proc Natl Acad Sci USA. 1998 Aug 4;95(16):9238–43.

Field JR, Henry LK, Blakely RD. Transmembrane Domain 6 of the Human Serotonin Transporter Contributes to an Aqueously Accessible Binding Pocket for Serotonin and the Psychostimulant 3,4-Methylene Dioxymethamphetamine. Journal of Biological Chemistry. 2010 Apr 2;285(15):11270–80.

Fog JU, Khoshbouei H, Holy M, Owens WA, Vaegter CB, Sen N, et al. Calmodulin Kinase II Interacts with the Dopamine Transporter C Terminus to Regulate Amphetamine-Induced Reverse Transport. Neuron. 2006 Aug;51(4):417–29.

Foloppe N, Nilsson L. Stabilization of the Catalytic Thiolate in a Mammalian Glutaredoxin: Structure, Dynamics and Electrostatics of Reduced Pig Glutaredoxin and its Mutants. Journal of Molecular Biology. 2007 Sep;372(3):798–816.

Forrest LR, Rudnick G. The rocking bundle: a mechanism for ion-coupled solute flux by symmetrical transporters. Physiology (Bethesda). 2009 Dec;24:377–86.

Forrest LR, Tavoulari S, Zhang YW, Rudnick G, Honig B. Identification of a chloride ion binding site in Na+/Cl -dependent transporters. Proc Natl Acad Sci USA. 2007 Jul 7;104(31):12761–6.

Forrest LR, Zhang YW, Jacobs MT, Gesmonde J, Xie L, Honig BH, et al. Mechanism for alternating access in neurotransmitter transporters. Proc Natl Acad Sci USA. 2008 Jul 7;105(30):10338–43.

Foster JD, Pananusorn B, Vaughan RA. Dopamine transporters are phosphorylated on N-terminal serines in rat striatum. J Biol Chem. 2002 Jul 12;277(28):25178–86.

Fuller RW. Mechanism by which uptake inhibitors antagonizep-chloroamphetamine-induced depletion of brain serotonin. Neurochem Res. Kluwer Academic Publishers-Plenum Publishers; 1980 Mar;5(3):241–5.

Gaffaney JD. Uptake Inhibitors but not Substrates Induce Protease Resistance in Extracellular Loop Two of the Dopamine Transporter. Mol Pharmacol. 2004 Mar 1;65(3):692–701.

Galli A, Blakely RD, DeFelice LJ. Patch-clamp and amperometric recordings from norepinephrine transporters: channel activity and voltage-dependent uptake. Proc Natl Acad Sci USA. National Acad Sciences; 1998;95(22):13260–5.

Galli A, Defelice LJ, Duke BJ, Moore KR, Blakely RD. Sodium-dependent norepinephrine-induced currents in norepinephrine-transporter-transfected HEK-293 cells blocked by cocaine and antidepressants. J Exp Biol. 1995 Oct;198(Pt 10):2197–212.

Gao X, Lu F, Zhou L, Dang S, Sun L, Li X, et al. Structure and Mechanism of an Amino Acid Antiporter. Science. 2009 Jun 18;324(5934):1565–8.

Gether U, Andersen PH, Larsson OM, Schousboe A. Neurotransmitter transporters: molecular function of important drug targets. Trends in Pharmacological Sciences. 2006 Jul;27(7):375–83.

Gillman PK. Tricyclic antidepressant pharmacology and therapeutic drug interactions updated. British Journal of Pharmacology. 2007 Jul;151(6):737–48.

Giros B, Jaber M, Jones SR, Wightman RM, Caron MG. Hyperlocomotion and indifference to cocaine and amphetamine in mice lacking the dopamine transporter. Nature. 1996 Feb 15;379(6566):606–12.

Goldberg NR, Beuming T, Soyer OS, Goldstein RA, Weinstein H, Javitch JA. Probing conformational changes in neurotransmitter transporters: a structural context. European Journal of Pharmacology. 2003 Oct 31;479(1-3):3–12.

Gouaux E. The molecular logic of sodium-coupled neurotransmitter transporters. Philosophical Transactions of the Royal Society of London B: Biological Sciences. The Royal Society; 2009 Jan 27;364(1514):149–54.

Grigoriadis DE, Wilson AA, Lew R, Sharkey JS, Kuhar MJ. Dopamine transport sites selectively labeled by a novel photoaffinity probe: 125I-DEEP. J Neurosci. 1989 Aug;9(8):2664–70.

Gu H, Wall SC, Rudnick G. Stable expression of biogenic amine transporters reveals differences in inhibitor sensitivity, kinetics, and ion dependence. J Biol Chem. 1994 Mar 11;269(10):7124–30.

Hahn MK, Blakely RD. Monoamine transporter gene structure and polymorphisms in relation to psychiatric and other complex disorders. The Pharmacogenomics Journal. 2002;2(4):217–35.

Hamilton PJ, Belovich AN, Khelashvili G, Saunders C, Erreger K, Javitch JA, et al. PIP2 regulates psychostimulant behaviors through its interaction with a membrane protein. Nat Chem Biol. 2014 Jun 1;10(7):582–9.

Hamilton PJ, Campbell NG, Sharma S, Erreger K, Hansen FH, Saunders C, et al. mp2013102a. Mol Psychiatry. Nature Publishing Group; 2013 Aug 27;:1–9.

Hansen FH, Skjørringe T, Yasmeen S, Arends NV, Sahai MA, Erreger K, et al. Missense dopamine transporter mutations associate with adult parkinsonism and ADHD. J Clin Invest. 2014 Jun 9;124(7):3107–20.

Harding MM. Metal–ligand geometry relevant to proteins and in proteins: sodium and potassium. Acta Crystallogr D Biol Crystallogr. 2002 Apr 26;58(5):872–4.

Hastrup H, Sen N, Javitch JA. The human dopamine transporter forms a tetramer in the plasma membrane: cross-linking of a cysteine in the fourth transmembrane segment is sensitive to cocaine analogs. J Biol Chem. 2003 Nov 14;278(46):45045–8.

Henry LK. Serotonin and Cocaine-sensitive Inactivation of Human Serotonin Transporters by Methanethiosulfonates Targeted to Transmembrane Domain I. J Biol Chem. 2003 Jul 24;278(39):37052–63.

Henry LK, Defelice LJ, Blakely RD. Getting the message across: a recent transporter structure shows the way. Neuron. 2006a Mar 3;49(6):791–6.

Henry LK, Field JR, Adkins EM, Parnas ML, Vaughan RA, Zou MF, et al. Tyr-95 and Ile-172 in transmembrane segments 1 and 3 of human serotonin transporters interact to establish high affinity recognition of antidepressants. J Biol Chem. 2006b Jan 27;281(4):2012–23.

Henry LK, Iwamoto H, Field JR, Kaufmann K, Dawson ES, Jacobs MT, et al. A Conserved Asparagine Residue in Transmembrane Segment 1 (TM1) of Serotonin Transporter Dictates Chloride-coupled Neurotransmitter Transport. Journal of Biological Chemistry. 2011 Aug 26;286(35):30823–36.

Henry LK, Meiler J, Blakely RD. Bound to be different: neurotransmitter transporters meet their bacterial cousins. Mol Interv. 2007 Dec;7(6):306–9.

Hess B, Bekker H, Berendsen H, Fraaije J. LINCS: a linear constraint solver for molecular simulations. Journal of computational …. 1997.

Hess B, Kutzner C, van der Spoel D, Lindahl E. GROMACS 4: Algorithms for Highly Efficient, Load-Balanced, and Scalable Molecular Simulation. J Chem Theory Comput. 2008 Mar;4(3):435–47.

Hilber B, Scholze P, Dorostkar MM, Sandtner W, Holy M, Boehm S, et al. Serotonin-transporter mediated efflux: a pharmacological analysis of amphetamines and non-amphetamines. Neuropharmacology. 2005 Nov;49(6):811–9.

Hill ER, Huang X, Zhan C-G, Ivy Carroll F, Gu HH. Interaction of tyrosine 151 in norepinephrine transporter with the 2β group of cocaine analog RTI-113. Neuropharmacology. 2011 Jul;61(1-2):112–20.

Hoffman B, Mezey E, Brownstein M. Cloning of a serotonin transporter affected by antidepressants. Science. 1991 Oct 25;254(5031):579–80.

Hoffman BJ, Mezey E. Distribution of serotonin 5-HT1C receptor mRNA in adult rat brain. FEBS Letters. 1989 Apr;247(2):453–62.

Huang T-L, Lin C-C. Advances in Biomarkers of Major Depressive Disorder. sciencedirectcom. Elsevier; 2015. pp. 177–204.

Huang X, Gu HH, Zhan C-G. Mechanism for Cocaine Blocking the Transport of Dopamine: Insights from Molecular Modeling and Dynamics Simulations. J Phys Chem B. 2009 Nov 12;113(45):15057–66.

Huang X, Zhan C-G. How Dopamine Transporter Interacts with Dopamine: Insights from Molecular Modeling and Simulation. Biophysical Journal. 2007 Nov;93(10):3627–39.

Humphrey W, Dalke A, Schulten K. VMD: Visual molecular dynamics. Journal of Molecular Graphics. 1996 Feb;14(1):33–8.

Humphreys CJ, Wall SC, Rudnick G. Ligand binding to the serotonin transporter: equilibria, kinetics, and ion dependence. Biochemistry. 1994 Aug 9;33(31):9118–25.

Ingram SL, Prasad BM, Amara SG. Dopamine transporter-mediated conductances increase excitability of midbrain dopamine neurons. Nat Neurosci. 2002 Oct;5(10):971–8.

Iversen L. Neurotransmitter transporters: fruitful targets for CNS drug discovery. Mol Psychiatry. 2000.

Iversen LL. Role of transmitter uptake mechanisms in synaptic neurotransmission. British Journal of Pharmacology. Blackwell Publishing; 1971 Apr 1;41(4):571.

Jang IS, Jeong HJ, Akaike N. Contribution of the Na–K–Cl Cotransporter on GABAAReceptor-Mediated Presynaptic Depolarization in Excitatory Nerve Terminals. J Neurosci. 2001.

Jardetzky O. Simple Allosteric Model for Membrane Pumps. Nature. 1966 Aug 27;211(5052):969–70.

Jo S, Lim JB, Klauda JB, Im W. CHARMM-GUI Membrane Builder for mixed bilayers and its application to yeast membranes. Biophys J. 2009 Jul 8;97(1):50–8.

Kanner BI. Structural biology: It's not all in the family. Nature. Nature Publishing Group; 2008 Jul 30;454(7204):593–4.

Kantcheva AK, Quick M, Shi L, Winther A-ML, Stolzenberg S, Weinstein H, et al. Chloride binding site of neurotransmitter sodium symporters. Proc Natl Acad Sci USA. 2013 May 2.

Kaufmann KW, Dawson ES, Henry LK, Field JR, Blakely RD, Meiler J. Structural determinants of species-selective substrate recognition in human and Drosophila serotonin transporters revealed through computational docking studies. Proteins. 2009 Feb 15;74(3):630–42.

Khafizov K, Perez C, Koshy C, Quick M, Fendler K, Ziegler C, et al. Investigation of the sodium-binding sites in the sodium-coupled betaine transporter BetP. Proc Natl Acad Sci USA. 2012 Oct 30;109(44):E3035–44.

Khoshbouei H, Sen N, Guptaroy B, Johnson L', Lund D, Gnegy ME, et al. N-terminal phosphorylation of the dopamine transporter is required for amphetamine-induced efflux. PLoS Biol. 2004 Mar;2(3):E78.

Kitayama S, Shimada S, Xu H, Markham L, Donovan DM, Uhl GR. Dopamine transporter site-directed mutations differentially alter substrate transport and cocaine binding. Proc Natl Acad Sci USA. 1992 Aug 15;89(16):7782–5.

Kniazeff J, Shi L, Loland CJ, Javitch JA, Weinstein H, Gether U. An Intracellular Interaction Network Regulates Conformational Transitions in the Dopamine Transporter. Journal of Biological Chemistry. American Society for Biochemistry and Molecular Biology; 2008 Apr 17;283(25):17691–701.

Koldsø H, Christiansen AB, Sinning S, Schiøtt B. Comparative Modeling of the Human Monoamine Transporters: Similarities in Substrate Binding. ACS Chem Neurosci. American Chemical Society; 2013 Feb 20;4(2):295–309.

Koldsø H, Noer P, Grouleff J, Autzen HE, Sinning S, Schiøtt B. Unbiased Simulations Reveal the Inward-Facing Conformation of the Human Serotonin Transporter and Na+ Ion Release. Livesay DR, editor. PLoS Comput Biol. 2011 Oct 27;7(10):e1002246.

Koldsø H, Severinsen K, Tran TT, Celik L, Jensen HH, Wiborg O, et al. The Two Enantiomers of Citalopram Bind to the Human Serotonin Transporter in Reversed Orientations. J Am Chem Soc. 2010 Feb 3;132(4):1311–22.

Krishnamurthy H, Gouaux E. X-ray structures of LeuT in substrate-free outward-open and apo inward-open states. Nature. Nature Publishing Group; 2012 Jan 9;481(7382):469–74.

Krishnamurthy H, Piscitelli CL, Gouaux E. Unlocking the molecular secrets of sodium-coupled transporters. Nature. 2009 May 21;459(7245):347–55.

Kristensen AS, Andersen J, Jørgensen TN, Sorensen L, Eriksen J, Loland CJ, et al. SLC6 Neurotransmitter Transporters: Structure, Function, and Regulation. Pharmacological Reviews. 2011 Sep 1;63(3):585–640.

Krueger BK. Kinetics and Block of Dopamine Uptake in Synaptosomes from Rat Caudate Nucleus. J Neurochem. 1990 Jul;55(1):260–7.

Kumar V, Rahbek-Clemmensen T, Billesbølle CB, Jørgensen TN, Gether U, Newman AH. Novel and High Affinity Fluorescent Ligands for the Serotonin Transporter Based on (S)-Citalopram. ACS Med Chem Lett. 2014 Jun 12;5(6):696–9.

Lapinsky DJ, Aggarwal S, Huang Y, Surratt CK, Lever JR, Foster JD, et al. A novel photoaffinity ligand for the dopamine transporter based on pyrovalerone. Bioorganic & Medicinal Chemistry. 2009 Jun 1;17(11):3770–4.

Lapinsky DJ, Aggarwal S, Nolan TL, Surratt CK, Lever JR, Acharya R, et al. (±)-2-(N-tert-Butylamino)-3"-[(125)I]-iodo-4-"azidopropiophenone: a dopamine transporter and nicotinic acetylcholine receptor photoaffinity ligand based on bupropion (Wellbutrin, Zyban). Bioorg Med Chem Lett. 2012 Jan 1;22(1):523–6.

Lapinsky DJ, Velagaleti R, Yarravarapu N, Liu Y, Huang Y, Surratt CK, et al. Azido-iodo-N-benzyl derivatives of threo-methylphenidate (Ritalin, Concerta): Rational design, synthesis, pharmacological evaluation, and dopamine transporter photoaffinity labeling. Bioorganic & Medicinal Chemistry. 2011 Jan;19(1):504–12.

Laskowski RA, MacArthur MW, Moss DS, Thornton JM. PROCHECK: a program to check the stereochemical quality of protein structures. J Appl Crystallogr. International Union of Crystallography; 1993 Apr 1;26(2):283–91.

Lever JR, Zou MF, Parnas ML, Duval RA, Wirtz SE, Justice JB, et al. Radioiodinated Azide and Isothiocyanate Derivatives of Cocaine for Irreversible Labeling of Dopamine Transporters: Synthesis and Covalent Binding Studies. Bioconjugate Chem. 2005 May;16(3):644–9.

Li L, Vorobyov I, Allen TW. Potential of Mean Force and p KaProfile Calculation for a Lipid Membrane-Exposed Arginine Side Chain. J Phys Chem B. 2008 Aug;112(32):9574–87.

Li LB, Chen N, Ramamoorthy S, Chi L, Cui XN, Wang LC, et al. The Role of N-Glycosylation in Function and Surface Trafficking of the Human Dopamine Transporter. Journal of Biological Chemistry. 2004 May 7;279(20):21012–20.

Lin F, Lester HA, Mager S. Single-channel currents produced by the serotonin transporter and analysis of a mutation affecting ion permeation. Biophysical Journal. 1996 Dec;71(6):3126–35.

Lingjærde O. Uptake of Serotonin in Blood Platelets in vitro. III: Effects of Acetate and Other Monocarboxylic Acids - Acta Physiologica Scandinavica - Wiley Online Library. 1971

Lochner M. Expanding the Small Molecular Toolbox to Study Big Biomolecular Machines. CHIMIA. 2010 Apr 28;64(4):241–6.

Loland CJ, Grånäs C, Javitch JA, Gether U. Identification of intracellular residues in the dopamine transporter critical for regulation of transporter conformation and cocaine binding. J Biol Chem. 2004 Jan 30;279(5):3228–38.

Loland CJ, Norregaard L, Gether U. Defining Proximity Relationships in the Tertiary Structure of the Dopamine Transporter. Journal of Biological Chemistry. 1999.

Mager S, Min C, Henry DJ, Chavkin C, Hoffman BJ, Davidson N, et al. Conducting states of a mammalian serotonin transporter. Neuron. 1994 Apr;12(4):845–59.

Marshall EF, Stirling GS, Tait AC, Todrick A. The Effect of Iproniazid and Imipramine on the Blood Platelet 5‑Hydroxytryptamine Level in Man. British journal of …. 1960;15(35):35–41.

Mazei-Robison MS, Bowton E, Holy M, Schmudermaier M, Freissmuth M, Sitte HH, et al. Anomalous Dopamine Release Associated with a Human Dopamine Transporter Coding Variant. J Neurosci. 2008 Jul 9;28(28):7040–6.

McCann UD, Szabo Z, Scheffel U, Dannals RF, Ricaurte GA. Positron emission tomographic evidence of toxic effect of MDMA ("Ecstasy") on brain serotonin neurons in human beings. Lancet. 1998 Oct 31;352(9138):1433–7.

Meiler J, Baker D. ROSETTALIGAND: Protein–small molecule docking with full side‑chain flexibility. Structure. 2006.

Meinild AK. Zinc Potentiates an Uncoupled Anion Conductance Associated with the Dopamine Transporter. Journal of Biological Chemistry. 2004 Aug 30;279(48):49671–9.

Mitchell P. Coupling of phosphorylation to electron and hydrogen transfer by a chemi-osmotic type of mechanism. Nature. 1961 Jul 8;191:144–8.

Mitchell SM, Lee E, Garcia ML, Stephan MM. Structure and function of extracellular loop 4 of the serotonin transporter as revealed by cysteine-scanning mutagenesis. J Biol Chem. 2004 Jun 4;279(23):24089–99.

Nelson MT, Blaustein MP. GABA efflux from synaptosomes: Effects of membrane potential, and external GABA and cations. J Membr Biol. Springer-Verlag; 1982 Oct;69(3):213–23.

Nelson PJ, Rudnick G. Coupling between platelet 5-hydroxytryptamine and potassium transport. J Biol Chem. 1979 Oct 25;254(20):10084–9.

Nelson PJ, Rudnick G. The role of chloride ion in platelet serotonin transport. J Biol Chem. 1982 Jun 10;257(11):6151–5.

Neubauer HA. Dissection of an Allosteric Mechanism on the Serotonin Transporter: A Cross-Species Study. Mol Pharmacol. 2006 Jan 18;69(4):1242–50.

Newman AH, Cha JH, Cao J, Kopajtic T, Katz JL, Parnas ML, et al. Design and Synthesis of a Novel Photoaffinity Ligand for the Dopamine and Serotonin Transporters Based on 2β-Carbomethoxy-3β-biphenyltropane. J Med Chem. American Chemical Society; 2006 Nov;49(22):6621–5.

Ni YG. A Lithium-induced Conformational Change in Serotonin Transporter Alters Cocaine Binding, Ion Conductance, and Reactivity of Cys-109. Journal of Biological Chemistry. 2001 Jun 14;276(33):30942–7.

Norgaard-Nielsen K, Norregaard L, Hastrup H, Javitch JA, Gether U. Zn(2+) site engineering at the oligomeric interface of the dopamine transporter. FEBS Letters. 2002 Jul 31;524(1-3):87–91.

Norregaard L, Frederiksen D, Nielsen EO, Gether U. Delineation of an endogenous zinc-binding site in the human dopamine transporter. EMBO J. 1998 Aug 3;17(15):4266–73.

Norregaard L, Loland CJ, Gether U. Evidence for Distinct Sodium-, Dopamine-, and Cocaine-dependent Conformational Changes in Transmembrane Segments 7 and 8 of the Dopamine Transporter. Journal of Biological Chemistry. 2003 Aug 15;278(33):30587–96.

Noskov SY. Molecular mechanism of substrate specificity in the bacterial neutral amino acid transporter LeuT. Proteins. United States; 2008 Dec;73(4):851–63.

Noskov SY, Roux B. Control of ion selectivity in LeuT: two Na+ binding sites with two different mechanisms. J Mol Biol. England; 2008 Mar 3;377(3):804–18.

O'Riordan C, Phillips OM, Williams DC. Two Affinity States for [3H]Imipramine Binding to the Human Platelet 5-Hydroxytryptamine Carrier: An Explanation for the Allosteric Interaction Between 5-Hydroxytryptamine and Imipramine. J Neurochem. 1990 Apr;54(4):1275–80.

Owens M, Nemeroff C. Role of serotonin in the pathophysiology of depression: focus on the serotonin transporter. Clinical Chemistry. Am Assoc Clin Chem; 1994 Feb 1;40(2):288.

Owens MJ, Knight DL, Nemeroff CB. Second-generation SSRIs: human monoamine transporter binding profile of escitalopram and R-fluoxetine. Biol Psychiatry. 2001 Sep 1;50(5):345–50.

Pacholczyk T, Blakely RD, Amara SG. Expression cloning of a cocaine-and antidepressant-sensitive human noradrenaline transporter. Nature. 1991 Mar 28;350(6316):350–4.

Pantanowitz S, Bendahan A, Kanner BI. Only one of the charged amino acids located in the transmembrane alpha-helices of the gamma-aminobutyric acid transporter (subtype A) is essential for its activity. J Biol Chem. 1993 Feb 15;268(5):3222–5.

Parnas ML, Gaffaney JD, Zou MF, Lever JR, Newman AH, Vaughan RA. Labeling of dopamine transporter transmembrane domain 1 with the tropane ligand N-[4-(4-azido-3-[125I]iodophenyl)butyl]-2beta-carbomethoxy-3beta-(4-chlorophenyl)tropane implicates proximity of cocaine and substrate active sites. Molecular Pharmacology. 2008 Apr;73(4):1141–50.

Partridge LD, Leach JK. Calcium Channels: Their Properties, Functions, Regulation, and Clinical Relevance. Boca Raton, FL: CRC Press; 1991. pp. 121–3.

Pastoor D, Gobburu J. Clinical pharmacology review of escitalopram for the treatment of depression. Expert Opin Drug Metab Toxicol. 2014 Jan;10(1):121–8.

Penmatsa A, Gouaux E. How LeuT shapes our understanding of the mechanisms of sodium-coupled neurotransmitter transporters. J Physiol (Lond). 2013 Jul 22.

Penmatsa A, Wang KH, Gouaux E. nature12533. Nature. Nature Publishing Group; 2013 Sep 15;:1–7.

Petersen CI, DeFelice LJ. Ionic interactions in the Drosophila serotonin transporter identify it as a serotonin channel. Nature Neuroscience. Nature Publishing Group; 1999;2(7):605–10.

Phillips JC, Braun R, Wang W, Gumbart J, Tajkhorshid E, Villa E, et al. Scalable molecular dynamics with NAMD. J Comput Chem. 2005 Dec;26(16):1781–802.

Piscitelli CL, Gouaux E. Insights into transport mechanism from LeuT engineered to transport tryptophan. EMBO J. 2012 Jan 4;31(1):228–35.

Piscitelli CL, Krishnamurthy H, Gouaux E. Neurotransmitter/sodium symporter orthologue LeuT has a single high-affinity substrate site. Nature. Nature Publishing Group; 2010 Dec 23;468(7327):1129–32.

Pizzo AB, Karam CS, Zhang Y, Ma CL, McCabe BD, Javitch JA. Amphetamine-induced behavior requires CaMKII-dependent dopamine transporter phosphorylation. Mol Psychiatry. 2013 Mar 19;19(3):279–81.

Plenge P, Gether U, Rasmussen SG. Allosteric effects of R- and S-citalopram on the human 5-HT transporter: Evidence for distinct high- and low-affinity binding sites. European Journal of Pharmacology. 2007 Jul;567(1-2):1–9.

Plenge P, Mellerup ET. Antidepressive drugs can change the affinity of [3H]imipramine and [3H]paroxetine binding to platelet and neuronal membranes. European Journal of Pharmacology. 1985 Dec 10;119(1-2):1–8.

Plenge P, Mellerup ET, Laursen H. Affinity modulation of [3H]imipramine, [3H]paroxetine and [3H]citalopram binding to the 5-HT transporter from brain and platelets. European Journal of Pharmacology: Molecular Pharmacology. 1991 Mar;206(3):243–50.

Plenge P, Shi L, Beuming T, Te J, Newman AH, Weinstein H, et al. Steric Hindrance Mutagenesis in the Conserved Extracellular Vestibule Impedes Allosteric Binding of Antidepressants to the Serotonin Transporter. Journal of Biological Chemistry. 2012 Nov 16;287(47):39316–26.

Plenge P, Wiborg O. High- and low-affinity binding of S-citalopram to the human serotonin transporter mutated at 20 putatively important amino acid positions. Neuroscience Letters. 2005 Aug;383(3):203–8.

Pramod AB, Foster J, Carvelli L, Henry LK. SLC6 transporters: Structure, function, regulation, disease association and therapeutics. Molecular Aspects of Medicine. 2013 Apr;34(2-3):197–219.

Quick M, Shi L, Zehnpfennig B, Weinstein H, Javitch JA. Experimental conditions can obscure the second high-affinity site in LeuT. Nat Struct Mol Biol. 2012 Jan 15;19(2):207–11.

Quick M, Winther AML, Shi L, Nissen P, Weinstein H, Javitch JA. Binding of an octylglucoside detergent molecule in the second substrate (S2) site of LeuT establishes an inhibitor-bound conformation. Proc Natl Acad Sci USA. 2009 Apr 7;106(14):5563–8.

Quick MW. Regulating the Conducting States of a Mammalian Serotonin Transporter. Neuron. 2003 Oct;40(3):537–49.

Rajabi M, de Leeuw E, Pazgier M, Li J, Lubkowski J, Lu W. The Conserved Salt Bridge in Human-Defensin 5 Is Required for Its Precursor Processing and Proteolytic Stability. Journal of Biological Chemistry. 2008 Jul 25;283(31):21509–18.

Ramachandran GN, Ramakrishnan C, Sasisekharan V. Stereochemistry of polypeptide chain configurations. Journal of Molecular Biology. 1963 pp. 95–9.

Ramamoorthy S, Bauman AL, Moore KR, Han H, Yang-Feng T, Chang AS, et al. Antidepressant- and cocaine-sensitive human serotonin transporter: molecular cloning, expression, and chromosomal localization. Proc Natl Acad Sci USA. 1993 Mar 15;90(6):2542–6.

Ramsey I. Serotonin transporter function and pharmacology are sensitive to expression level. Journal of Biological Chemistry. 2002.

Ransom RW, Lee JD, Bolger MB, Shih JC. Photoinactivation of serotonin uptake by an arylazido derivative of 5-hydroxytryptamine. Mol Pharmacol. 1985 Aug;28(2):185–90.

Rehavi M, Tracer H, Rice K, Skolnick P, Paul SM. [3H]2-nitroimipramine: A selective "slowly-dissociating" probe of the imipramine binding site ('serotonin transporter') in platelets and brain. Life Sci. 1983 Feb;32(6):645–53.

Reith MEA. The Uptake Inhibitors Cocaine and Benztropine Differentially Alter the Conformation of the Human Dopamine Transporter. Journal of Biological Chemistry. 2001 Jun 6;276(31):29012–8.

Reith MEA. Neurotransmitter transporters: structure, function, and regulation. 2nd ed. Humana Press. 2002

Reith MEA, Xu C, Coffey LL. Binding domains for blockers and substrates on the cloned human dopamine transporter studied by protection against N-Ethylmaleimide-induced reduction of 2β-carbomethoxy-3β-(4-fluorophenyl)[3H]tropane ([3H]WIN 35,428) binding. Biochem Pharmacol. 1996 Nov;52(9):1435–46.

Ressl S, Terwisscha van Scheltinga AC, Vonrhein C, Ott V, Ziegler C. Molecular basis of transport and regulation in the Na+/betaine symporter BetP. Nature. 2009 Mar 5;458(7234):47–52.

Rodriguez GJ, Roman DL, White KJ, Nichols DE, Barker EL. Distinct recognition of substrates by the human and Drosophila serotonin transporters. J Pharmacol Exp Ther. 2003 Jul;306(1):338–46.

Rothman RB, Baumann MH. Monoamine transporters and psychostimulant drugs. European Journal of Pharmacology. 2003 Oct;479(1-3):23–40.

Rudnick G. Chemical Modification Strategies for Structure-Function Studies. In: Quick MW, editor. Transmembrane Transporters. Hoboken, NJ, USA: John Wiley & Sons, Inc; 2002. pp. 125–41.

Rudnick G. Serotonin transporters--structure and function. J Membr Biol. 2006;213(2):101–10.

Rudnick G, Krämer R, Blakely RD, Murphy DL, Verrey F. The SLC6 transporters: perspectives on structure, functions, regulation, and models for transporter dysfunction. Archives of the European Journal of Physiology. 2014 Jan;466(1):25–42.

Rudnick G, Nelson PJ. Platelet 5-hydroxytryptamine transport, an electroneutral mechanism coupled to potassium. Biochemistry. American Chemical Society; 1978 Oct;17(22):4739–42.

Rudnick G, Wall SC. p-Chloroamphetamine induces serotonin release through serotonin transporters. Biochemistry. 1992a Jul;31(29):6710–8.

Rudnick G, Wall SC. The molecular mechanism of" ecstasy"[3, 4-methylenedioxy-methamphetamine (MDMA)]: serotonin transporters are targets for MDMA-induced serotonin release. Proc Natl Acad Sci USA. National Acad Sciences; 1992b;89(5):1817–21.

Sakrikar D, Mazei-Robison MS, Mergy MA, Richtand NW, Han Q, Hamilton PJ, et al. Attention Deficit/Hyperactivity Disorder-Derived Coding Variation in the Dopamine Transporter Disrupts Microdomain Targeting and Trafficking Regulation. J Neurosci. 2012 Apr 18;32(16):5385–97.

Sallee FR, Fogel EL, Schwartz E, Choi SM, Curran DP, Niznik HB. Photoaffinity labeling of the mammalian dopamine transporter. FEBS Letters. 1989 Oct 9;256(1-2):219–24.

Sarker S, Weissensteiner R, Steiner I, Sitte HH, Ecker GF, Freissmuth M, et al. The High-Affinity Binding Site for Tricyclic Antidepressants Resides in the Outer Vestibule of the Serotonin Transporter. Mol Pharmacol. 2010 Nov 16;78(6):1026–35.

Sastry GM, Adzhigirey M, Day T, Annabhimoju R, Sherman W. Protein and ligand preparation: parameters, protocols, and influence on virtual screening enrichments. J Comput Aided Mol Des. 2013 Mar;27(3):221–34.

Schicker K, Uzelac Z, Gesmonde J, Bulling S, Stockner T, Freissmuth M, et al. Unifying Concept of Serotonin Transporter-associated Currents. Journal of Biological Chemistry. 2011 Dec 30;287(1):438–45.

Scholze P, Zwach J, Kattinger A, Pifl C, Singer EA, Sitte HH. Transporter-mediated release: a superfusion study on human embryonic kidney cells stably expressing the human serotonin transporter. J Pharmacol Exp Ther. 2000 Jun 1;293(3):870–8.

Schroeter S, Blakely RD. Drug Targets in the Embryo. Ann N Y Acad Sci. 1996 Oct;801(1 Cellular and):239–55.

Schulze S, Köster S, Geldmacher U, Terwisscha van Scheltinga AC, Kühlbrandt W. Structural basis of Na+-independent and cooperative substrate/product antiport in CaiT. Nature. Nature Publishing Group; 2010 Sep 9;467(7312):233–6.

Screpanti E, Hunte C. Discontinuous membrane helices in transport proteins and their correlation with function. Journal of Structural Biology. 2007 Aug;159(2):261–7.

Segonzac A, Raisman R, Tateishi T, Schoemaker H, Hicks PE, Langer SZ. Tryptamine, a Substrate for the Serotonin Transporter in Human Platelets, Modifies the Dissociation Kinetics of [3H]Imipramine Binding: Possible Allosteric Interaction. J Neurochem. 1985 Feb;44(2):349–56.

Sette M, Ruberg M, Raisman R, Zivkovic B, Agid Y, Langer SZ. [3H]Impramine binding in subcellular fractions of rat cerebral cortex after chemical lesion of serotonergic neurons. European Journal of Pharmacology. 1983 Nov;95(1-2):41–51.

Shaffer PL, Goehring A, Shankaranarayanan A, Gouaux E. Structure and Mechanism of a Na+-Independent Amino Acid Transporter. Science. 2009 Aug 20;325(5943):1010–4.

Sherman W, Day T, Jacobson MP, Friesner RA, Farid R. Novel procedure for modeling ligand/receptor induced fit effects. J Med Chem. 2006 Jan 26;49(2):534–53.

Shi L, Quick M, Zhao Y, Weinstein H, Javitch JA. The Mechanism of a Neurotransmitter:Sodium Symporter—Inward Release of Na+ and Substrate Is Triggered by Substrate in a Second Binding Site. 2008 Jun 20;30(6):667–77.

Shi L, Weinstein H. Conformational rearrangements to the intracellular open states of the LeuT and ApcT transporters are modulated by common mechanisms. Biophys J. 2010 Dec 15;99(12):L103–5.

Shimamura T, Weyand S, Beckstein O, Rutherford NG, Hadden JM, Sharples D, et al. Molecular Basis of Alternating Access Membrane Transport by the Sodium-Hydantoin Transporter Mhp1. Science. 2010 Apr 22;328(5977):470–3.

Simonson T, Carlsson J, Case DA. Proton binding to proteins: pK(a) calculations with explicit and implicit solvent models. J Am Chem Soc. 2004 Apr 7;126(13):4167–80.

Singh SK, Piscitelli CL, Yamashita A, Gouaux E. A Competitive Inhibitor Traps LeuT in an Open-to-Out Conformation. Science. 2008 Dec 12;322(5908):1655–61.

Singh SK, Yamashita A, Gouaux E. Antidepressant binding site in a bacterial homologue of neurotransmitter transporters. Nature. 2007 Aug 8;448(7156):952–6.

Sinning S, Musgaard M, Jensen M, Severinsen K, Celik L, Koldso H, et al. Binding and Orientation of Tricyclic Antidepressants within the Central Substrate Site of the Human Serotonin Transporter. Journal of Biological Chemistry. 2010 Mar 5;285(11):8363–74.

Sitte HH, Freissmuth M. Amphetamines, new psychoactive drugs and the monoamine transporter cycle. Trends in Pharmacological Sciences. 2015 Jan;36(1):41–50.

Sitte HH, Hiptmair B, Zwach J, Pifl C, Singer EA, Scholze P. Quantitative analysis of inward and outward transport rates in cells stably expressing the cloned human serotonin transporter: inconsistencies with the hypothesis of facilitated exchange diffusion. Molecular Pharmacology. ASPET; 2001;59(5):1129–37.

Sitte HH, Huck S, Reither H, Boehm S, Singer EA, Pifl C. Carrier-mediated release, transport rates, and charge transfer induced by amphetamine, tyramine, and dopamine in mammalian cells transfected with the human dopamine transporter. J Neurochem. 1998 Sep;71(3):1289–97.

Sitte HH, Scholze P, Schloss P, Pifl C, Singer EA. Characterization of carrier-mediated efflux in human embryonic kidney 293 cells stably expressing the rat serotonin transporter: a superfusion study. J Neurochem. 2000 Mar;74(3):1317–24.

Smith CA, Kortemme T. Backrub-like backbone simulation recapitulates natural protein conformational variability and improves mutant side-chain prediction. J Mol Biol. 2008 Jul 18;380(4):742–56.

Smith E, Collins I. Photoaffinity labeling in target- and binding-site identification. Future Medicinal Chemistry. Future Science Ltd London, UK; 2015 Feb;7(2):159–83.

Sneddon JM. Sodium-dependent accumulation of 5-hydroxytryptamine by rat blood platelets. British Journal of Pharmacology. Blackwell Publishing; 1969 Nov 1;37(3):680.

Sneddon JM. Blood platelets as a model for monoamine-containing neurones. Prog. Neurobiol. 1973. pp. 151–98.

Sonders MS, Amara SG. Channels in transporters. Current Opinion in Neurobiology. 1996 Jun;6(3):294–302.

Sonders MS, Zhu SJ, Zahniser NR, Kavanaugh MP, Amara SG. Multiple ionic conductances of the human dopamine transporter: the actions of dopamine and psychostimulants. J Neurosci. 1997 Feb 1;17(3):960–74.

Stockner T, Montgomery TR, Kudlacek O, Weissensteiner R, Ecker GF, Freissmuth M, et al. Mutational Analysis of the High-Affinity Zinc Binding Site Validates a Refined Human Dopamine Transporter Homology Model. Noskov S, editor. PLoS Comput Biol. 2013 Feb 21;9(2):e1002909.

Sucic S, Dallinger S, Zdrazil B, Weissensteiner R, Jørgensen TN, Holy M, et al. The N terminus of monoamine transporters is a lever required for the action of amphetamines. J Biol Chem. United States; 2010 Apr 4;285(14):10924–38.

Sulzer D, Sonders MS, Poulsen NW, Galli A. Mechanisms of neurotransmitter release by amphetamines: a review. Prog Neurobiol. 2005 Apr;75(6):406–33.

Sung U, Blakely RD. Calcium-dependent interactions of the human norepinephrine transporter with syntaxin 1A. Molecular and Cellular Neuroscience. 2007 Feb;34(2):251–60.

Swanson JMJ, Henchman RH, McCammon JA. Revisiting free energy calculations: a theoretical connection to MM/PBSA and direct calculation of the association free energy. Biophys J. 2004 Jan;86(1 Pt 1):67–74.

Tatsumi M, Groshan K, Blakely RD, Richelson E. Pharmacological profile of antidepressants and related compounds at human monoamine transporters. European Journal of Pharmacology. 1997 Dec;340(2-3):249–58.

Tavoulari S, Rizwan AN, Forrest LR, Rudnick G. Reconstructing a chloride-binding site in a bacterial neurotransmitter transporter homologue. J Biol Chem. 2011 Jan 28;286(4):2834–42.

Vaughan RA. Photoaffinity-labeled ligand binding domains on dopamine transporters identified by peptide mapping. Mol Pharmacol. 1995 May;47(5):956–64.

Vaughan RA, Agoston GE, Lever JR, Newman AH. Differential binding of tropane-based photoaffinity ligands on the dopamine transporter. J Neurosci. 1999 Jan 15;19(2):630–6.

Vaughan RA, Foster JD. Mechanisms of dopamine transporter regulation in normal and disease states. Trends in Pharmacological Sciences. 2013 Sep;34(9):489–96.

Vaughan RA, Huff RA, Uhl GR, Kuhar MJ. Protein Kinase C-mediated Phosphorylation and Functional Regulation of Dopamine Transporters in Striatal Synaptosomes. Journal of Biological Chemistry. 1997 Jun 13;272(24):15541–6.

Vaughan RA, Kuhar MJ. Dopamine Transporter Ligand Binding Domains: Structural and Functional Properties Revealed by Limited Proteolysis. Journal of Biological Chemistry. 1996.

Vaughan RA, Parnas ML, Gaffaney JD, Lowe MJ, Wirtz S, Pham A, et al. Affinity labeling the dopamine transporter ligand binding site. Journal of Neuroscience Methods. 2005 Apr;143(1):33–40.

Veenstra-VanderWeele J, Muller CL, Iwamoto H, Sauer JE, Owens WA, Shah CR, et al. Autism gene variant causes hyperserotonemia, serotonin receptor hypersensitivity, social impairment and repetitive behavior. Proc Natl Acad Sci USA. 2012 Apr 3;109(14):5469–74.

Wall SC, Gu H, Rudnick G. Biogenic amine flux mediated by cloned transporters stably expressed in cultured cell lines: amphetamine specificity for inhibition and efflux. Mol Pharmacol. 1995 Mar;47(3):544–50.

Wang H, Goehring A, Wang KH, Penmatsa A, Ressler R, Gouaux E. nature12648. Nature. Nature Publishing Group; 2013 Oct 13;:1–6.

Wang H, Gouaux E. Substrate binds in the S1 site of the F253A mutant of LeuT, a neurotransmitter sodium symporter homologue. EMBO Rep. Nature Publishing Group; 2012

Wang KH, Penmatsa A, Gouaux E. Neurotransmitter and psychostimulant recognition by the dopamine transporter. Nature. Nature Publishing Group; 2015 May 11;521(7552):322–7.

Wang LC, Cui X-N, Chen N, Reith MEA. Binding of cocaine-like radioligands to the dopamine transporter at 37°C: effect of Na+ and substrates. Journal of Neuroscience Methods. 2003 Dec;131(1-2):27–33.

Watanabe A, Choe S, Chaptal V, Rosenberg JM, Wright EM, Grabe M, et al. The mechanism of sodium and substrate release from the binding pocket of vSGLT. Nature. Nature Publishing Group; 2010 Dec 5;468(7326):988–91.

Wenge B, Bönisch H. The Role of Cysteines and Histidins of the Norepinephrine Transporter. Neurochem Res. Springer US; 2013 Mar 23;38(7):1303–14.

Wennogle LP, Ashton RA, Schuster DI, Murphy RB, Meyerson LR. 2-Nitroimipramine: a photoaffinity probe for the serotonin uptake/tricyclic binding site complex. EMBO J. European Molecular Biology Organization; 1985 Apr 1;4(4):971.

Weyand S, Shimamura T, Beckstein O, Sansom MSP, Iwata S, Henderson PJF, et al. The alternating access mechanism of transport as observed in the sodium-hydantoin transporter Mhp1. J Synchrotron Rad. International Union of Crystallography; 2010 Nov 5;18(1):20–3.

Weyand S, Shimamura T, Yajima S, Suzuki S, Mirza O, Krusong K, et al. Structure and molecular mechanism of a nucleobase-cation-symport-1 family transporter. Science. 2008 Oct 31;322(5902):709–13.

Yamashita A, Singh SK, Kawate T, Jin Y, Gouaux E. Crystal structure of a bacterial homologue of Na+/Cl--dependent neurotransmitter transporters. Nature. 2005 Sep 9;437(7056):215–23.

Yu H, Noskov SY, Roux B. Two mechanisms of ion selectivity in protein binding sites. Proc Natl Acad Sci USA. 2010 Nov 11;107(47):20329–34.

Zdravkovic I, Zhao C, Lev B, Cuervo JE, Noskov SY. Atomistic models of ion and solute transport by the sodium-dependent secondary active transporters. Biochim Biophys Acta. 2012 Feb;1818(2):337–47.

Zhang P, Cyriac G, Kopajtic T, Zhao Y, Javitch JA, Katz JL, et al. Structure−Activity Relationships for a Novel Series of Citalopram (1-(3-(Dimethylamino)propyl)-1-(4-fluorophenyl)-1,3-dihydroisobenzofuran-5-carbonitrile) Analogues at Monoamine Transporters. J Med Chem. 2010 Aug 26;53(16):6112–21.

Zhang YW, Rudnick G. The cytoplasmic substrate permeation pathway of serotonin transporter. J Biol Chem. 2006 Nov 11;281(47):36213–20.

Zhao C, Stolzenberg S, Gracia L, Weinstein H, Noskov S, Shi L. Ion-Controlled Conformational Dynamics in the Outward-Open Transition from an Occluded State of LeuT. Biophysical Journal. 2012 Sep;103(5):878–88.

Zhao Y, Terry D, Shi L, Weinstein H, Blanchard SC, Javitch JA. Single-molecule dynamics of gating in a neurotransmitter transporter homologue. Nature. 2010 May 13;465(7295):188–93.

Zhou Z, Zhen J, Karpowich NK, Goetz RM, Law CJ, Reith MEA, et al. LeuT-Desipramine Structure Reveals How Antidepressants Block Neurotransmitter Reuptake. Science. 2007 Sep 7;317(5843):1390–3.

Zhou Z, Zhen J, Karpowich NK, Law CJ, Reith MEA, Wang D-N. Antidepressant specificity of serotonin transporter suggested by three LeuT–SSRI structures. Nat Struct Mol Biol. NIH Public Access; 2009 May 10;16(6):652–7.

Zoete V, Cuendet MA, Grosdidier A, Michielin O. SwissParam: a fast force field generation tool for small organic molecules. J Comput Chem. 2011 Aug;32(11):2359–68.

Zomot E. The Interaction of the -Aminobutyric Acid Transporter GAT-1 with the Neurotransmitter Is Selectively Impaired by Sulfhydryl Modification of a Conformationally Sensitive Cysteine Residue Engineered into Extracellular Loop IV. Journal of Biological Chemistry. 2003 Aug 11;278(44):42950–8.

Zomot E, Bendahan A, Quick M, Zhao Y, Javitch JA, Kanner BI. Mechanism of chloride interaction with neurotransmitter:sodium symporters. Nature. Nature Publishing Group; 2007 Aug 19;449(7163):726–30.

Zou MF, Kopajtic T, Katz JL, Newman AH. Structure−Activity Relationship Comparison of (S)-2β-Substituted 3α-(Bis[4-fluorophenyl]methoxy)tropanes and (R)-2β-Substituted 3β-(3,4-Dichlorophenyl)tropanes at the Dopamine Transporter. J Med Chem. 2003 Jul;46(14):2908–16.

Zou MF, Kopajtic T, Katz JL, Wirtz S, Justice JB, Newman AH. Novel Tropane-Based Irreversible Ligands for the Dopamine Transporter. J Med Chem. 2001 Dec;44(25):4453–61.